TECHNICAL REPORT STANDARD TITLE PAGE

1. Report No.	2. Government Accession No.	3. Recipient's Catalog No.
FHWA/TX-86/60+372-1F(revised)		

4. Title and Subtitle	5. Report Date
Effects of Tire Pressures on Flexible Pavements	August 1986
	6. Performing Organization Code

7. Author(s)	8. Performing Organization Report No.
F. L. Roberts, J. T. Tielking, D. Middleton, R. L. Lytton, and K. Tseng	Research Report 372-1F

9. Performing Organization Name and Address	10. Work Unit No.
Texas Transportation Institute The Texas A&M University System College Station, Texas 77843	11. Contract or Grant No. Study No. 2-8-83-372
	13. Type of Report and Period Covered Final - September 1982 August 1986
12. Sponsoring Agency Name and Address Texas State Department of Highways and Public Transportation; Transportation Planning Division P. O. Box 5051 Austin, Texas 78763	14. Sponsoring Agency Code

15. Supplementary Notes

Research performed in cooperation with DOT, FHWA.
Research Study Title: Effects of Truck Tire Pressures on Flexible Pavements.

16. Abstract

This study includes the results of (1) a field study to determine the tire inflation pressures currently being carried by Texas highways, (2) a literature and analytical study to determine what tire contact pressures are actually being applied by modern tires to pavements, and (3) an analytical study to evaluate the effect of thse contact pressures on the stresses and strains in typical Texas flexible pavements.

Descriptions of the analytical studies include discussions of the finite element computer programs used to model the tire carcass and the flexible pavements. The tires included in the analytical study include both truck and passenger car tires operated at typical loads and inflation pressures.

The field study showed that tire inflation pressures are much higher on the road than those typically used in design procedures or even in analysis. Truck tire pressures average between 95 and 100 psi on the road and 75-80 psi is typically used in design. However, these high truck tire inflation pressures translate to contact pressures in the range of 150 to 200 psi. The effect of these high contact pressures is especially detrimental for thin surfaced roads. The analytical pavement studies show that, for pavements typical of the Texas Farm to Market System, the fatigue lives can be reduced by more than 50 percent. These studies indicate that thin, flexible surfaces or thick stiff surfaces offer the best protection against these high contact pressures.

17. Key Words	18. Distribution Statement
Contact pressure, inflation pressure, truck tires, finite element, field study, fatigue, rutting, permanent deformation, ILLIPAVE	No restriction. This document is available to the public through the National Technical Information Service 5285 Port Royal Road Springfield, Virginia 22161

19. Security Classif. (of this report)	20. Security Classif. (of this page)	21. No. of Pages	22. Price
Unclassified	Unclassified	245	

Form DOT F 1700.7 (8-69)

EFFECTS OF TIRE PRESSURES ON FLEXIBLE PAVEMENTS

by

Freddy L. Roberts

John T. Tielking

Dan Middleton

Robert L. Lytton

and

Kuo-Hung Tseng

Research Report 372-1F
Research Study Number 2-8-83-372
Effects of Truck Tire Pressures on Flexible Pavements

Sponsored by

Texas State Department of Highways and Public Transportation
in cooperation with
U. S. Department of Transportation, Federal Highway Administration

August 1986

TEXAS TRANSPORTATION INSTITUTE
The Texas A&M University System
College Station, Texas

METRIC (SI*) CONVERSION FACTORS

APPROXIMATE CONVERSIONS TO SI UNITS

Symbol	When You Know	Multiply By	To Find	Symbol
LENGTH				
in	inches	2.54	millimetres	mm
ft	feet	0.3048	metres	m
yd	yards	0.914	metres	m
mi	miles	1.61	kilometres	km
AREA				
in²	square inches	645.2	millimetres squared	mm²
ft²	square feet	0.0929	metres squared	m²
yd²	square yards	0.836	metres squared	m²
mi²	square miles	2.59	kilometres squared	km²
ac	acres	0.395	hectares	ha
MASS (weight)				
oz	ounces	28.35	grams	g
lb	pounds	0.454	kilograms	kg
T	short tons (2000 lb)	0.907	megagrams	Mg
VOLUME				
fl oz	fluid ounces	29.57	millilitres	mL
gal	gallons	3.785	litres	L
ft³	cubic feet	0.0328	metres cubed	m³
yd³	cubic yards	0.0765	metres cubed	m³

NOTE: Volumes greater than 1000 L shall be shown in m³.

TEMPERATURE (exact)

°F	Fahrenheit temperature	5/9 (after subtracting 32)	Celsius temperature	°C

APPROXIMATE CONVERSIONS TO SI UNITS

Symbol	When You Know	Multiply By	To Find	Symbol
LENGTH				
mm	millimetres	0.039	inches	in
m	metres	3.28	feet	ft
m	metres	1.09	yards	yd
km	kilometres	0.621	miles	mi
AREA				
mm²	millimetres squared	0.0016	square inches	in²
m²	metres squared	10.764	square feet	ft²
km²	kilometres squared	0.39	square miles	mi²
ha	hectores (10 000 m²)	2.53	acres	ac
MASS (weight)				
g	grams	0.0353	ounces	oz
kg	kilograms	2.205	pounds	lb
Mg	megagrams (1 000 kg)	1.103	short tons	T
VOLUME				
mL	millilitres	0.034	fluid ounces	fl oz
L	litres	0.264	gallons	gal
m³	metres cubed	35.315	cubic feet	ft³
m³	metres cubed	1.308	cubic yards	yd³

TEMPERATURE (exact)

°C	Celsius temperature	9/5 (then add 32)	Fahrenheit temperature	°F

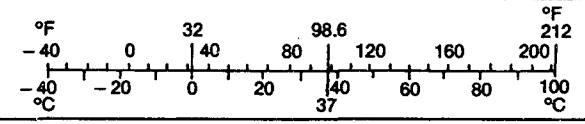

These factors conform to the requirement of FHWA Order 5190.1A.

* SI is the symbol for the International System of Measurements

DISCLAIMER

The contents of this report reflect the views of the authors, who are responsible for the facts and the accuracy of the data presented herein. The contents do not necessarily reflect the official views or policies of the Federal Highway Administration. This report does not constitute a standard, specification, or regulation.

PREFACE

This is the final report describing the truck tire inflation pressures measured on Texas highways and the effect of those tire pressures on flexible pavements. The report includes a description of not only the field study but the background data on tire contact pressure distributions that has been available to the tire industry for many years but has only recently come to the attention of pavement designers. The authors have included some of this tire contact pressure distribution data and presented the effect of these higher contact pressures on thin flexible pavements. This report should be instrumental in making the highway industry aware of the importance of considering the interactions between the tire and the road surface in analysis of pavement stresses and strains.

This report was completed with the assistance of many people. Special appreciation is extended to (1) Captains Collins and Johnson, Sergeants Mitchell, Kemp, and Kersey, and Trooper Bailey of the Texas Department of Public Safety, for their help in organizing and conducting the field study, (2) Messrs. James L. Brown and Robert L. Mikulin of the Texas State Department of Highways and Public Transportation for their support and encouragement as well as their constructive suggestions, (3) Messrs. Dan Walker, Randy Strickland and Dr. Ted Chira-Chavala of the Texas Transportation Institute for their field work and help in analysis of the data, (4) to Smithers Laboratories for making the tire sections available for the analytical study, and (5) the secretarial staff of the Pavement Materials, and Construction Division who prepared the manuscript materials. The support of the Federal Highway Administration, Department of Transportation, is gratefully acknowledged.

Freddy L. Roberts
John T. Tielking
Dan Middleton
Robert L. Lytton
Kuo-Hung Tseng

SUMMARY

This report summarizes the results of a field study and a series of analytical studies to determine the magnitude of truck tire inflation pressures currently on Texas highways and the effect of those tire pressures are on stresses and strains in flexible pavements. Analysis of field data showed that inflation pressure varies with tire construction, radials showing on the average 10 psi higher than for bias ply tires; AASHTO truck classification, the 3-S2 vehicles having the highest pressures followed by 2-S2, SU-3 and SU-2; and tread depth, worn tires having about a 4 psi lower inflation pressure than tires with tread depth less than 8/32-inch. Interestingly, for the small amount of axle weight data obtained, there was only a slight correlation between axle weight and inflation pressure.

Results from the analytical study of the tire, using a finite element model, indicated that for a common 10 x 20 bias truck tire the highest contact pressure in the tire contact patch is about two times the inflation pressure for inflation pressures of both 75 and 125 psi. For passenger car tires analyzed, similar results were obtained both from the finite element model and from limited literature found on the subject.

The analytical studies on pavements were conducted primarily on thin pavements, since the effects of the tire pressure are most pronounced in thinner sections. A set of computer runs were performed using the contact pressure distribution previously described. The results indicate that these truck contact pressures should produce premature fatigue cracking in thin surfaces, especially those between 1 and 3 inches. The studies using automobile tires indicate that the tensile strains are high enough, even for wheel loads as low as 800 pounds, to lead to fatigue cracking for intermediate thickness surfaces on thin, weak granular bases. In general the studies indicate that to provide adequate fatigue life these surfaces should be thin and flexible or thick and stiff over stiff granular bases.

IMPLEMENTATION STATEMENT

Based on the findings of this study it is apparent that measured truck tire inflation pressures are considerably higher than those typically assumed for design of flexible pavements. It is also apparent that to accurately reflect the effect of these high inflation pressures, pavements designers must also include tire contact pressure rather than inflation pressures.

Results of analytical studies indicate that thin asphalt surfaces should be used with caution. For relatively thin flexible pavements with unbound bases, conventional hot-mixed asphalt concrete should probably not be used. This suggestion results from the observation that high truck tire contact pressures produce tensile strains at the bottom of these surfaces that can lead to very premature fatigue cracking.

Evaluations of tensile strains show that for flexible pavements over unbound, granular bases that asphalt surfaces of

(1) 1-inch or less should be surface treatments on very stiff bases,

(2) 4 -inches or greater should be strong and stiff and strong and placed on stiff bases, and

(3) 1 to 3-inches should probably not be built since the strains are very high and early cracking is expected.

The primary reason for recommending caution in the use of 1 to 3-inch asphalt surfaces is that the high truck tire contact pressures produced the greatest increase in tensile strains for surface moduli ranging from 200 to 600 ksi, which is the modulus range for these materials during most of the Spring through Fall. Therefore, intermediate surface thicknesses should be used only after a careful analysis of each pavement structure to ensure that overstressing does not occur.

Analysis of the effect of passenger car tires contact pressures indicate that pavement designers should consider the strains induced by these vehicles especially for intermediate surface thicknesses.

TABLE OF CONTENTS

CHAPTER

CHAPTER 1
INTRODUCTION

This study was established originally (1) to determine the inflation pressures currently being used on trucks traveling Texas highways and (2) to evaluate the effect of these tire pressures on flexible pavement deterioration rates. Therefore, the study included a field study to accomplish the first objective and a series of analytical studies to accomplish the second objective. The scope of the study was expanded once it was determined that the tire pressure assumption most often used in pavement design was badly in error. In pavement design the tire-pavement contact pressure is assumed to be equal to the tire inflation pressure. Because this assumption was greatly in error, the study was expanded to include additional analytical work using a computer model capable of estimating the tire contact pressure distribution across a tire using data measured from a slice of tire. Having these non-linear contact pressure distributions produced a need for a pavement analysis program capable of accepting such loads. Such a program was obtained by modifying an existing finite element program that was originally developed at the University of California.

The original work plan called for an evaluation of the effect of tire pressures on both fatigue cracking and permanent deformation in flexible pavements. A considerable amount of effort was expended to evaluate both these distresses but with more success on fatigue cracking. A set of models were developed to estimate permanent deformation using results from creep tests, however, those efforts were not entirely successful and additional research work remains before those models can be used with confidence. However, a set of analyses were conducted to evaluate the effect of changing the inflation pressures from the rated values included in the Tire and Rim Manual to higher values actually measured in the field. Results from these analyses as well as the field study are included in this report.

CHAPTER 2

TIRE PRESSURES ON TEXAS HIGHWAYS

INTRODUCTION

Preliminary evidence from the field indicates that truck tire pressures on Texas Highways are higher than is typically assumed in design. The effect of such increases on pavements is an accelerated rate of deterioration. On asphaltic concrete pavements, increases in truck tire inflation pressures produce a more rapid occurrence of alligator cracking and rutting, and probably increase the rate of reflection cracking in overlays. One consequence of increased deterioration is an attendent increase in major maintenance and rehabilitation.

Prior to this study, little information was available to determine the distribution of tire pressures on Texas highways and to identify the magnitude of the effects of increased tire pressures on flexible pavements. None of the previous studies evaluating the effects of truck traffic and changing legal load limits have included tire pressures as an explicit variable although inflation pressures were assumed to increase somewhat as the legal load limit increased.

The objectives of this part of the study were two-fold: 1) to determine, using field measurements, the distribution of tire pressures and the contact area of the tire footprint on Texas pavements; and 2) to evaluate the effect of these tire pressures on the life and cost of typical flexible pavements.

It should be noted that in a companion study entitled "The Effect of Tire Inflation Pressures and Loading on the Tire-Pavement Interface" the contact areas of truck tires under various loads were measured in a laboratory setting. The study was conducted by the Center for Transportation Research (CTR) at the University of Texas in Austin and their findings are being used to supplement the results of Project 372.

SELECTION OF DATA COLLECTION SITES

The License and Weight Division of the Texas Department of Public Safety (DPS) is involved in an ongoing enforcement program in which trucks are stopped to check weights, vehicle registration, etc. The most logical means of collecting tire pressure information was to join the DPS weighing operations at selected sites in the state.

Three primary factors were considered in making site selection:

(1) Commodities being hauled through the area,
(2) Roadside safety considerations at the site, and
(3) Availability of DPS personnel and equipment.

The normal procedure used by project staff to schedule field data collection with the Department of Public Safety was to identify a geographic area in the State where desired commodity movements occurred. The DPS designated a captain in Austin to be the project contact man who could designate the proper person to contact in the vicinity of interest. A sergeant usually coordinated the schedule of the various troopers and made the necessary commitments for DPS personnel to meet project staff at specific times and places. After initial contact in a local area, scheduling other data collection efforts were made directly with these same troopers.

Because the DPS equipment was limited, scheduling difficulties occurred often. These semi-portable platform scales were trailer-mounted, pulled by a van or carry-all, and were rotated to the various DPS offices within a given region on a scheduled basis. Therefore, data collection depended not only on the availability of DPS personnel but also on the location of the semi-portable scales.

Another important factor in choosing data collection sites was traffic around the site. Only a few sites had adequate capacity for stopping several trucks at a time without the queue extending into the through traffic lanes. Even some of the specially paved weigh strips were too short to accommodate all of the stopped vehicles. In a few

cases, paved shoulders were used for weighing trucks if there was a parking lot or other clear area available for project equipment and vehicle parking.

In many cases, DPS staff had already planned to work a location which met project staff needs, but in other cases DPS plans were modified to accommodate project staff needs. In almost all cases DPS weighed the trucks, but in many cases project staff were unable to record the weights because of other data collection requirements.

The commodities selected in this study are those identified in Project 420, "Identification of Special-Use Truck Traffic" and aggregated into three industries: timber, agriculture, and surface mining. Specific commodities included in each category are listed below:

TIMBER	AGRICULTURE	SURFACE MINING
Raw Timber &	Grain	Sand/Gravel
Wood Products	Beef Cattle	Limestone
	Produce	
	Cotton	

For the selected sites, the primary timber products were found in a forty county area in east Texas. Agricultural produce was found at the site near Riviera on Highway 77 while beef cattle were found in the Panhandle area of the state. The primary surface mining products such as crushed stone and sand/gravel were found south of Dallas in the Trinity River bottom and in Wise County on Highway 114. Other sites such as I-45 north of Huntsville, Highway 79 near Taylor, I-10 east of Seguin, and I-35 near San Marcos, yielded data on a more general cross-section of cargo.

There were very few, if any, ideal sites for collecting truck tire and weight data. Even where weigh strips were available for stopping trucks, there were almost always parallel roads which were available for by-passing the enforcement activities. The percentage of trucks avoiding the scales could not be determined, however, the survey results are not necessarily biased because of potential avoidance. In fact, discussions

with truckers indicates that changes in tire inflation pressure are made only when a tire is underinflated.

DATA TO BE COLLECTED

A standard data collection form was developed and a copy is included in Appendix A. Each portion of the data collection form is described below. Each "block" of information gathered (two per sheet) represents one truck. Since very few trucks had more than five axles, the data form allowed space for recording one inflation pressure per axle as was the case for almost all trucks.

Each truck surveyed on a particular day was given a unique "test number" for that day, the first truck being test No.1, the second, test No.2, etc. The test numbers were therefore duplicated from one day to the next. During data assimilation, each truck was given a unique "truck number" to alleviate this duplication in test numbers.

Other information recorded in the top two lines of each block pertain to the vehicle or the site, whereas the remainder of the data was primarily tire information. Specifically, the data included: state, license tag no., AASHTO truck classification, commodity, pavement temperature, air temperature, date, location, weather, and comments. Some of these data were recorded for each vehicle (test number, state license, AASHTO classification, and commodity); others were recorded approximately hourly (pavement temperature, air temperature, and weather); while data and location were usually recorded once per day.

The remainder of each block was used primarily for tire information. The information on vehicle length, width, and headlight height was originally selected in an attempt to camouflage the tire pressure data collection efforts. The researchers anticipated that there was a remote chance that truckers would alter their normal tire pressures if they realized that the real intent of the data collection effort was to monitor pressure. These superfluous measurements were not taken, however, since time was not available.

Another item included in the original data collection plan was the tire "footprint". Several methods of tire footprint measurement were considered and some were actually tested in the field, however, none proved to be feasible. In fact, using the measurement systems investigated, the amount of tire pressure data collected would have been significantly reduced if contact areas had been measured because of the time intensity of the measurement process. Again, the length of time required to make these measurements was a deterrent as well as the lack of a practical and accurate means of making the measurement.

The remaining tire information included tire manufacturer, tire construction (radial or bias), tire size, inflation pressure, tread depth, and axle load. The tire manufacturer, whether radial or bias, and tire size were simply read from the tire and recorded. The "1st pressure" was the air pressure measured near the scales soon after the truck was stopped. In a few instances, a second reading of pressure was taken ("2nd pressure" on the data form) at least an hour after the truck was stopped initially. These were cases where the truck and driver were detained by the Department of Public Safety (DPS) for a relatively long period of time. The reason for the second reading was to determine whether or not a change in pressure occurred as the tires cooled down.

The tread depth varied in many cases across the width of the tire. The measurements were taken at a distance of approximately two inches from the outside edge of the tire.

A limited amount of axle weight data was collected by project personnel as DPS weighed the vehicle. Since different personnel recorded the weights and tire information, truck license numbers were used to combine the two data sets.

PROCEDURE AT THE SITE

At each data collection site, the personnel requirements included at least two project personnel to collect tire pressure information and two DPS officers to weigh trucks. At an enforcement site all trucks, whether

loaded or empty, were required to stop. Empty vehicles were often waved on by DPS but often vehicle registration and/or operator license checks were performed.

The typical data collection procedure involved measuring and recording data on the outside tire along the passenger side of the truck only, starting at either the front or rear. The inside tire of a dual was measured only if some problem occurred on the outside tire. Securing information such as brand name for the inside tire was much more difficult than for the outside tire.

Project personnel activities during data collection included the following:

Surveyor No. 1: Remove cap from tire valve stem, measure tire inflation pressure, replace cap on valve stem, and measure tread depth.

Surveyor No. 2: (Works with No.1) Record information on tire manufacturer, construction (radial/bias), AASHTO vehicle classification, truck license number, tire inflation pressure, and tread depth. Surveyor No.2 also records test number, weather, date, location, temperature at appropriate times, and asks the truck driver what commodity is being hauled, if not visible.

Surveyor No. 3: (Not always used) Works at the scales to record axle weights and truck license numbers.

Collection of the required project data took longer than the time required for the DPS to weigh trucks. Therefore, at busy locations, such as the I-35 and I-45 weigh strips, the truck queue length increased significantly often producing a safety problem for vehicles in the main freeway lanes. Therefore, data collection procedures were modified to check as many trucks as possible either before or after being weighed. The researchers recognized that checking only those trucks found to have a

violation could introduce bias, if a correlation was found to exist between vehicle weight and tire pressure.

In most cases, truck drivers permitted the tire pressures to be checked. Since the DPS was always present during data collection, their presence may have been a factor in the high level of cooperation experienced. In some cases, project staff asked permission to check the tire pressures. Several drivers expressed concern that the valve stems would leak air and their concern was valid since some valves stems did stick partially open after the pressure measurement. That problem was corrected relatively quickly, however.

A limited sample of data was taken at night between 6:00 P.M. and 6:00 A.M.. The data collection procedure was identical to the daytime operations, except that flashights were required even if overhead security lights were present. Oftentimes, shadows cast by overhead lights made data collection difficult.

ANALYSIS OF TIRE PRESSURE DATA

The objective of preliminary analyses of tire measurements was to identify significant factors affecting tire pressure and to develop tire pressure distributions. Because of various implementation constraints imposed by the field conditions, there was a significant amount of missing data for most variables. This required that the data be purified before final analysis could be completed. The data were basically divided into sets by AASHTO truck class. Analysis of tire pressure measurements were carried out separately for each AASHTO truck class: 3-S2, 2-S2, SU-2, and SU-1.

Purification of Data File

A number of coding errors were identified in the early stage of tire pressure data analysis including:

1) missing AASHTO class codes for 42 percent of the data,
2) miscoding of AASHTO classes,
3) miscoding of axle locations for over 100 3-S2 trucks, and
4) coding errors in tire pressure valves.

The high percent missing codes on AASHTO class could be relatively easily rectified. Miscoding of axle locations and thus related tire pressure information was observed for over 100 trucks. These trucks were in the first group surveyed and the field sheets were updated. Corrections of axle locations were relatively straight forward. The majority of these cases were obviously 3-S2 trucks since complete information was available on the pressures for all 5 axles. They were thus recoded as 3-S2. Some other 40 trucks, upon examining the hard-copy reports, had AASHTO class information recorded on the side of the reports. Such information was, therefore, used to identify the missing AASHTO classes. There were some trucks with 3 tire pressure readings only; they were assumed to be SU-3. Those with only 2 tire pressure readings were recoded as SU-2. This editing procedure reduced the proportion of missing AASHTO classes from 42 percent to 13 percent.

Coding errors in tire pressure values were, fortunately, not very common. Those few cases, which were characterized by unusually low tire pressures (1 to 20 psi) and/or unrealistically large differences between two tire pressure readings taken some 30 minutes apart, were corrected by reviewing each of the hard-copy reports.

Preliminary Analysis

The sample included measurements on a total of 1,486 trucks. As shown in Table 1, 70 percent were 3-S2, 6 percent SU-3, 6 percent SU-2, 4 percent 2-S2, 2 percent other truck types, and 13 percent unknown truck types.

Table 2 contains the distribution of commodities by truck type for the sample. The 3-2S trucks were used to transport almost all the 16

Table 1. Number of Trucks in the Sample

AASHTO	# of Vehicles	Percent
3S2	1033	69.5
2S2	52	3.5
SU3	90	6.1
SU2	86	5.8
Double (3-2)	11	0.7
Double (2-S1-2)	6	0.4
2S1	13	0.9
Missing/Unknown	195	13.1
Total	1486	100.0

Table 2. Number of Trucks by Major Commodities

Commodity	# of Trucks			
	3S2	2S2	SU3	SU2
Cattle	17			
Cement	18		5	
Construction Equip.	9			
Grain	18			
Gasoline	40			
Limestone	27			
Lumber (finished)	15			3
Steel Pipe	9			
Produce	21		5	4
Rock	45	4		
Sand/Gravel	37			
Steel	37			
Tar	14			
Timber (log)	21			
Empty	48	6	9	7
Mail/UPS		3		
Beverage				3
Unknown	546	26	50	47

major commodities while 2-S2 trucks primarily hauled rock and mail/UPS cargo. Single-unit trucks were used for produce, cement, finished lumber, and beverage. There is a large proportion of missing data in Table 2, primarily because this data was collected as time allowed.

Table 3 shows the distribution of truck types at each of the 12 survey locations. At the majority of these locations, virtually all trucks passing the survey station were stopped for tire measurements. These locations were Nacogdoches, Weslaco, Dallas, Wells, Teneha, and Lufkin. At Huntsville, only those trucks stopped by the DPS officers for violations were surveyed for tire pressures. At Seguin, tire pressure measurements were taken for those trucks selected as part of a WIM demonstration project.

Descriptive statistics of tire-pressure measurements are summarized in Table 4 by AASHTO truck class, tire construction (radial/bias), and axle location. For 3-S2 trucks, radial tires occurred more than twice as often as bias tires. However, for 2-S2, SU-3, and SU-2 trucks the number of bias tires exceeded the number of radial tires. Radial tires had inflation pressure from 12-23 psi higher than bias tires. Figures 1 through 8 show cumulative distribution plots of tire pressures for each AASHTO class, by tire construction (radial/bias) and with the front axle separated from all other axles. Figure 9 shows the cumulative distributions of front axle tire pressures among the 4 AASHTO classes by tire construction. The difference in inflation pressure between bias and radials is clearly indicated in Figure 9. For a particular AASHTO vehicle, the radial tires had higher inflation pressures than did the bias tires. The differences between AASHTO class, though smaller, can also be seen from this figure. For bias tires, 3-S2 trucks had higher pressures than did SU-3 trucks, 2-S2 trucks, and SU-2 trucks, in that order. For radial tires, the highest tire-pressures were measured for the 3-S2 trucks followed by SU-3, 2-S2, and SU-2 trucks.

Table 5 summarizes tire inflation pressure data by major tire manufacturer for the 3-S2 trucks. There is little variation in the average inflation pressure among manufacturers after adjusting for tire construction. Table 6 shows tire inflation pressure data for the 3-S2

Table 3. Survey Locations and Percent Truck Type at Each Location

Location	Highway Classification	Percent Truck Type					Total Number of Trucks
		3S2	2S2	SU3	SU2	Other	
Nacogdoches, US 259 & SH 204	US 259, 2-lane, rural	86.0	3.0	7.0	4.0	---	29
Taylor, US 79	2-lane, rural	81.0	2.0	7.0	7.0	3.0	85
Seguin, I10	Interstate, rural	72.0	8.0	8.0	10.0	2.0	245
Weslaco, US 83	4-lane divided, rural	61.0	5.0	11.0	17.0	7.0	127
Dallas FM 1389	2-lane, rural	78.0	---	16.0	3.0	3.0	64
Wells, US 69	2-lane, rural	96.0	4.0	---	---	---	22
Huntsville, I45	Interstate, rural	78.0	6.0	7.0	6.0	3.0	167
Teneha, US 59	2-lane, rural	90.0	---	2.0	8.0	---	39
US77 Riviera	4-lane divided, rural	86.0	2.0	5.0	3.0	4.0	205
Amarillo, US 287	4-lane divided, rural	86.0	2.0	1.0	3.0	8.0	80
Vega, US 385	2-lane, rural	94.0	---	3.0	---	3.0	34
Lufkin, SH 103	4-lane divided	91.0	2.0	3.0	4.0	---	128

Table 4. Descriptive Statistics of Tire Pressures

AASHTO	Axle	Radial/Bias	TIRE PRESSURE (Min, Max)	Mean	S.D.	# of Axles
3S2	F	R	52,140	99.6	12.8	504
		B	43,120	87.5	11.8	208
	1	R	44,150	99.1	13.8	634
		B	30,130	84.5	15.6	181
	2	R	32,153	97.9	14.9	637
		B	41,128	85.5	14.5	173
	3	R	30,140	96.6	14.2	526
		B	28,132	85.5	15.7	273
	4	R	28,136	97.1	15.0	510
		B	10,128	83.1	18.1	253
2S2	F	R	85,120	98.8	10.1	17
		B	43,104	78.2	16.3	23
	1	R	68,112	96.4	12.3	24
		B	40,110	73.1	17.6	21
	2	R	40,122	91.4	22.2	14
		B	23,124	75.1	19.0	31
	3	R	71,120	94.7	14.6	15
		B	20,112	75.7	18.7	29
SU3	F	R	68,120	98.0	12.9	24
		B	50,110	80.4	14.5	43
	1	R	74,122	95.7	12.2	36
		B	28,110	83.0	16.4	45
	2	R	70,122	95.4	13.2	32
		B	38,121	83.6	13.9	40
SU2	F	R	62,114	88.3	19.3	19
		B	20,102	71.5	19.6	54
	1	R	52,114	91.5	18.0	20
		B	27,104	71.7	15.4	58

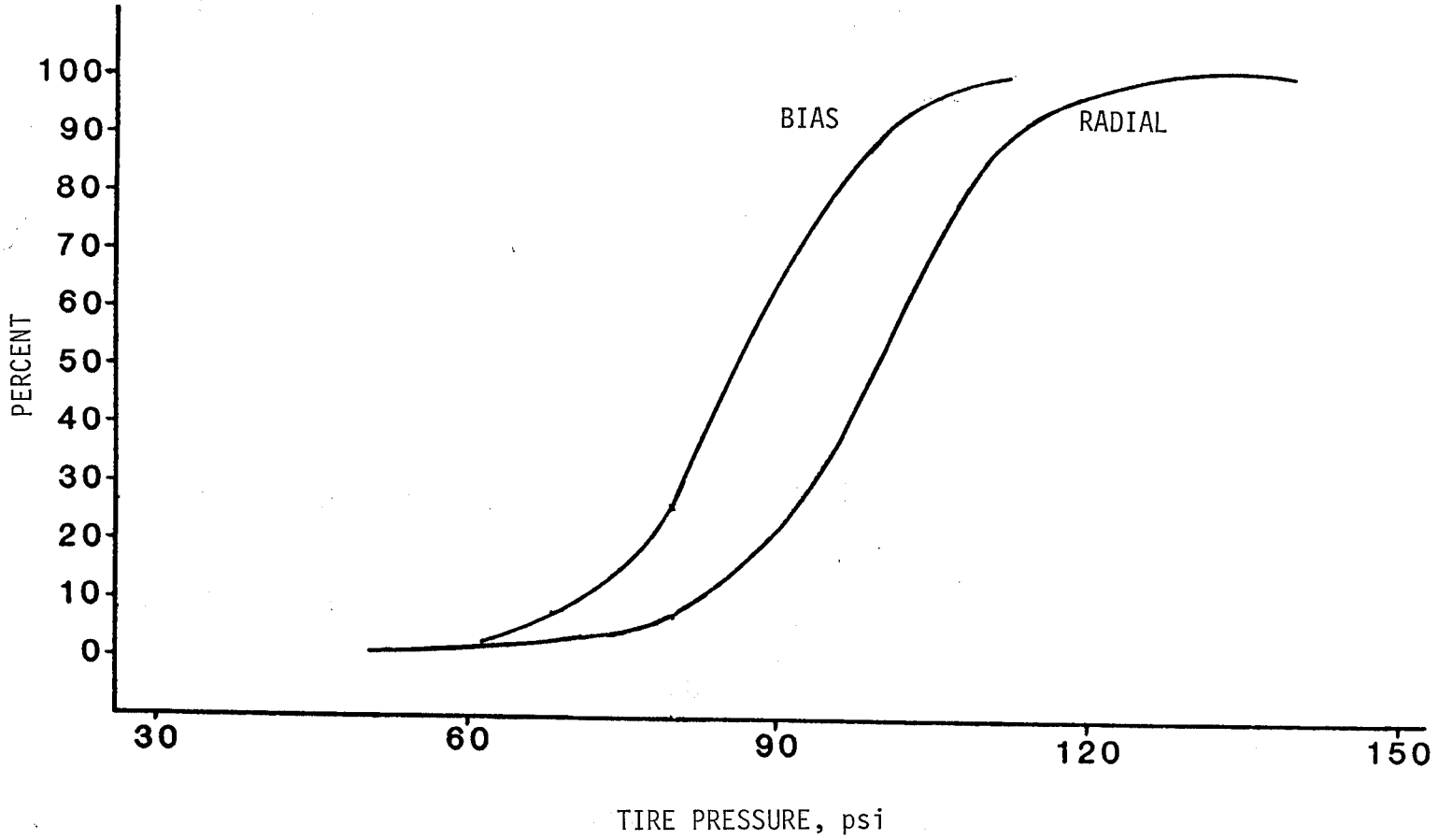

Figure 1. Cumulative distribution of tire pressures for front axles of 3-S2 trucks

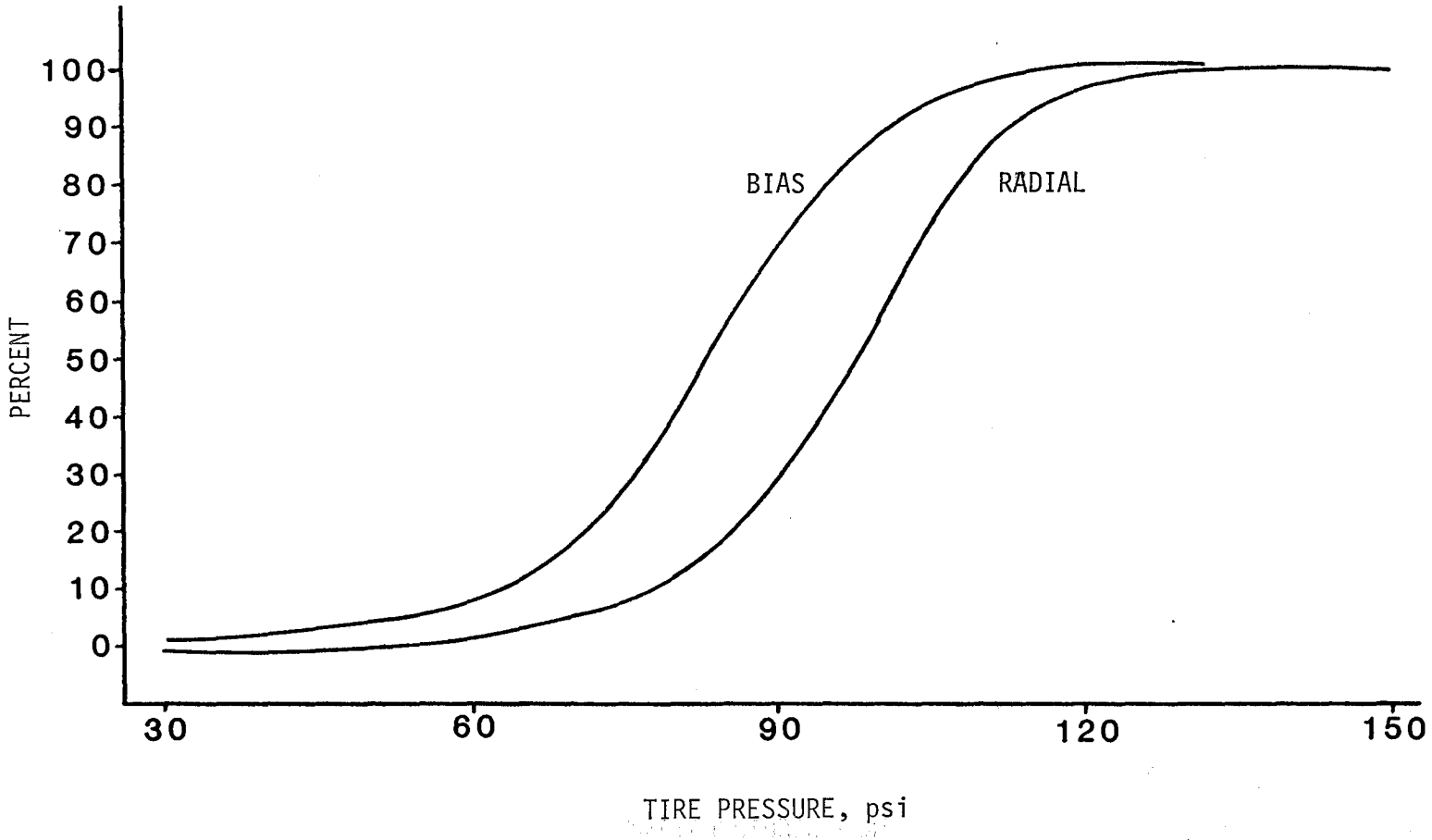

Figure 2. Cumulative distribution of tire pressures for non-front axles of 3-S2 trucks

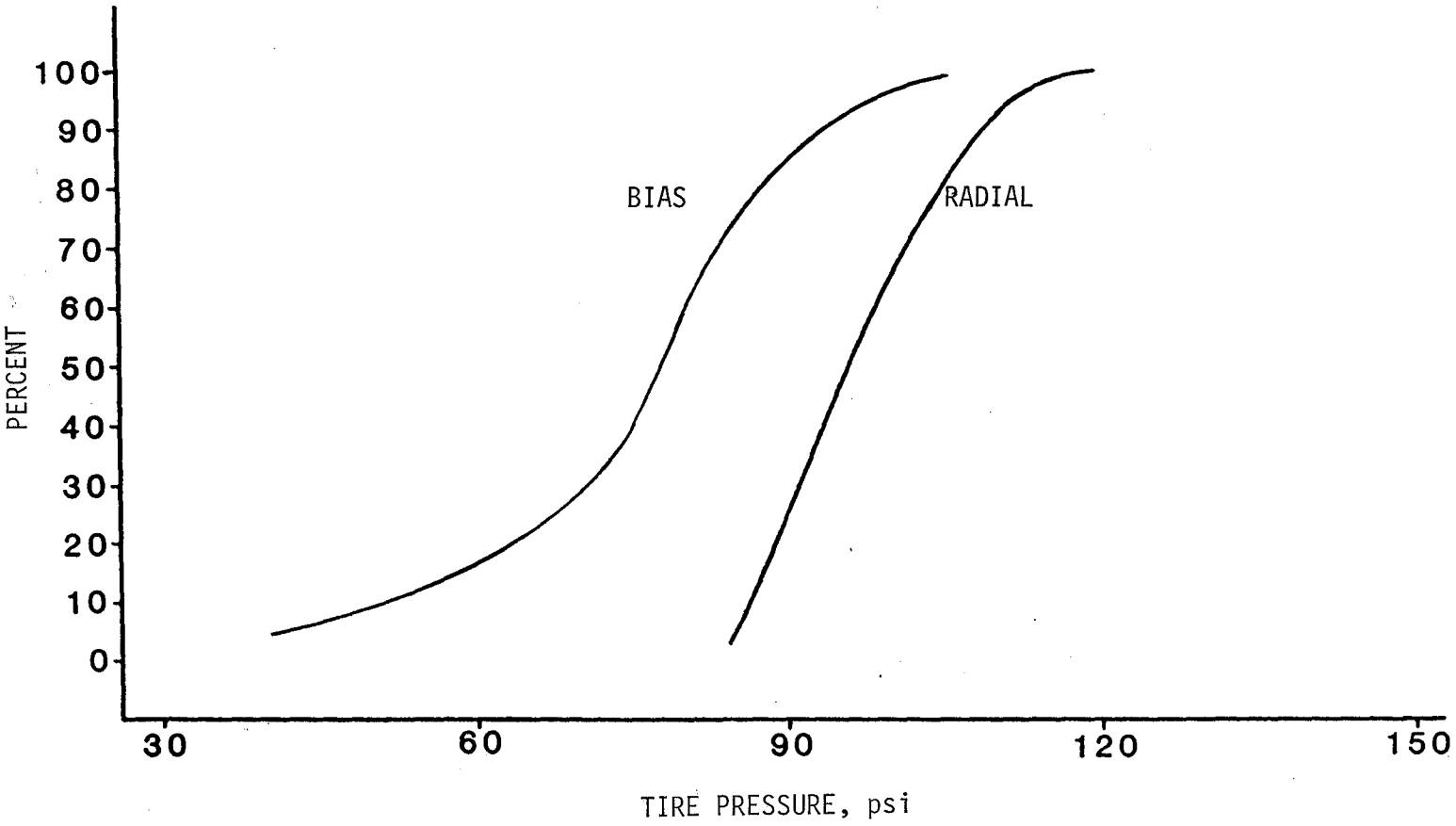

Figure 3. Cumulative distribution of tire pressures for front axles of 2-S2 trucks

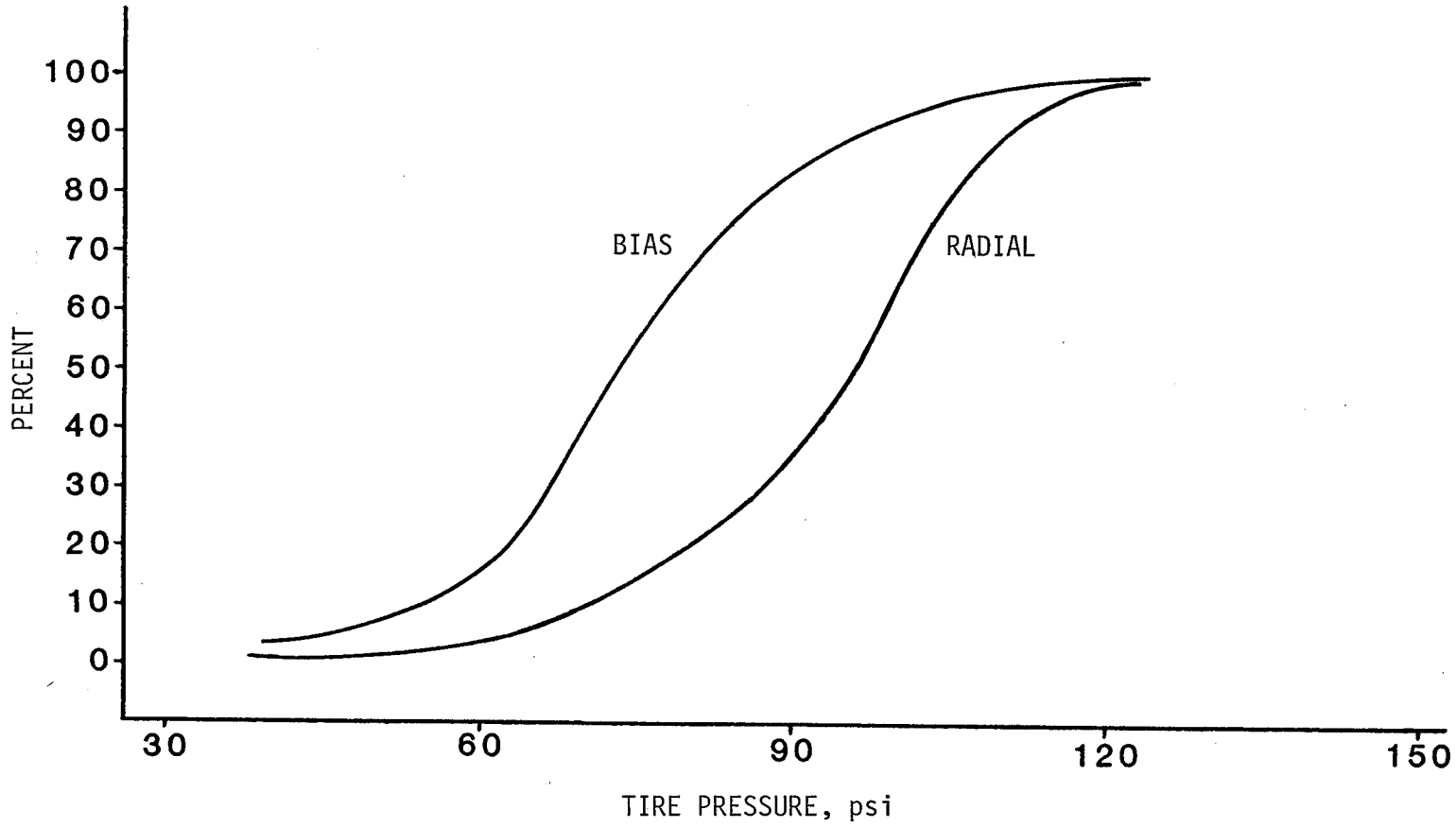

Figure 4. Cumulative distribution of tire pressures for non-front axles of 2-S2 trucks

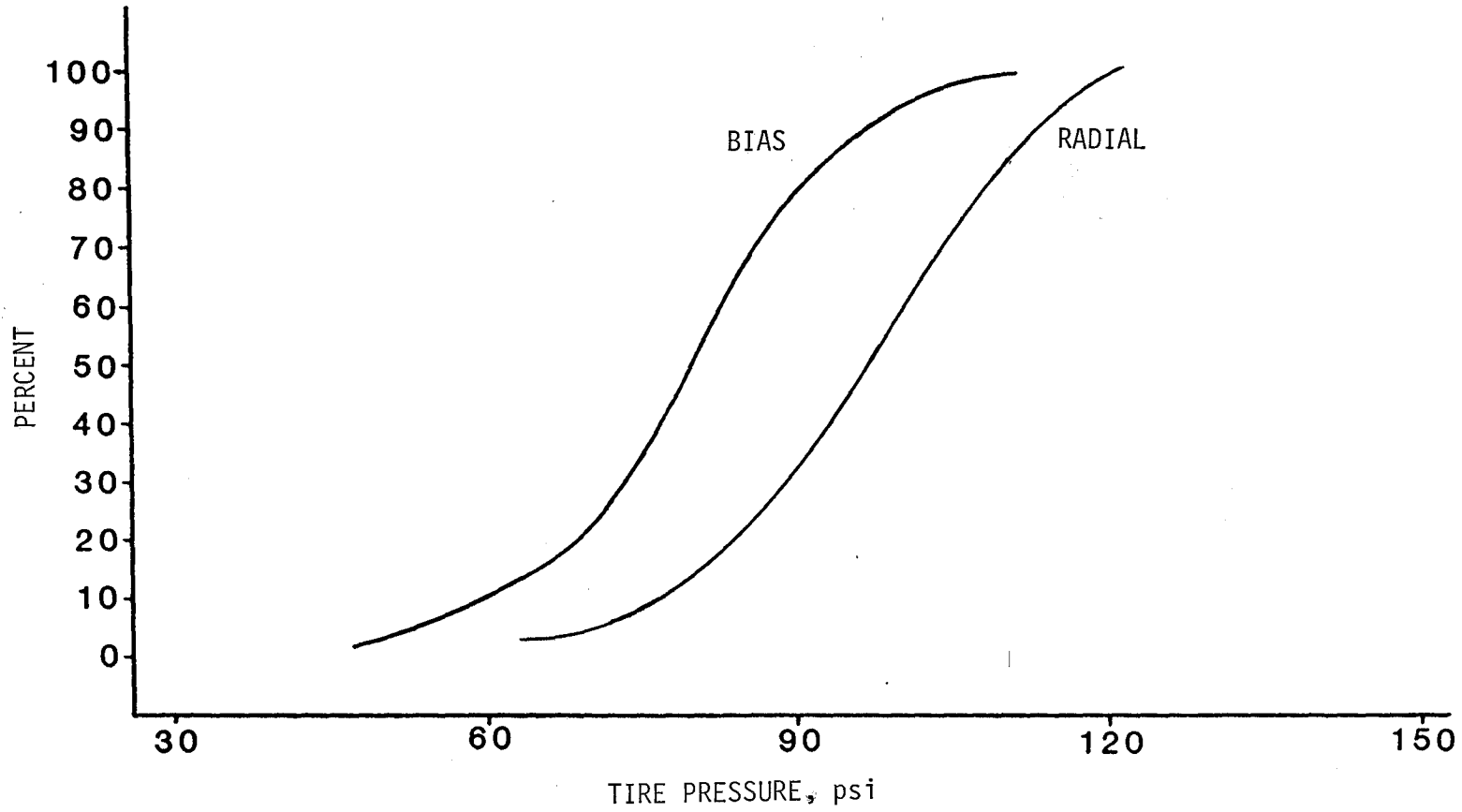

Figure 5. Cumulative distribution of tire pressures for front axles of SU-3 trucks

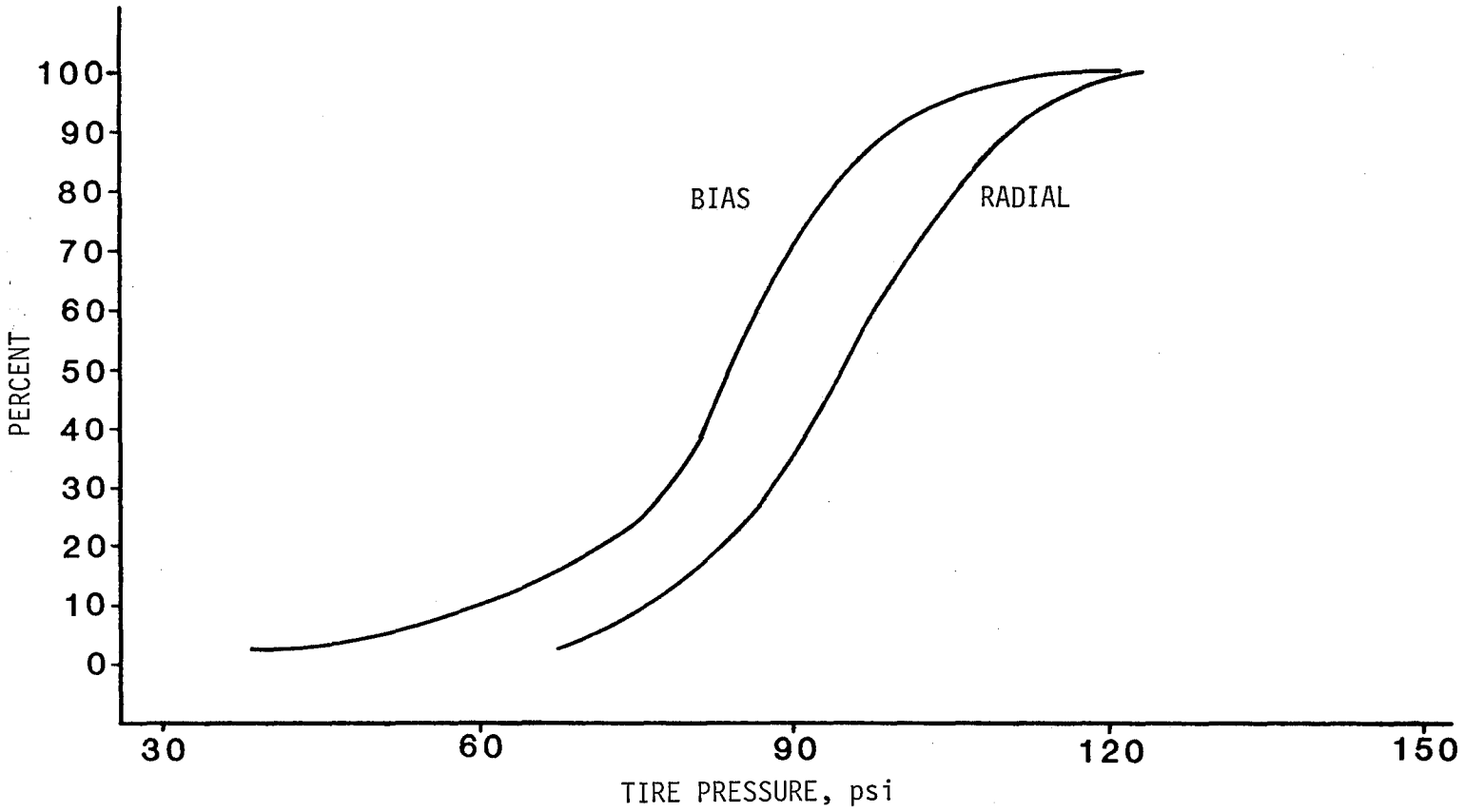

Figure 6. Cumulative distribution of tire pressures for non-front axles of SU-3 trucks

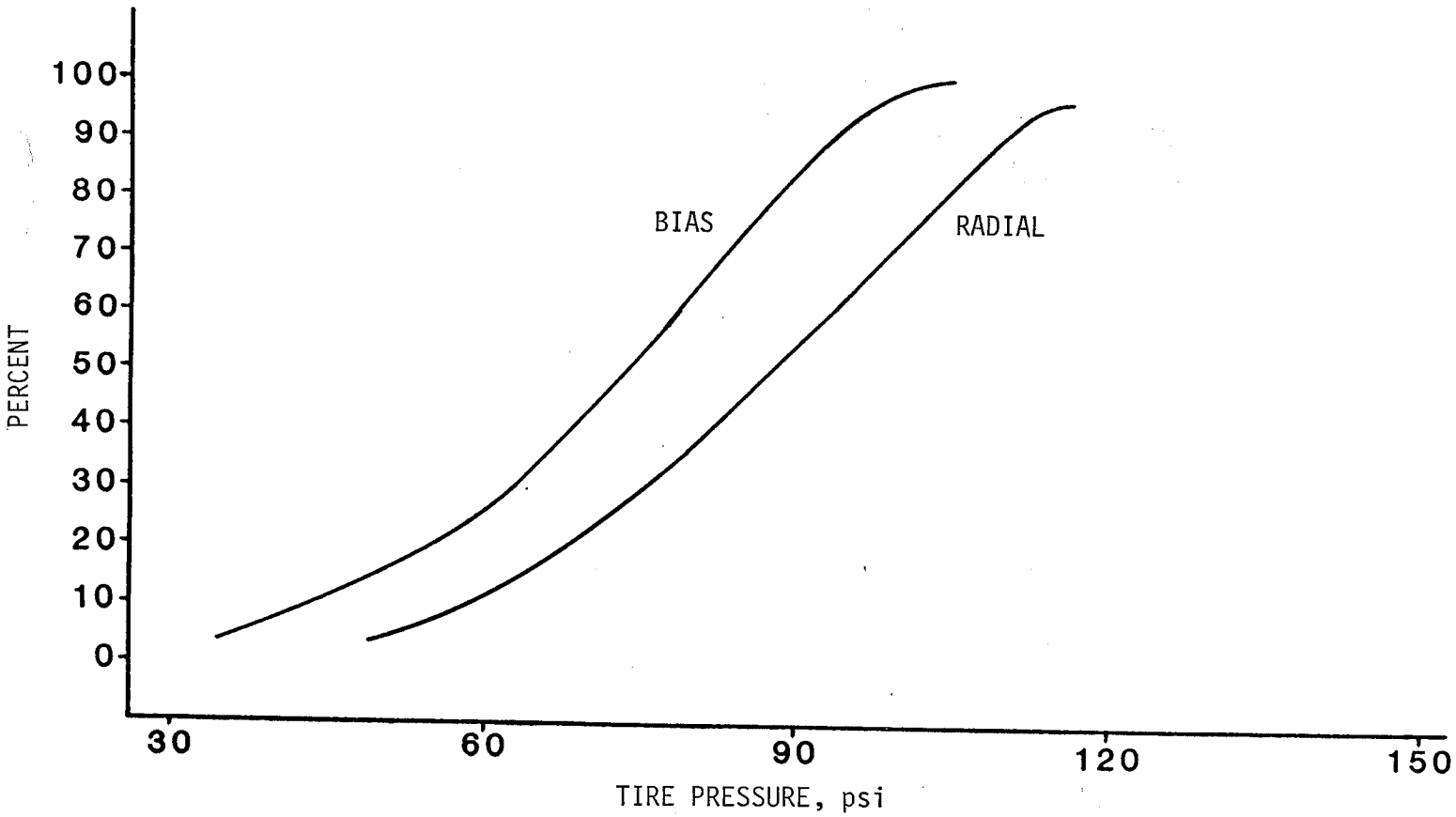

Figure 7. Cumulative distribution of tire pressures for front axles of SU-2 trucks

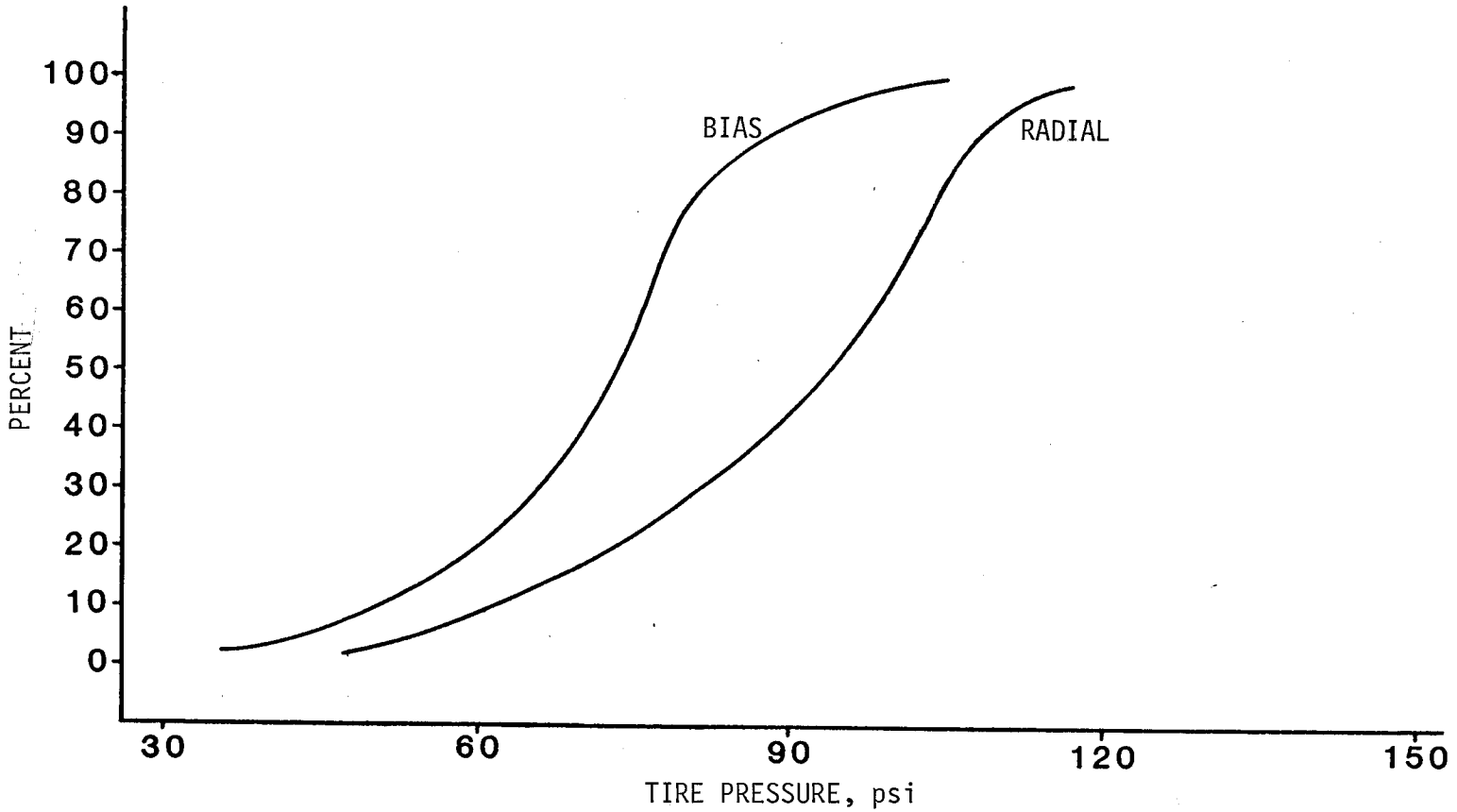

Figure 8. Cumulative distribution of tire pressures for non-front axles of SU-2 trucks

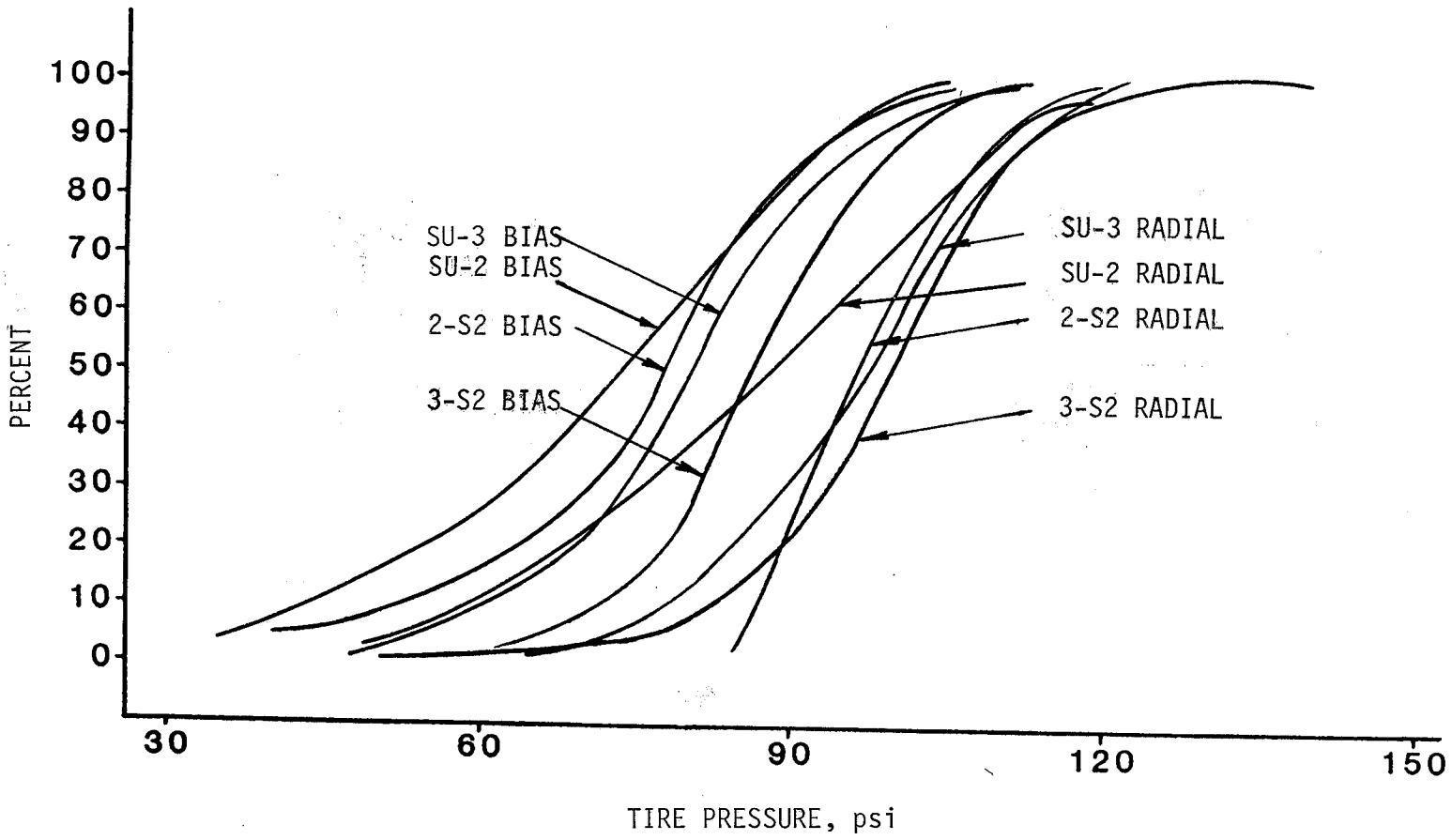

Figure 9. Cumulative distributions of tire pressures by tire construction and AASHTO class

Table 5. Tire Pressures by Major Manufacturers for 3S2

Manufacturer	Radial/ Bias	TIRE PRESSURE		
		Mean	S.D.	# of Axles
Michelin	R	99.0	13.2	730
	B	94.9	11.1	11
Goodyear	R	98.1	13.9	656
	B	85.5	16.0	222
Bridgestone	R	99.2	14.9	322
	B	87.7	14.5	53
Firestone	R	99.8	16.0	116
	B	83.7	15.1	106
Dunlop	R	98.6	16.5	110
	B	87.7	17.8	33
General	R	95.4	16.1	80
	B	84.4	15.8	58
Goodrich (B.F.G.)	R	97.7	13.2	70
	B	83.8	14.6	96
Cooper	R	94.6	11.7	17
	B	77.9	14.1	48
Next Top 10	R	95.3	15.0	283
	B	86.6	14.3	171
All Other	R	94.9	14.3	264
	B	85.2	15.8	265

Table 6. Tire-Pressure Distribution by 10 Major Commodities for 3-S2 Trucks Only

Commodity	RADIAL			BIAS		
	# of Axles	Mean	S.D.	# of Axles	Mean	S.D.
Produce	95	106.2	12.1	10	79.1	20.7
Grain	39	105.6	13.7	11	90.2	14.0
Cattle	36	101.6	19.8	10	87.3	9.1
Lumber	39	100.6	12.6	27	81.8	19.1
Steel	113	98.8	17.5	55	87.9	13.1
Rock/Sand/ Gravel/Limestone	257	97.8	12.4	117	84.0	12.2
Logs	62	96.2	13.4	13	87.7	5.8
Cement	62	95.1	15.6	22	87.6	16.4
Empty	138	95.2	12.2	40	83.8	12.8
Gasoline	121	95.1	13.2	26	85.1	12.1

trucks by commodities hauled. The inflation pressure was highest for trucks hauling produce and grain on radial tires with an average pressure of 105 psi. For bias tires, the differences in average inflation pressure among different commodities was relatively small.

Figures 10(a) through 10 (d) contain histograms of the axle weight data collected for some of the 3-S2, 2-S2, SU-3, and SU-2 vehicles, respectively.

Statistical Analysis

The statistical analysis of tire pressures involved an in-depth investigation of the variability in tire pressures and the factors affecting this variability. Based on the result of the preliminary analysis, the following independent variables were examined:

(1) Tire construction (radial/bias)
(2) AASHTO truck class
(3) Axle location (front, rear, other)
(4) Tire size (diameter)
(5) Tread depth (<8/32", $\geq$ 8/32")
(6) Commodity carried
(7) Axle weight
(8) Survey location

Tread depth was included as a dichotomous variable to reflect whether the tread depth was low or of reasonable depth.

The collection of axle weight and commodity data was not as complete as the data on other variables. Axle weight, in particular, was found to have a very high percentage of missing data (about 80 percent) as shown in Table 7. For commodity, the proportion of cases with missing information was about 55 percent as shown in Table 8.

The high percentage of missing data on axle weight and commodity, as well as the fact that a large majority of trucks in the sample were 3-S2 trucks led to the conduct of the following four analyses:

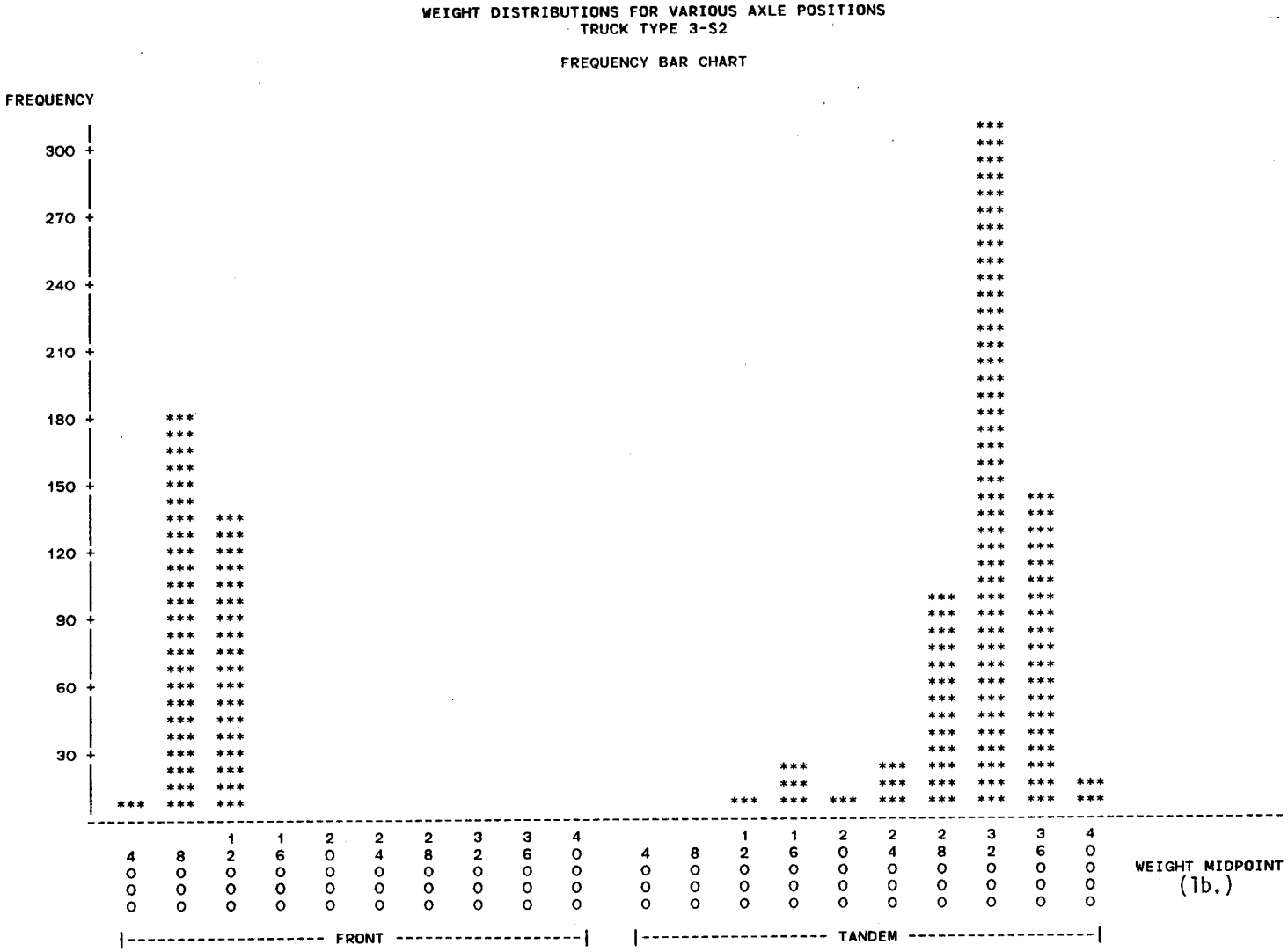

Figure 10(a). Histogram of axle weights for 3-S2 trucks

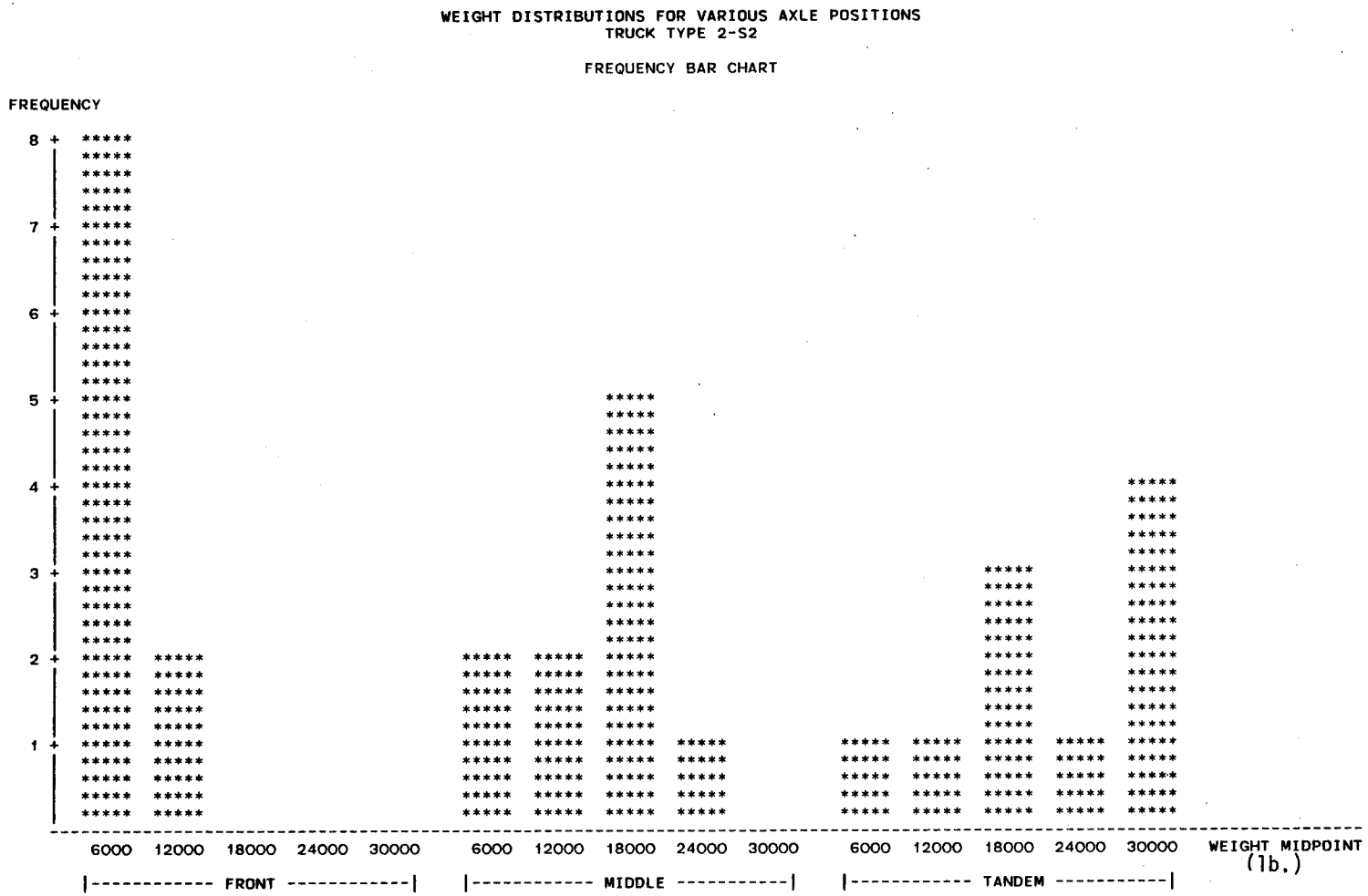

Figure 10(b). Histogram of axle weights for 2-S2 trucks

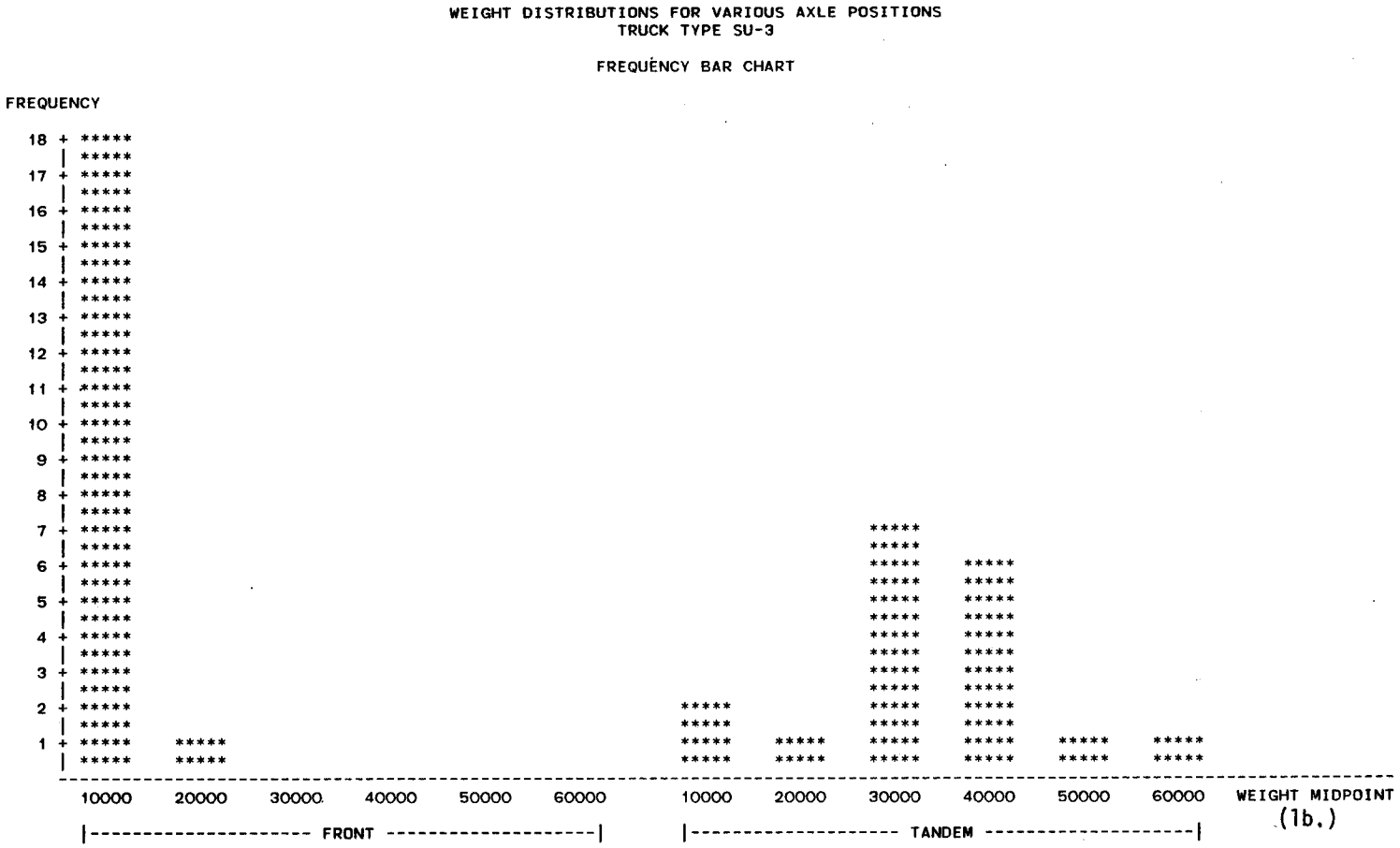

Figure 10(c). Histogram of axle weights for SU-3 trucks

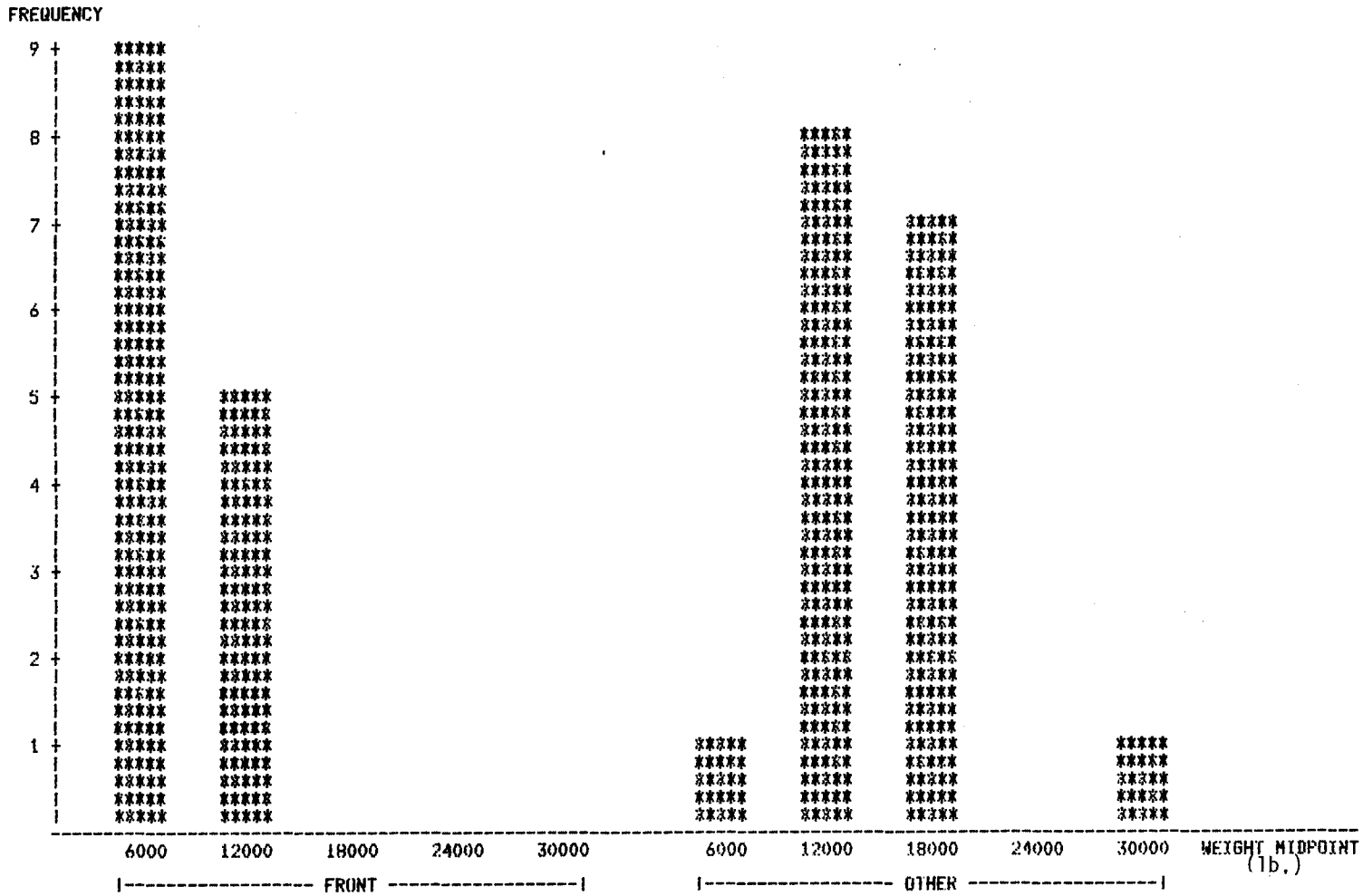

Figure 10(d). Histogram of axle weights for SU-2 trucks

Table 7. Percentage of Missing Data on Axle Weight

AASHTO	# of Complete Axles	# of Missing Axles	Percent Missing
3-S2	871	3028	77.7
2-S2	29	145	83.3
SU-3	47	173	78.6
SU-2	22	129	85.4

Table 8. Percentage of Missing Data on Commodity

AASHTO	# of Complete Trucks	# of Missing Trucks	Percent Missing
3-S2	487	546	52.9
2-S2	26	26	50.0
SU-3	40	50	55.6
SU-2	39	47	54.7

1. analyze the effects of tire and trucks factors, variables 1 through 5,
2. analyze the effect of axle weights for 3-S2 trucks only,
3. analyze the effect of commodity for 3-S2 trucks only, and
4. analyze the distribution of tire inflation pressures by survey locations.

Effect of Tire Construction, AASHTO Class, Axle Location, Tire Size, and Tread Depth. An analysis of variance (ANOVA) was first conducted to determine the effect of the following 5 variables on tire pressures:

Variable	Level
Tire Construction	Radial or Bias
AASHTO Class	3-S2, 2-S2, SU-3, SU-2
Axle Location	Front or All Other
Tire Diameter	$\leq$22.5 or >22.5
Tread Depth	<8/32" or $\geq$8/32"

Table 9 shows the 5-variable ANOVA results for all the significant factors. Tire construction, AASHTO class, and tread depth were found to be significant in explaining the variability in tire pressures. Among these 3 variables, tire construction was by far the most significant in explaining the differences in tire pressures, followed by AASHTO class. The influence of tread depth was the smallest. Tire diameter and axle location were not significant nor were any of the 2-factor interactions among the 5 variables.

Table 10 shows a summary of tire pressures by tire construction, AASHTO class and tread depth. Again, Table 10 indicates that, of the 3 significant variables, tire construction was the most important. After adjusting for the other two variables, radial tires on the average showed up to 20 psi higher pressures than did bias tires. The next most significant variable was AASHTO class in which 3-S2 trucks showed higher average tire pressures than did 2-S2, SU-3, and SU-2 trucks. The largest

Table 9. 5-Variable ANOVA Result (Unbalanced Design)

Variable	F-Value *	p-Value	Remark
Tire Construction	144.92	.0000	Significant
AASHTO	14.92	.0001	Significant
Tread Depth	8.54	.0035	Significant

*Based on Type III SS (see SAS)

Table 10. Summary of Tire pressures by Tire Construction, AASHTO Class, and Tread Depth

ASSHTO Class	Tread Depth	Radial/Bias	Tire Pressure		
			# of Axles	Mean	S.D
3-S2	<8/32"	Radial	422	95.1	14.9
		Bias	222	81.2	15.2
	≥8/32"	Radial	1997	98.5	13.6
		Bias	709	86.1	14.4
2-S2	<8/32"	Radial	10	90.9	22.0
		Bias	28	78.0	18.5
	≥8/32"	Radial	51	95.3	13.0
		Bias	61	74.6	17.5
SU-3	<8/32"	Radial	19	91.6	14.9
		Bias	23	77.4	17.9
	≥8/32"	Radial	56	97.9	12.5
		Bias	94	83.6	14.2
SU-2	<8/32"	Radial	1	101.0	--
		Bias	34	65.7	20.0
	≥8/32"	Radial	35	88.3	18.8
		Bias	75	73.4	15.3

difference in average tire pressures (10-15 psi) was detected beteen 3-S2 trucks and SU-2 trucks. The effect of tread depth was relatively small, particularly for 3-S2 and 2-S2. Reasonable condition tires of these trucks showed about 4 psi higher average inflation pressure than did worn tires. For SU-2 and SU-3 trucks, this difference was about 6-7 psi. The table also shows that there was only one tire pressure observation for SU-2 trucks with a radial tire and tread depth of <8/32". In order to reduce the importance of this single observation on the overall result, another ANOVA analysis was conducted without this observation to re-test the effect of tire construction, AASHTO class, and tread depth. The result of this analysis is shown in Table 11 which indicates that the significance of all three variables remained unaltered.

Effect of Axle Weight for 3-S2 Trucks. Because of the small samples of SU-2, SU-3, and 2-S2 trucks with complete axle-weight information, only the 3-S2 truck subset was analyzed. A regression analysis was conducted to assess the influence of axle weight on tire pressures. The detail of this analysis is described in Appendix B. Axle weight was found to be significant in explaining the variability in tire pressures. The following relationships were obtained from the analysis for all combinations of tire construction and tread depth.

a) Radial, <8/32": Pressure = 83.03 + 0.0007 (Axle Weight)
b) Radial, ≥8/32": Pressure = 88.70 + 0.0007 (Axle Weight)
c) Bias, <8/32": Pressure = 70.34 + 0.0007 (Axle Weight)
d) Bias, ≥8/32": Pressure = 76.01 + 0.0007 (Axle Weight)

where pressure is the measured inflation pressure in psi and the axle weight is in pounds. The above equations suggest that in order to change the inflation pressure one psi, axle weight must increase by about 1,400 lbs. This magnitude of pressure-weight elasticity may be considered by many to be practically non-significant. Figures 11 through 14 are plots of tire pressures versus axle weight for 3-S2 trucks for all combinations of tire construction and tread depth.

Table 11. ANOVA Result* on Tire Construction, AASHTO Class, and Tread Depth

Variable	F-Value	p-Value	Remark
Tire Construction	91.57	.0000	Significant
ASSHTO Class	18.97	.0001	Significant
Tread Depth	7.87	.0051	Significant

*Excluding one observation (see text).

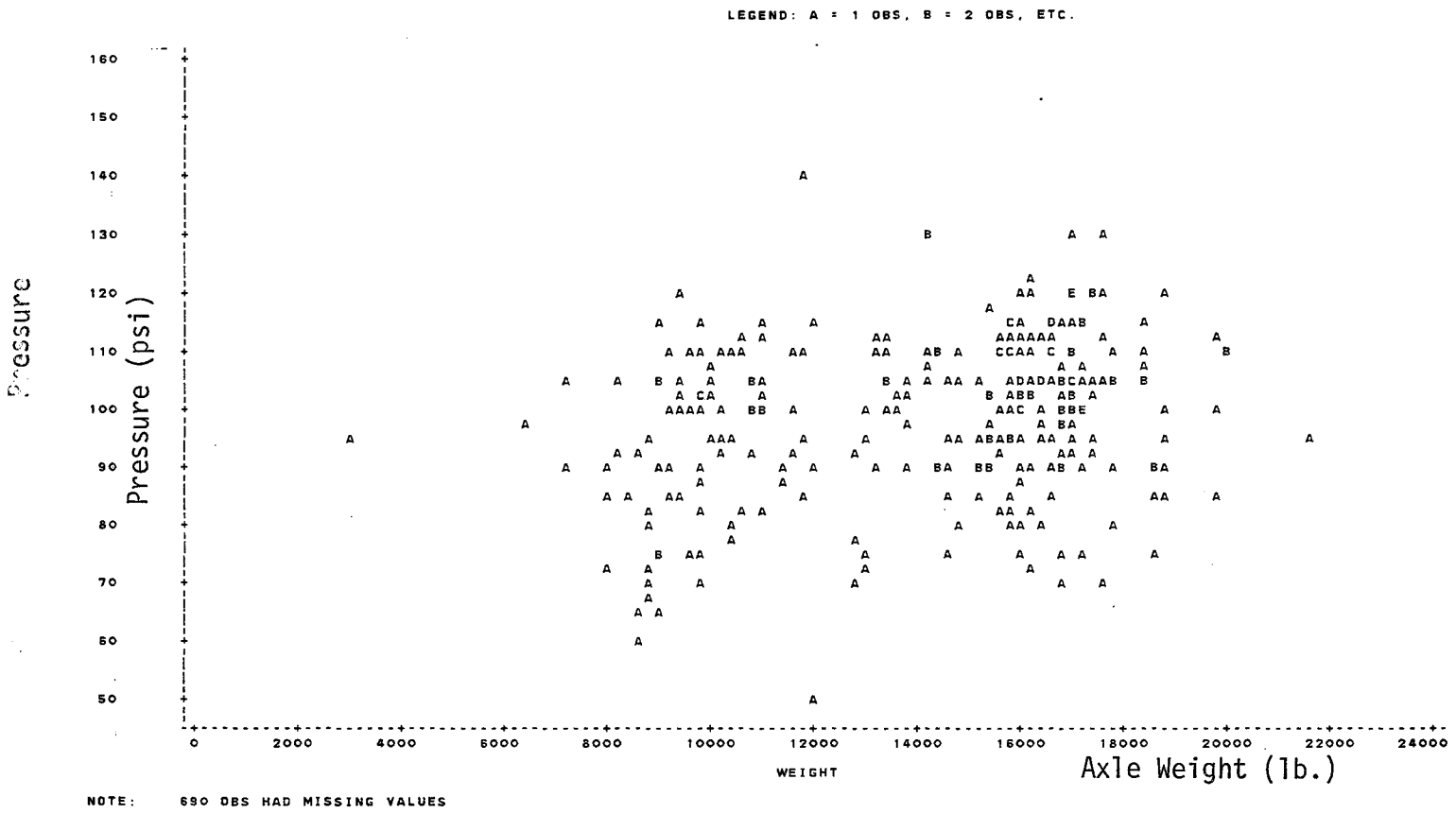

Figure 11. Tire pressures vs. axle weights for radial tires, $\geq$ 8"/32 tread depth (3-S2)

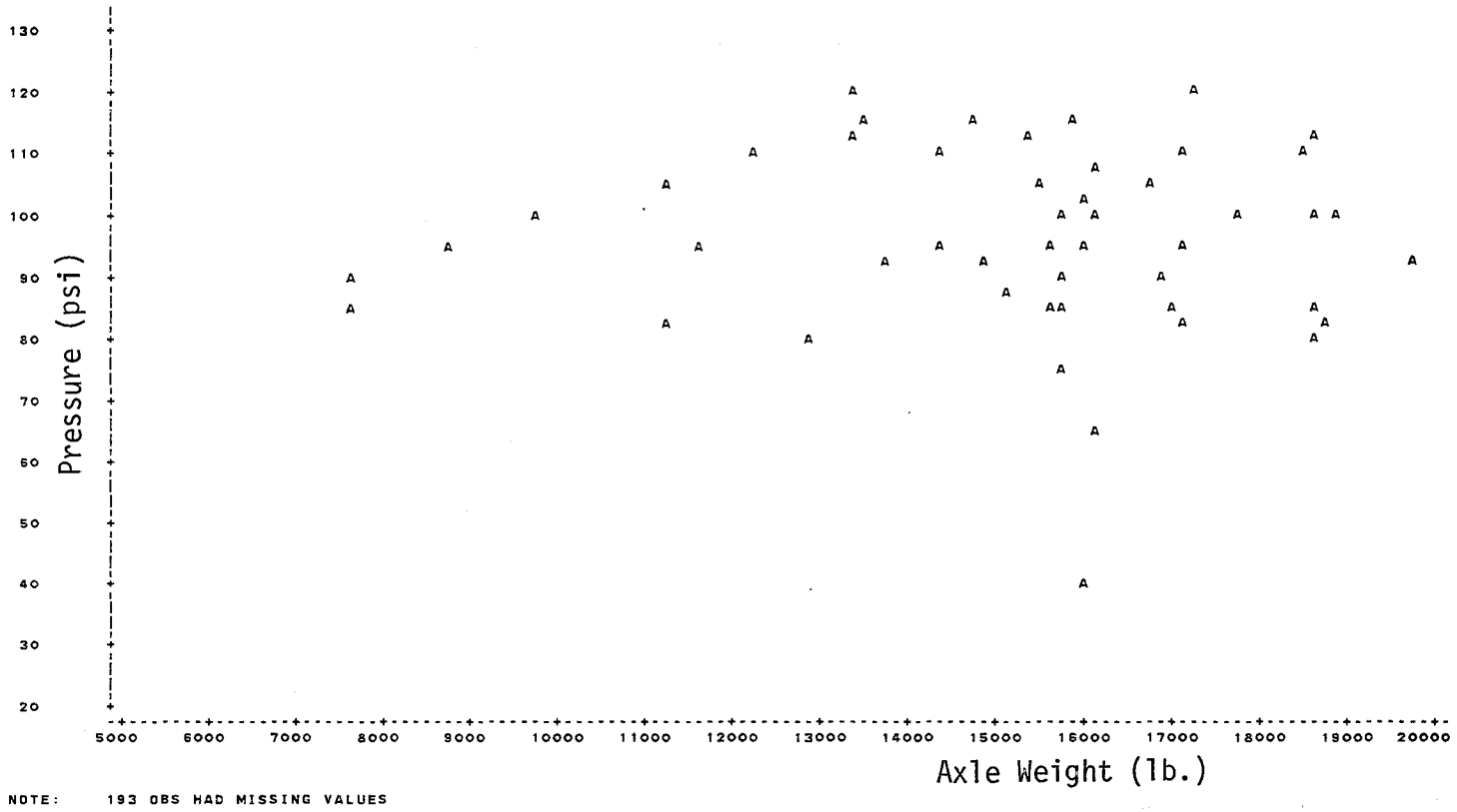

Figure 12. Tire pressure vs. axle weights for radial tires, $\leq$ 8"/32 tread depth (3-S2)

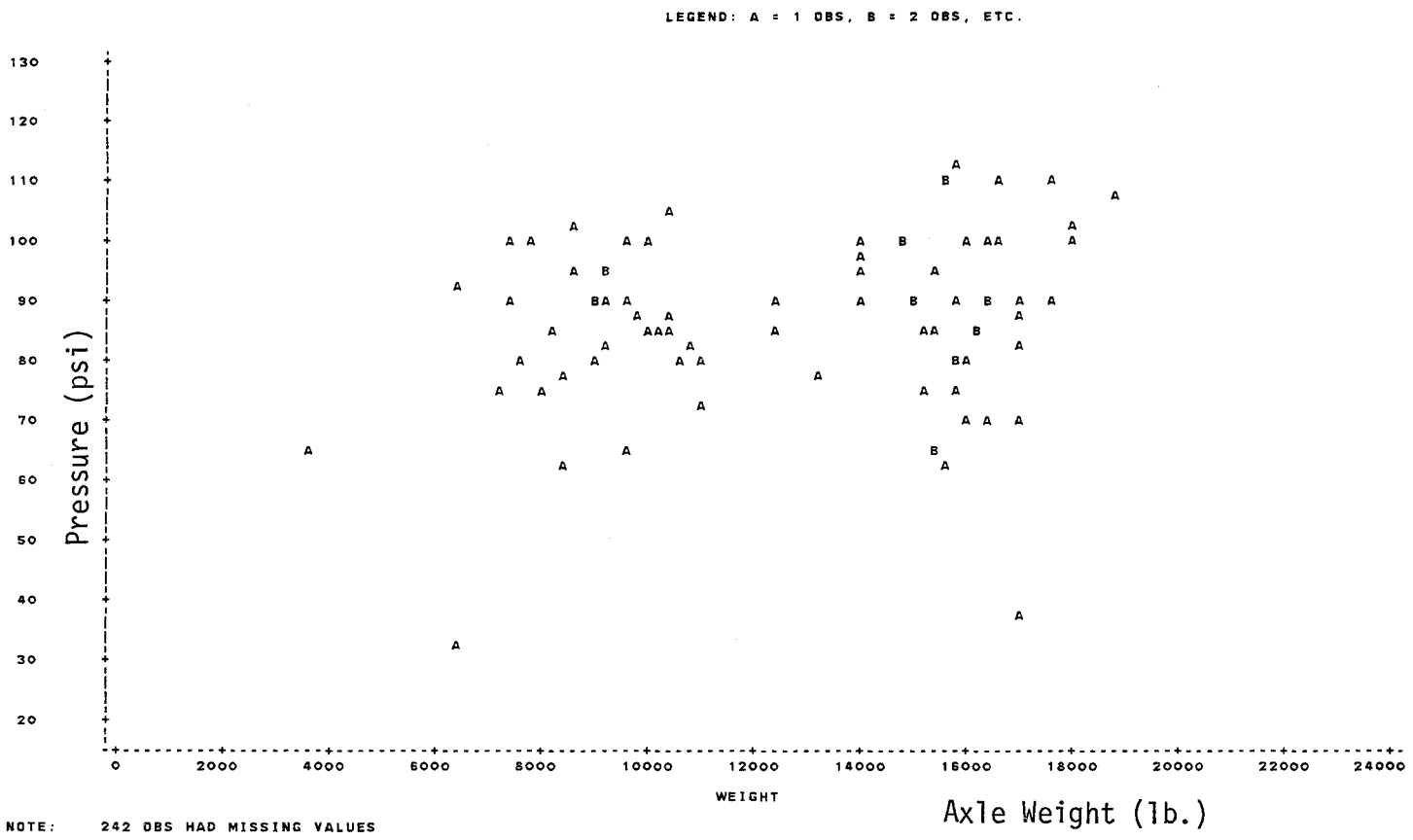

Figure 13. Tire pressure vs. axle weights for bias tires, $\geq$ 8"/32 tread depth (3-S2)

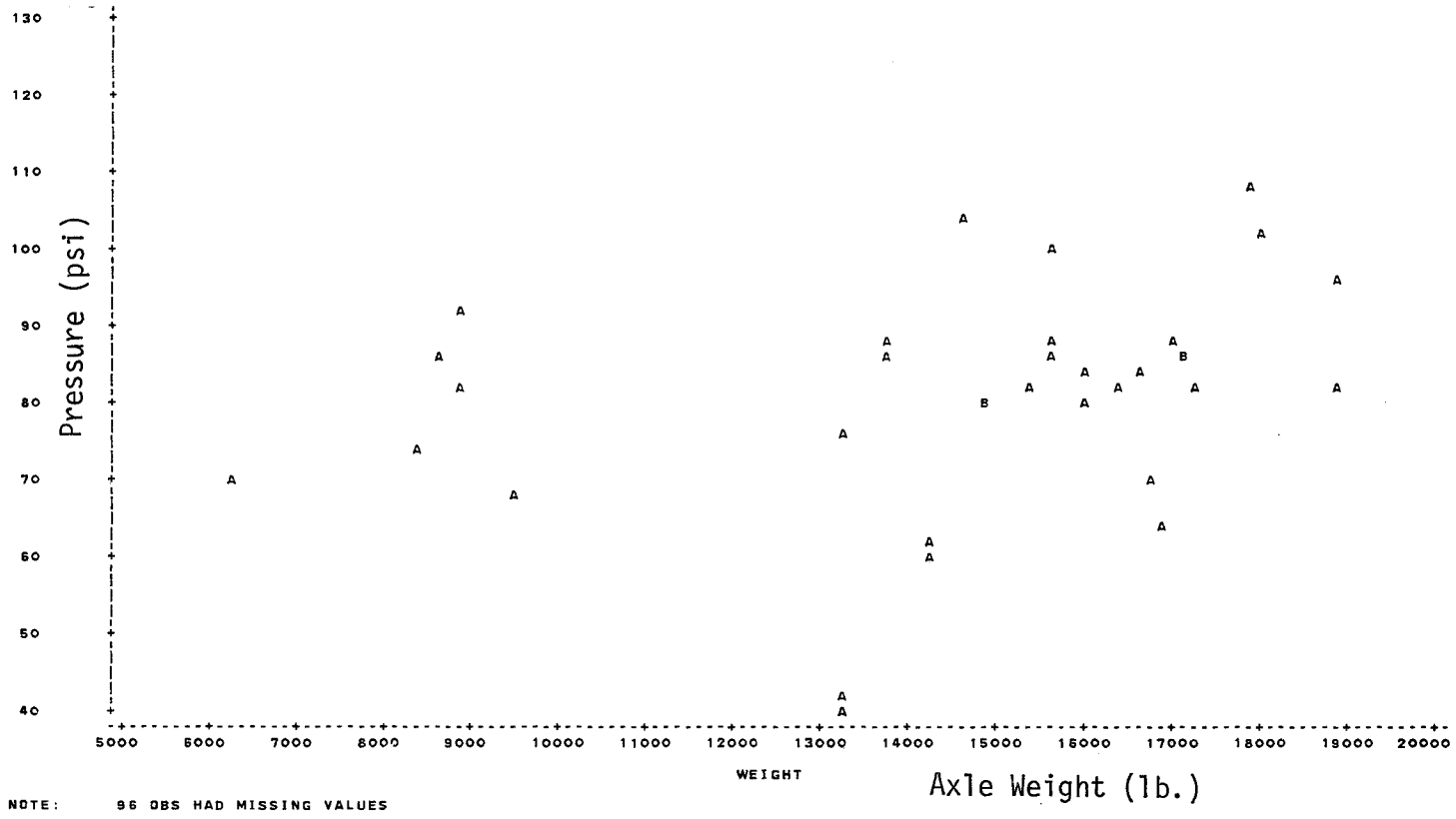

Figure 14. Tire pressures vs. axle weights for bias tires, < 8"/32 tread depth (3-S2)

Effect of Commodity for 3-S2 Trucks. An analysis of variance was conducted to test the effect of commodity and tire construction for 3-S2 trucks only. The result is shown in Table 12. The table indicates that the averages of tire pressure were affected by the main effects of tire construction and commodity types; the interaction effect between tire construction and commodity was not statistically significant at an alpha level of 0.02. The tire pressure distributions by major commodity types 3-S2 trucks are shown in Table 6. For ANOVA purposes, commodity types were rearranged into 10 categories as shown in Appendix C.

Distribution of Tire Pressures for 3-S2 Trucks by Survey Locations. Out of the 12 survey locations, Vega, Amarillo, and Wells, showed relatively small samples of the 3-S2 trucks with complete tire inflation pressure information especially for trucks with bias tires. Table 13 shows the number of axles with complete tire pressure values by tire construction and the survey locations. The table indicates that, after adjusting for tire construction, the average of tire pressure values at different survey locations still differed. Because the commodities at different survey locations were different, the difference in tire pressure distributions seen here was probably attributable to different commodities. Figures 15 through 26 shows the cumulative distributions of tire pressures at each of the 12 survey locations.

RELEVANCE OF TIRE PRESSURE IN PAVEMENT CONSIDERATIONS

The primary objective in conducting this field study was to provide data on the level of the truck tire pressures on Texas highways so that the effect of those tire pressures on the development of pavement distress could be evaluated. In order to accomplish that objective it was desirable to determine if there were significant differences between tire pressures for tires of different construction, with axle load, with truck type, and with commodity type. The most important of these factors are discussed below.

Table 12: Result of ANOVA on Commodity and Tire Construction For 3-S2 Trucks

Source	TYPE III S.S.*	D.F.	p-value
Tire Construction	9241.95	1	.0001
Commodity	7616.03	9	.0001
Tire Construction x Commodity	3885.52	9	.0229**

* see SAS (1982 Edition)
** not significant at α = .02

Table 13: Summary of Tire Pressures for 3-S2 Trucks by Survey Locations

Survey Location	Tire Construction	Mean	S.D.	# of Axles
Nacogdoches	Radial	87.8	7.6	89
	Bias	82.2	8.0	30
Taylor	Radial	95.6	13.2	235
	Bias	80.9	15.0	99
Seguin	Radial	98.4	13.6	612
	Bias	88.1	14.1	185
Weslaco	Radial	99.1	13.4	219
	Bias	78.6	15.4	152
Dallas	Radial	93.5	11.6	155
	Bias	86.1	13.5	91
Wells	Radial	95.2	14.1	64
	Bias	86.1	8.8	14
Huntsville	Radial	93.4	14.2	332
	Bias	82.1	13.4	164
Teheha	Radial	100.6	16.9	92
	Bias	89.6	23.8	54
Riviera	Radial	103.3	12.1	555
	Bias	88.2	14.8	163
Amarillo	Radial	101.8	14.9	68
	Bias	98.0	8.7	3
Vega	Radial	99.2	8.5	10
	Bias	--	--	--
Lufkin	Radial	98.4	17.2	323
	Bias	89.3	16.3	131

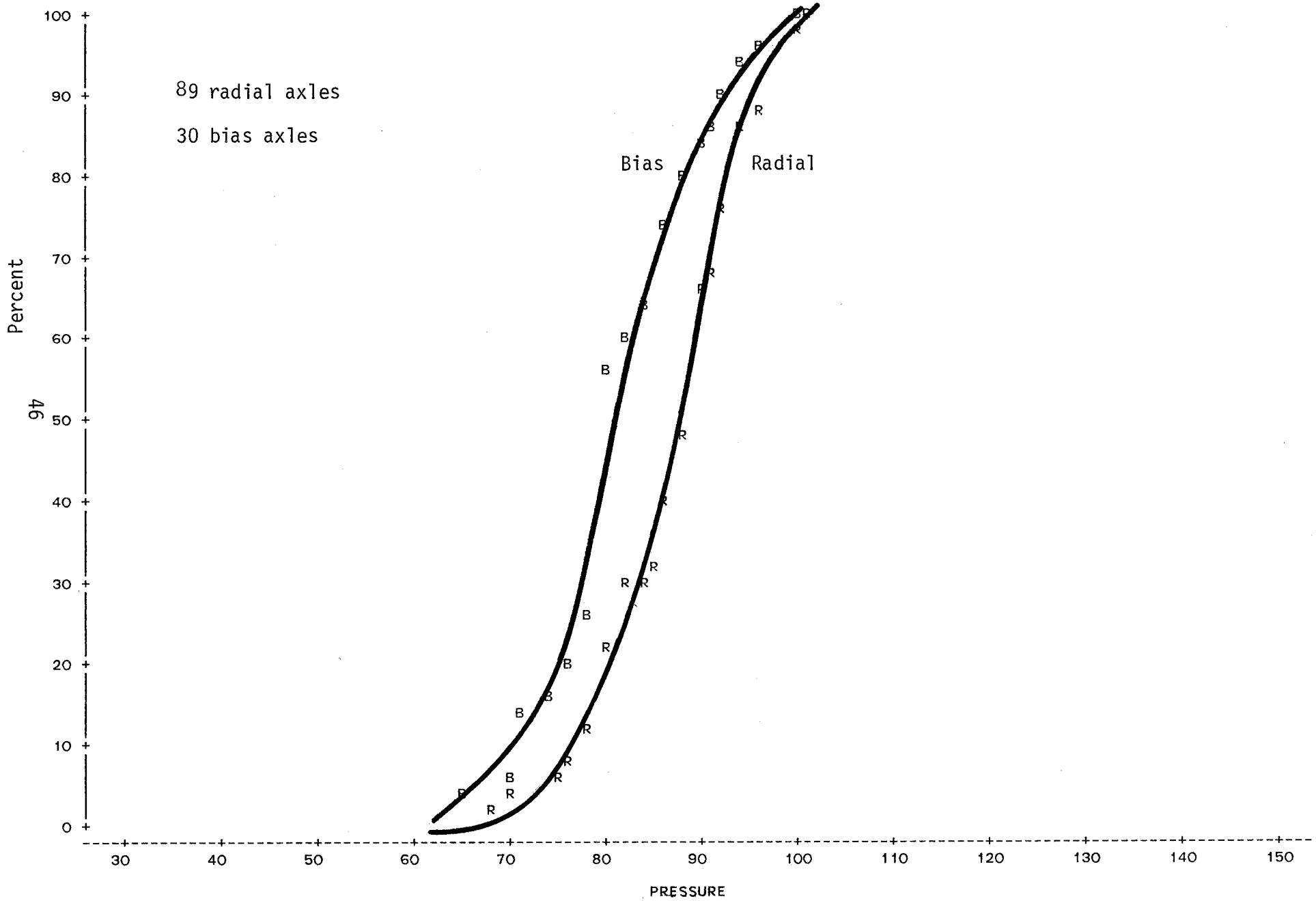

Figure 15. Cumulative distribution of tire pressures for 3-S2 at Nacogdoches

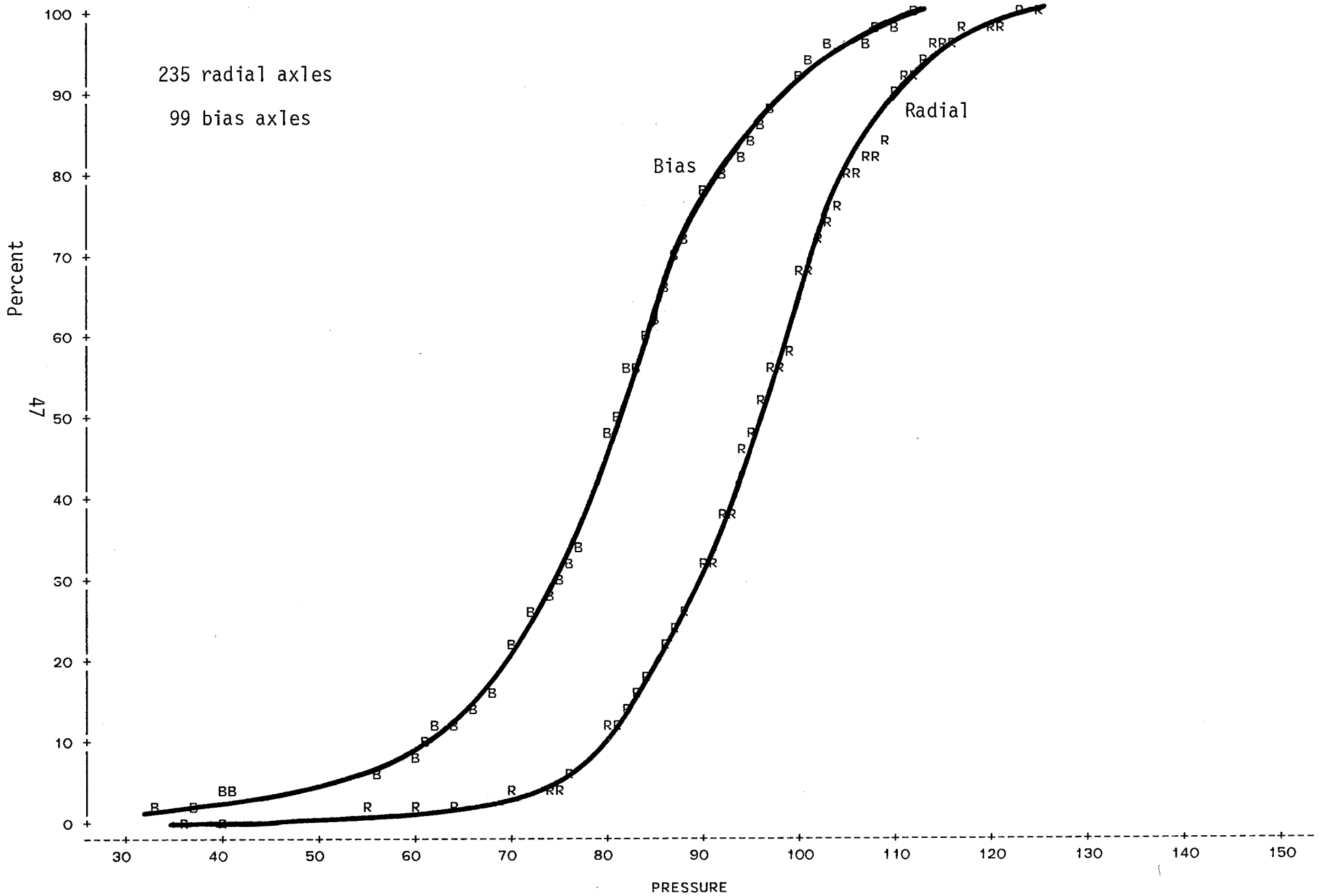

Figure 16. Cumulative distribution of tire pressures for 3-S2 at Taylor

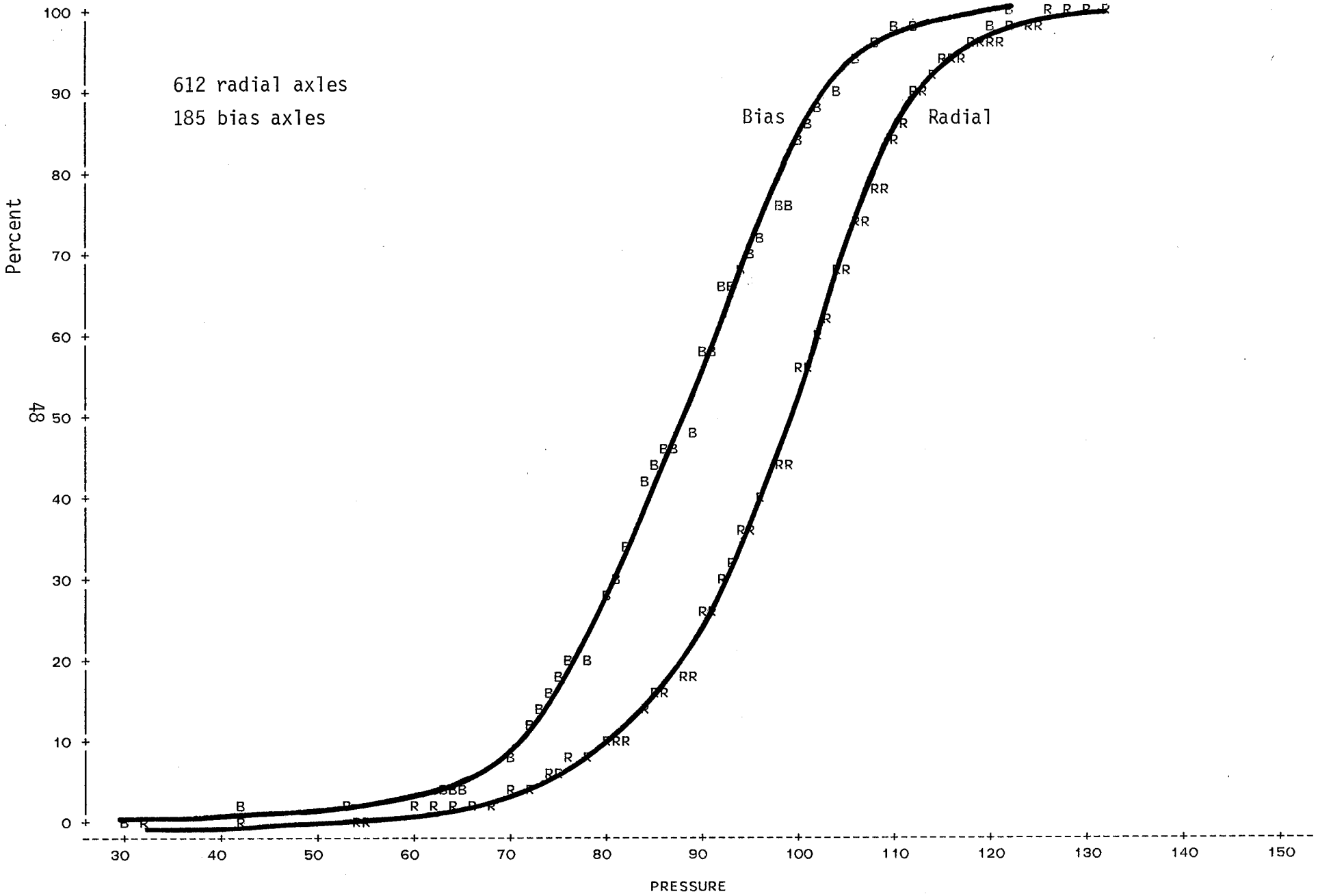

Figure 17. Cumulative distribution of tire pressures for 3-S2 at Seguin

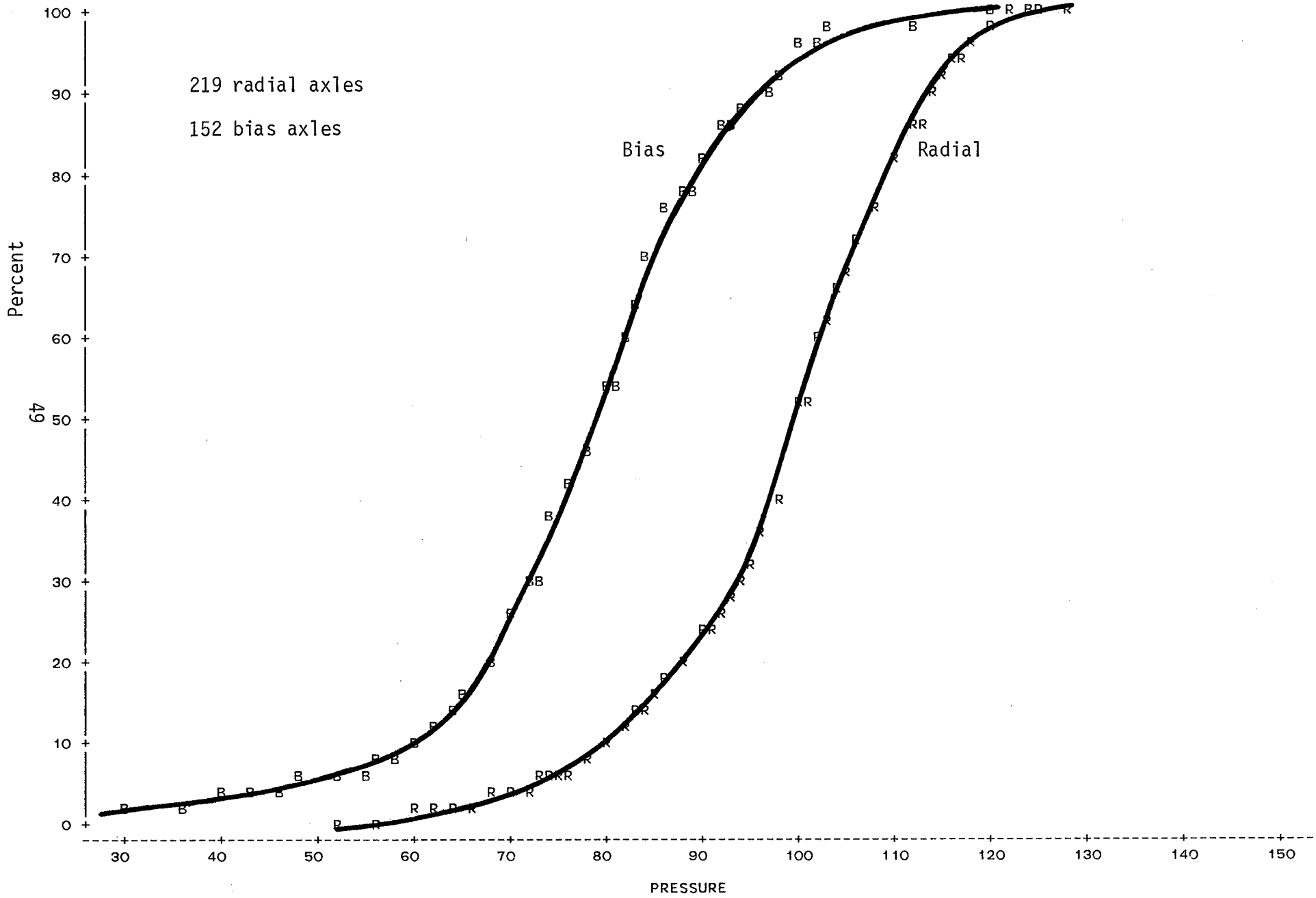

Figure 18. Cumulative distribution of tire pressures for 3-S2 at Weslaco

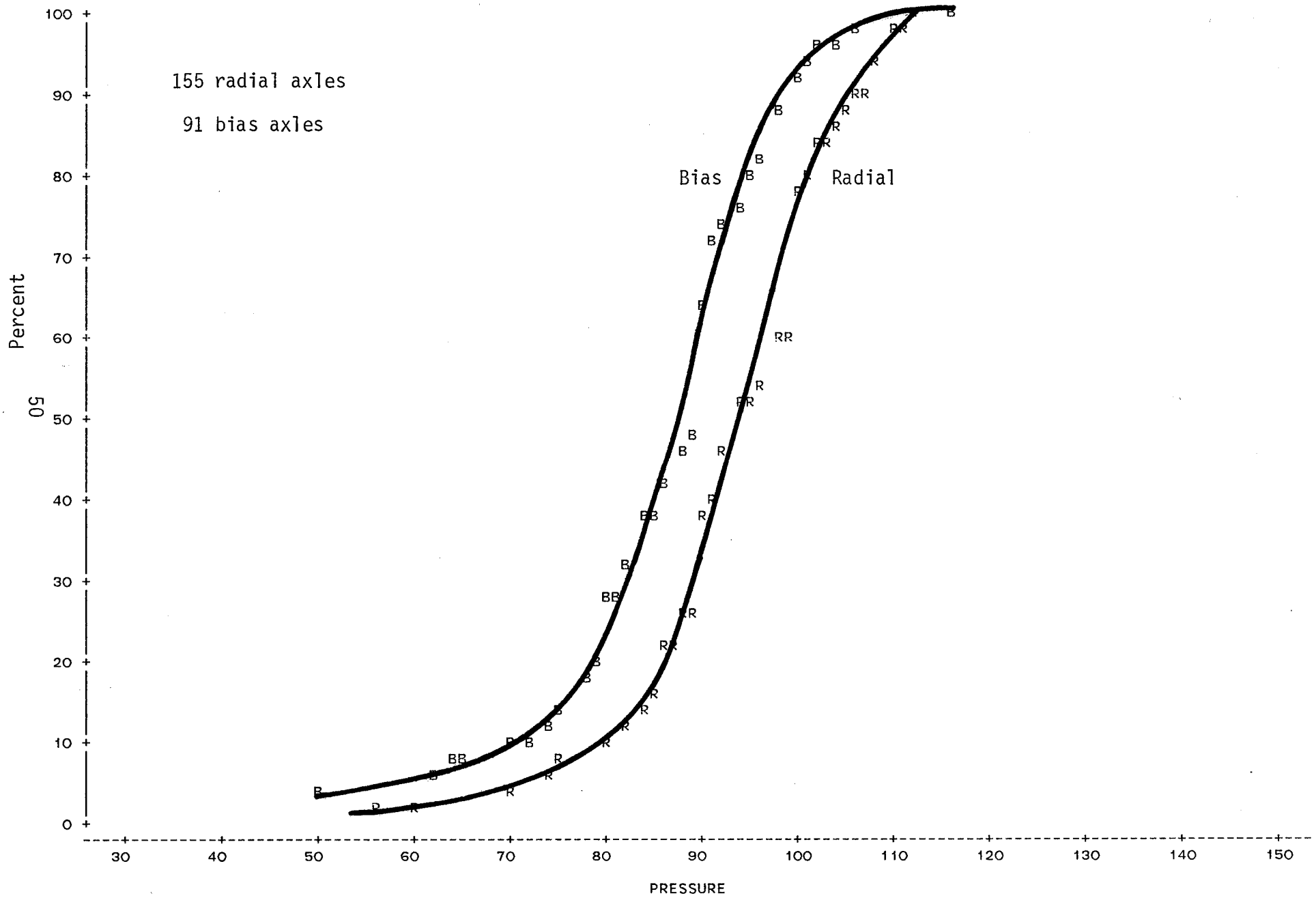

Figure 19. Cumulative distribution of tire pressures for 3-S2 at Dallas

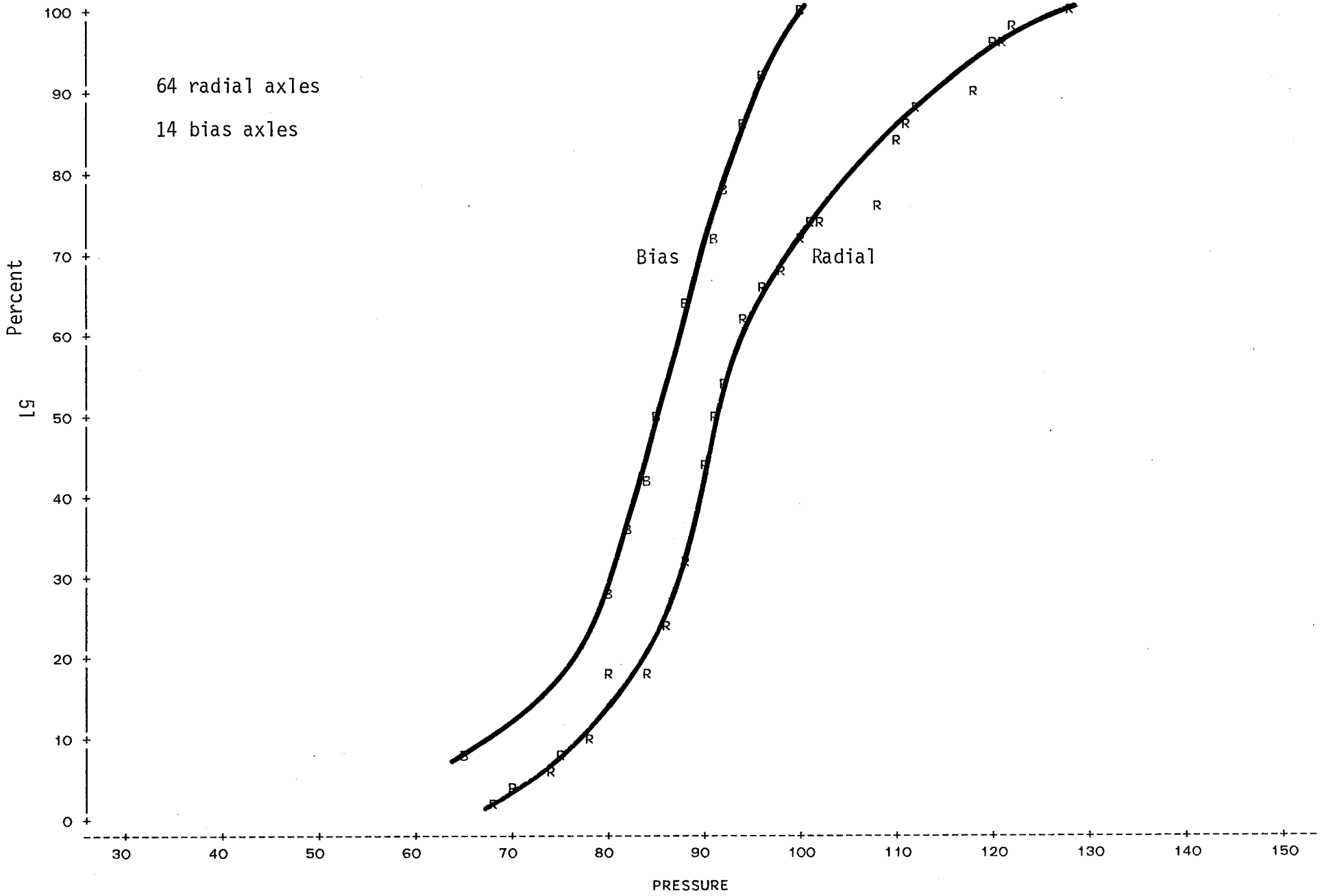

Figure 20. Cumulative distribution of tire pressures for 3-S2 at Wells

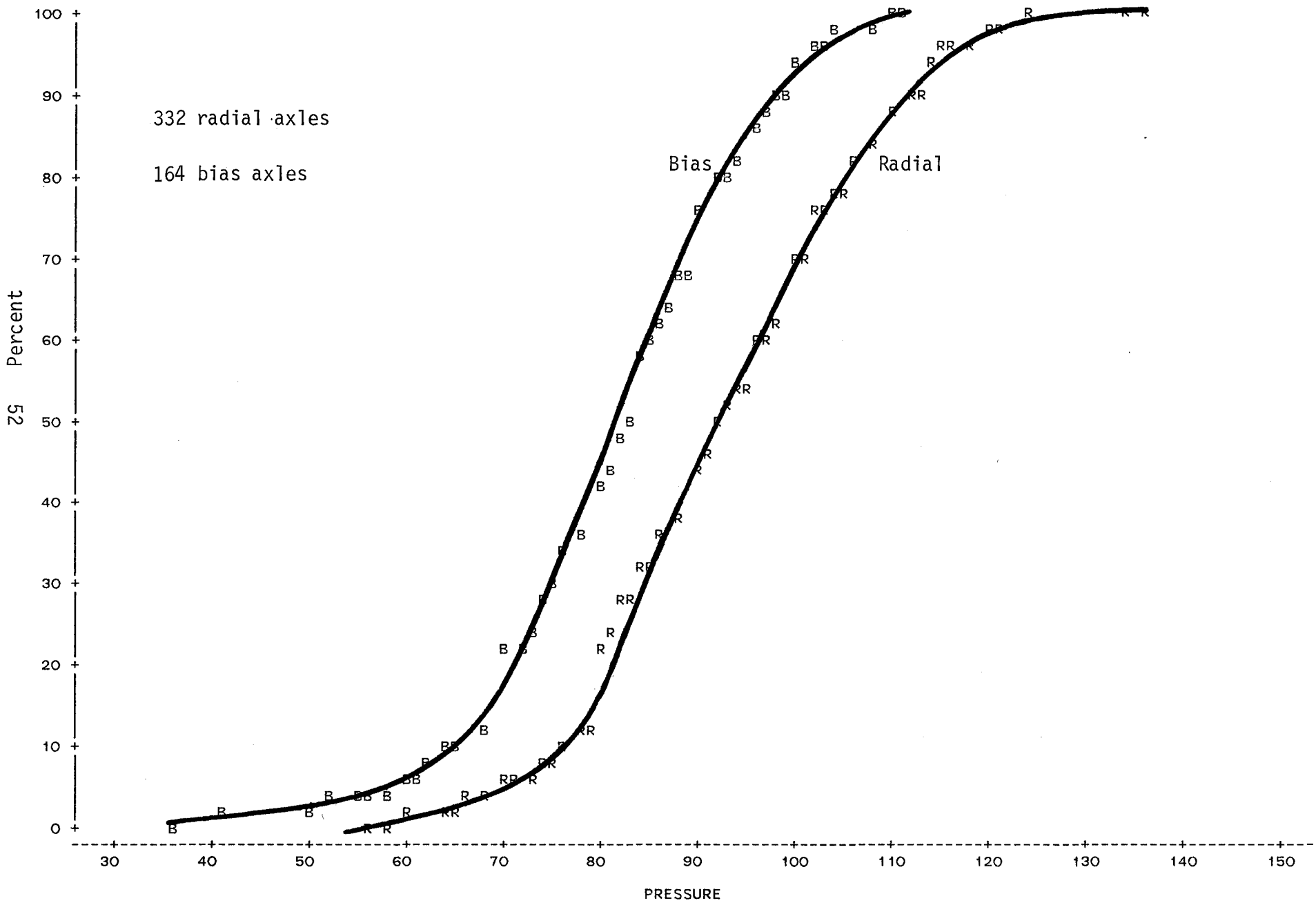

Figure 21. Cumulative distribution of tire pressures for 3-S2 at Huntsville

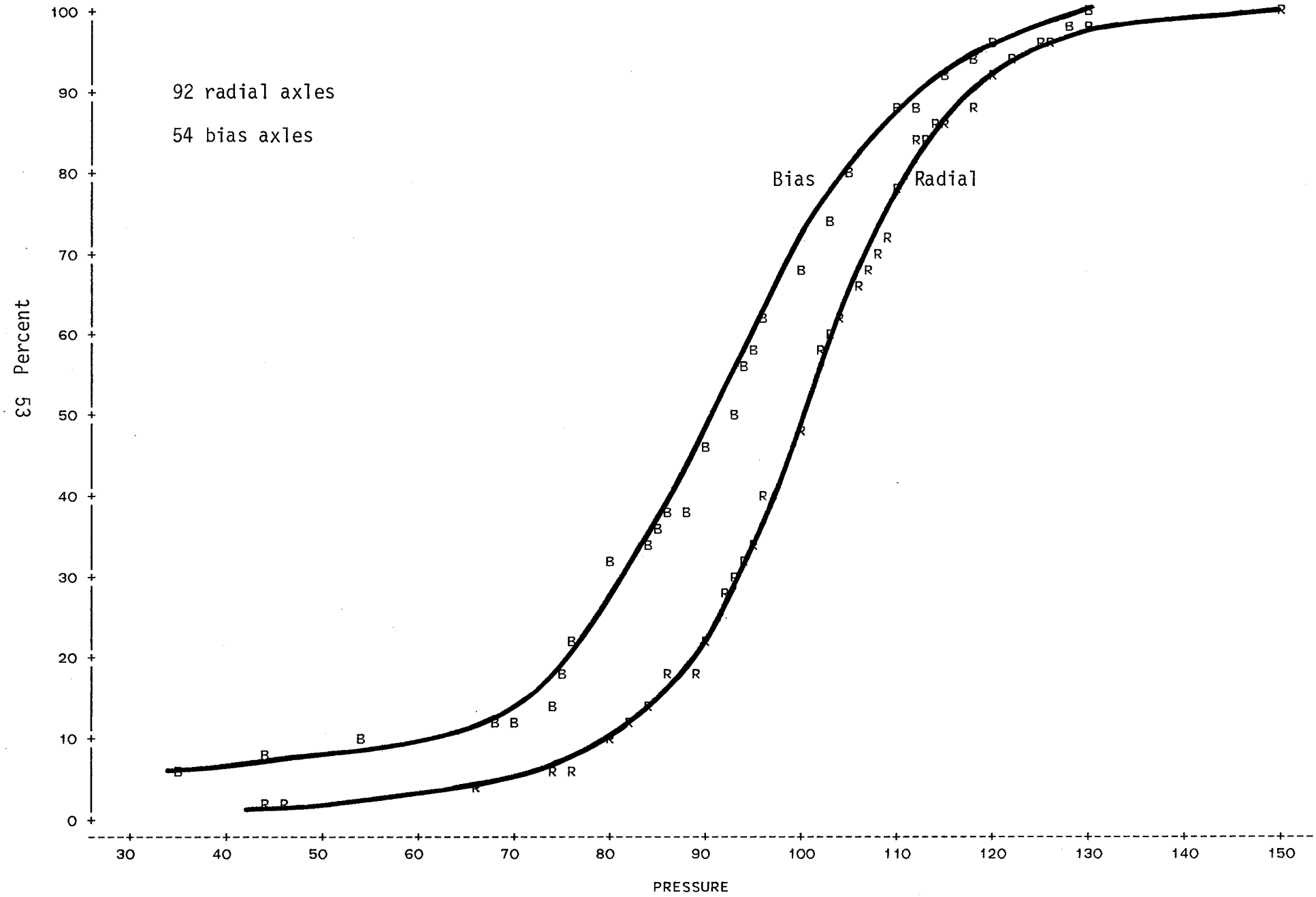

Figure 22. Cumulative distribution of tire pressures for 3-S2 at Teneha

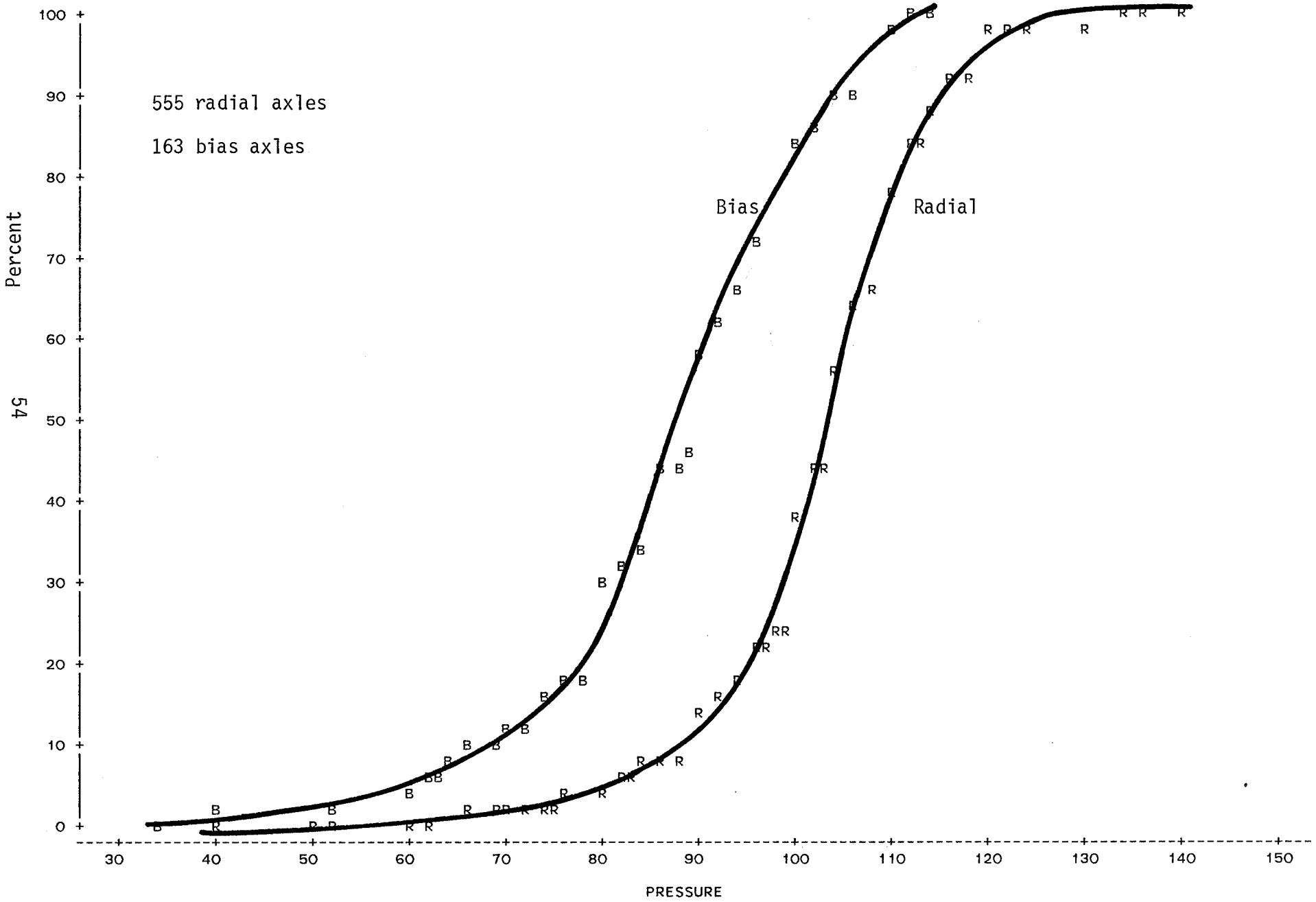

Figure 23. Cumulative distribution of tire pressures for 3-S2 at Riviera

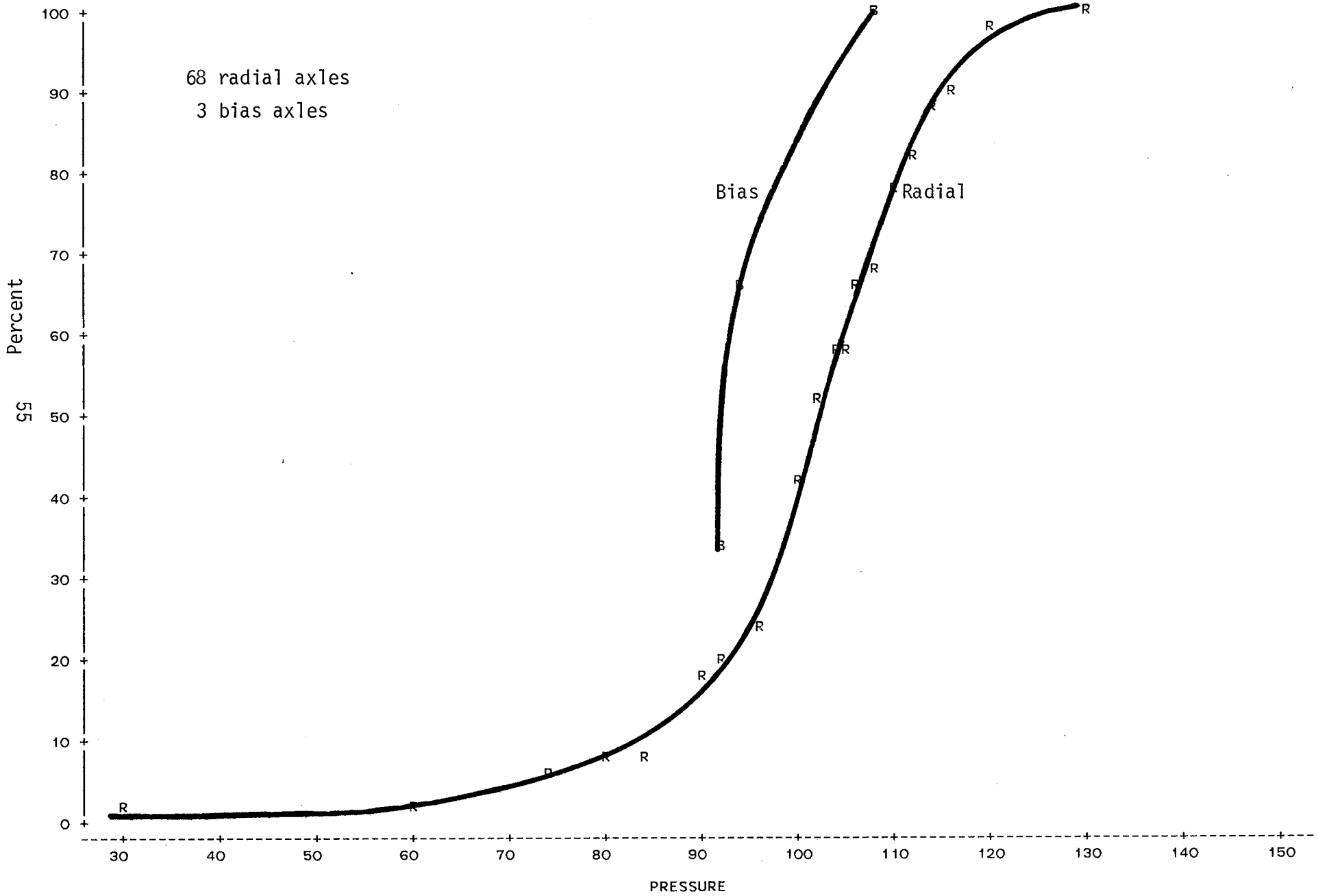

Figure 24. Cumulative distribution of tire pressures for 3-S2 at Amarillo

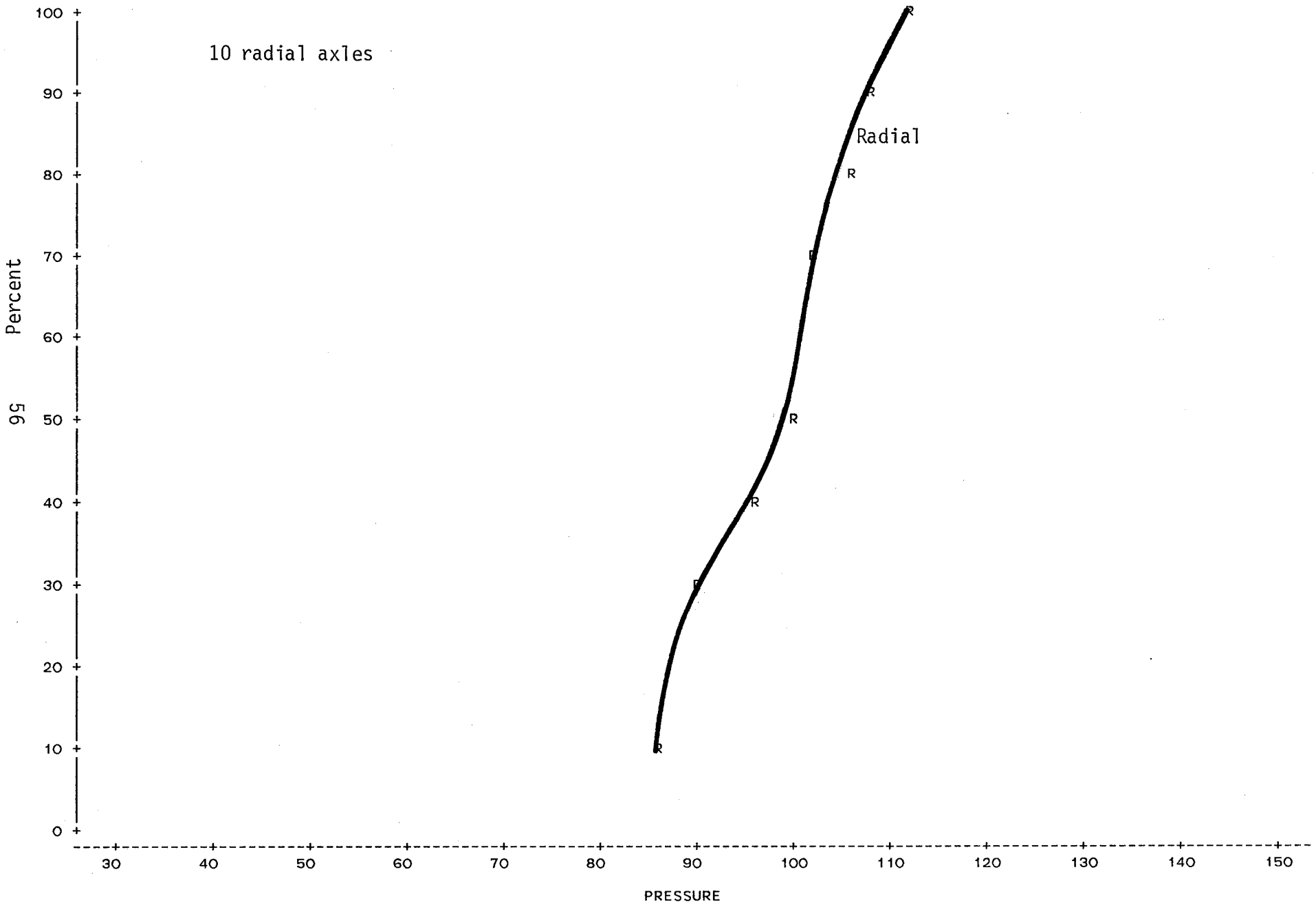

Figure 25. Cumulative distribution of tire pressures for 3-S2 at Vega

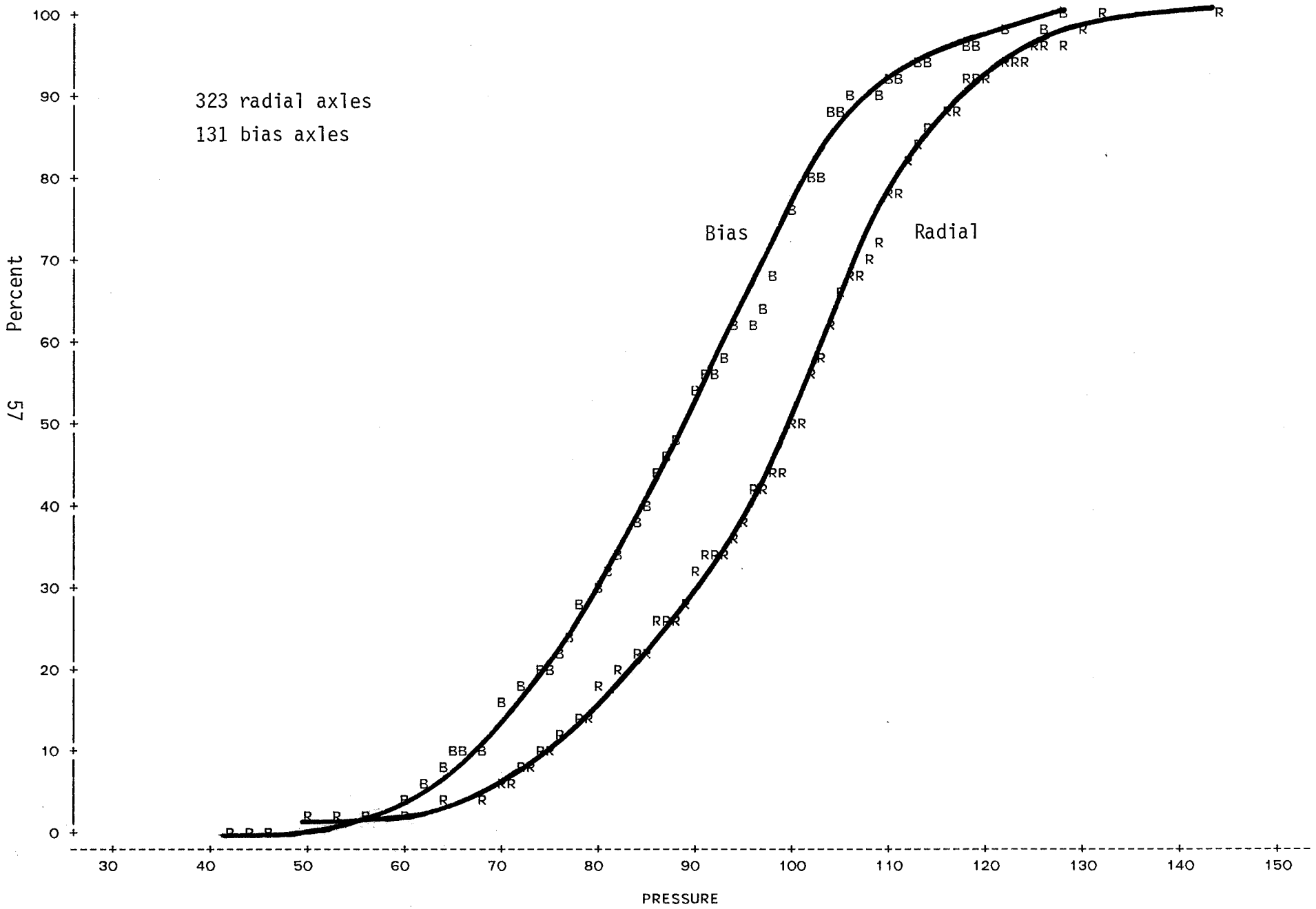

Figure 26. Cumulative distribution of tire pressures for 3-S2 at Lufkin

Tire Construction

Since the tire construction greatly affects the pressure transmitted to the roadway surface, it was imperative that an assessment be made of the variation in tire pressure with type of tire construction. The average tire pressure by vehicle type and tire construciton is shown in Table 4 and Figure 9. The ANOVA and multiple regression analysis performed indicated that tire pressures for radials were considerably higher than those for bias tires. After accounting for truck types and tread depth, radial tires on the average showed 12-21 psi higher pressure than did bias tires.

From a practical standpoint, an evaluation of the effect of the mean tire pressure differences between radial and bias construction must come from analyses similar to those described in Chapter 5. Even though the tire pressures of the radial tires are higher than those of the bias, it is probably that, for the 3-S2 vehicle, the difference in damage will not be significant.

Axle Load

The data on tire pressure variation versus axle loads almost certainly has some bias because of the nature of the data collection efforts. While all trucks were stopped once data collection efforts began, at some sites only those vehicles detained for weight or other violations were included in the tire pressure survey. It is instructive, however, to review that data for trends. The analysis conducted indicated that tire pressure was statistically significantly related to axle weight for at least the 3-S2 vehicles. One cannot argue with the fact that tire pressure is affected by axle load and ambient temperature. However, because tire carcass design affects heat built up and therefore tire pressure, it is difficult in an uncontrolled field experiment to confirm all the relationships that should occur.

Figures 11 through 14 show the scatter plots between axle load and tire pressure for the 3-S2 vehicles for both tire types. These figures do attest to the very wide variation in tire pressure and also that there is a large, though expected difference between load on the steering axle and the other axles of the vehicle.

Commodity

Table 6 summarizes the variation in tire pressures with selected commodity being hauled for the 3-S2 vehicle. It is interesting to note that only four showed the mean tire pressures above 100 psi: farm produce, grain, cattle, and lumber. For most commodities, the mean tire pressures were around 95 psi. Because of the small sample size for the other vehicle types, trends of tire pressure with commodity in that data will not be very reliable.

CONCLUSIONS

Tire pressure data collected on Texas highways indicate that the mean tire pressures are considerably higher than the values historically used in the design of pavement structures and higher than those of the AASHO Road Test for which load equivalence factors were developed. ANOVA on the collected data indicate that observed tire pressures are significantly affected by tire construction, truck type, tread depth, commodity, and axle weight. However, relatively small sample sizes for trucks other than the 3-S2 in this sample do not allow very definite statements to be made for the other vehicle types.

CHAPTER 3

EFFECT OF TIRE INFLATION PRESSURE AND LOAD ON PAVEMENT CONTACT PRESSURE

INTRODUCTION

The interfacial pressure between a free-rolling tire and the pavement exhibits a highly nonuniform two-dimensional distribution over the contact area (tire footprint). The nonuniformity is due to bending stiffness in the tire structure and is therefore influenced by tire design. For a given tire, the contact pressure distribution is significantly influenced by certain basic operating variables, such as inflation pressure and tire load. Tire load here refers to the vertical force applied to the tire. This is the resultant of the vertical component of the pavement contact pressure.

The study of tire-pavement contact pressure is experimentally difficult and, until recently, was not addressed analytically. The recent development of nonlinear finite element techniques has made possible the construction of comprehensive mathematical tire models which are sensitive to tire operating variables as well as to tire design details.

This chapter begins with a review of present knowledge about tire-pavement contact pressure, from experiments reported in the literature. The Texas A&M finite element tire model, used to calculate tire contact pressures for the flexible pavement study, is then described in some detail. Examples of contact pressures calculated for selected tires are given as well as comparisons to measured pressures available in the literature.

The discussion of contact pressure here is restricted to the case of straight-ahead, free rolling tires; the pressure distributions are significantly altered by steering and braking maneuvers, which were not included in the present study.

DEFINITION OF CONTACT PRESSURE

A tire supports an axle load by establishing a relatively small contact region (footprint) between the tread and the pavement. The tire responds to change in axle load by changing significantly the shape and size of the footprint, with imperceptible change in inflation pressure. This is in contrast to an air spring, where changes in load are balanced mainly by changes in inflation pressure. Conversely, the tire load can be held fixed and the footprint changed by adjusting the inflation pressure. As will be seen later, changing either tire load or tire pressure will significantly change the shape of the distribution of pressure in the footprint and the two effects are not interchangable.

When an inflated tire is deflected against a pavement, the doubly-curved surface of the tread is forced to become a flat surface. The flattening is accompanied by tangential motion of points on the tread surface, scrubbing against the pavement. When the tire is deflected vertically against a flat surface, the general tangential motion is toward the center of the footprint, as shown in Figure 27b. This is in contrast to contact of a solid body, for which the tangential motion is directed away from the center of contact. The tangential motion is restrained by friction between tire and pavement, thereby generating two perpendicular tangential (shear) components of contact pressure.

Longitudinal Shear Pressure

The shear pressure is redirected when the footprint is generated by rolling contact, due to the superposition of an angular velocity of the tread surface. By using a simple rolling contact model (1), it can be shown that the longitudinal sliding velocity of tread surface points changes direction twice in the footprint during rolling contact. Thus, the longitudinal component of tire force on the pavement may be expected to change direction twice, as sketched in Figure 27a. The location of a point where the force distribution is zero is determined by the amount of

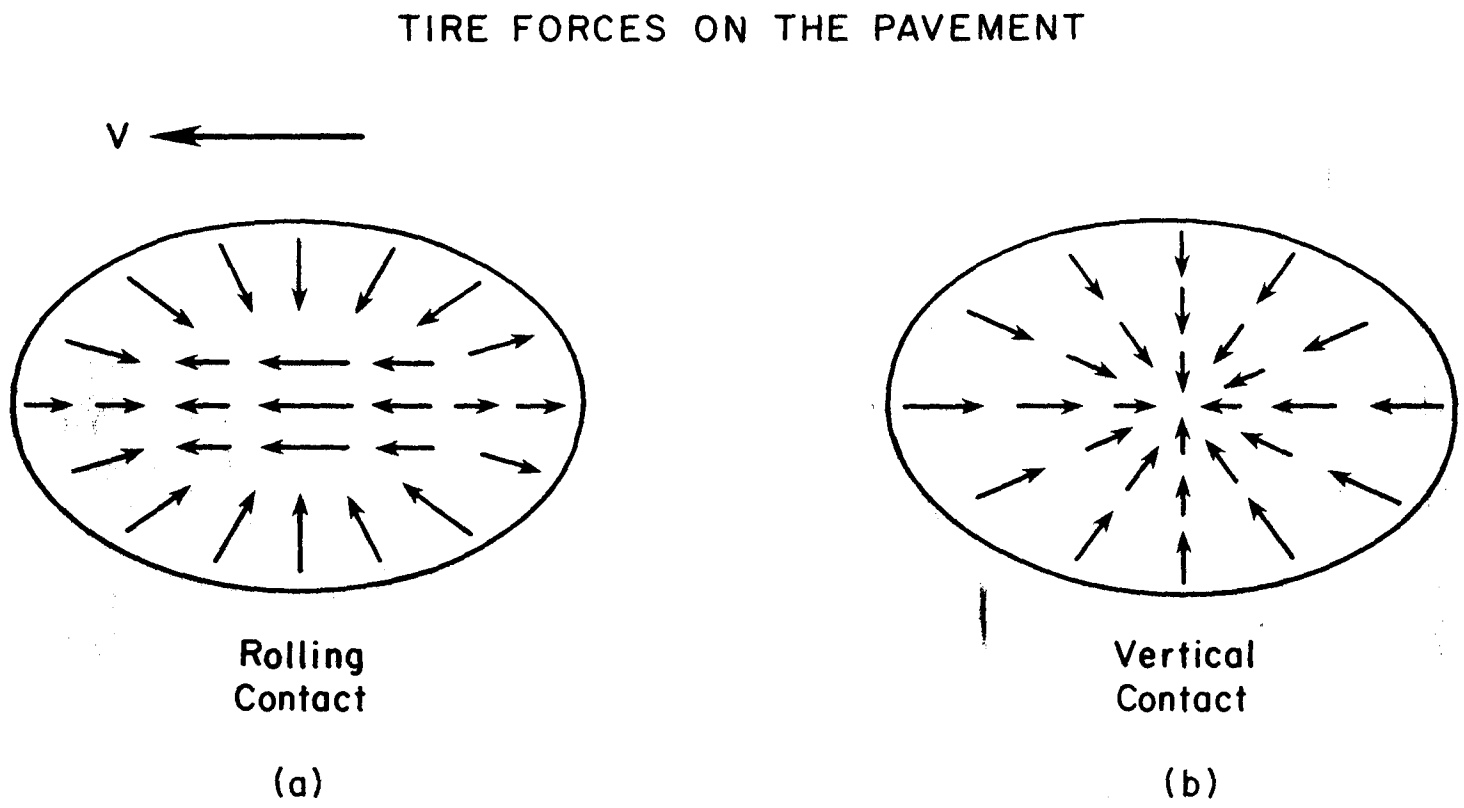

Figure 27. Direction of tire shear forces under a standing tire (vertical contact) and under a rolling tire.

friction between tire and pavement. Even a low level of friction will retard the reversal of longitudinal force. In Figure 28, which shows laboratory data taken from Reference 2, the reversals occur well toward the rear (exit) of the footprint. The second reversal is often not seen, with the distribution of longitudinal pressure then appearing to be nearly axisymmetric.

Transverse Shear Pressure

A less complex mechanism causes the generation of transverse (side-to-side) shear pressure on the pavement surface. The top part of Figure 29 shows the paths of the ribs of a tire in the contact region of a rolling tire. A rib is drawn toward the center of the footprint as the tread is flattened against the pavement. The inward movement of the rib is inhibited by friction, thereby developing the transverse component of tire-pavement shear pressure. The transverse shear pressure is significantly affected by tire construction, with radial tires producing lower peak values than bias-ply (diagonal) tires do. Representative laboratory data (3) on transverse shear pressure, shown at the bottom of Figure 29, indicates that the peak pavement force developed by a radial tire is about half of the peak force developed by a bias-ply tire.

The three components of contact pressure for a small radial passenger car tire (165 SR 13) are shown in Figure 30. These data were obtained with the tire rotating on a laboratory roadwheel at the University of Munich, Germany (4). Since the normal pressure for a free-rolling tire is relatively independent of friction, the distribution in Figure 30a is representative of the normal pressure between a tire and the pavement. The shear pressures, however, are strongly influenced by the friction characteristic of the tread and the contacting surface. Thus, the distributions shown in Figures 30b and 30c, which were measured with the tire rolling on a metal surface, may not be entirely similar to the shear pressures applied by a tire to the pavement. Despite the differences in laboratory and on-the-road data, it is generally believed that transverse

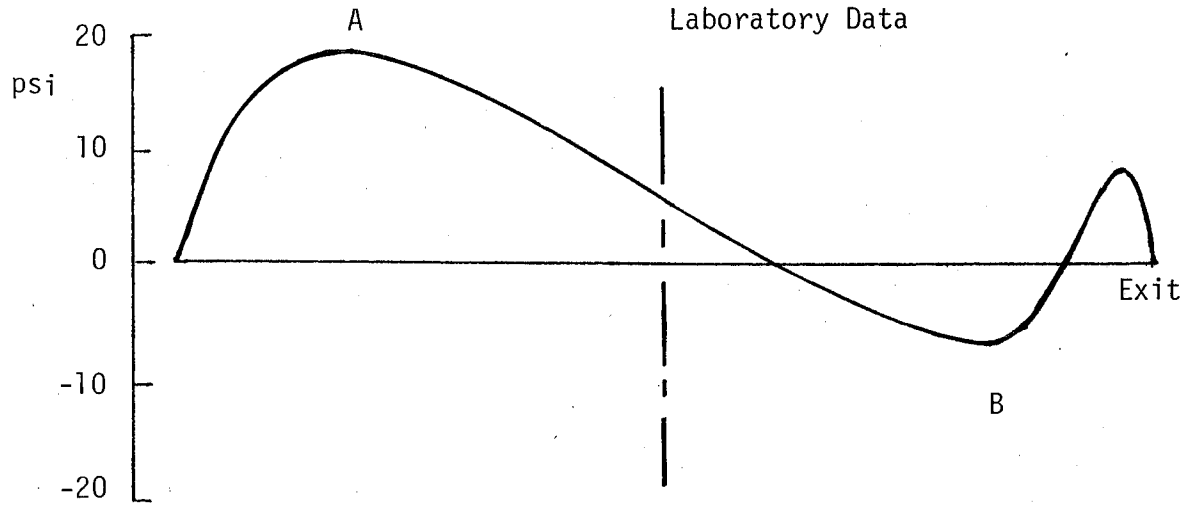

Figure 28. Laboratory measurement of the longitudinal shear pressure distribution (2).

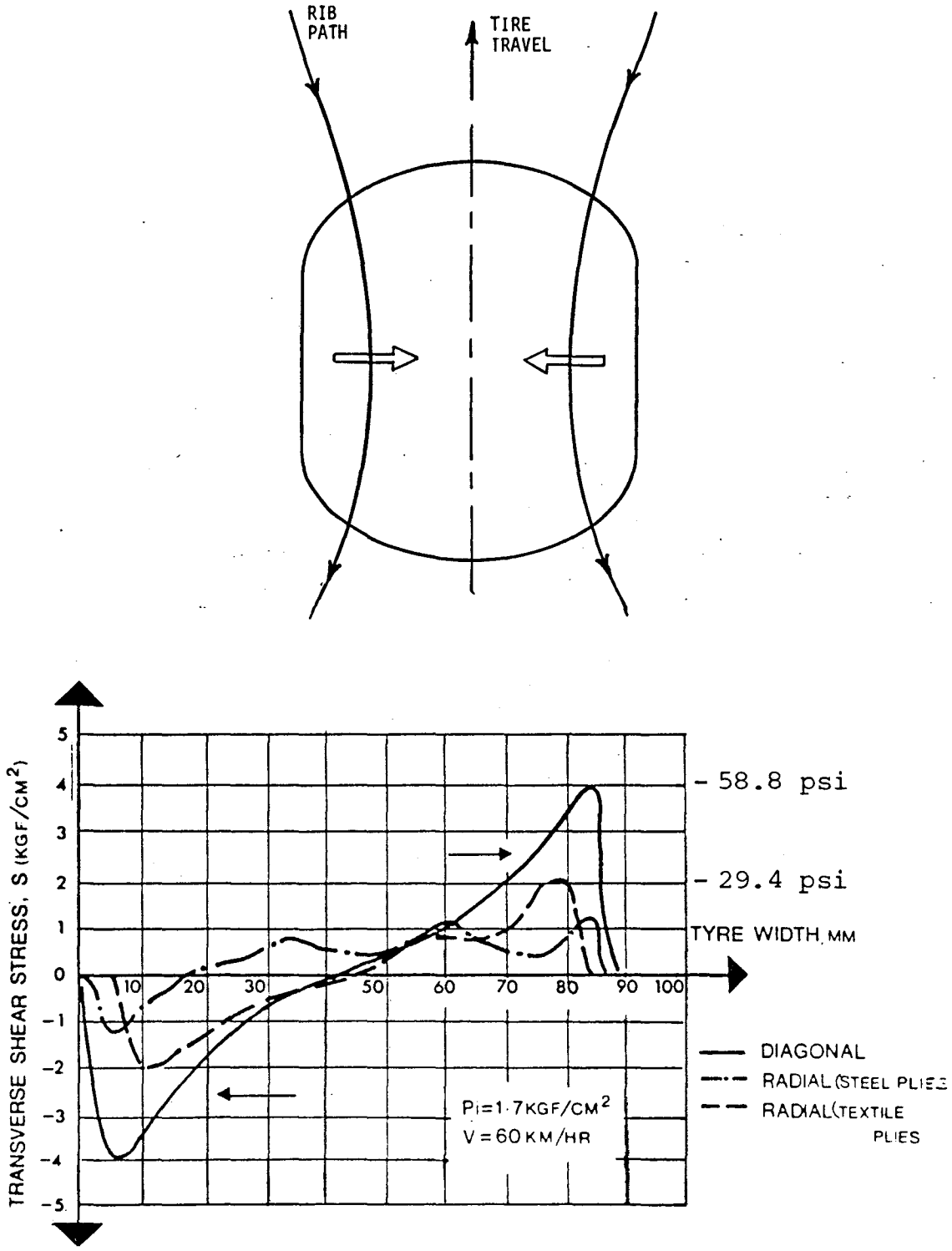

Figure 29. Transverse shear stress distributions across the footprint of radial and bias-ply (diagonal) tires during free-rolling (3).

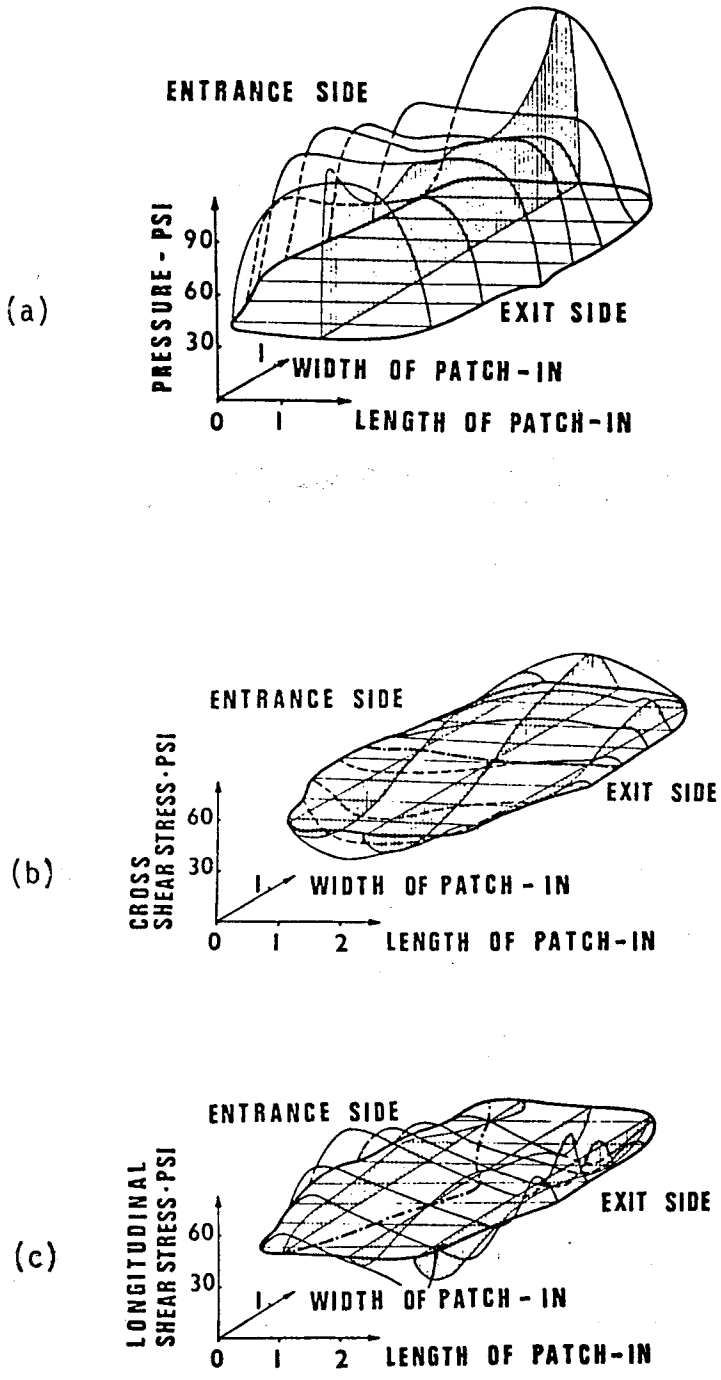

Figure 30. Laboratory measurement of tire contact pressure components. (a) normal pressure, (b) transverse shear pressure, (c) longitudinal shear pressure.

shear pressure applies a higher stress to the pavement than the longitudinal shear pressure does.

Contact pressure data such as shown in Figure 30 are difficult to measure but are very valuable for understanding the complex system of forces generated between a tire and the pavement.

FACTORS AFFECTING CONTACT PRESSURE DISTRIBUTIONS

Most experimental studies have focused on the normal contact pressure distribution, since it is more easily measured than the shear pressure. Only factors affecting the normal component of contact pressure for a free-rolling tire are discussed in this section.

Speed

It has been established experimentally that speed has only a minor influence on the contact pressure for a free-rolling tire. The roadwheel data given in Figure 31 show that the footprint is slightly enlarged as speed increases (4). This is a consequence of centrifugal stiffening of the tire carcass. Radial tires have a smaller increase in footprint area than bias-ply tires with increase in speed. Figure 32, Reference 5, shows the effect of speed on the longitudinal (fore-aft) distribution of normal pressure for a bias-ply tire. About a ten percent increase in contact length is indicated here between zero and highway speeds.

The minor effect of speed on contact pressure permits normal pressure distributions measured (or calculated) for a standing tire to be used in studies of highway degradation.

Inflation Pressure and Tire Load

The non-uniformity of the contact pressure distribution is due entirely to bending stiffness in the tire structure. In the absence of

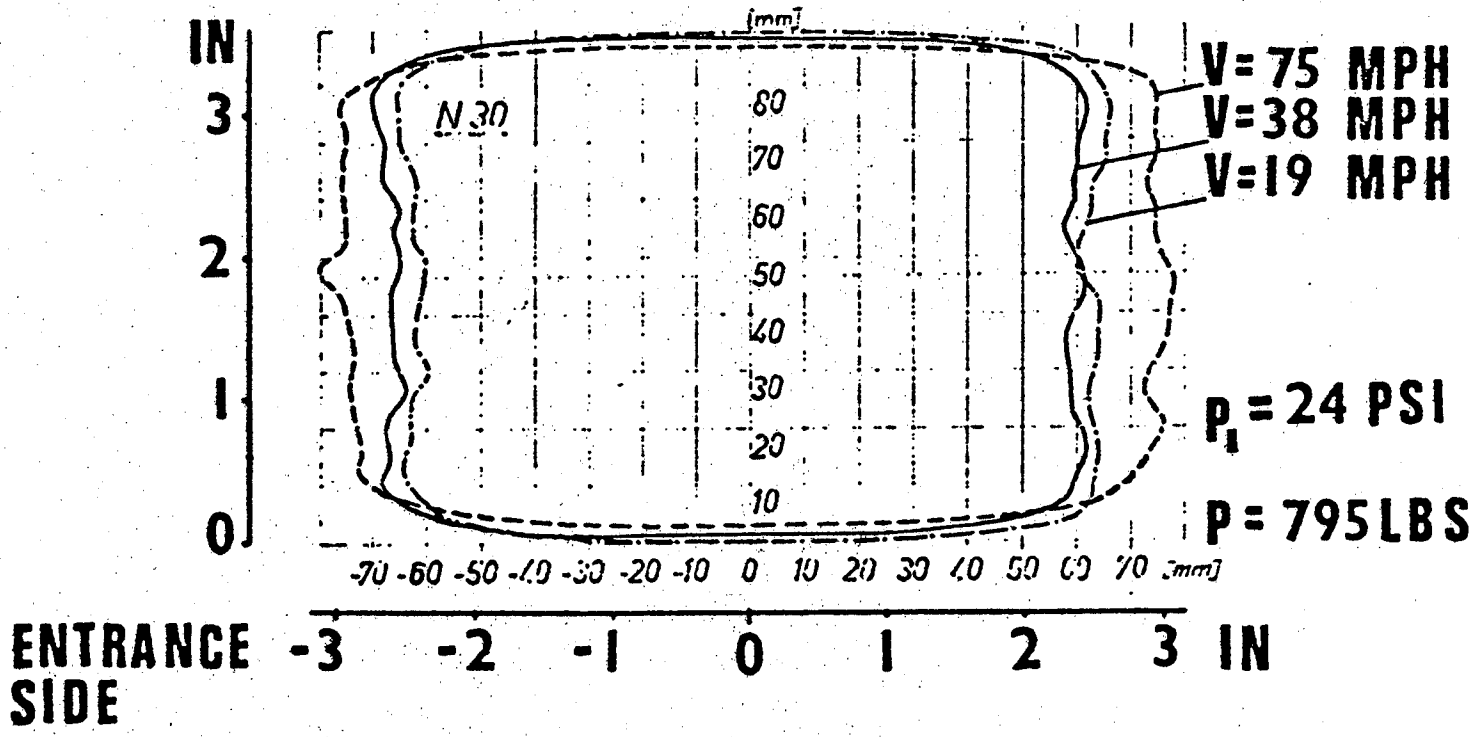

Figure 31. Effect of speed on the footprint of a bias-ply tire (4).

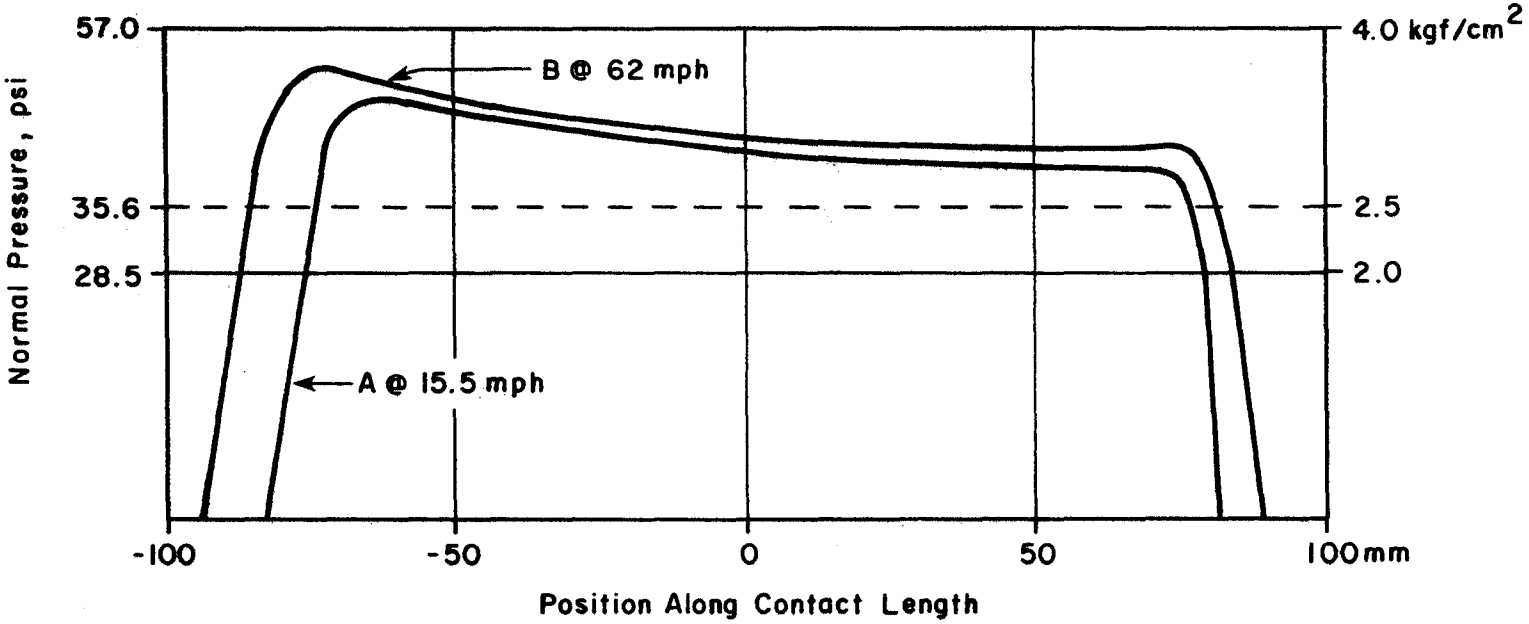

Figure 32. Effect of speed on the normal contact pressure distribution for a bias-ply tire with inflation pressure p = 35.6 psi (5).

bending stiffness, e.g., an inner tube, the contact pressure is uniform and equal to the inflation pressure. Since bending stiffness of the tire is significantly influenced by the inflation pressure, the contact pressure distribution is changed by a change in the inflation pressure. This effect is most conveniently investigated using a computer tire model, due to the difficulty and expense of measuring a large number of contact pressure distributions for a real tire. The finite element computer tire model used in the project is described in the next section. The next two figures contain calculated data, made with this tire model, showing the effect of inflation pressure and tire load on the normal contact pressure distribution for a truck tire.

Figure 33 shows the effect of increasing the inflation pressure, while keeping the tire load fixed at 4500 lbs. The contact pressure distributions here are calculated on one-half of the tire meridian passing through the center of the footprint. The effect of increasing the tire load while keeping the inflation pressure fixed at 100 psi is shown in Figure 34. A second peak in the contact pressure distribution is found at the 8500 lb. tire load. However, it should be noted that this size tire (10.00-20, 12PR) is designed to operate at a maximum load of 4760 lb. (as a dual) at 75 psi inflation pressure. The computer tire model assumes that the tire is symmetric about its equator (center rib or groove) so the contact pressure along only one-half of a meridian is calculated. A real tire, due to complex manufacturing processes or uneven wear, will not be perfectly symmetric so measurements of contact pressure should be taken across the complete contact width (shoulder-to-shoulder). Figure 35 gives a very detailed set of measurements showing the effect of inflation pressure and load on the normal pressure for a truck tire without a tread pattern.

Despite the asymmetry in these measured data, it is evident that the contact pressure tends to peak near the shoulders of the tire. Figure 35 was reproduced from the discussion of tire-road contact in Chapter 5 of Reference 6. The size of the truck tire tested for the data in Figure 35 is not known.

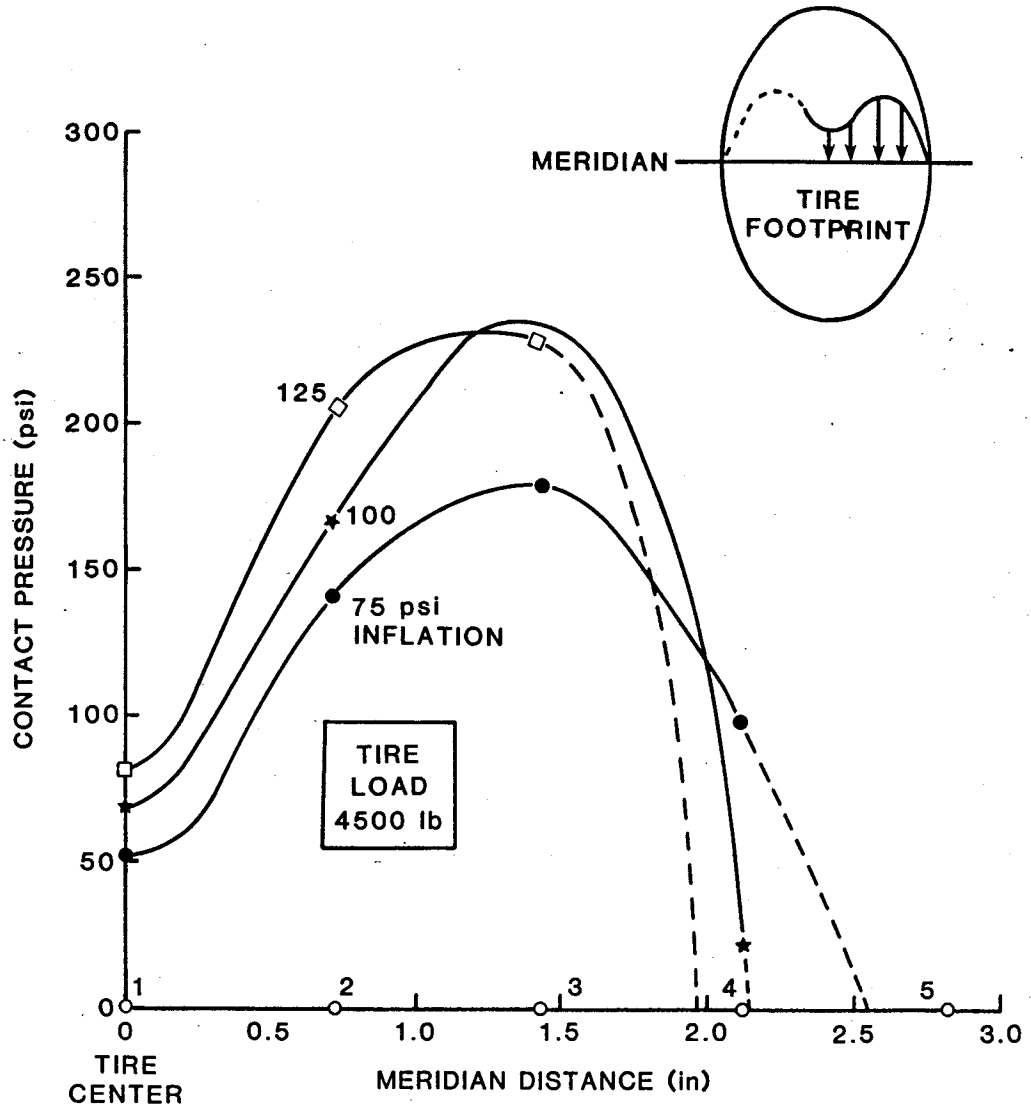

Figure 33. Effect of inflation pressure on contact pressure calculated for a 10.00-20 truck tire with a 4500 lb. load.

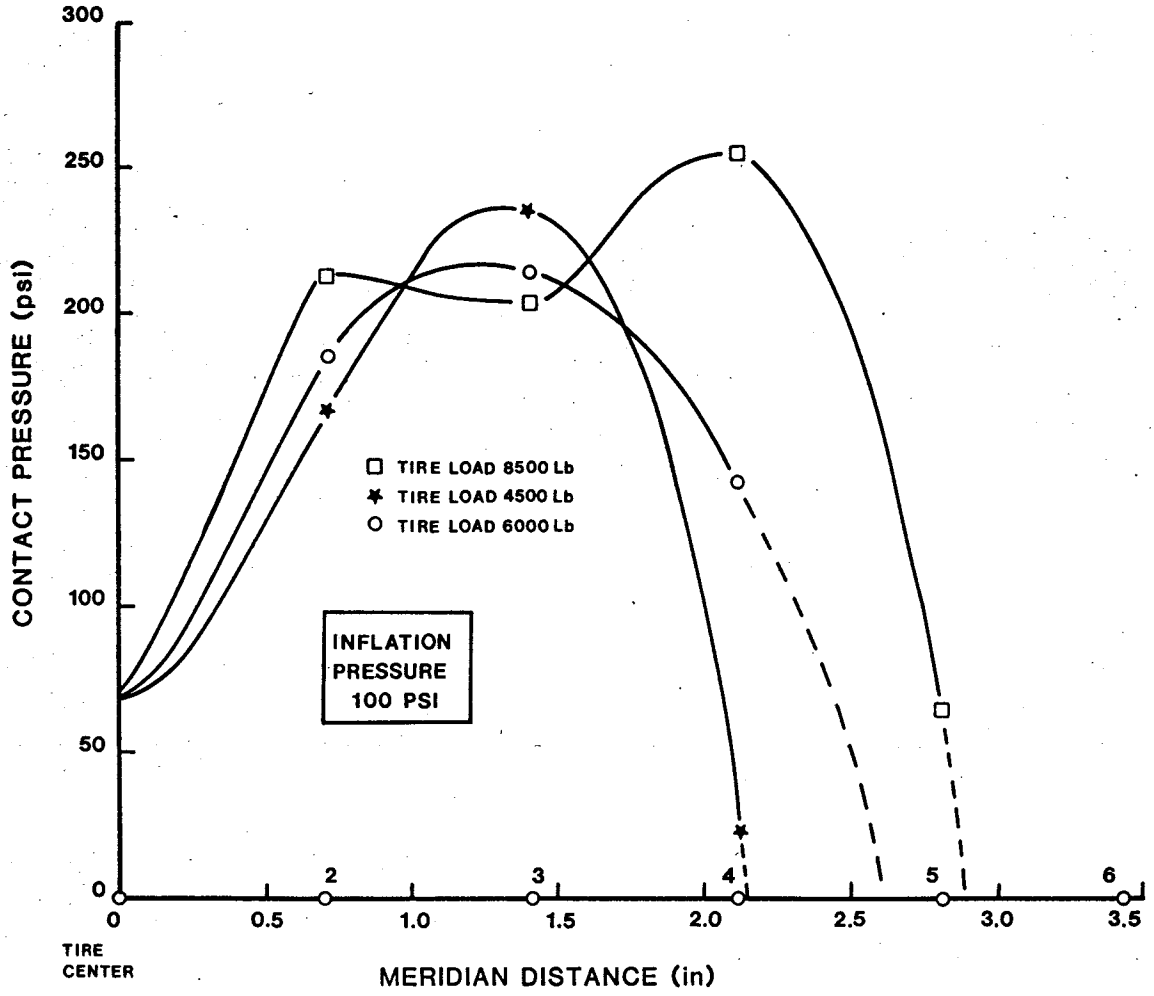

Figure 34. Effect of tire load on contact pressure calculated for a 10.00 truck tire with 100 psi inflation pressure.

Identification of Curves in Figure 35

Curve	Inflation	Load
a	50 psi	3700 lb
b	70	3700
c	90	3700
d	90	8250

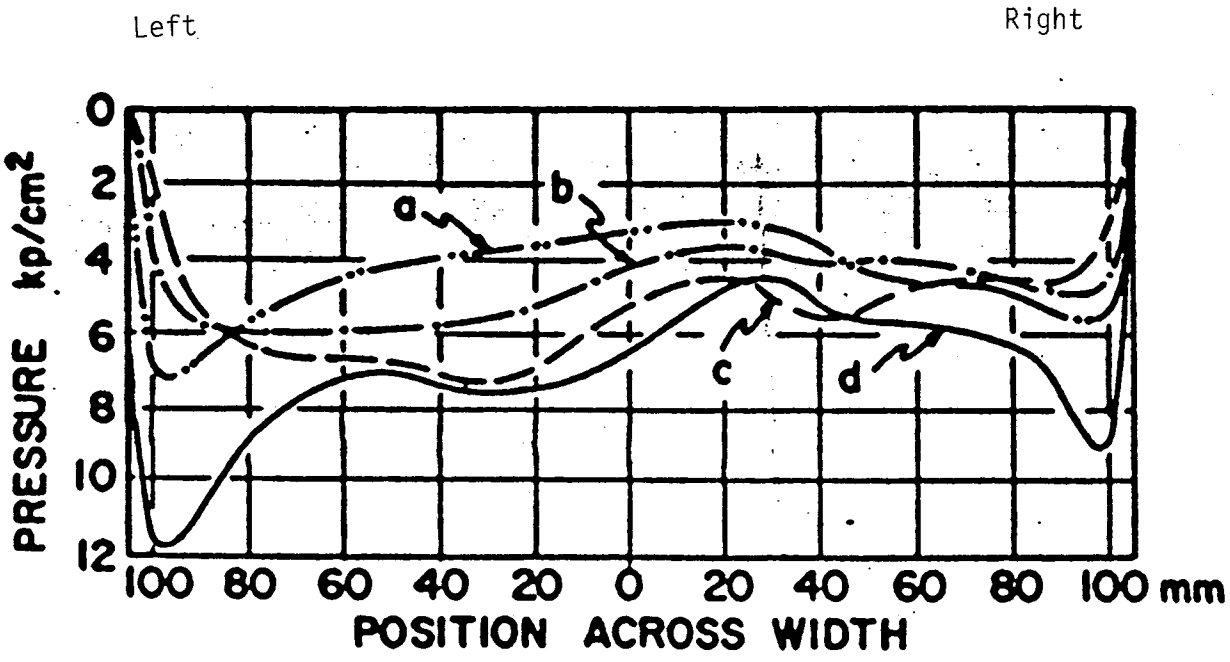

Figure 35. Effect of tire load and inflation pressure on contact pressure measured for a smooth-treaded truck tire (6). Data identification in table above. (1 kp/cm^2 = 14.22 psi)

Pavement Friction

An experimental study of the effect of pavement friction on the normal pressure distribution for a free-rolling tire does not appear to have been made. Analytical studies on contact loading of a solid rubber disk (7), and a cordless tire (8), indicate that there is very little difference in static deflection against a no-slip surface and a frictionless surface. The calculated pressure data for a rubber disk shown in Figure 36 have been confirmed by laboratory experiments.

Conclusion

In view of the small effects of speed and pavement friction on the normal pressure distribution for a free-rolling tire, it is believed that normal contact pressures calculated with a non-rotating tire model deflected against a frictionless surface are realistic representations of the normal pressures under a real tire travelling at highway speed. The significant effects of inflation pressure and tire load on normal pressure can thus be analytically studied with the standing tire model, and the calculated contact pressures can be utilized in investigations of pavement degradation accelerated by changes in inflation pressure and/or tire load.

A description of the finite element tire model used in this project is given in the next section.

COMPUTER MODEL FOR CALCULATING CONTACT PRESSURE DISTRIBUTIONS

A finite element tire model was developed at Texas A&M University for the purpose of investigating tire-pavement interaction during vehicle maneuvering (9). A comprehensive description of the details of the tire construction is input to the model, thereby permitting study of the

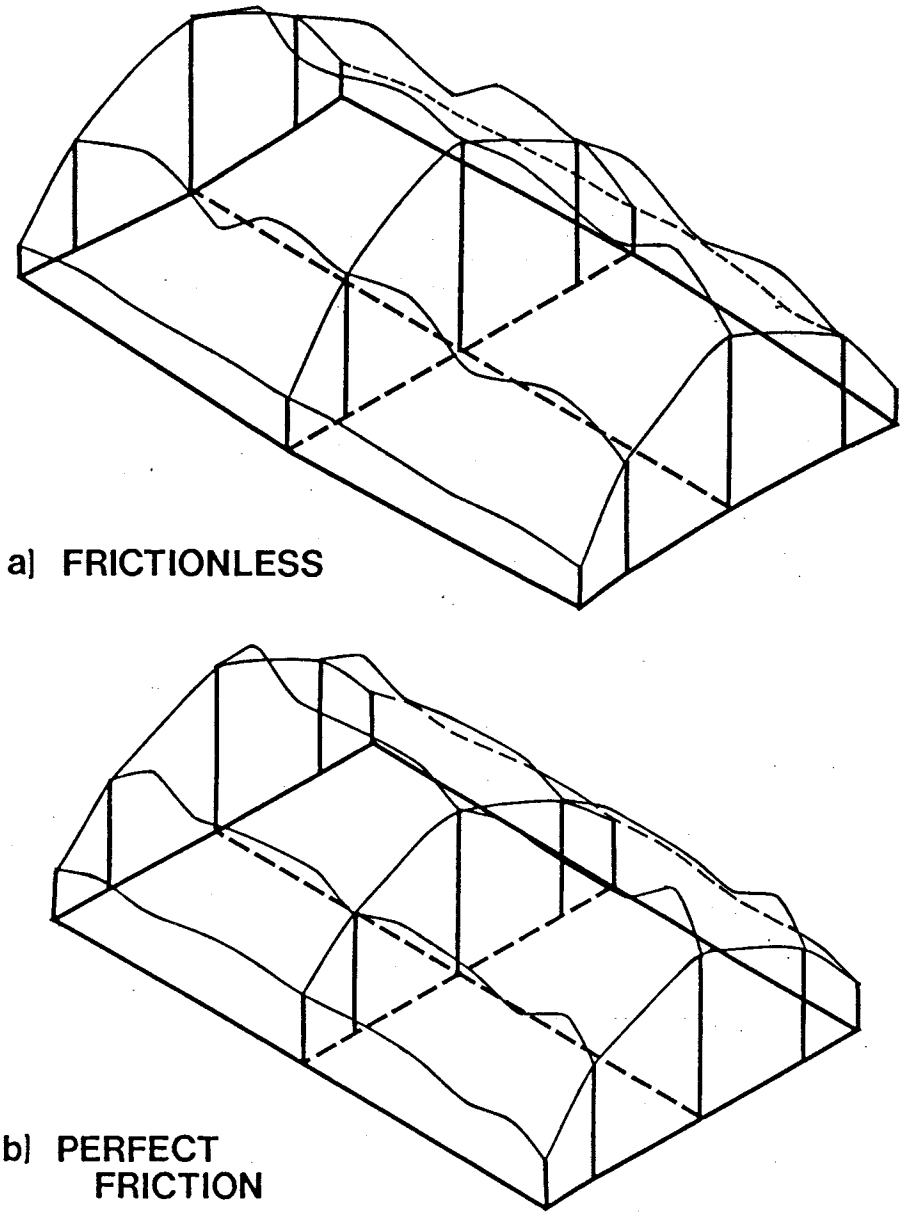

Figure 36. Normal contact pressure distributions calculated (7) for a solid rubber disk in contact with (a) a frictionless surface, and (b) a no-slip surface.

influence of factors such as tire materials and size, as well as the effect of inflation pressure and load on pavement contact pressure.

Tire Model

The tire model was developed from a relatively general finite element nonlinear shell-of-revolution computer program (10,11). This established program was enhanced for tire modeling by (1) adding the capability to work with laminated material properties, representing a tire carcass, and (2) utilizing a Fourier transform procedure (12) for solving the large deformation contact problem which is defined by a loaded tire in contact with the pavement.

The computer tire model consists of an assembly of axisymmetric shell elements positioned along the carcass mid-ply surface. Figure 37 shows an assembly of 17 elements representing the midsurface of a 10-ply 10.00-20 truck tire for which calculated contact pressures are shown in Figures 33 and 34. The ply structure in each finite element is specified separately to define the laminated cord-rubber tire carcass. Specifying the lamination of each element separately allows tire construction features such as belts, sidewall reinforcements, and bead turn-ups to be included in the tire model. Calculations made with the model reflect the influence of these components on tire behavior.

The finite elements are homogeneous orthotropic, with moduli determined by the laminated carcass. The elements are connected at the node points, which are numbered as shown in Figure 37. Node 18 (Figure 37) is a fixed node, representing the tire bead clamped on a rigid rim. The rim design, as it determines the distance between the two beads of a tire, also has an influence on pavement contact pressure.

An example of the construction data (geometry and material properties) needed by the tire model is given in Figure 38. Some of these data are difficult to acquire, particularly for a large tire. This work could not have been accomplished without the assistance of Smithers laboratories of Akron, Ohio who provided detailed physical data on the

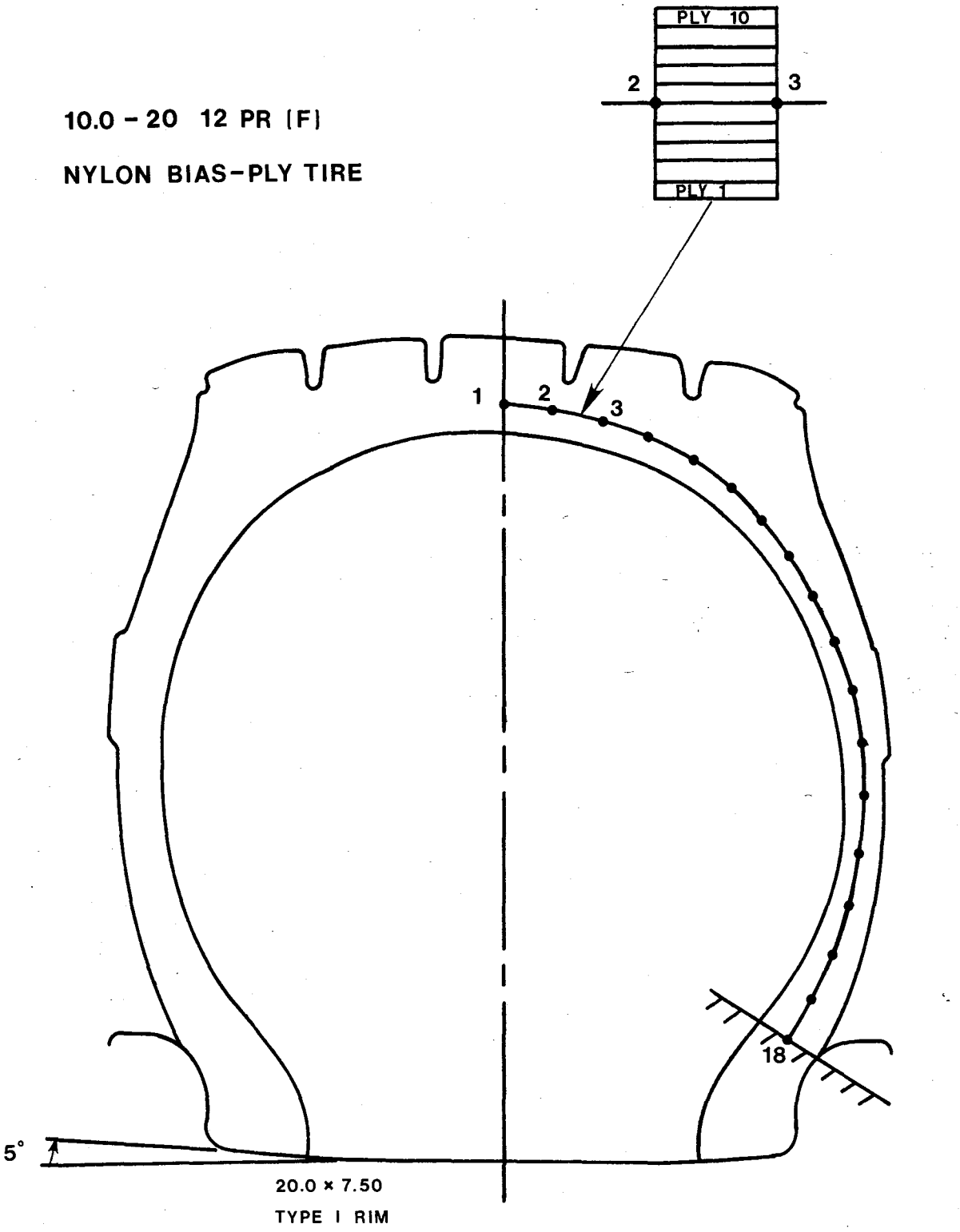

Figure 37. Assembly of finite element modeling a 10.00-20 truck tire.

10.00-20 12 PR (F)

Sidewall 8 plies nylon

Tread 10 plies nylon

Design Data (T&R)		
Tire Use	Inflation Pressure	Load Limit
Dual	75 psi	4760 lb
Single	85 psi	5430 lb

Construction Data

Cord diameter $d = 0.026$ in

Cord count at crown
$n = 22$ epi (in sidewall plies)
$n = 14$ epi (in breaker plies)

Cord angle $\beta = 38$ deg (at crown, in all plies)

Cord modulus $E_C = 150{,}000$ psi (Nylon 66, 1260/2)

Rubber moduli $E_R = 450$ psi , $\nu_R = 0.49$ (Poisson ratio)

Ply thickness $h = 0.043$ in (all plies)

Figure 38. Construction data input to the computer model of the 10.00-20 truck tire.

10.00-20 truck tire and a section of this tire. Figure 39 is an example of the tire carcass measurements included in the Smithers report. The geometrical data in Figure 39 is needed to correctly position the finite element mid-ply line shown in Figure 37.

Tire Model Loading

Figure 40 shows the coordinate system used to locate points on the tire model. Cylindrical coordinates (r,θ,z) are used, with the r-θ plane perpendicular to the pavement. The unloaded tire is symmetric about the z coordinate axis, located at the wheel axle.

The tire model is loaded first by specifying the inflation pressure. An axisymmetric solution for the inflated shape is obtained. The structural stiffness of the inflated tire is then calculated, prior to applying the axle load. The model is brought into contact with the pavement by specifying the axle height, R_ℓ, shown in Figure 40. This is equivalent to specifying the tire deflection against the pavement. At present, the computer tire model is deflected against a frictionless, flat rigid surface. Laboratory tests, discussed in the preceding section, show that interfacial friction has very little influence on the normal component of contact pressure for a free-rolling tire.

Neither the contact pressure distribution nor the contact area are known *a priori*. These are calculated by the computer program during the contact solution procedure. The contact pressure distribution is integrated over the contact area to find the tire load that will deflect the axle to the specified height, R_ℓ. Reference 12 describes the mathematical procedures used to calculate the contact pressure distribution and the deformation of the tire deflected against the pavement.

An example calculation for a G78-14 passenger tire is shown in Figures 41 and 42. The longitudinal distribution of contact pressure, along the centerline of the tire, is determined by the force at the contacting points, spaced 11.25 degrees apart shown in Figure 41. The

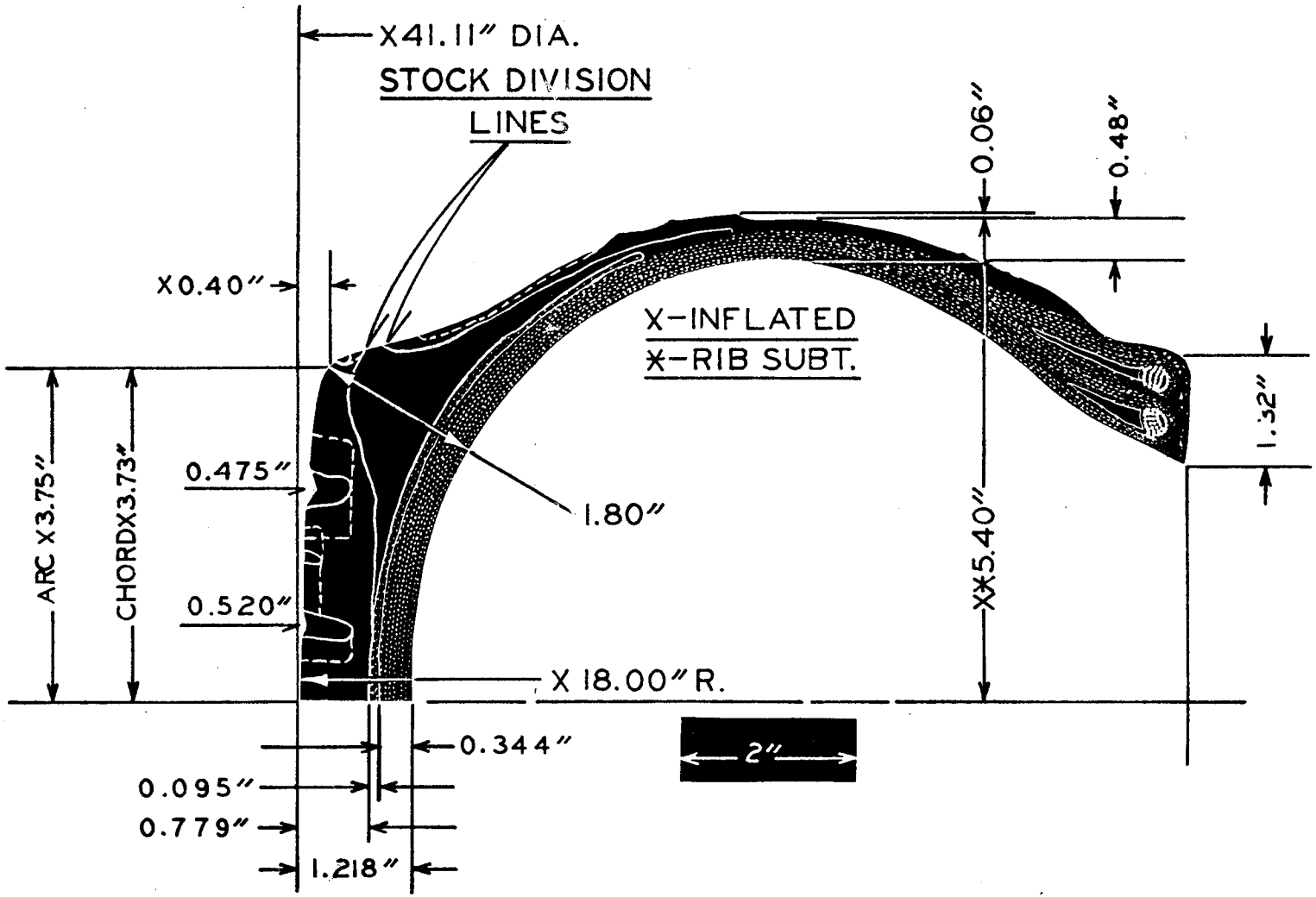

Figure 39. Details of a 10.00-20 truck tire carcass.

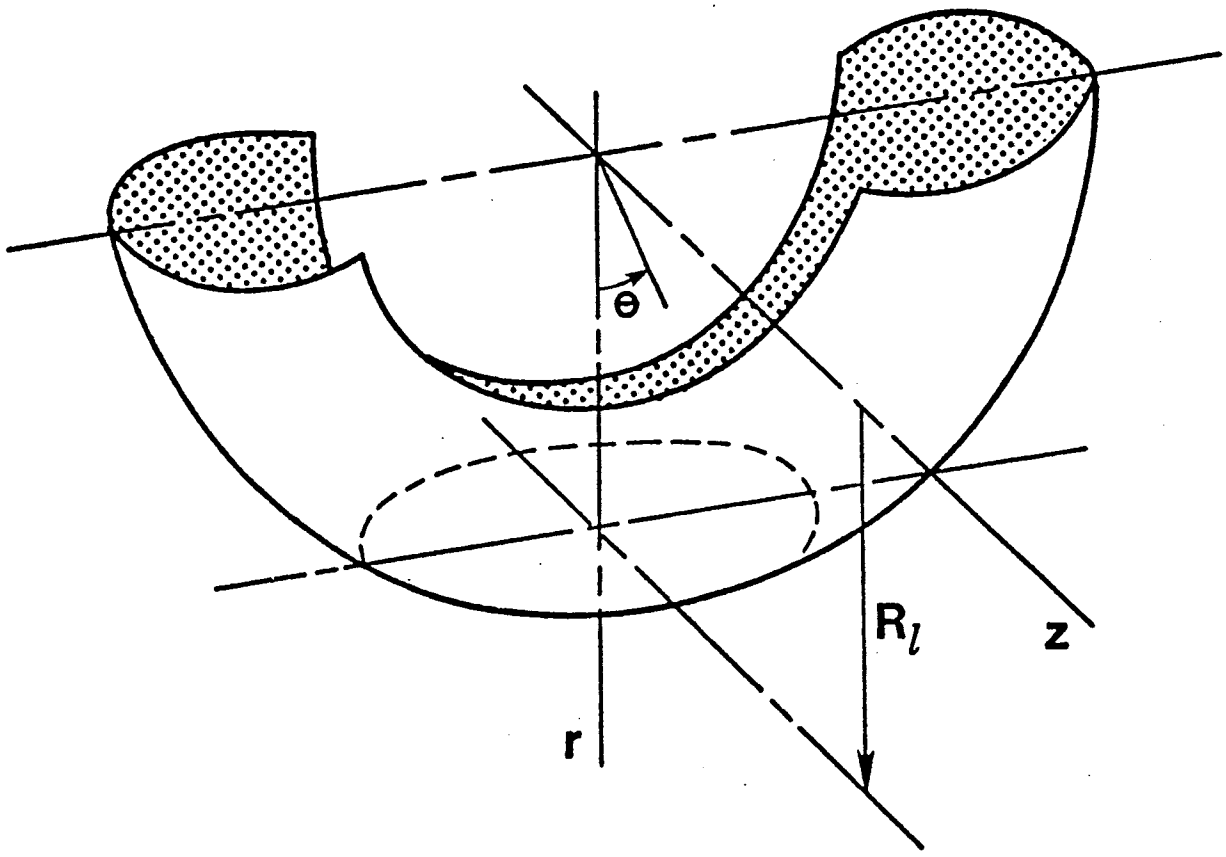

Figure 40. Tire model coordinates, r, θ, z and contact surface located at the loaded radius R_ℓ

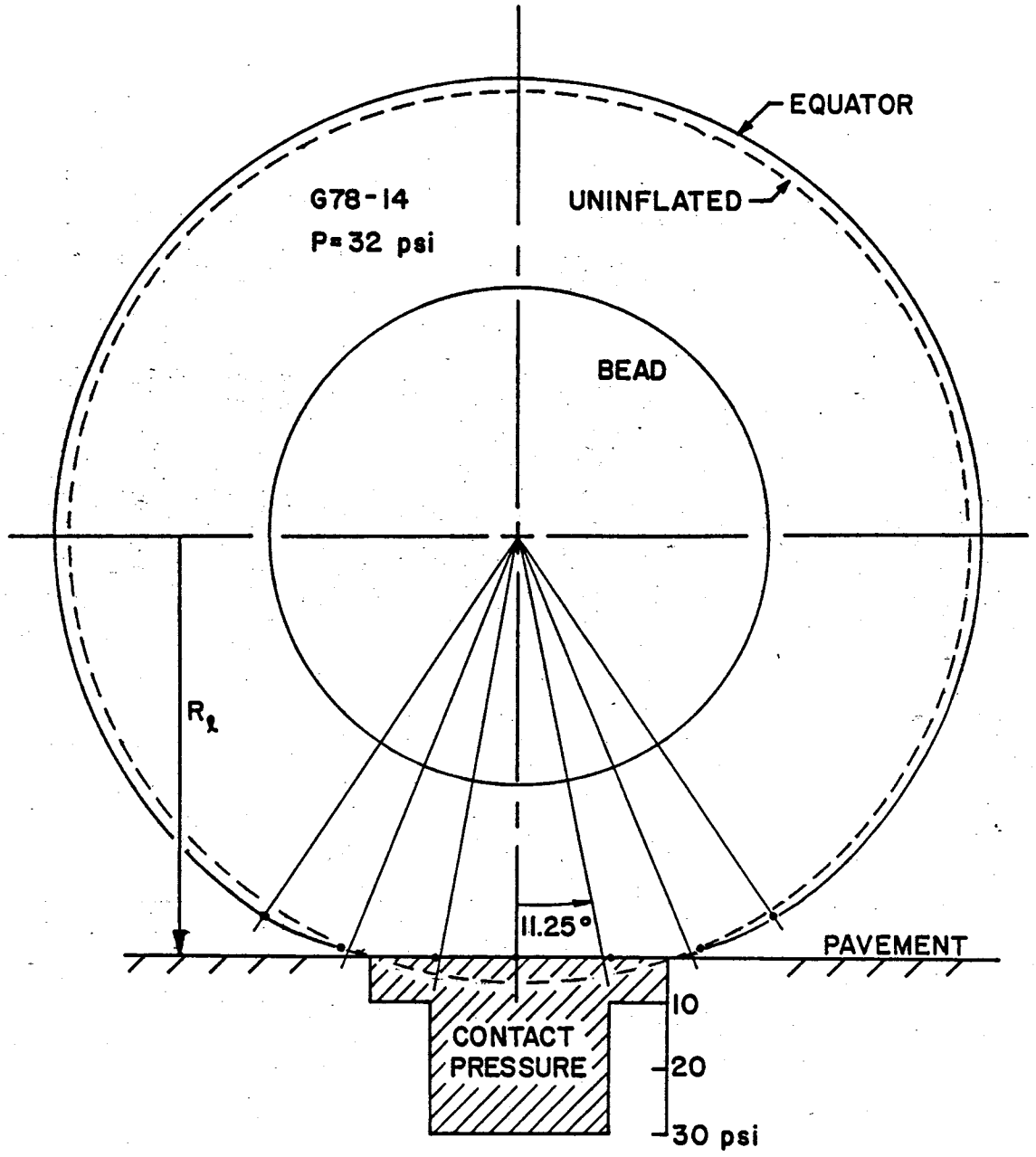

Figure 41. Passenger tire deflected 0.9 in and longitudinal distribution of the calculated contact pressure along the centerline.

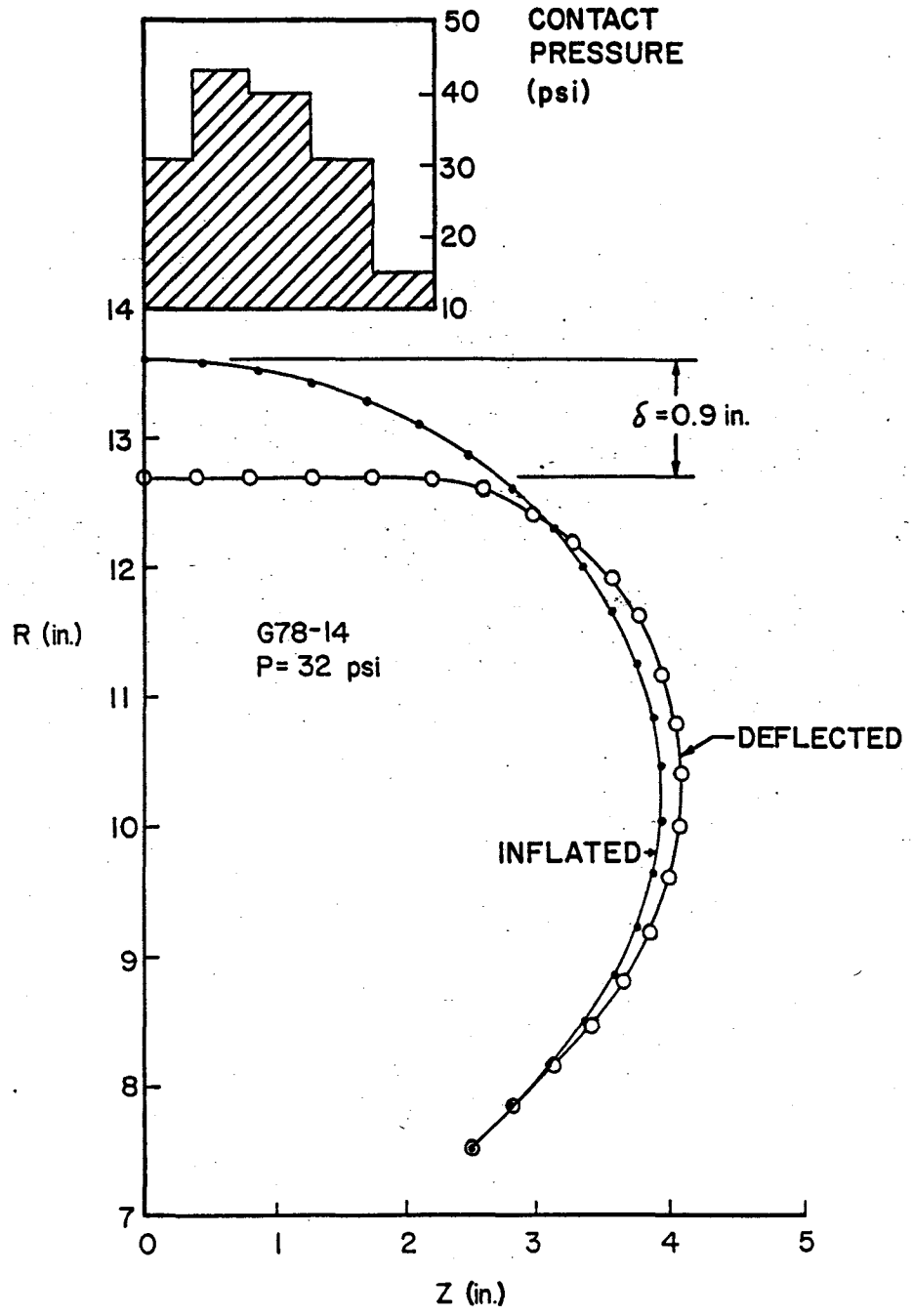

Figure 42. Meridian of passenger tire deflected 0.9 in. and lateral distribution of the calculated contact pressure.

lateral distribution of contact pressure, along the tire meridian passing through the center of the footprint, is determined by the force at four contacting points on the meridian (Figure 42). The footprint point forces, which are determined by the contact solution procedure, are divided by the area surrounding the points to obtain the normal contact pressures. Summing the point forces gives the tire load. For the G78-14 tire example here, with 0.9 inch specified deflection, the calculated tire load is 850 pounds.

Experimental Verification

Surprisingly little data on basic tire behavior, such as static load versus deflection, have appeared in the literature. With published data, the tire is often insufficiently described to allow a set of tire model input data to be developed. As there has not been a specific project to quantitatively validate the computer tire model, its validity rests on its ability to qualitatively reproduce various tire data. Figure 43 gives an example of load-deflection data calculated for the 10.00-20 truck tire. The dashed curve in Figure 43 follows experimental data obtained from a tire company on the same size tire at 75 psi inflation pressure. The calculated load-deflection data at 75 psi show that the tire model has approximately the same vertical stiffness as the test tire (the data curves have similar slopes). Without access to more details of the experiment (the test data were obtained in 1977) it is not possible to explain why the measured data are offset from the calculated data.

The contact pressure distributions calculated by the tire model are seen to be qualitatively similar to the peak contact force distributions measured by an instrumented stud embedded in a highway (13). Vertical force data from Reference 13 is reproduced in Figure 44, for comparison with the calculated contact pressure distributions shown in Figures 33 and 34. The calculated data are clearly similar to these measured data. The effect of inflation pressure shown in Figures 44a and 44b, for

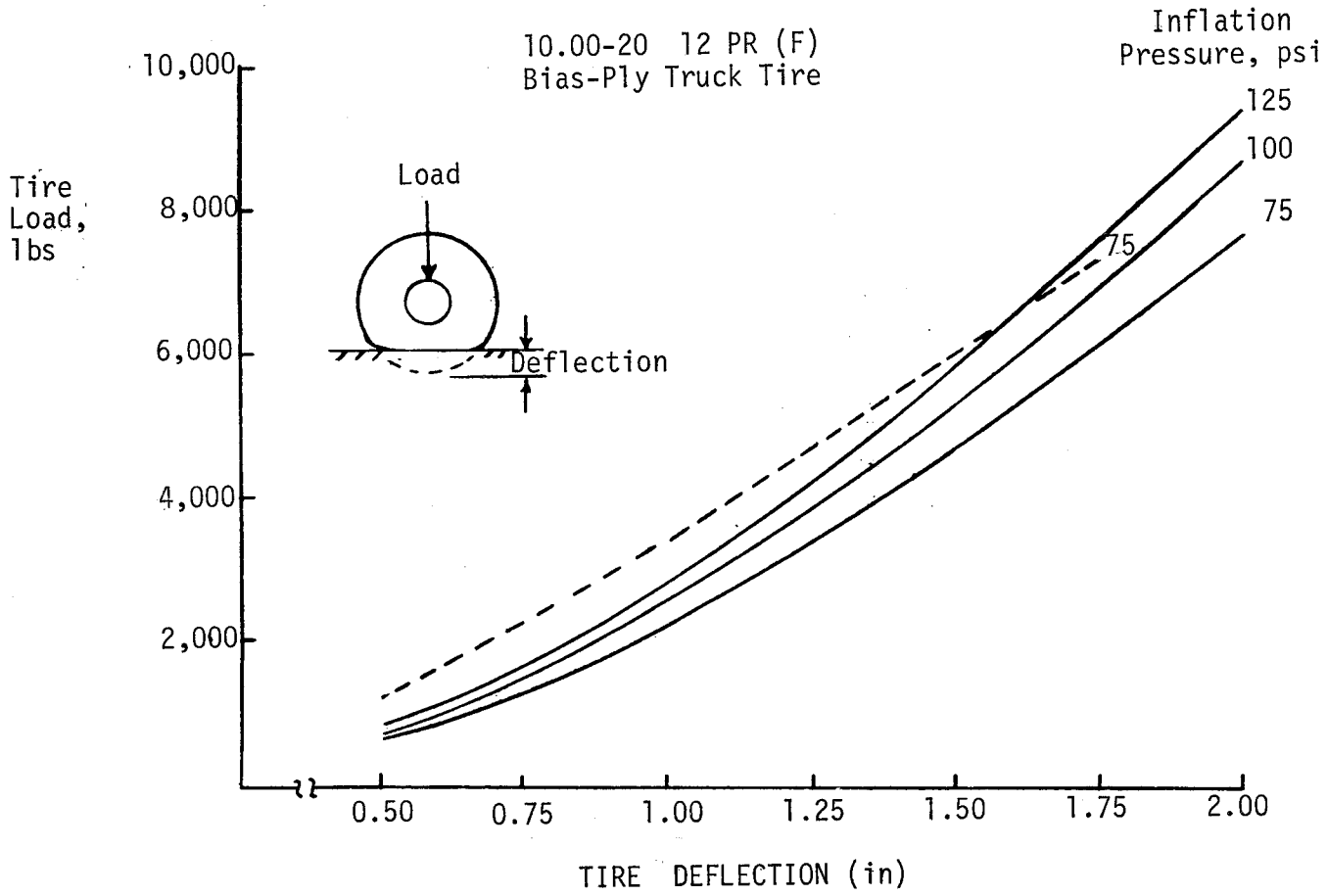

Figure 43. Influence of inflation pressure on load-deflection data calculated for a truck tire (solid curves). Measured data at 75 psi (dashed curve).

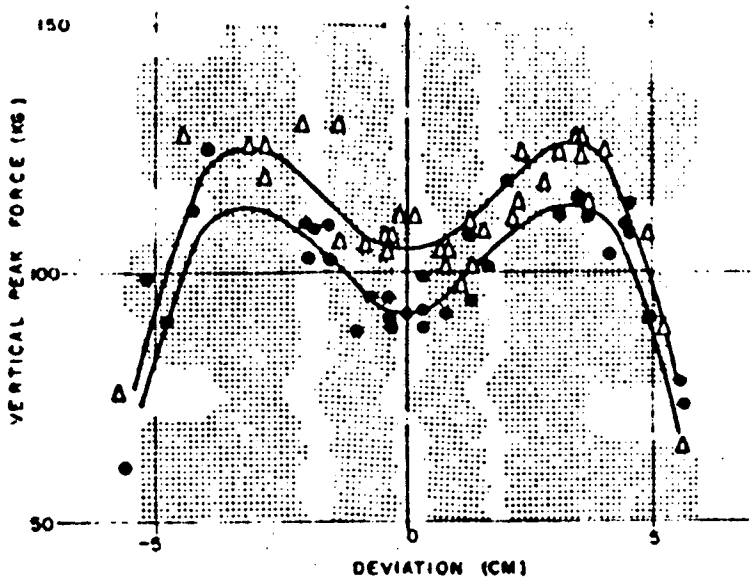

(a) Land Rover, influence of inflation pressure.

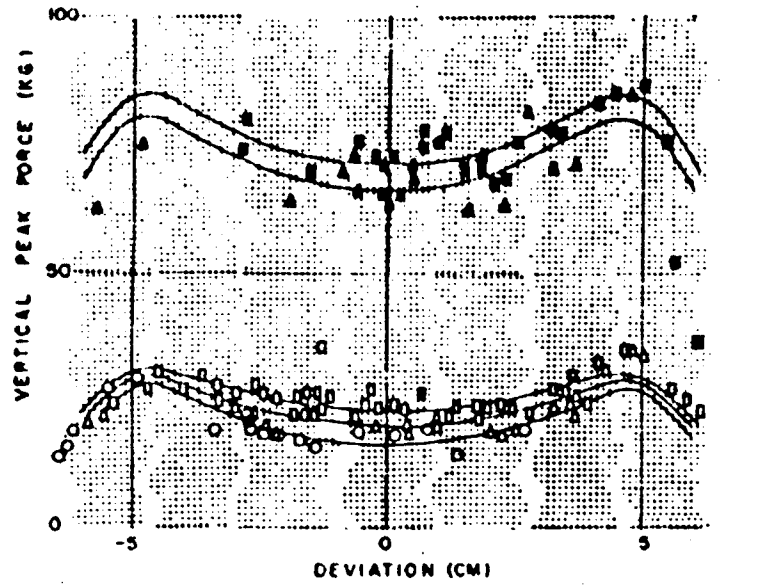

(b) Chevrolet station wagon, influence of inflation pressure.

Figure 44. Measured normal force distributions for several passenger car tires (13).

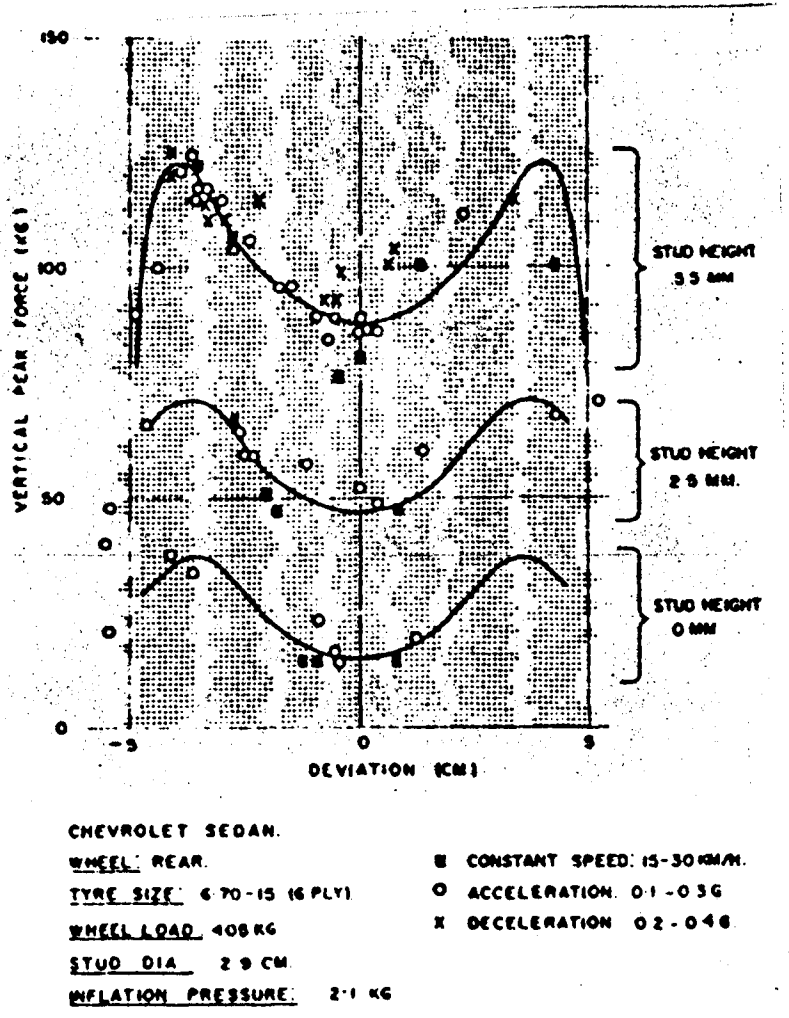

(c) Chevrolet sedan, influence of measuring stud height and vehicle acceleration.

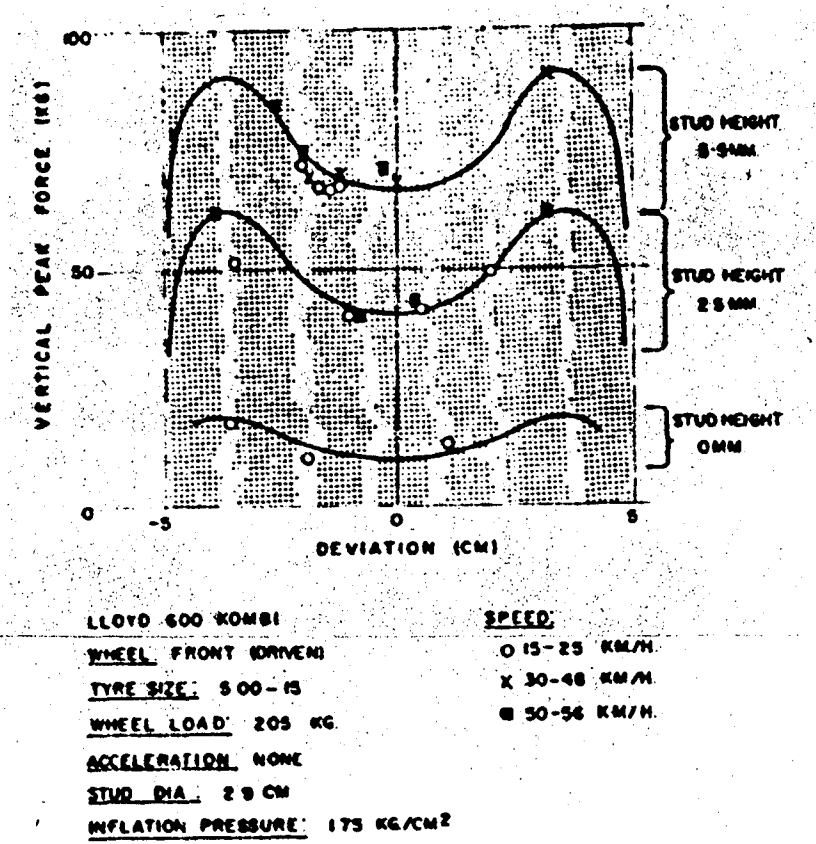

(d) Lloyd van, influence of stud height and vehicle speed.

Figure 44. (Continued)

example, is generally reproduced by the effect of inflation pressure on the calculated data in Figure 33. The negligible effect of speed, discussed earlier, is confirmed by the data in Figure 44d. The considerable scatter that always occurs in on-the-road tire tests is present in Figure 44, but the qualitative behavior is clear. It is of interest to note that the test program reported in Reference 13 was conducted over 25 years ago by the National Institute for Road Research in Pretoria, South Africa. Continuation of this type of experimental investigation, with modern technology and modern tires, would be of great benefit to both tire modeling and road research.

Summary

The Texas A&M finite element tire model is capable of calculating normal tire-pavement contact pressure distributions that are sensitive to a wide range of tire construction parameters and tire operating variables. It is the only cord-reinforced finite element tire model that is capable of economically calculating a contact pressure distribution for a specified tire deflection. The economy is due to the use of axisymmetric shell elements, instead of the 3-D elements used by all other finite element tire contact models.

At present, few experimental data have been found to validate the model. However, the calculated results are qualitatively reasonable. The model is, at present, not 'user friendly', as it requires running five separate programs to get from raw tire data to a contact pressure solution. Additional development work on the model is needed. Continued development will include implementation of a friction theory to enable the model to calculate detailed distributions of longitudinal and transverse shear pressures.

CONTACT PRESSURE DISTRIBUTIONS FOR SELECTED TIRES

Calculated distributions of normal contact pressure for the tires considered in this project are shown here.

Radial Passenger Car Tires

Geometric and material property data were acquired for a small and a medium-size radial tire. These are standard load tires with sizes and load limits (14) listed in the table below. The small tire (P185/80R13) is used on cars such as the Ford Pinto, Mercury Bobcat, Buick Skyhawk, and Pontiac Sunbird. The medium-size tire (P205/75R14) is believed to represent the average passenger car tire on the road today, used on cars such as the Ford LTD, Chevrolet Monte Carlo, Buick Skylark, and Pontiac LeMans. Both tires have a polyester cord body and are steel-belted, the most common radial tire construction in use today.

Tire Size	Tire Design Load (26 psi inflation)	Tire Maximum Load (35 psi inflation)
P185/80R13	1124 lb	1301 lb
P205/75R14	1323	1532

Figure 45 shows distributions of contact pressure along the meridian passing through the center of the footprint. These distributions are symmetric about the tire centerline because the finite element tire model does not account for differences between the right and left half of a tire. Slight right-left differences exist in all tires and influence the actual contact pressure distribution to some extent, but usually have negligible influence on tire performance. A more significant influence on contact pressure is the shape of the tire meridian. The P205/75R14 is seen to exhibit a contact pressure distribution with two peaks, which is the shape most commonly found. The P185/80R13 pressure distribution is unusual in that three peaks are seen. The meridian profiles of these two tires appear quite similar, although they are produced by two different

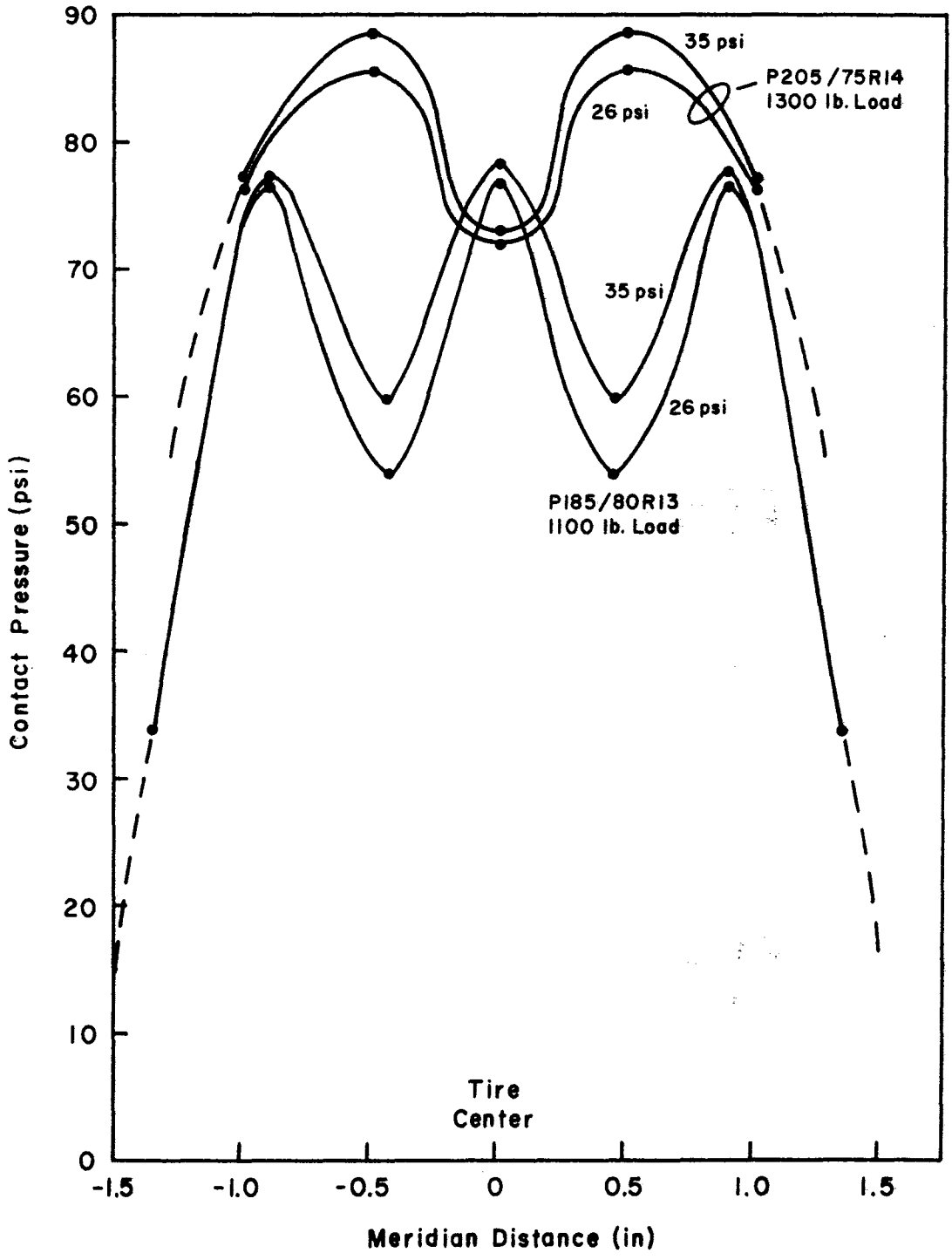

Figure 45. Effect of inflation pressure on footprint pressure for radial passenger car tires.

major tire companies. It has been the experience of the developer of the finite element tire model (Tielking) that a slight repositioning of finite elements in the tread region (corresponding to a slight redesign of the tire meridian shape) can cause the contact pressure distribution to exhibit a peak at the center. Which profile is better for tire performance would be debatable as many other factors (besides normal contact pressure) have a significant influence on tire performance. In Figure 46, which shows the longitudinal distributions of contact pressure along the fore-aft centerline in the footprint, there is little evidence of the effect of meridian shape. The longitudinal distributions are always smoother than the meridianal, and usually (for a standing tire) exhibit a single peak at the center. Finally, it is noted that the contact pressure peaks in Figures 45 and 46 are accentuated, appearing to be sharper than peaks that are usually measured. This is due to excessive laminate stiffness inherent in the present finite element tire model. Continued improvement of the tire model will focus on the laminate stiffness problem, with consequent improvement in the calculated contact pressure distributions. Experimental data to confirm calculated data, such as shown in Figures 45 and 46, is not yet available.

Figure 47 compares the load-deflection behavior of the two radial passenger car tires and shows the effect of inflation pressure.

Bias-Ply Truck Tire

Data for a 10.00-20/F, nylon cord truck tire were acquired. The 10.00-20 size is the most common bias-ply size for 18-wheel truck applications, and nylon is believed to be currently the most common bias-ply truck tire cord. Truck tire load limits are different for dual and single truck tire usage. The table below gives the load specifications in Reference (14). In this table, a letter in parentheses indicates the load range (ply rating: F = 12PR, G = 14PR, H = 16PR) and is adjacent to the maximum load for that load range.

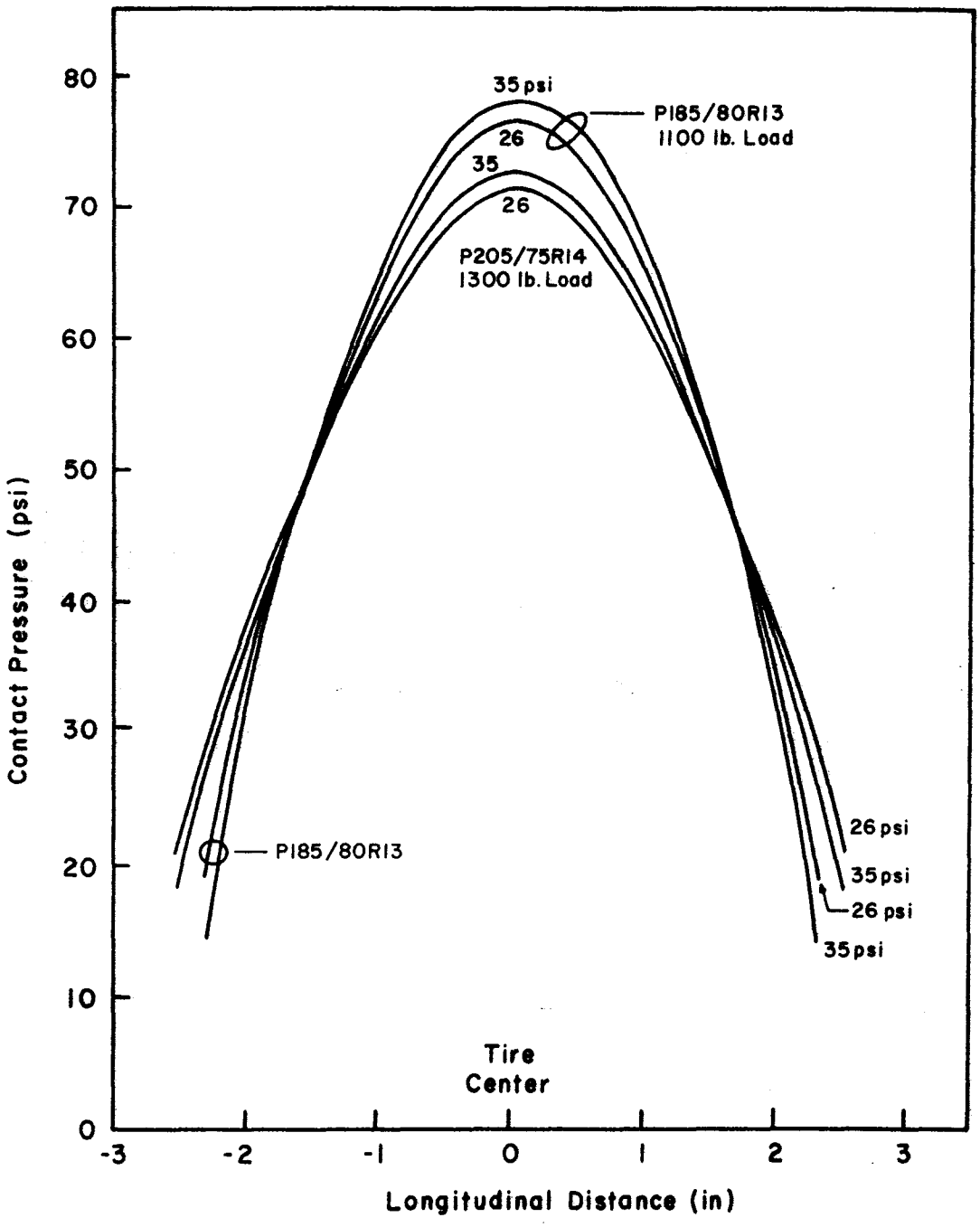

Figure 46. Effect of inflation pressure on footprint pressure distribution along the centerline of radial passenger car tires.

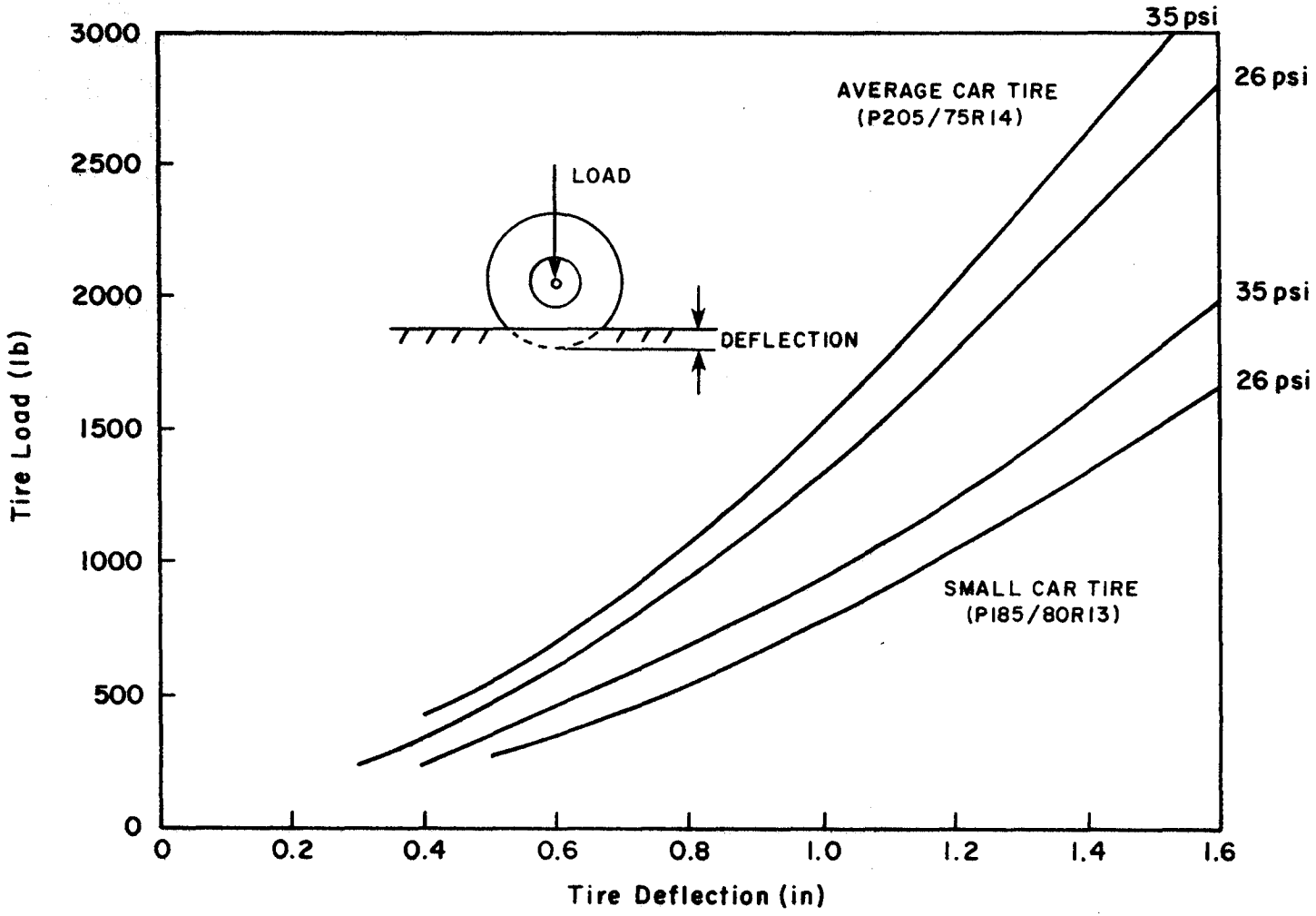

Figure 47. Effect of inflation pressure on load-deflection behavior of radial passenger car tires.

Load Limits (lbs) for a 10.00-20 Bias-Ply Truck Tire
at Various Cold Inflation Pressures (psi)

Use	75	80	85	90	95
Dual	4580	4760(F)	4950	5120	5300(G)
Single	4770	4990	5220	5340(F)	5640

Use	100	105	110	115	120
Dual	5470	5630	5800(H)		
Single	5840	6040(G)	6240	6430	6610(H)

Figure 48 shows a full scale plot with dimensions locating the points where the contact pressure is calculated. These dimensions change slightly with inflation pressure because the finite element model represents the mounted but uninflated tire. The tire model is first inflated (giving the point locations shown in Figure 48 at 100 psi) and then brought into contact with the pavement. Due to symmetry in the model, only points in one-quarter of the footprint (including the medians) are included in the contact pressure calculations. The symmetry was used to lay out Figures 49 and 50, showing pressures (psi) in the complete footprint. If the load is increased (Figure 49) or the pressure is decreased (Figure 50) more contact points will be included in the footprint. The point spacing will change slightly with the inflation pressure; the total number of points in the footprint for a specified pressure and tire load is determined by the number of finite elements used to represent the uninflated tire.

Plots of meridional pressure distributions for the 10.00-20 truck tire are shown in Figures 33 and 34 in this chapter.

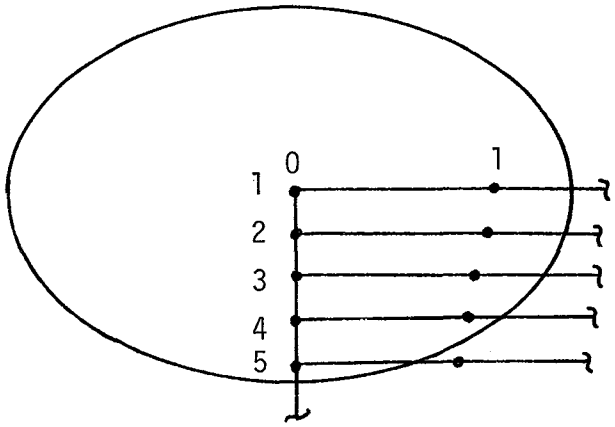

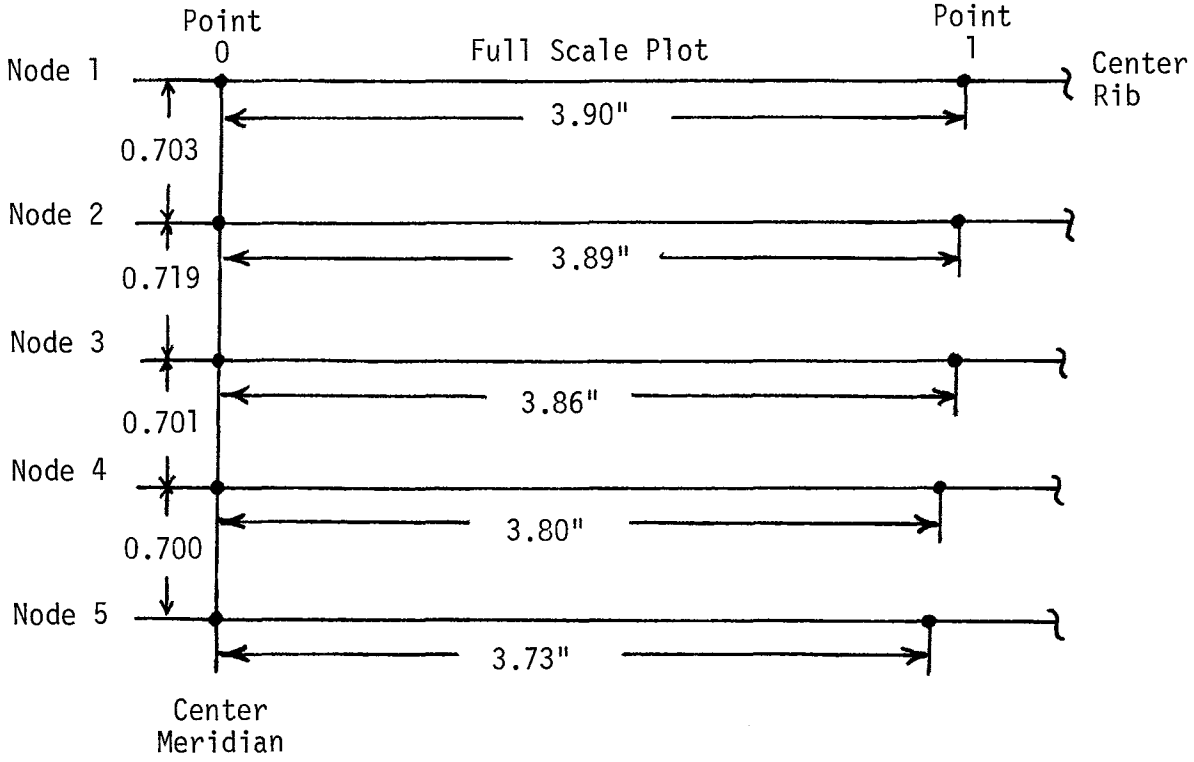

Figure 48. Pressure data locations in 1/4 footprint of the 10.00-20 truck tire with 100 psi inflation pressure.

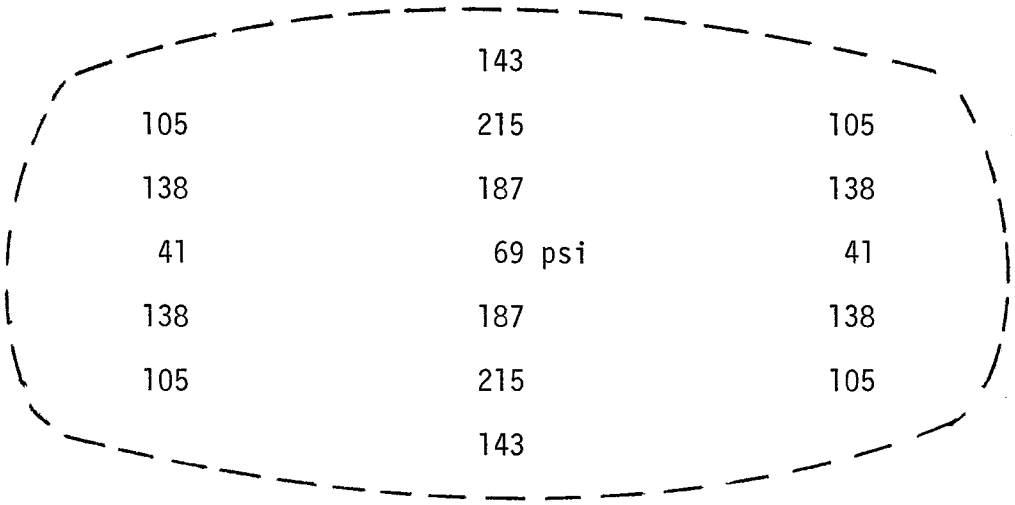

(a) 6,000 lb. load, 1.6 in. deflection

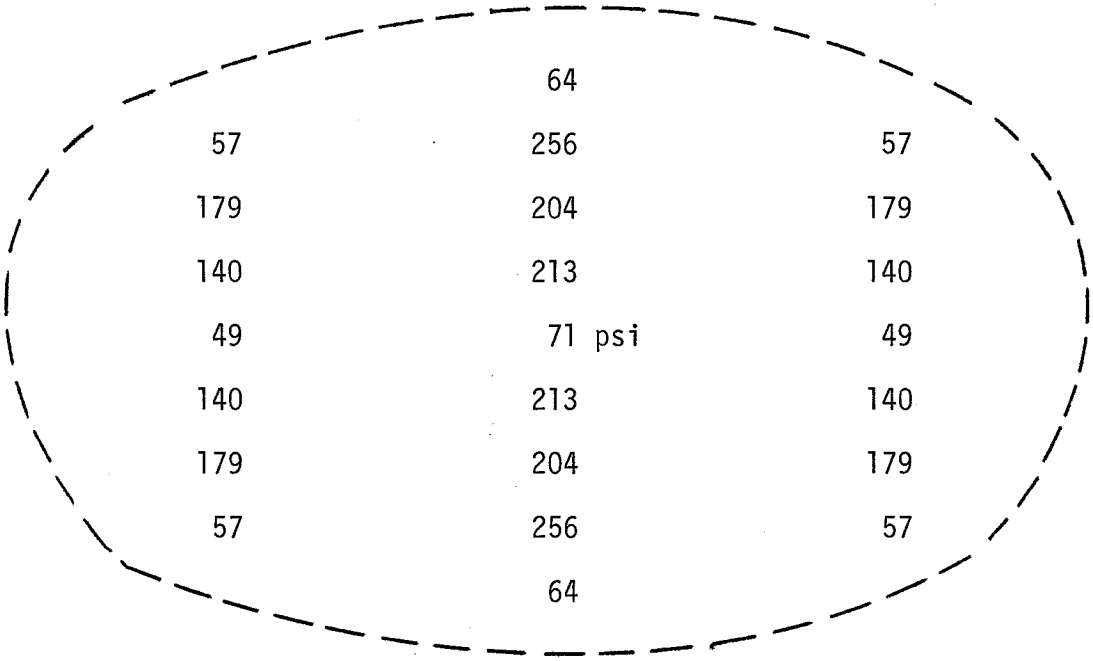

(b) 8,500 lb. load, 2.0 in. deflection

Figure 49. Contact pressures in footprint of the 10.00-20 truck tire with 100 psi inflation pressure.

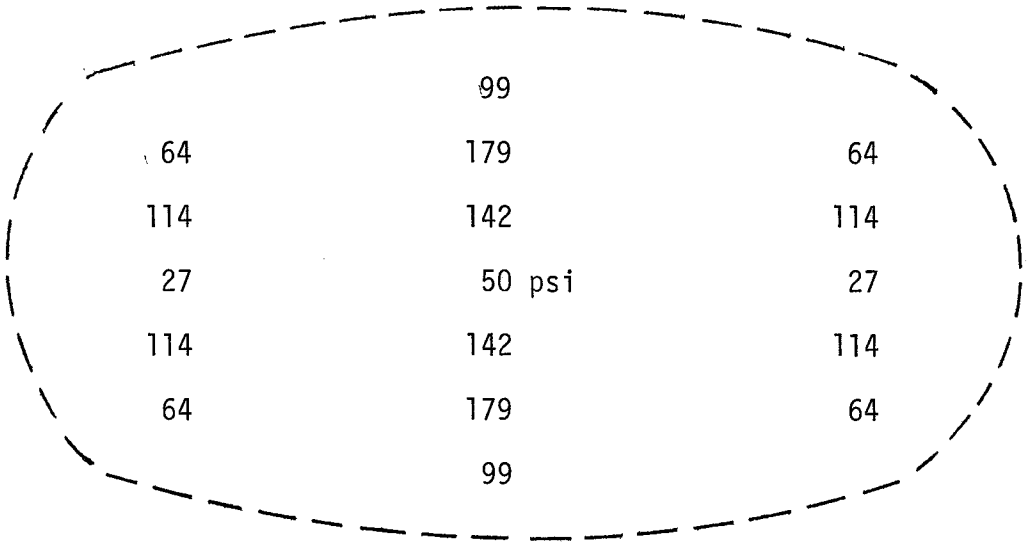

(a) 75 psi inflation, 1.5 in. deflection

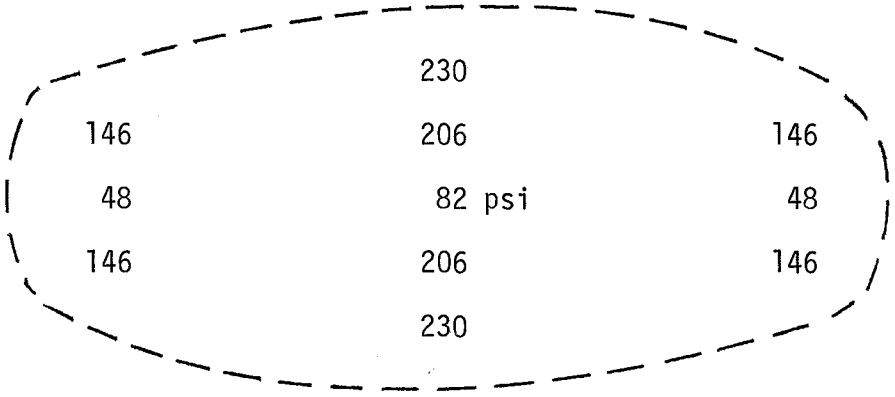

(b) 125 psi inflation, 1.3 in. deflection

Figure 50. Contact pressures in footprint of the 10.00-20 truck tire under 4,500 lb. load.

CHAPTER 4

ANALYSIS PROGRAM

INTRODUCTION

A large number of computer programs have been developed that calculate the state of stresses and displacements in highway pavements resulting from wheel loads. These programs can generally be divided into two categories: elastic-layered programs and finite element programs. Elastic-layered systems are based on a generalized assumption that the pavement consists of materials that can be characterized by a modulus of elasticity and Poisson's ratio as was assumed by Burmister for a two-layered structure (15). Material characterization in layered systems is in terms of linearly elastic behavior. However, most pavement materials exhibit nonlinear stress-strain behavior. A finite element method can be alternatively used to handle this nonlinearity. A program for flexible pavements based on finite element method incorporating nonlinear material properties of materials was developed by Duncan et.al.(16). This program was made user-friendly and improved, to include a failure model for granular and subgrade soils based on the Mohr-Coulomb theory (17) and renamed ILLIPAVE. The program adequately predicts the flexible pavement response to loadings and the results compared favorably with field test data (18). Additional modifications of ILLIPAVE were made during this study. The modified version of ILLIPAVE has been expanded to include the ability to predict the performance of inservice pavements. The current version of ILLIPAVE includes linear and nonlinear characterization of materials, interface relationships between the substructure of the pavement component materials, together with a finite element technique, and predicts rut depth, slope variance, fatigue cracking, and present serviceability index (PSI) with time. These additions to ILLIPAVE should make it very useful for analysis and design of future pavement structures.

DESCRIPTION OF ILLIPAVE

The ILLIPAVE computer program (19) consists of a two-dimensional half-section of asymmetrical solid of resolution that was used to model a three-dimensional section of a pavement structure. The half-section structure to be analyzed is divided into a set of quadrilateral elements which are then automatically divided into four triangles by the computer program to produce a set of elements like those shown in Figure 51. Consistent with plane stress or plane strain models of finite element analysis, the displacements are assumed to vary linearly within each triangles. Thus the equilibrium equation, in terms of unknown nodal point displacements, were developed at each nodal point of the finite element system. A solution to the system is produced by the application of Gauss elimination to this set of equilibrium equations. The current program includes a series of features that will be discussed in the subsequent sections of this chapter.

Resilient Modulus Models

One of the most significant features of the ILLIPAVE finite element program for flexible pavement analysis is the ability to incorporate both linear and nonlinear stress-strain behavior of the pavement materials. Besides finite element configuration to represent pavement cross sections, load conditions and material properties are required inputs in the program. Unit weight, Poisson's ratio, earth-pressure coefficient at rest, as well as modulus for stress dependent materials must be specified. Three alternative models are available for describing the resilient modulus for stress dependent granular and subgrade soil under repeated loads. For the granular soils the resilient modulus, Er, can be expressed as function of either the sum of the three principal stresses; θ,or minor principal stress, σ_3 . They are respectively given by:

$$Er = k_1 \theta^{k2} \qquad (1)$$

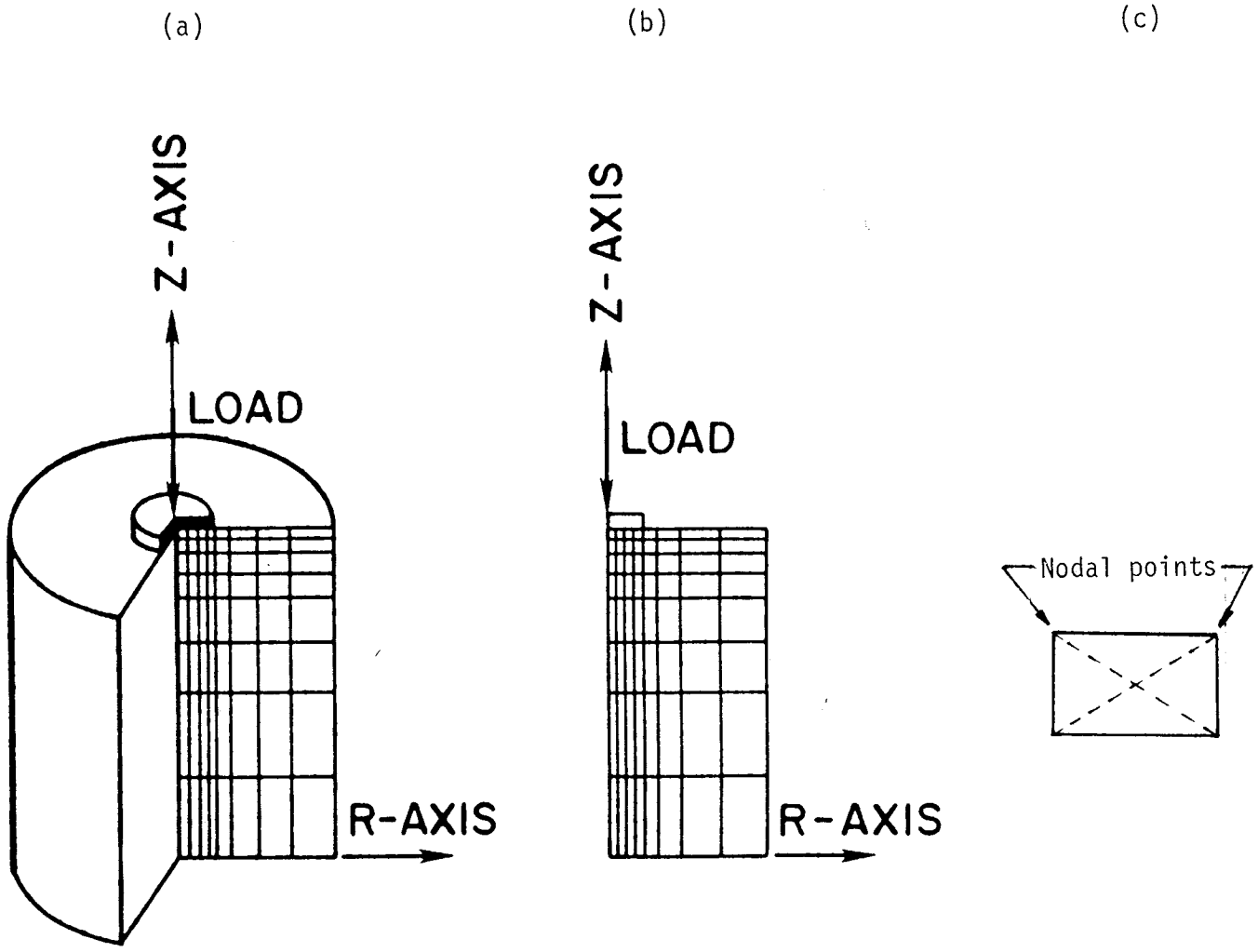

Figure 51. Finite element model in ILLIPAVE: (a) 3-dimensional view; (b) half-section; (c) typical element.

or

$$Er = k_1' \ \sigma_3^{\ k_2'} \qquad (2)$$

in which

Er = resilient modulus

$\theta = \sigma_1 + \sigma_2 + \sigma_3$

k_1 , k_2 , k_1', k_2' = experimental test constants

For the subgrade soils, as shown in Figure 52, the variation of resilient modulus is introduced by means of the following two expressions as

$$Er = c_2 + c_3 \ [c_1 - (\sigma_1 - \sigma_3)] \ ; \ c_1 > (\sigma_1 - \sigma_3) \qquad (3)$$

and

$$Er = c_2 \ + c_4 \ \ [(\sigma_1 - \sigma_3) - c_1] \ \ c_1 < (\sigma_1 - \sigma_3) \qquad (4)$$

in which

$(\sigma_1 - \sigma_3)$ = deviator stress

c_1, c_2 = material constants

c_3, c_4 = the rate of change of Er with repeated deviator stress

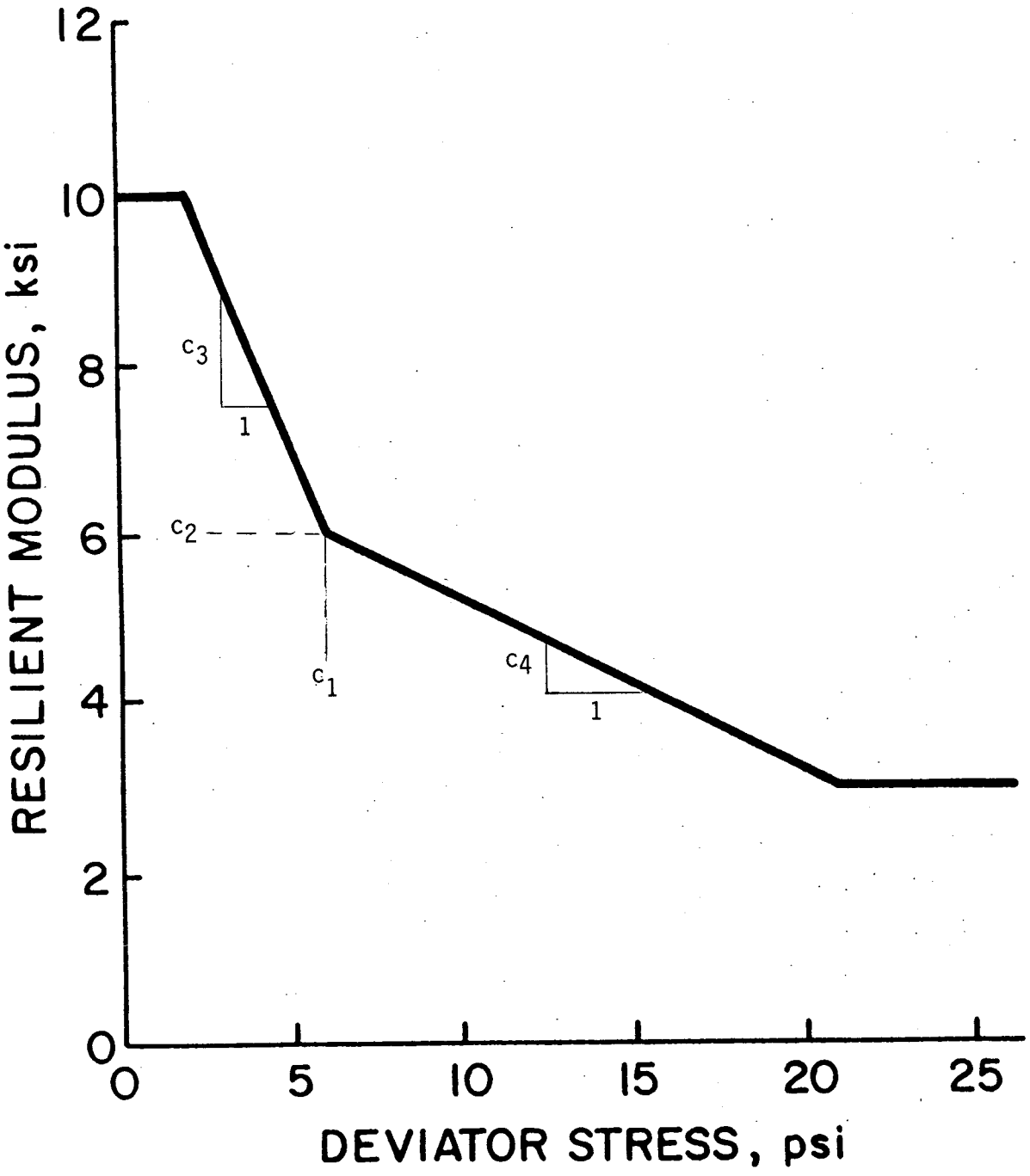

Figure 52. Variation of subgrade resilient modulus with deviator stress.

Permanent Deformation Characterization

The method used to represent permanent deformation characteristics of the materials in this study is in terms of three parameters, i.e., ε_o, β, and ρ. These parameters are developed by fitting a curve that relates permanent strains to loading cycles. These data are developed from creep or repeated load triaxial laboratory tests of each pavement material. A typical permanent strains versus loading curve is shown in Figure 53. The curve describing this relationship is represented by

$$\varepsilon_a = \varepsilon_o e^{-\left(\frac{\rho}{N}\right)^{\beta}} \qquad (5)$$

in which

ε_a = permanent strains

N = Cycles of load

and ε_o, β, and ρ = material parameters

The subsequent steps should be followed to find the three parameters ε_o, β, ρ.

Step 1. Finding β

The derivative of Equation 5 is

$$\frac{\partial \varepsilon_a}{\partial N} = \frac{\varepsilon_a}{N} (\beta \rho^{\beta}) N^{-\beta} \qquad (6)$$

Equation 6 can be expressed as

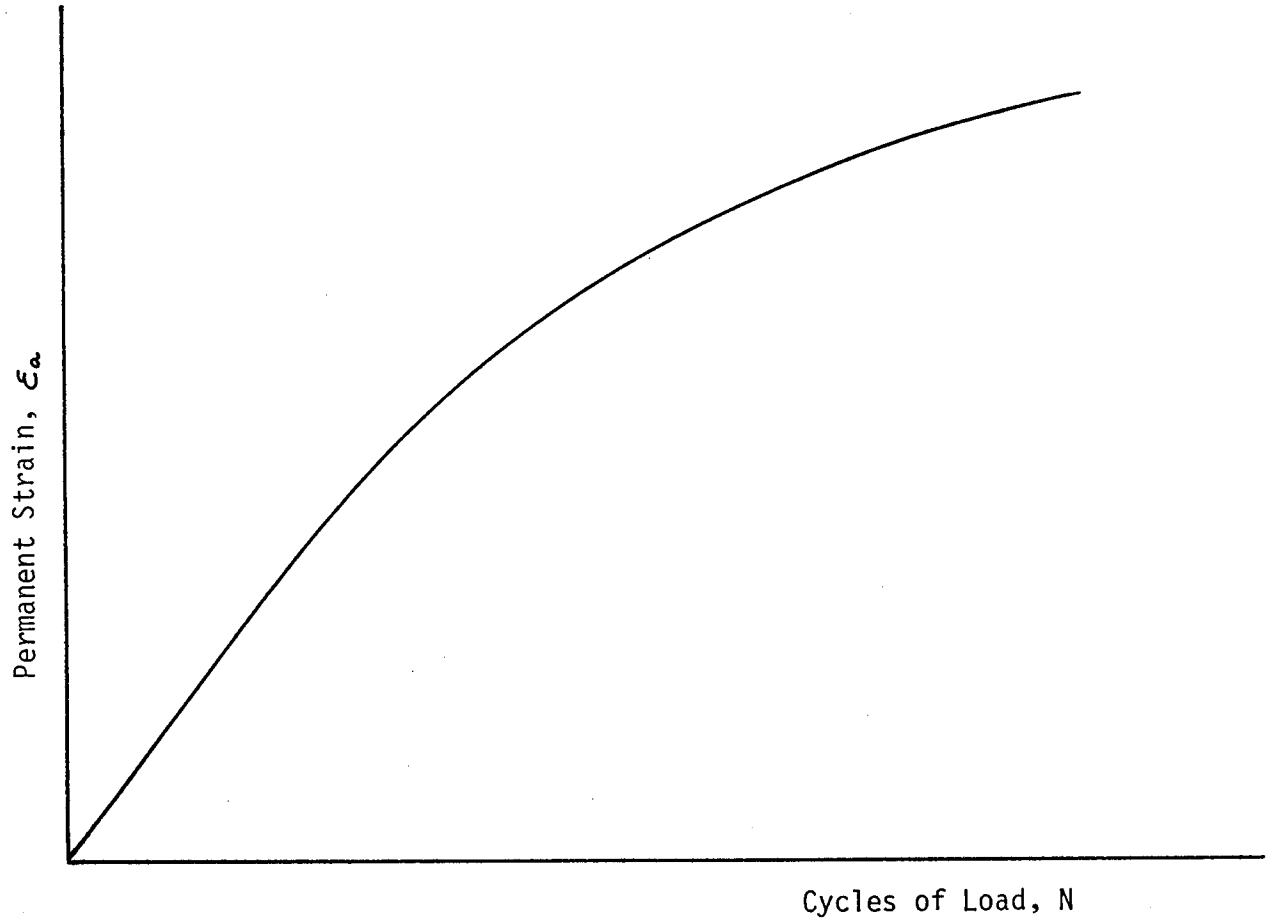

Figure 53. Relationship between permanent strain versus cycles of load.

$$\frac{\partial(\ln \varepsilon_a)}{\partial(\ln N)} = \beta \rho^{\beta} N^{-\beta} \tag{7}$$

Taking the logrithm of both sides of equation 7 yields

$$\log \left[\frac{\partial(\ln \varepsilon_a)}{\partial(\ln N)} \right] = \log (\beta \rho^{\beta}) - \log N^{\beta} \tag{8}$$

Equation 8 can be redefined as:

$$y = c - x^{\beta} \tag{9}$$

in which

$$y = \log \frac{\partial(\ln \varepsilon_a)}{\partial(\ln N)}$$

$$c = \log \beta \rho^{\beta}$$

$$x = \log N$$

Since Equation 8 is a straight line, β and c are the slope and intercept of the equation and can be found by plotting log versus log N as shown in Figure 54.

Step 2. Finding ρ

Once β and c were obtained from Step 1, the equation for ρ can be expressed as

$$\rho = \left(\frac{10^c}{\beta}\right)^{\frac{1}{\beta}} \tag{10}$$

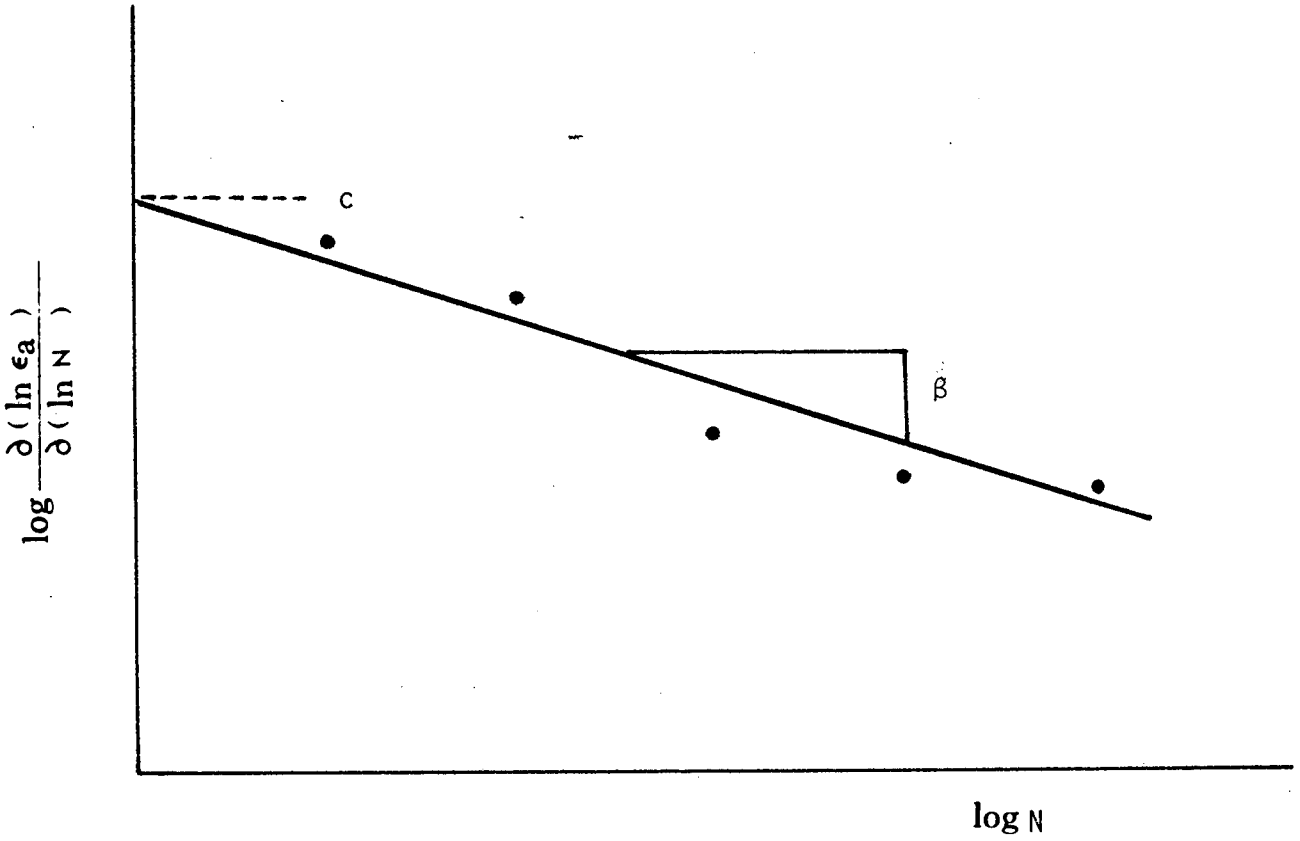

Figure 54. Relationships of $\log \frac{\partial(\ln \epsilon_a)}{\partial(\ln N)}$ Versus $\log N$

Step 3. Finding ε_o

From equation 5 ε_o can be obtained by averaging the values of permanent strains against cycles of load. The equation for Es is:

$$\varepsilon_o = \frac{1}{m} \sum_{i=1}^{m} \frac{(\varepsilon_a)i}{e^{-(\frac{\rho}{N})^{\beta}}} \qquad (11)$$

in which m = number of reading from material testing

The results from use of this three parameter method are presented as graphs in the form of permanent strain versus load repetitions as shown in Appendix F, those measured data were obtained from References (20), (21), and (22). Comparisons between measured deformations and estimated values are in reasonable agreement.

Development of the Rut Depth Prediction

The depth of ruts in the wheel path of a flexible pavements is attributed to accumulation of permanent deformations produced by repetitive traffic loads. The rut depth predictive model included in ILLIPAVE uses the finite element analysis to obtain the stress and strain in the pavement structure along with the permanent deformation material characterizations described previously. Theoretically, this approach can be applied to not only a single axle load but also multiple axle loads on the surface. The material properties developed from either creep or repeated load triaxial compression test are used in a set of simplified constitutive equations. The finite element analysis is used to calculate the stresses in the nonlinear pavement materials. The mathematical derivation of the equations to predict rut depth is described below for rutting from a single axle load as well as from multiple axle loads, respectively.

Rutting for a Single Axle Load. To estimate the permanent strain from a single load, it is assumed that the stress-strain relationship is of the form shown in Figure 55.

Using geometry, it can be shown that

$$\Delta\varepsilon_a = \sigma \left(\frac{1}{E_1} - \frac{1}{E_u}\right) \tag{12}$$

The fractional increase of the total strain, F(N), that is permanent with load repetition is

$$F(N) = \frac{\Delta\varepsilon_a}{\varepsilon_r + \Delta\varepsilon_a} \tag{13}$$

If it is assumed that the resilient strain, ε_r, is large in comparison to the increase of the permanent strain with each load repetition, then the following approximation can be used:

$$F(N) = \frac{\Delta\varepsilon_a}{\varepsilon_r} \tag{14}$$

since

$$\Delta\varepsilon_a \simeq \frac{\partial \varepsilon_a}{\partial N} \tag{15}$$

The fractional increase of the total strain, F(N), can be expressed as

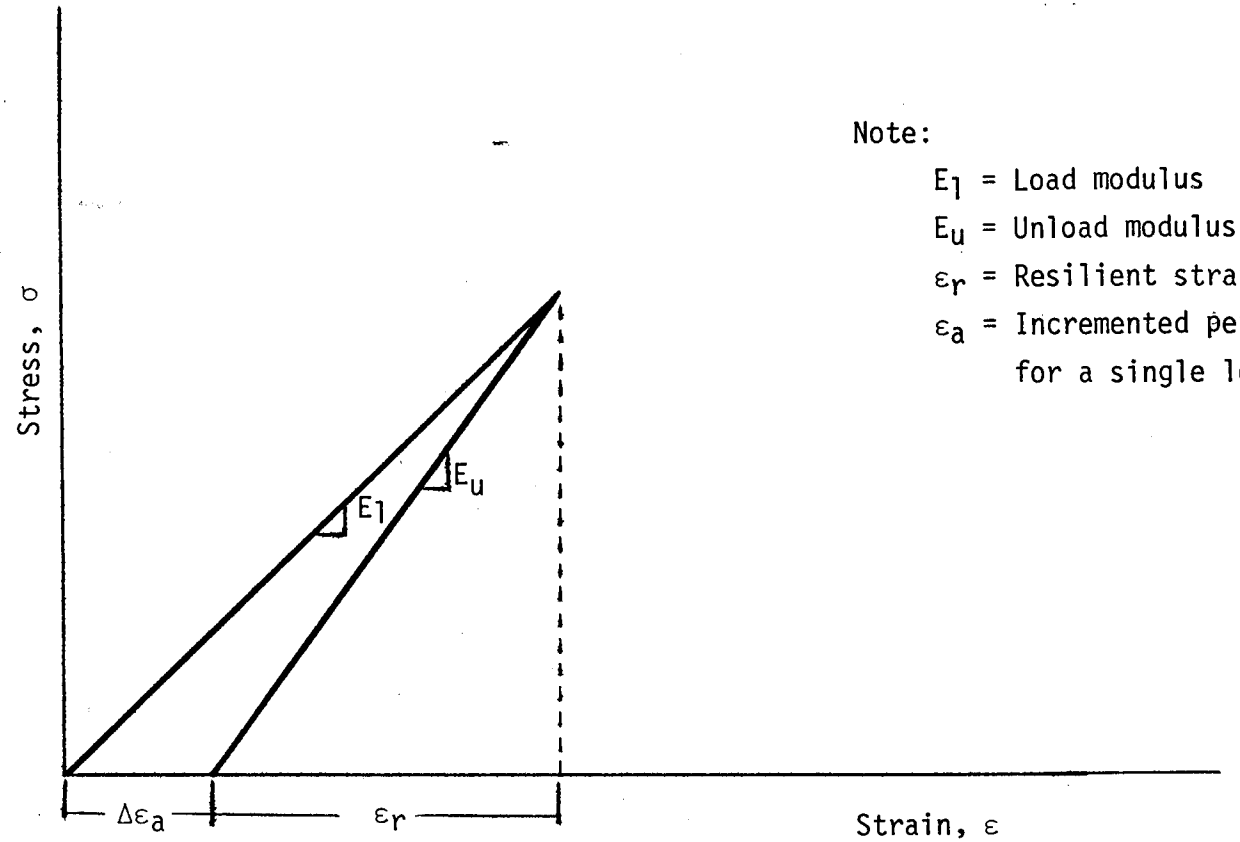

Note:

E_l = Load modulus

E_u = Unload modulus

ε_r = Resilient strain

ε_a = Incremented permanent strain for a single load repetition

Figure 55. Relationship Between Stress Versus Strain for a Single Load Repetition

$$F(N) = \frac{\partial \varepsilon_a}{\varepsilon_r \partial N} = \frac{Eu}{E_1} - 1 \qquad (16)$$

If the first derivative of Equation 5 with respect to N is substituted into Equation 16, F(N) becomes

$$F(N) = \frac{1}{\varepsilon_r} \cdot \frac{\partial \varepsilon_a}{\partial N} = \frac{\varepsilon_o \beta \rho^{\beta}}{\varepsilon_r} \cdot e^{-(\frac{\rho}{N})^{\beta}} N^{-(\beta + 1)} \qquad (17)$$

Then the rut depth, $\delta_a(N)$, may be determined by

$$\delta_a(N) = \int_0^{\varepsilon_a (N)} d\varepsilon_a (N)$$

$$= \int_0^{N} \int_0^{Z\ max} \varepsilon_c (Z)\ F(N)\ dZ\ dN \qquad (18)$$

in which

Zmax = depth of the pavement layer

$\varepsilon_c (Z)$ = compressive strain at depth Z

Equation 18 may be extended to include all the pavement layers as follows:

$$\delta_a(N) = \int_0^N \int_0^{d_1} \varepsilon_c(Z)\, F_1(N)\, dZdN + \int_0^N \int_{d_1}^{d_2} \varepsilon_c(Z)\, F_2(N)\, dZdN$$

$$+ \ldots + \int_0^N \int_{dn-1}^{dn} \varepsilon_c(Z)\, F_n(N)\, dZdN \qquad (19)$$

in which $d_1, d_2, \ldots, d_n$ are the depths of each layer in the pavement, and $F_1, F_2, \ldots, Fn$ are the fractional increases of the total strain for each layer.

By substituting Equation 17 into 19, the rut depth becomes

$$\delta_a(N) = \sum_{i=1}^{n} \int_0^N \nu_i e^{-\left(\frac{\rho i}{N}\right)^{\beta i}} N^{-(\beta+1)}\, dN \int_{d_{i-1}}^{d_i} \varepsilon c\,(Z)\, dZ \qquad (20)$$

in which

n = number of layers

$$\nu = \frac{\varepsilon_o\, \beta\, \rho^{\beta}}{\varepsilon_r}$$

The first integral on the right side of Equation 20 may be solved as

$$\int_0^n \nu_i \, e^{-(\frac{\rho i}{N})^{\beta i}} \, N^{-(\beta_i + 1)} = \frac{\varepsilon_{oi}}{\varepsilon_{ri}} \, e^{-(\frac{\rho i}{N})^{\beta i}} \qquad (21)$$

The second integral on the right side of Equation 20 can be solved numerically using the trapezoidal rule for the given nodal compressive strains computed from finite element analysis. Therefore, the rut depth in Equation 20 becomes

$$\delta_a (N) = \sum_{i=1}^{n} \left\{ \frac{\varepsilon_{oi}}{\varepsilon_{ri}} \, e^{-(\frac{\rho i}{N})^{\beta i}} \int_{d_{i-1}}^{d_i} \varepsilon_c (Z) \, dz \right\} \qquad (22)$$

Rutting for a Dual Axle Load. For a dual axle load on the surface, ε_u and ε_1 are assumed to be the same during the loading and unloading conditions. The relationships between stresses and strains are shown in Figure 56.

Using the geometry in Figure 56, it can be shown that the incremental strain from the first axle (1), is:

$$(\Delta \varepsilon_a)_1 = \sigma_m \left(\frac{1}{E_1} - \frac{1}{E_u}\right) \qquad (23)$$

and the incremental strain from the second axle, (2), is:

$$(\Delta \varepsilon_a)_2 = \Delta\sigma \left(\frac{1}{E_1} - \frac{1}{E_u}\right) \qquad (24)$$

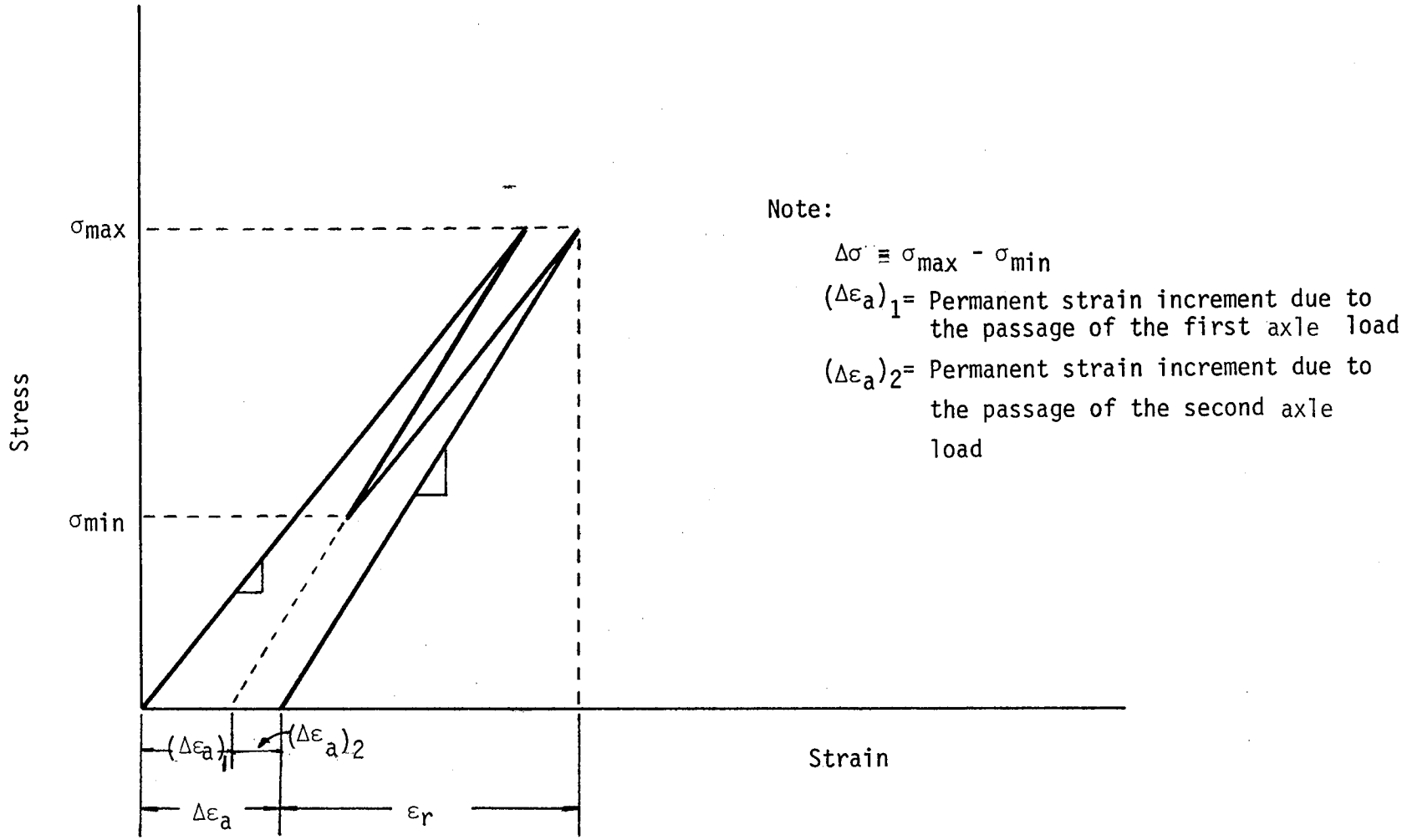

Figure 56. Relationship Between Stress and Strain During the Passage of a Double Axle Load

The total incremental strain from axles 1 and 2 is:

$$\Delta\varepsilon_a = (\Delta\varepsilon a)_1 + (\Delta\varepsilon_a)_2$$

$$= (\sigma_m + \Delta\sigma) \left(\frac{1}{E_1} - \frac{1}{E_u}\right) \tag{25}$$

From Equation 14, the fractional increase of the total strain, F(N), due to a dual axle load can be expressed as

$$F(N) = \left(1 + \frac{\Delta\sigma}{\sigma_m}\right) \left(\frac{E_u}{E_1} - 1\right) \tag{26}$$

Note that $\left(\frac{E_u}{E_1} - 1\right)$ in Equation 26 is the permanent strain resulting from one wheel load as described in equation 16. Equation 26 may be rewritten by substituting Equation 17 in for $\left(\frac{E_u}{E_1} - 1\right)$ as:

$$F(N) = \left(1 + \frac{\Delta\sigma}{\sigma_m}\right) \frac{\varepsilon_0 \beta \rho^\beta}{\varepsilon_r} e^{-\left(\frac{\rho}{N}\right)^\beta} N^{-(\beta + 1)} \tag{27}$$

or

$$F(N) = \left(1 + \frac{\Delta\sigma}{\sigma_m}\right) \nu e^{-\left(\frac{\rho}{N}\right)^\beta} N^{-(\beta + 1)} \tag{28}$$

in which

$$\nu = \frac{\varepsilon_0 \beta \rho^\beta}{\varepsilon_r}$$

As described in the previous section, the rut depth at some specific number of load repetitions can be calculated as:

$$\delta_a(N) = \int_0^N \int_0^{Zmax} \varepsilon_c(Z)F(N)\, dZdN$$

$$= \sum_{i=1}^{n} \left\{ \frac{\varepsilon_{oi}}{\varepsilon_{ri}} e^{-\left(\frac{\rho i}{N}\right)^{\beta i}} \int_{d_{i-1}}^{d_i} \left(1 + \frac{\Delta\sigma(Z)}{\sigma_m(Z)}\right)\varepsilon_c(Z)dZ \right\} \quad (29)$$

in which

$$r_i = \frac{\varepsilon_{oi}}{\varepsilon_{ri}} e^{-\left(\frac{\rho i}{N}\right)^{\beta i}} \qquad \delta_i = \int_{d_{i-1}}^{d_i} \left(1 + \frac{\Delta\sigma(Z)}{\sigma_m(Z)}\right)\varepsilon_c(Z)\, dZ$$

or

$$\delta_a(N) = \sum_{i=1}^{n} r_i \delta_i \quad (30)$$

σmax is determined by superposition as the vertical stress under a single wheel plus the overlap vertical stress at a distance corresponding to the dual axle spacing. σ min is simply twice the vertical stresses at half the dual axle spacing. The distribution of the vertical stresses is assumed to be symmetric and the interaction of the dual tires is ignored. The term $\Delta\sigma$ is the difference between σ max and σ min. The individual values of σ max, σ min, and ε_c varied with the depth of the pavement and the loads. For a particular solution the value for each term is taken from the defined nodal points in the finite element analysis. δ_i for each layer can be calculated by numerical integration using the trapezoidal rule and the estimate for total rut depth at the surface is the summation of r_i times δ_i for each layer (Equation 30).

Rutting for other Multiple Axle Configurations. For a multiple axle configuration shown in Figure 57, the permanent strain increment can be expressed as

$$\Delta\varepsilon_a = (\Delta\varepsilon_a)_1 + (\Delta\varepsilon_a)_2 + \ldots + (\Delta\varepsilon_a)_n \quad (31)$$

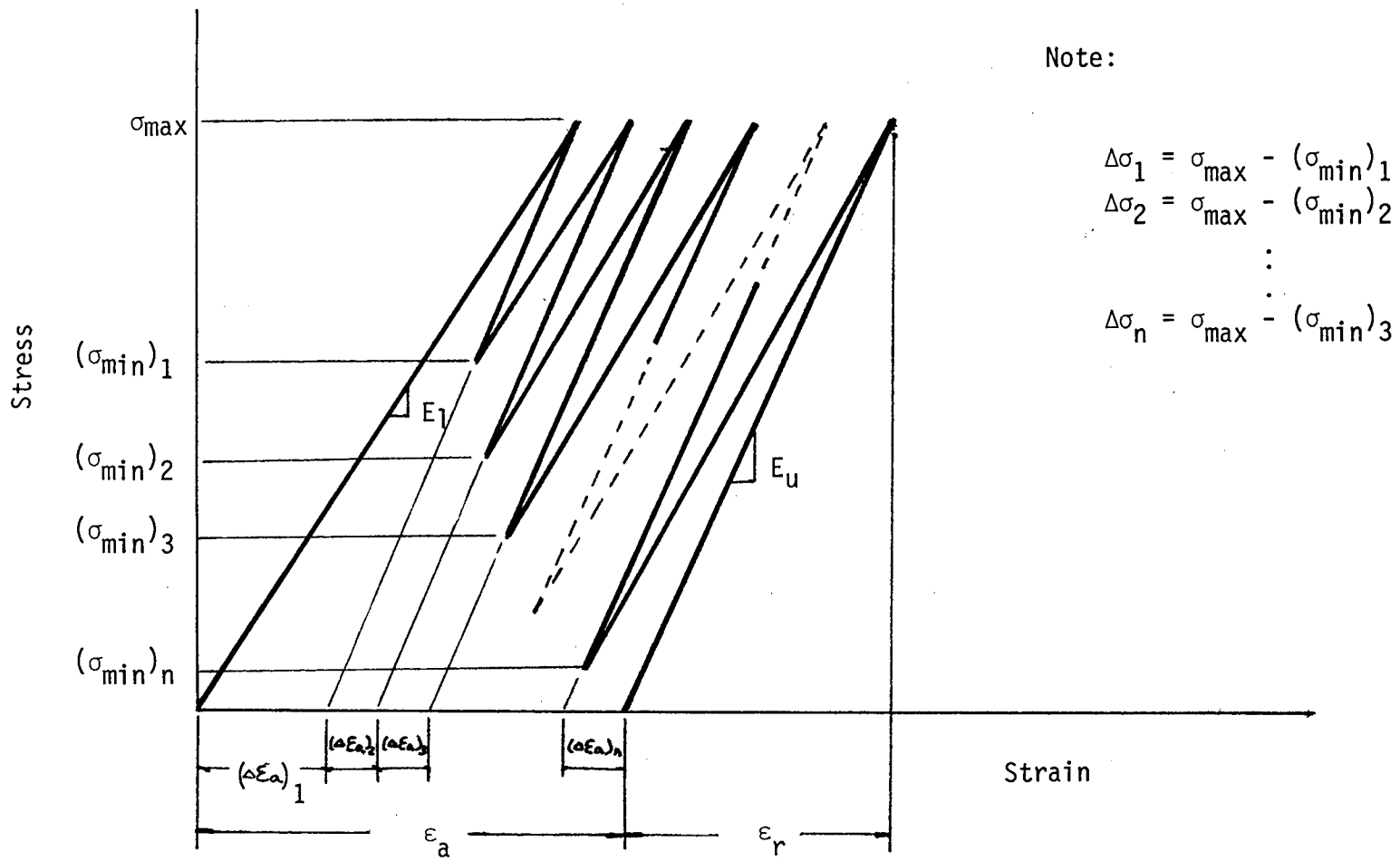

Figure 57. Stress - Strain Relationship for the Multiple Axle Configuration

The subscript n of $\Delta\varepsilon a$ designates the permanent strain increment due to nth axle load in the axle group. Using the geometry relations in Figure 57 the fractional increase of the total strain, F(N), may be formulated as:

$$F(N) = \left(\frac{\Delta\varepsilon_a}{\varepsilon_r}\right) = \left(1 + \frac{\Delta\sigma_1}{\sigma_m} + \frac{\Delta\sigma_2}{\sigma_m} + \ldots + \frac{\Delta\sigma_n}{\sigma_m}\right)\left(\frac{E_u}{E_1} - 1\right) \qquad (32)$$

Equation 16 of the previous section defines the permanent strain due to one wheel load and is also equal to $\nu\, e^{-(\frac{\rho}{N})^{\beta}} N^{-(\beta+1)}$ in Equation 28. Replacement of this value in Equation 32 gives the following equation for F(N):

$$F(N) = \left(1 + \frac{\Delta\sigma_1}{\sigma_m} + \frac{\Delta\sigma_2}{\sigma_m} + \ldots + \frac{\Delta\sigma_n}{\sigma_m}\right) \nu\, e^{-(\frac{\rho}{N})^{\beta}} N^{-(\beta+1)} \qquad (33)$$

Thus, the equation for rut depth is of the same form as before

$$r_i(N) = \frac{\varepsilon_{oi}}{\varepsilon_{ri}} e^{-(\frac{\rho i}{N})^{\beta i}} \qquad (34)$$

$$\delta_i(Z) = \int_{d_{i-1}}^{d_i} \left[1 + \sum_{j=1}^{k} \frac{\Delta\sigma_j}{\sigma_m}\right] \varepsilon_c(Z)\, dZ \qquad (35)$$

in which k = number of axles in axle group

And the rut depth is

$$\delta_a(N) = \sum_{i=1}^{n} r_i(N)\, \delta_i \qquad (36)$$

Slope Variance

The calculation of slope variance for use in the AASHO equation for present serviceability index (PSI) is based on the following equation that was developed by Soussou, et. al. (23).

$$E\,[sv] = \frac{2B}{C^2}\,\sigma_n\,(E[\delta a]^2 + Var\,[\delta a]) \qquad (37)$$

in which

E[sv] = expected value of slope variance in radians x 10^6

Var[δa] = rut depth variance

E[δa] = expected value of rut depth

σ_n^2 = variation of deflection response

B and C = roughness properties

Equation 37 is based on the auto-correlation function for surface deformation which is derived from the spatial correlation of the material properties. It has been shown in Reference (24) that the mean slope variance in Equation 37 may be approximated as

$$E\,[sv] = \frac{2B}{C^2}\quad Var\,[\delta a] \qquad (38)$$

Rauhut et.al. (24) reported that the values of B and C used in Equation 38 were obtained by running regression on field studies of pavement roughness measurements. Values of B = 1 and C = 0.058, as proposed by Kenis (25), provide reasonable estimates of roughness. An expression for the variance of rut depth has been derived on the basis of probabilistic analysis as

$$\text{Var}\,[\delta_a(N)] = \sum_{i=1}^{n} [\delta_i]^2\ \text{Var}[r_i(N)] + \sum_{i=1}^{n} [r_i(N)]^2\ \text{Var}\,[\delta_i] \tag{39}$$

If one assumes that the compressive strain, ε_c, is a constant, and that and $\Delta\sigma_j$ in Equation 35 are independent, the var $[\delta i]$ may be written as

$$\text{Var}[\delta_i] = \varepsilon_c^{\,2}\,(d_i - d_{i-1})^2 \left(\frac{\text{c.v.}^2[\sigma_{mi}]}{\sigma_{mi}^2} + \sum_{j=1}^{k} \frac{\text{Var}[\Delta\sigma_j]}{\sigma_{mi}^2}\right) \tag{40}$$

$$= \varepsilon_c^{\,2}(d_i - d_{i-1})^2 \left(\frac{\text{c.v.}^2[\sigma_{mi}]}{\sigma_{mi}^2} + \text{c.v.}[\Delta\sigma_j] \sum_{j=1}^{k} \frac{\Delta\sigma_j}{\sigma_{mi}}\right)^2 \tag{41}$$

in which

$\text{c.v.}[\sigma_m]$ = Coefficient of variation of σ_m

$\text{c.v.}[\Delta\sigma]$ = Coefficient of variation of $\Delta\sigma$

Equation 41 can be further simplified by assuming that the squared coefficient of the variation terms are zero. Equation 41 becomes

$$\text{Var}[\delta_i] = \varepsilon_c^{\,2}(d_i - d_{i-1})^2\ (\text{c.v.}[\Delta\sigma_j] \sum_{j=1}^{k} \frac{\Delta\sigma_j}{\sigma_{mi}})^2 \tag{42}$$

For specific material in a pavement structure, r_i is a function of the number of load cycles, N. If N is assumed to follow a Poisson distribution; then the variance of r_i may be written as

$$\text{Var}[r_i] = \frac{\varepsilon_{oi}}{\varepsilon_{ri}}\, e^{-\left(\frac{\rho i}{N}\right)^{\beta i}} \tag{43}$$

in which N = mean number of load cycles. Thus, the mean slope variance, E[SV], in Equation 38 can be solved in terms of Equation 39 in conjunction with Equations 42, 43, 34, and 35.

Fatigue Cracking

The estimation of fatigue cracking made in this study are to be used in a cracking model presented by Rauhut et.al. (24). The estimates of fatigue cracking are one component in a cracking term called cracking index. Cracking index is based on a modified stochastic Miners Hypothesis progression of cracking damage in asphalt concrete surface materials. The primary contribution to this cracking is produced by tensile strains occurring at the bottom of the surface layer. These strains induce a fatigue failure. The equation for cracking index used in this program is :

$$C_j = \sum_{i=1}^{j} \frac{n_i}{N_i} \tag{44}$$

in which

C_j = crack index at times j

n_i = number of cycles of load during the ith time interval,

N_i = number of cycles to failure for the ith time interval

The relationship of N_i is

$$\frac{1}{N_i} = \frac{\epsilon^{k_{2i}}}{K_{1i}} \tag{45}$$

in which

K_{1i} = fatigue coefficient for ith time interval

K_{2i} = fatigue exponent for ith time interval

ε = radial strain

It is futher assumed that C_j takes on a normal distribution with mean $E[C_j]$. Thus, the expected area of cracking, in terms of square yards of cracking per 1000 square yard of surface, is given by the probability of C_j being greater than 1. Detailed development of the cracking index equations can be found in Reference 24.

EXAMPLE PROBLEM

Use of the modified ILLIPAVE to predict the performance of pavements requires input of data in the form of pavement and loading geometry, environment, traffic characteristics, material properties, and pavement system performance bound.

Development of Input Data. A detailed description of the major input data is given below and classified as structural properties, distress properties, stocastic coefficients, traffic volume, seasonal temperature, and loading geometry. The finite element mesh used in this example shown in Figure 58. This problem does not include interface elements, or analysis of the interface, i.e., complete bond is assured between layers. A listing of the input data used in this example problem is contained in Tables 15,16,17,18 and 19.

Structural Properties. The resilient modulus is one of the major descriptors that define the structural behavior in pavements. Since the modulus of asphalt concrete materials changes with seasonal temperature, a graph such as that included in Figure 59 can be developed from a series of repeated load testing or static indirect tensile tests at different

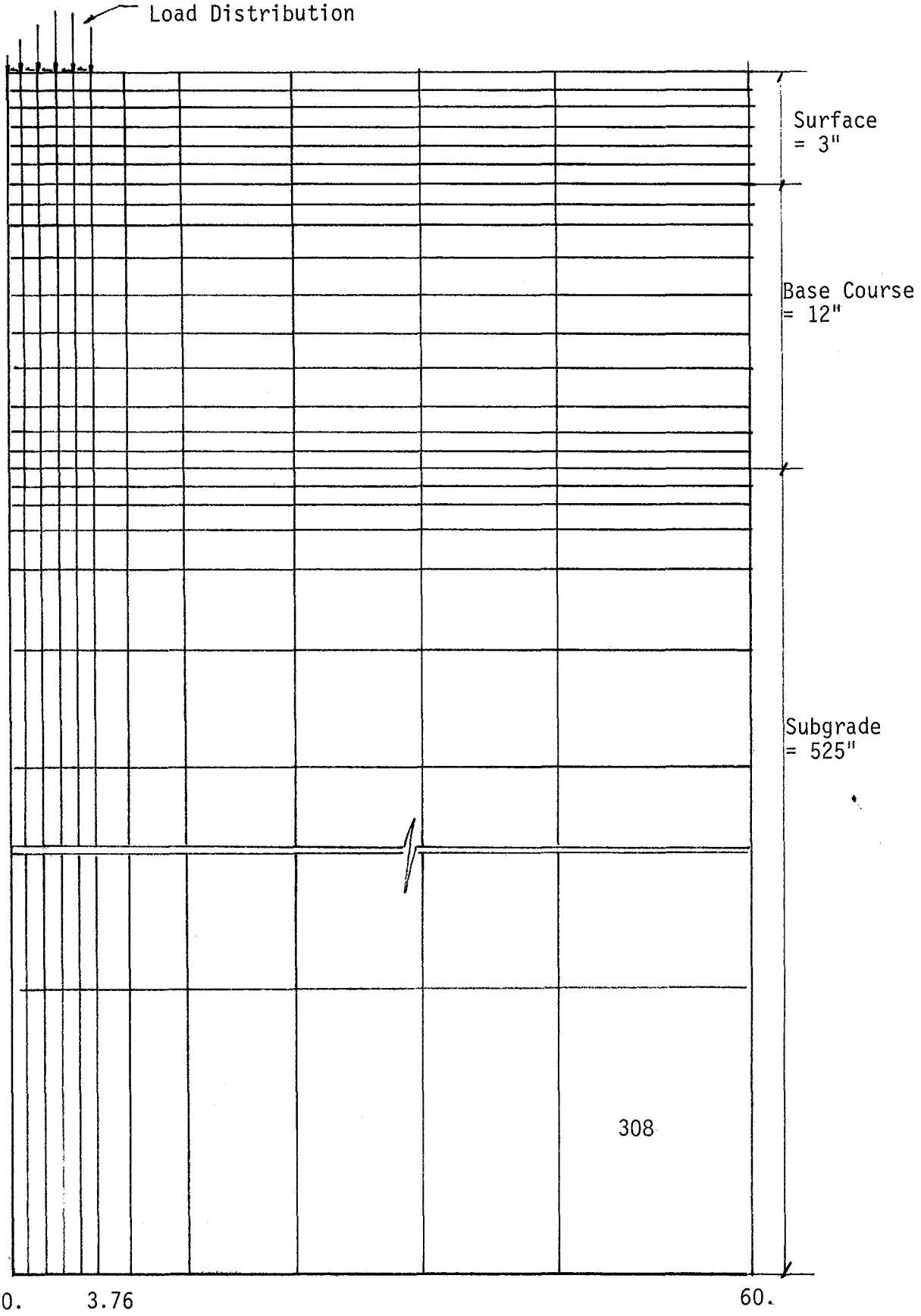

Figure 58. Finite Element Mesh for Example Problem

Table 15. Example Problem General Input Data

Length of the Analysis Period in Years	20
Intial Number of 18 kip Equivalent Single Axle Loads/day	150
Final Number of 18 kip ESAL/day	150
Radius of Loaded Circular Area, inches	3.76
Intensity of Loading	(shown in Table 6)
Thickness of Surface Course, inches	3
Thickness of Base Course, inches	12
Thickness of Subgrade Course, inches	525
Serviceability Index at Time Zero	4.2
Roughness Property B	1
Roughness Property C	0.058
Coefficient of Variance K_1	0.2
Coefficient of Variance K_2	0.04
Coefficient of Covariance K_1, K_2	-0.9

Table 16. Load Inputs for Example Problem

Node	Force, lb.	
	Normal	Tangential
1	-8.15	0.0
2	-70.12	-17.87
3	-171.68	-51.20
4	-233.36	-74.59
5	-179.59	-59.87
6	-58.33	-20.05

Table 17. Seasonal Temperature Variations Within a Year For the Site of the Example Problem

Length of Season, Months	Temperature, (°F)	
	Summer	Winter
7	77	
5		56.3

Table 18. Resilient Moduli of Each Layer for the Example Problem

Resilient Moduli, ε_r, in psi			
Surface		Base	Subgrade
at 77°F	at 56.3°F		
380,000	1,100,000	$\varepsilon_r = k_1\ \theta^{k_2}$ $k_1 = 3746.1$ $k_2 = 0.532$	8,450

Table 19. Material Properties for Calculating Distress for the Example Problem

	Fatigue Parameters				Permanent Deformation Properties			
	at 77°F		at 56.3°F					
	k_1	k_2	k_1	k_2	ε_o	β	ρ	ε_r
ASP. Conc. With Limestone Agg. Surface	3.112×10^{-6}	3.138	7.799×10^{-8}	3.541	0.649×10^{-2}	0.098	0.573×10^{8}	0.264×10^{-4}
Crushed Granite Gneiss Base					0.171×10^{-1}	0.173	0.363×10^{4}	0.123×10^{-2}
Moscow Soil (CH) Subgrade					0.157	0.135	0.242×10^{9}	0.114×10^{-2}

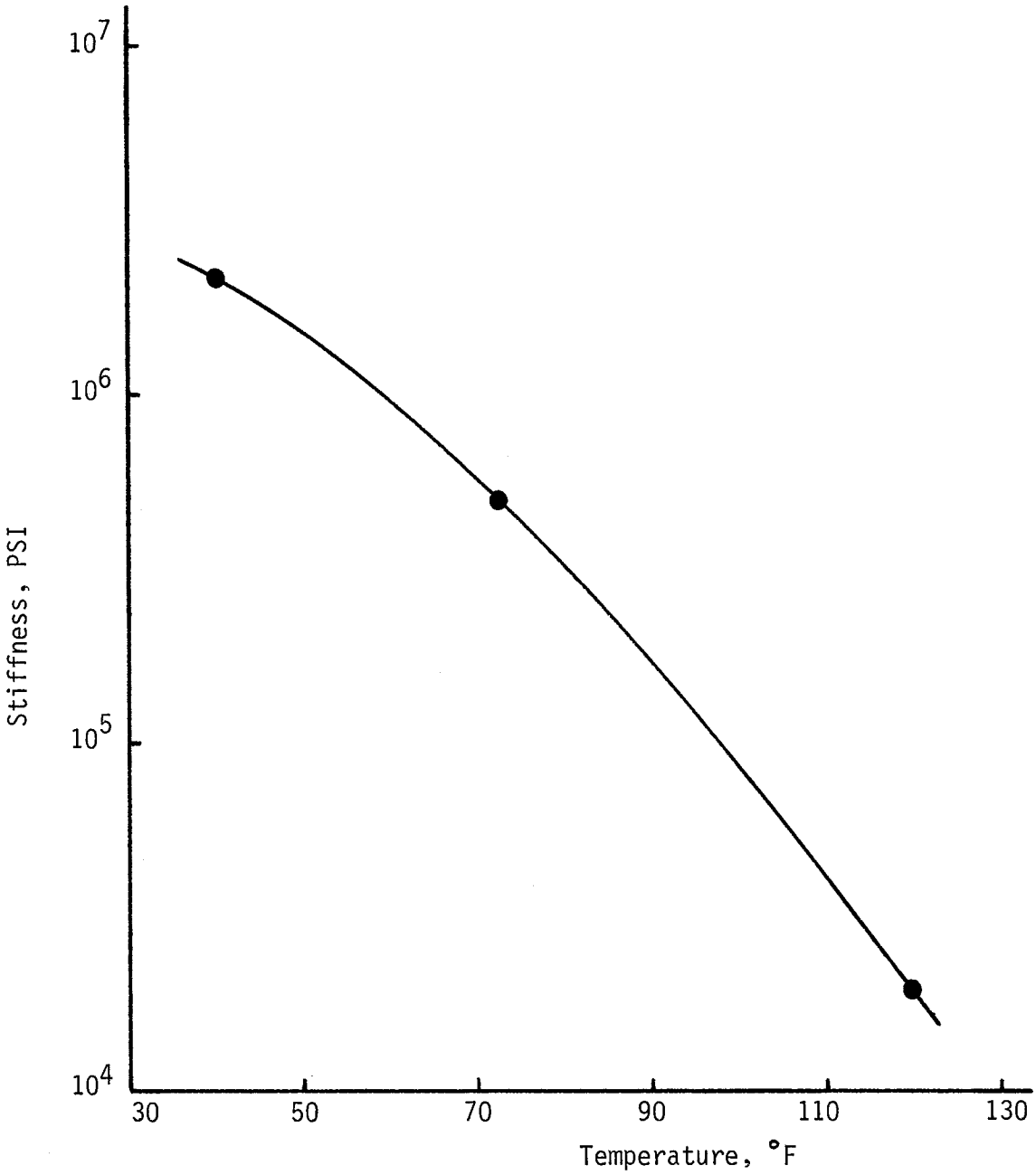

Figure 59. Relationship of Stiffness Versus Various Temperature

temperatures. Other methods such as the regression equation developed by Witczak (26) may also be used to estimate the resilient modulus of asphalt concrete. In addition to above methods, the Van der Poel and Huekelom nomographs (27 and 28) may be used where mixture laboratory test results are not avaiable. To determine mixture stiffness using these nomographs the following properties are required: (1) percent air voids in the compacted mixture, (2) ring-and-ball softening point penetration index of the bitumen, and (3) volume concentration of the aggregate in the compacted mass.

The modulus of a base material an be expressed in terms of the sum of the three principal stresses as mentioned in Equation 1. Two parameter, k_1 and k_2, are determined using results of repeated triaxial tests by plotting on log-log paper the modulus versus the sum of the three principal stresses. Rada and Witczak (29) performed an extensive study to evaluate the resilient moduli of granular materials and summarized the average values and ranges of k_1 and k_2.

The modulus of subgrade soils is greatly influenced by environmental factors and stress state. The resilient modulus of a soil may be obtained by developing a relation similar to that shown in Figure 2. These data can be developed from repeated load triaxial tests or from dynamic deflection measurements with representative traffic loads in situation (30). Edris (22) conducted a comprehensive study on subgrade soils which included soils with different clay contracts ranging from 20% to 70%. The regression equations have been developed for these soils with their temperature correction factors. The resilient moduli for the three materials used in this example problem are included in Table 18. The data were developed from information in Reference 21, 22, and 23.

Distress Properties. Distress Properties include the parameters to characterize the development of permanent deformation and fatigue in the pavement structure. Three parameters, ε_o, β , and ρ , are used to represent the permanent deformation in each pavement layer, as previously described in this chapter. The permanent deformation relationships used in this example problem are included in Table 19. It should be noted

that, while temperature affects the permanent deformation parameters, the temperature effects are ignored in this problem because of a lack of data to decribe those effects.

The fatigue parameters, k_1 and k_2, can be obtained from plots of strain versus the number of loads to failure of asphalt concrete at different temperatures. In the modified ILLI-PAVE program the fatigue parameters k_1 and k_2 have been related to an average seasonal temperature. As shown in Table 17, only two seasonal changes are considered summer and winter which are of length seven and five months, respectively. Several methods are available for estimating the variation in fatigue parameters with temperature, including the procedures by Witczak (32) and Rauhut (24). Witczak assumes that the parameter k_2 is constant and the parameter k_1 varies with temperature, while Rauhut includes some variations of k_2 with temperature.

Stochastic Coefficients. The Stochastic Coefficients required as input to the program are the coefficients of variation of the fatigue parameters and the roughness properties as shown in Table 19. The coefficients of variation of the fatigue parameters are used in conjunction with the fatigue parameters and strains at various conditions to calculate the mean and variation in the number of load cycles to failure. These data are in turn used to calculate a cracking index.

Roughness properties are used to calculate slope variance, as described in the previous section. This slope variance and the predicted distress is used to predict the serviceability in References 24, 25, and 33 which include detailed discussion of these variables.

Seasonal Variation. In the program seasonal variation can be evaluated by up to 12 different periods. The number of seasons selected should reflect the effect of environment on the properties of various pavement layers during a year. For each season, the input temperatures should represent the average over that length of time. The program evaluates the structural response of the pavement for each season.

Traffic Volume. The traffic volumes are generally obtained from the traffic and planning personnel who estimate current traffic and then project it over the length of the design period. The traffic inputs to the program are based on the traffic characteristics having a significant influence on pavement behavior. For this example problem the equivalent 18 kips axle loads provided by AASHTO INTERIM GUIDE are used as input to the program. The above method requires the data such as initial ADT, projected 20-year ADT (average daily traffic), percent of truck, and loadometer station data. Therefore, the input data shown in Table 15 represents the average number of equivalent 18 kip single axle load applications per day in the design lane.

Description of Program Output. The output from modified ILLIPAVE for the example problem is included in Table 20. The first two pages of the output are a printout of the input data including the finite element configuration, load conditions, modulus characteristics of each pavement material, traffic data, fatigue and permanent deformation properties, and stochastic coefficients.

In the input data section several things should be mentioned. Several options were available in the original ILLIPAVE program to describe the stress-strain behavior of the pavement materials. A value of 3 assigned to the surface and subgrade in the "MAT PROP" section of the "SUMMARY OF MATERIAL PROPERTIES" means that the moduli of these materials is constant. Alternatively, a value of 5 for the base course means that the resilient moduli of the asphalt concrete has two values, 380,000 and 1,100,000, to reflect the seasonal temperature change while the modulus of the subgrade is constant. However, the user may vary the modulus of subgrade varied with temperature or seasonal change. Since the modulus of the base course is a function of bulk stress, the coefficients k_1 and k_2 are shown in as "K1" and "K2", respectively. It should be noted that for the base material, the value of 8,000 in "MODULUS" is the modulus of the material at failure rather than the

Table 20. Example Problem Output for Modified ILLIPAVE.

```
O  IH - HIGH THICKNESS, T.P.=  75 PSI (TEMP - PORT ARTHUR) (BOND CASE)

 NUMBER OF NODAL POINTS------        348

 NUMBER OF ELEMENTS----------        308

 NUMBER OF DIFF. MATERIALS---          3

 NUMBER OF APPROXIMATIONS----          1

 PAVEMENT THICKNESS----------      15.00

 SUBGRADE THICKNESS----------     525.00

 RADIUS OF LOADED AREA ------       3.76

 SURFACE PRESSURE -----------     101.32

 TOTAL PLATE LOAD -----------    4500.00

 TOTAL NUMBER OF STEPS TO BE PRINTED OUT ---          1
 THE INDIVIDUAL STEP NUMBERS TO PRINTED OUT ARE
                                                      1

 ********************************************************************************************************************
SUMMARY OF MATERIAL PROPERTIES
********************************************************************************************************************

MTYPE=  1   DENSITY=145.00000   KZERO=  0.67   THICKNESS=    3.00

        MODULUS         POIS RA           K1           K2           K3           K4        MAT PROP
      380000.00            0.36          0.0          0.0          0.0          0.0            3.00

     1100000.00            0.32          0.0          0.0          0.0          0.0            3.00


MTYPE=  2   DENSITY=137.00000   KZERO=  0.60   THICKNESS=   12.00

        MODULUS         POIS RA           K1           K2           K3           K4        MAT PROP
        8000.00            0.40      3746.10         0.53        10.00         0.10            5.00


MTYPE=  3   DENSITY=106.00000   KZERO=  0.82   THICKNESS=  525.00

        MODULUS         POIS RA           K1           K2           K3           K4        MAT PROP
       12000.00            0.45          0.0          0.0          0.0          0.0            3.00


 ********************************************************************************************************************
AXLE LOAD CONDITION, REQUIRED ANALYSIS PERIOD, AND TRAFFIC RATE
********************************************************************************************************************
NUMBER OF AXLE LOAD                    =    1
NUMBER OF INCREMENTAL ANALYSIS PERIOD  =    8

      INCREMENTAL
     ANALYSIS PERIOD       TRAFFIC RATE
       (YEAR)           (TRUCK/LN/DAY)
     --------------       ------------

          1.0                150.0
          2.0                150.0
          4.0                150.0
          6.0                150.0
          8.0                150.0
         10.0                150.0
         15.0                150.0
         20.0                150.0
```

Table 20. (Continued)

PERMANENT DEFORMATION PROPERTIES

LAYER 1

SEASONAL CHANGE	EO/ER	RHO	BETA
1	0.246D+03	0.573D+08	0.983D-01
2	0.246D+03	0.573D+08	0.983D-01

LAYER 2

SEASONAL CHANGE	EO/ER	RHO	BETA
1	0.139D+02	0.363D+04	0.173D+00
2	0.139D+02	0.363D+04	0.173D+00

LAYER 3

SEASONAL CHANGE	EO/ER	RHO	BETA
1	0.137D+03	0.242D+09	0.135D+00
2	0.137D+03	0.242D+09	0.135D+00

COEFFICIENTS OF ROUGHNESS PROPERTIES AND VARIATION COEF. FATIGUE PROPERTIES

ROUGHNESS PROPERTY COEFFICIENT B = 1.000
ROUGHNESS PROPERTY COEFFICIENT C = 0.058
COEFFICIENT OF VARIATION K1 = 0.200
COEFFICIENT OF VARIATION K2 = 0.040
CORRELATION COEFFICIENT OF K1 AND K2 = -0.900
CHECK WRIOUT= 0

RUT DEPTH

YEARS	LOADING CYCLE	RUT DEPTH	VARIANCE RUT DEPTH
1.0	54750.0	0.13035D+00	0.10696D-02
2.0	109500.0	0.15540D+00	0.13012D-02
4.0	219000.0	0.18391D+00	0.15674D-02
6.0	328500.0	0.20222D+00	0.17397D-02
8.0	438000.0	0.21595D+00	0.18694D-02
10.0	547500.0	0.22701D+00	0.19743D-02
15.0	821250.0	0.24803D+00	0.21741D-02
20.0	1095000.0	0.26364D+00	0.23231D-02

FATIGUE CRACKING

TEMPERATURE DEGREE-F	RADIAL STRAIN	K1	K2	FAIL CYCLES
77.0	0.4444D-03	0.3112D-05	0.3138D+01	0.76944D+05
56.3	0.2207D-03	0.7799D-07	0.3541D+01	0.44997D+06

YEARS	DAMAGE INDEX	AREA CRACKED
1.0	0.4655D+00	0.2824D-03
2.0	0.9310D+00	0.3237D+03
4.0	0.1862D+01	0.1000D+04
6.0	0.2793D+01	0.1000D+04
8.0	0.3724D+01	0.1000D+04
10.0	0.4655D+01	0.1000D+04
15.0	0.6983D+01	0.1000D+04
20.0	0.9310D+01	0.1000D+04

Table 20. (Continued)

PERFORMANCE

INITIAL PRESENT SERVICEABILITY INDEX = 4.2

YEARS	SLOPE VARIANCE	AREA CRACKED	RUT DEPTH	SERVICEABILITY
1.0	0.6359D+00	0.2824D-03	0.1304D+00	0.3768D+01
2.0	0.7736D+00	0.3237D+03	0.1554D+00	0.3511D+01
4.0	0.9319D+00	0.1000D+04	0.1839D+00	0.3291D+01
6.0	0.1034D+01	0.1000D+04	0.2022D+00	0.3238D+01
8.0	0.1111D+01	0.1000D+04	0.2159D+00	0.3199D+01
10.0	0.1174D+01	0.1000D+04	0.2270D+00	0.3169D+01
15.0	0.1293D+01	0.1000D+04	0.2480D+00	0.3111D+01
20.0	0.1381D+01	0.1000D+04	0.2636D+00	0.3068D+01

resilient modulus which is in the "MAT-PROP" and is defined as 5, a function of bulk stress.

The last two pages of output are the predicted distress analysis; including predictions of rut depth, fatigue cracking, and present serviceability. Since one of the primary objectives for the modified ILLIPAVE is to predict the distresses and performance of pavement, the listing of deflections and stresses for each nodal point and element included in ILLI-PAVE has been eliminated. The calculation of rut depth for specific loading cycles is based on equation 36 and required the use of the strains and stresses (in case of multiple axles) in each layer and the permanent deformation properties of each material. The variance of rut depth was calculated using equation 38.

The prediction of fatigue cracking is based on the model presented by Rauhut et.al.(24). "RADIAL STRAIN" in the "FATIGUE CRACKING" section of the output varies with temperature. In the program "FAIL CYCLES" is calculated using the expected value of the Taylor series expansion of the reciprocal of the number of cycles to failure. It should be noted that the variation of radial strain is ignored in the calculation of "FAIL CYCLES". Therefore, the modified ILLIPAVE value of "FAIL CYCLES" will be slightly larger than that of "FAIL CYCLES" by Rauhut. "AREA CRACKED" represents the estimate of the square yards of cracking per thousand square yards surface area and is computed from the assumed normal distribution of damage index based on probabilities Miner's hypothesis. For this approach, a damage index of 1.0 represents a pavement with 100% of the area cracked.

The overall structural performance of pavements is often expressed in terms of present serviceability index developed first at the AASHO road test (31). This index is predicted from factors measured on a pavement surface including, rut depth, slope variance, cracking and patching, and predicted from the following equation:

$$PSI = 5.03 - 1.91 \log_{10} (1 + SV) - 0.01\sqrt{C+P} - 1.38 (RD)^2 \text{ in which} \quad (46)$$

PSI = present serviceability index

SV = slope variance

C + P = amount of cracking and patching on the paving surface, square feet per 1000 square feet of surface area.

RD = rut depth, inches

Since no prediction is made for the area of patching, that term has been left out in the program.

CHAPTER 5
EVALUATION OF THE EFFECTS OF TIRE PRESSURES ON FLEXIBLE PAVEMENTS

INTRODUCTION

This chapter includes a description of a series of studies to evaluate the effects of tire pressures on flexible pavements in Texas. These studies included contact pressure distributions for both truck and automobile tires. These results are from two SDHPT studies that were being conducted at the same time and which shared efforts and results. The first section in this chapter is a summary of an analytical study reported by Roberts and Rosson (34) to determine the material properties required for thin asphalt concrete pavements to perform properly. The second section is a summary of a study by Roberts and Urruela (35) to evaluate the effects of passenger car tires on thin asphalt concrete pavements. These first two studies were performed with the original ILLIPAVE program modified to allow input of nonuniform contact pressure distributions. The third section contains the results of a study using the modified ILLIPAVE program described in Chapter 4 of this report.

TRUCK TIRE STUDY WITH ILLIPAVE

For this study, a typical 10.00-20 bias-ply truck tire carcass was obtained; the input data for the Tielking tire model was developed by performing measurements on a section of the tire; and the tire pressure distributions were calculated. Figure 60 shows the vertical and horizontal contact pressure distributions for this tire inflated to 125 psi.

Two tire pressures were selected for this analysis, 75 psi and 125 psi. These two values were selected because the first value represents a typical historical value used for design and analysis of highway pavements structures, and the second value represents a value typical of the current inflation pressure on Texas highways.

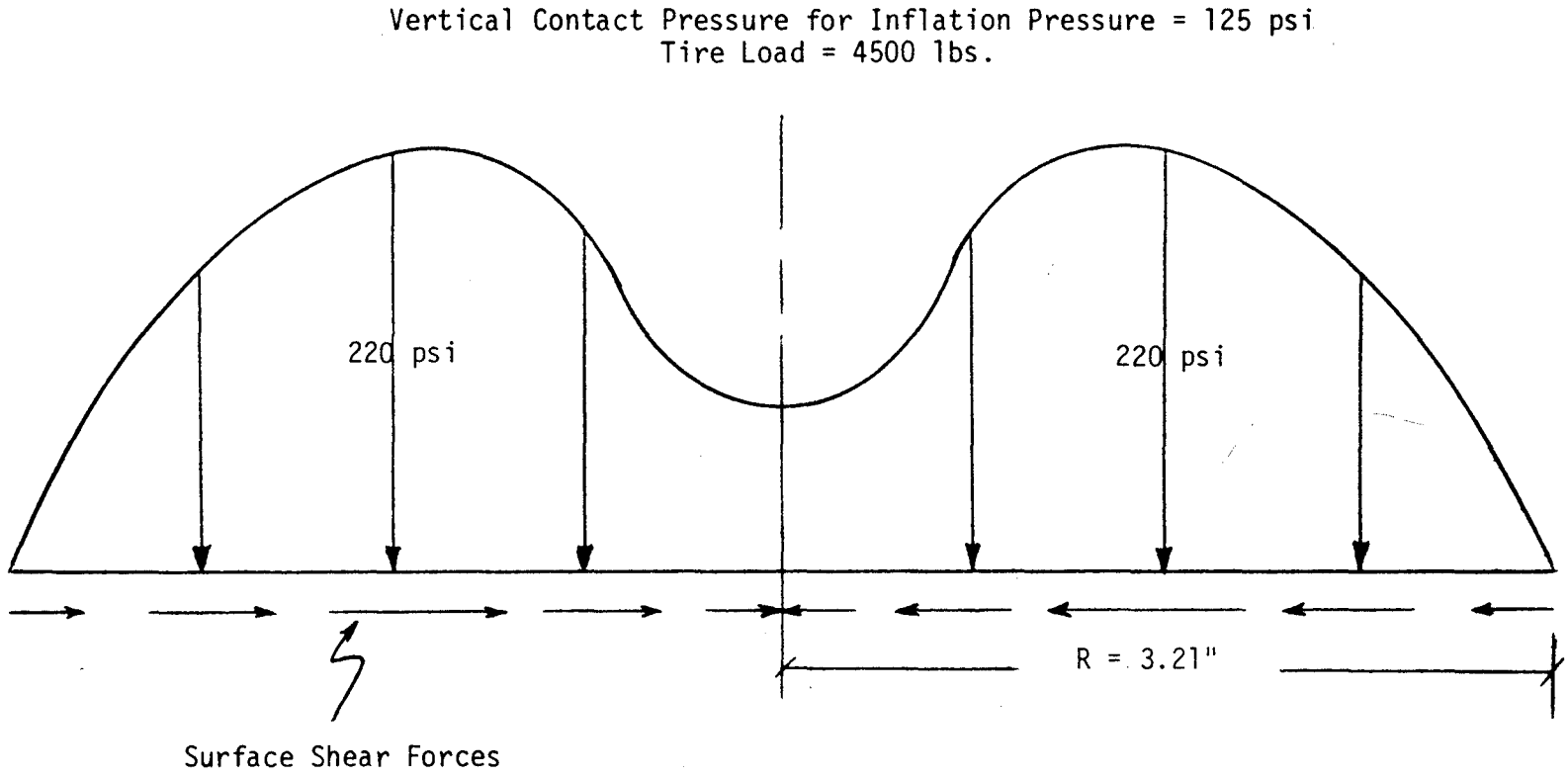

Figure 60. Non-linear vertical tire pressure distribution with lateral surface shear forces as developed using finite element model by Tielking.

Study Parameters

The basic objective of this portion of the report is to evaluate the effects of increased tire pressure on thin asphalt concrete pavements that are typically used on the Texas farm to market system. Therefore, the following series of material combinations and layer thicknesses were used to determine the stress and strain state for two different tire inflation pressures and a 4500 lb. single wheel load:

Surface

Thicknesses: 1, 1.5, 2, and 4 inches

Elastic Moduli: 50, 100, 200, 400, and 800 ksi

Base

Thicknesses: 8 inches

Elastic Moduli: Stress-Sensitive

Equation	Typical Base Moduli, psi
$4886\ \Theta^{0.239}$	20,000
$7000\ \Theta^{0.325}$	40,000
$8787\ \Theta^{0.365}$	60,000

where Θ = bulk stress

Subgrade

Thicknesses: Infinite

Elastic Moduli: As defined in Figure 61

NOTE: Only one subgrade soil was included in this analysis.

Study Results

Several types of comparisons were made using results from the ILLIPAVE computer runs. Comparisons in this report include plots to show the effects of tire pressure on horizontal tensile strain at the bottom of the surface. Reference 34 includes additional plots to evaluate the effects of base modulus on tensile strain and the effects of both surface thickness and modulus on strains. An additional analysis included in this report evaluates the effect of the tensile strains on predicted

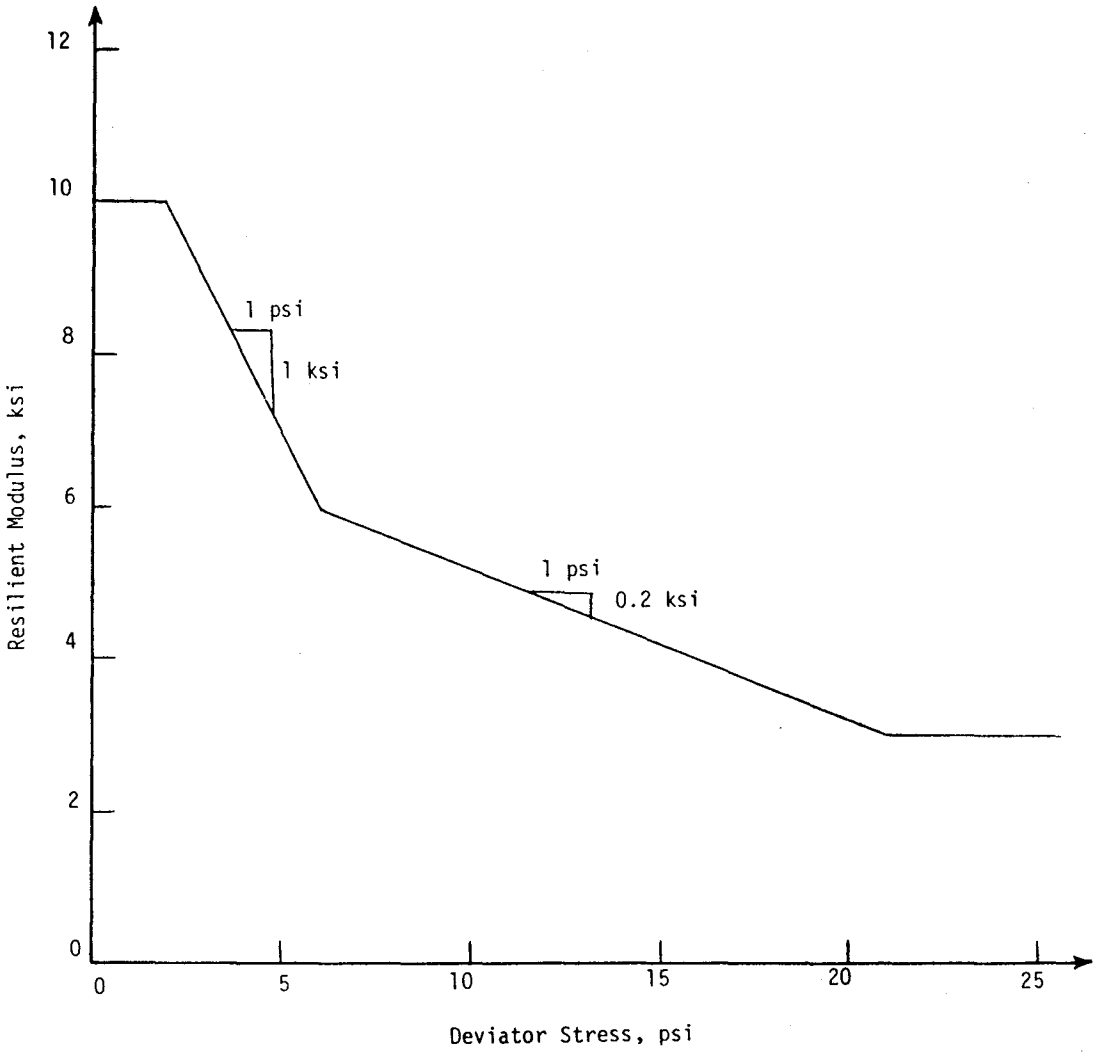

Figure 61. Resilient modulus-deviator stress relationship for subgrade soil.

fatigue damage. Each analysis will be presented seperately in the following section.

Tire Pressure Effects. The series of computer runs used in this analysis is the same set described in the study parameters section. All runs for this analysis included a 4500 lb. load with nonuniform vertical pressure and with lateral surface shear forces. To describe the effects of tire pressure on tensile strain Figures 62 and 63 have been prepared. Figure 62 shows the change in tensile strain for a surface of varying thickness and with a modulus of 400 ksi while Figure 63 shows the same information for a surface with a modulus of 50 ksi.

The increase in tire contact pressure produces increases in the strain ranging from 20 to 30 percent for the 1-inch surface data in Figure 62 with the 30 percent increase occurring for the stiffest base layer. Notice that the effect of increased tire pressure decreases with increasing surface thickness and that the relative increase for a 4-inch surface is less than 10 percent.

Figure 63 shows that at 75 psi inflation pressure a surface one inch thick is in compression for the moderate and strong bases and that the tensile strain is low for the weak base. However, when the inflation pressure increases to 125 psi, the 1-inch surface still remains in compression for the moderate and strong bases but the tensile strain increases dramatically for the weak base condition. In fact, for the low modulus base all the thicknesses experience strains near or in excess of 0.001 in./in. which Monismith says is the upper limit of linear behavior of these materials: "...for strains exceeding 0.001 in./in., asphalt concrete mixtures are nonlinear, rate dependent materials with different properties in tension and compression" (36).

The increases in strain for the 2-inch surface range from about 30 to 55 percent for the weak to strong bases, indicating the significance of the effect of increasing tire pressures on surfaces having low moduli. Therefore, it is important to recognize that the general advice often given, to make thin pavements flexible, must be conditioned by adding that the surface thickness should be limited to less than 1.5 inches for moderate and strong bases. In fact, these very flexible asphalt concrete type materials should probably not be used in combination with weak

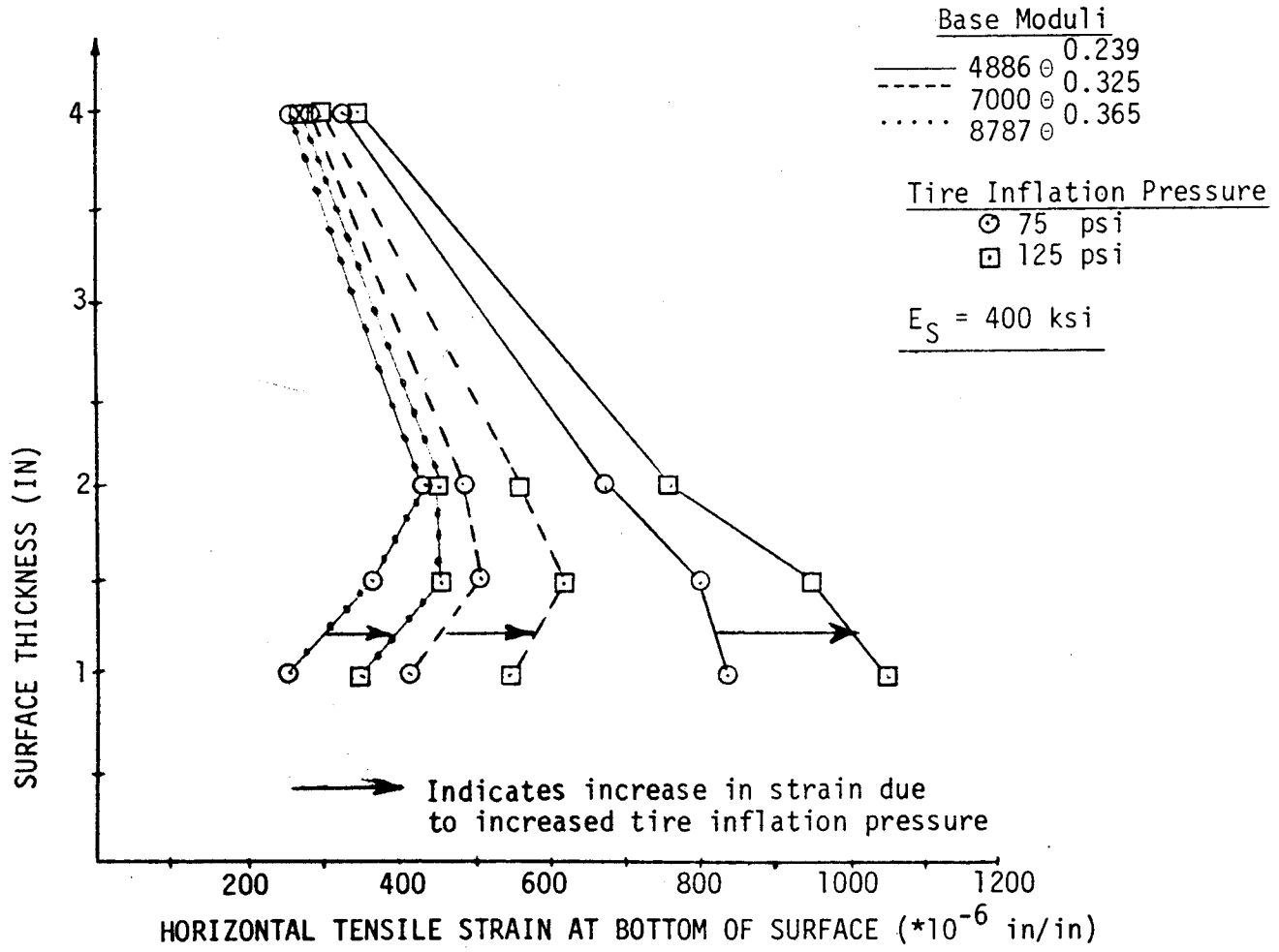

Figure 62. Effects of increased tire pressure on tensile strain for a surface modulus of 400 ksi.

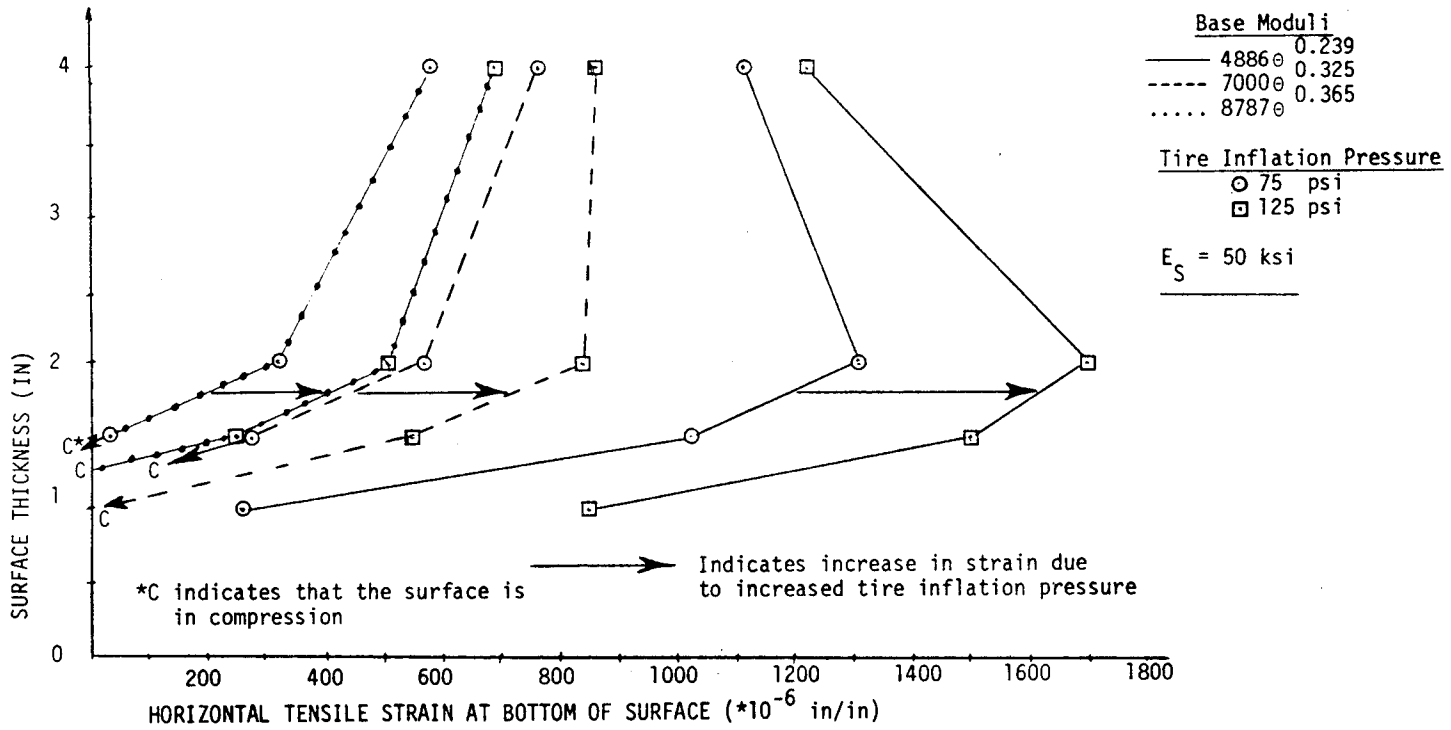

Figure 63. Effects of increased tire pressure on tensile strain for a surface modulus of 50 ksi.

granular bases, especially since tire pressures have increased substantially over the last few years.

For the thick flexible surfaces, the increase in tire pressure produces a smaller increase in tensile strain than for the thinner surface. But the increase in strain for the more flexible surfaces in Figure 63 is much larger than that experienced by the stiffer surfaces included in Figure 62. In general, as the surface thickness increases, the surface modulus is more important in determining the strain level than the base modulus; however, as the surface thickness decreases, the effect of the base modulus becomes more significant.

Surface Modulus and Thickness Effects. To evaluate the effects of surface modulus on strains for different base moduli and tire pressures, Figures 64-66 have been prepared. Each figure contains plots of tensile strain (microinches per inch) at the bottom of the surface for each combination of surface thickness and surface modulus. The plot on the top of each figure is the strain for a 125 psi inflation pressure. The contour lines on each figure represent lines of equal strain.

To resist fatigue damage, the tensile strains in the pavement structure must be kept fairly low, the exact level depending on the total traffic to be carried on the roadway and the characteristics of the surfacing layer. Since low strians are desirable, the first analysis of the plots in Figures 64-66 involved identifying the low strain areas. For purposes of discussion the authors have selected a strain level of 300 microinches/inch to be a level below which reasonably adequate performance can be achieved and above which performance begins to be significantly impaired.

Strain levels below 300 occur in both the upper right and the lower left corners in Figures 64 and 65, but only in the upper right corner in Figure 66. Notice also that increasing the tire pressure from 75 to 125 psi results in the higher strain levels being wedged between the areas of low strain level thereby compressing and driving these low strain levels more toward opposite corners. In fact, the increased tire pressure for the weak base condition, Figure 66, resulted in there being no strain level below 300 for the low modulus surface combinations in the bottom left corner.

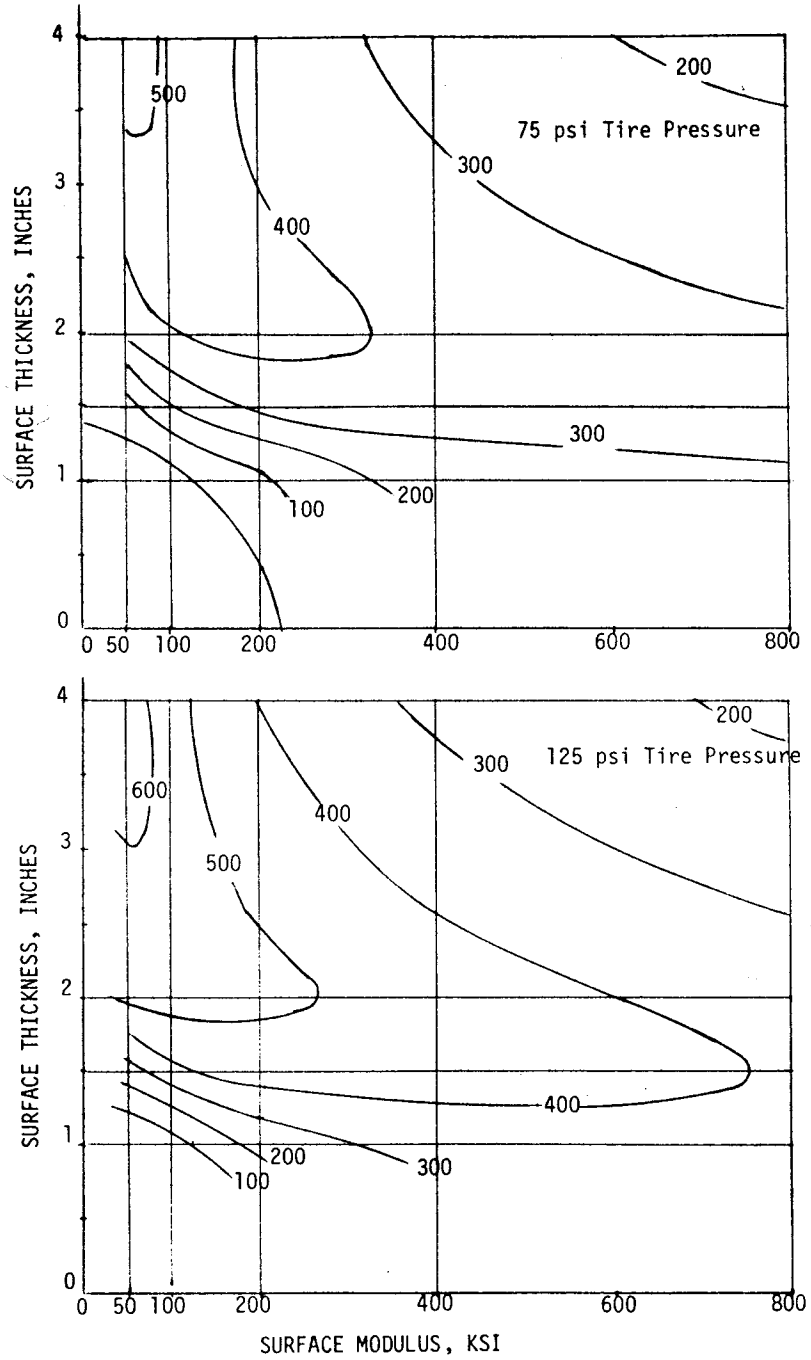

Figure 64. Tensile strain contours for $8787\theta^{0.365}$ base modulus.

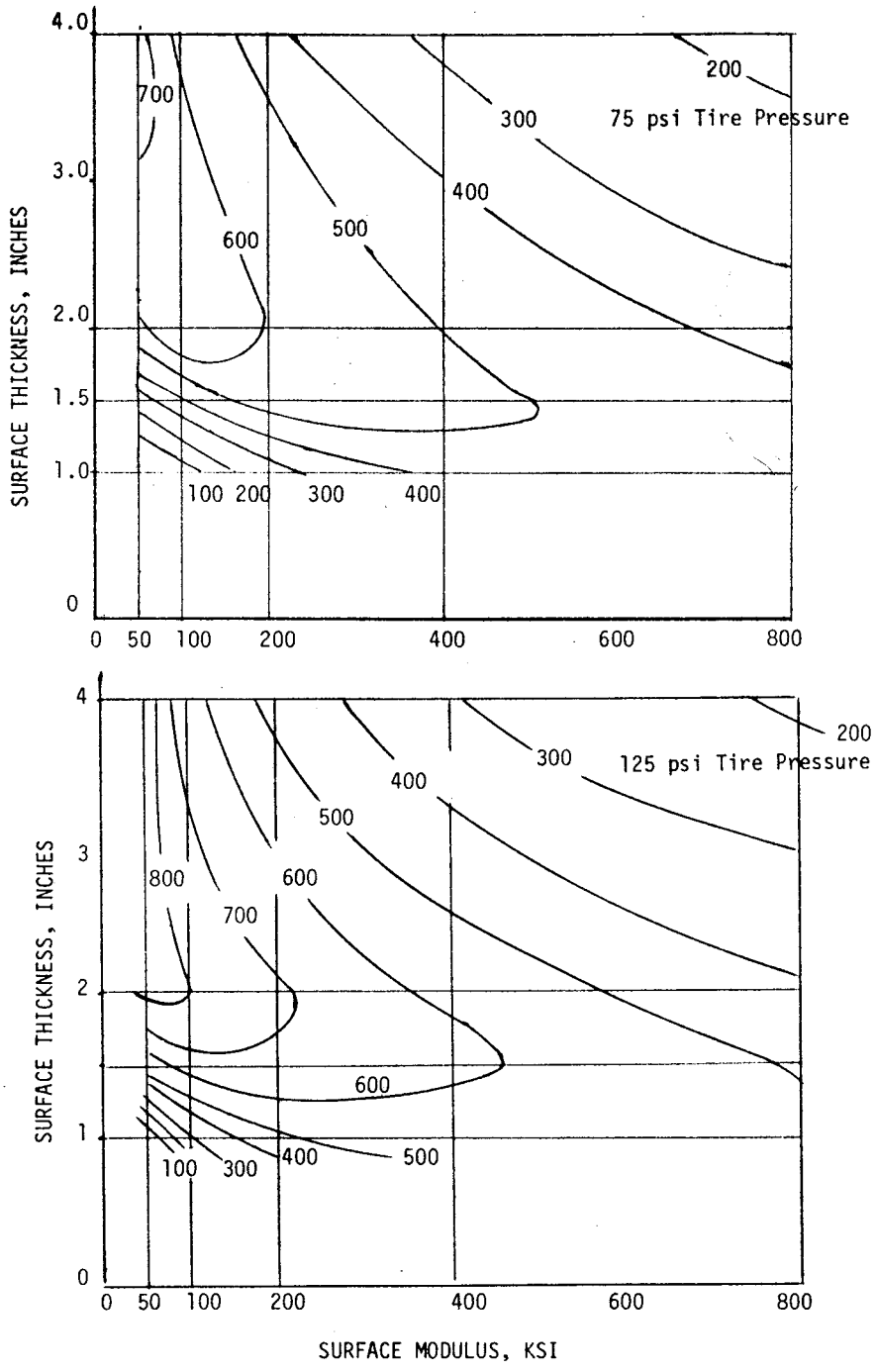

Figure 65. Tensile strain contours for $7000\theta^{0.325}$ base modulus.

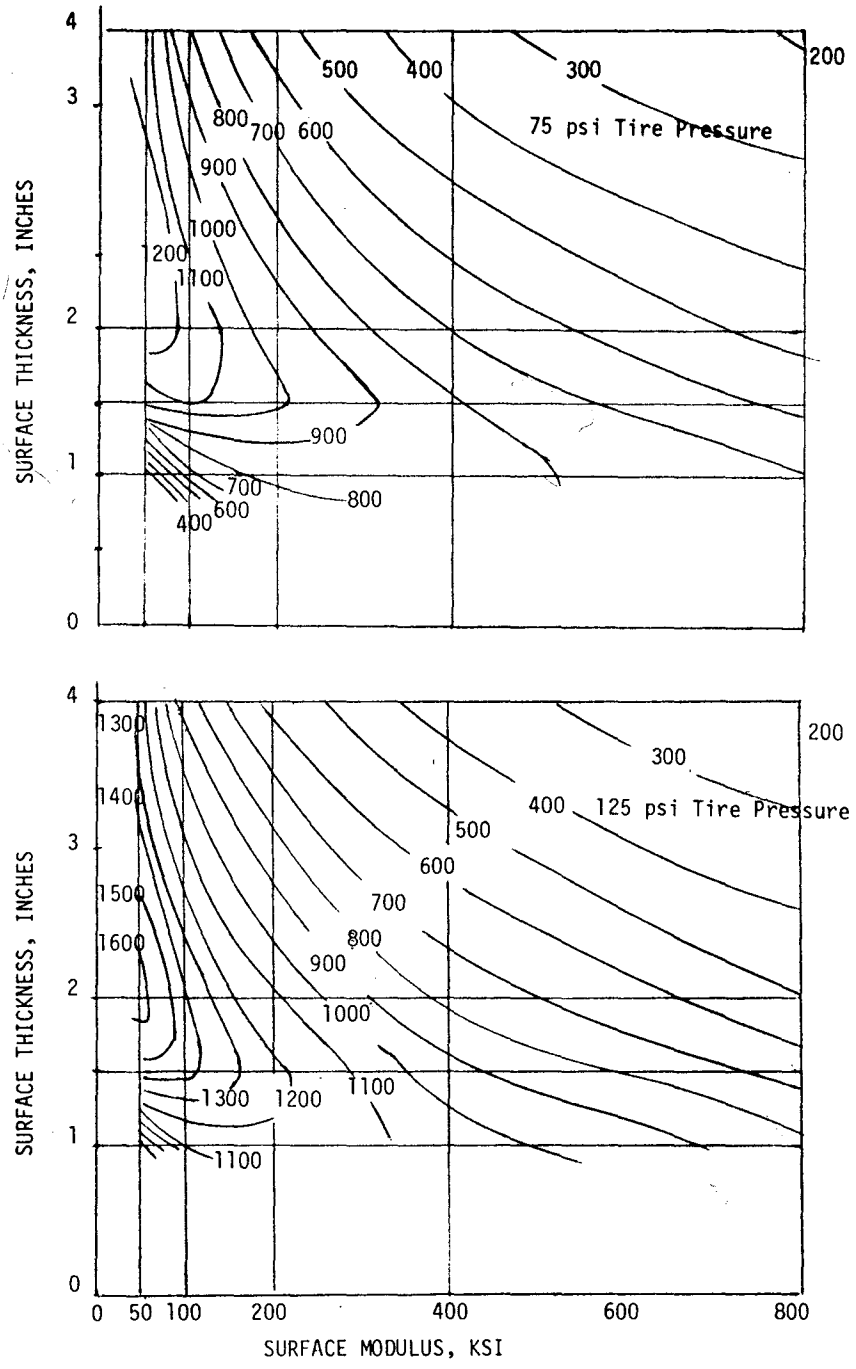

Figure 66. Tensile strain contours for $4886\theta^{0.239}$ base modulus.

Review of these isostrain lines in Figures 64-66 leads to the conclusion that for thin asphalt concrete surfaces the surface moduli should be low and the base moduli for the flexible bases should be high. Only with this combination of materials can the tensile strains be reduced to levels that will provide adequate fatigue resistance.

The strain levels for surface thickness of 1.5 to 2 inches are quite high except for the high base modulus combined with surface moduli over 300 ksi. At these strain levels reduced service life will occur but pavements with several years of life should result, depending on the traffic levels. But for the moderate and weak bases, these high tire pressures produce strains too high to provide even marginal lengths of service life.

To provide a more definite indication of the effects of the interaction between tire pressure and surface thickness and moduli on fatigue cracking, an analysis was conducted to estimate the additional fatigue damage produced by the increase in tire pressure from 75 to 125 psi. To perfrom this analysis, a fatigue equation developed from AASHO Road Test results was selected (37) as a model for developing the equation used in this study. The equation was developed by using the observed number of weighted 18-kip ESAL required to produce Class 2 fatigue cracking, and the calculated tensile strain at the bottom of the surface layer was developed by using ILLIPAVE. That equation is as follows:

$$W_{18} = 5.0957 \times 10^{-13} \left(\frac{1}{\varepsilon_t}\right)^{4.65644}$$

where:

W_{18} = number of weighted 18-kip axle loads to produce Class 2 cracking; and

ε_t = tensile strain at bottom of the surface

The above regression equation has a standard error of estimate of 0.495 and R^2 term of 0.7796.

First to be discussed will be the fatigue effects due to the tensile strains at the bottom of the surface. As the base modulus becomes weaker, the fatigue effects become more pronounced; this is shown in

Figures 67 through 69. Notice that for the weak base condition, Figure 69, the number of applications until Class 2 cracking for all surface thickness and modulus combinations is well below that required for a low volume road. A low volume road is defined in the literature as having approximately 500 ADT. This would correspond to a road that has normal traffic and a life of the pavement of 5 years, an ESAL of 20,000 load applications. This value or higher is shown only in the bottom left and upper right corners of the figures representing the ESAL for the strong and weak base condition.

The surface modulus and thickness have a significant effect on the number of ESAL applications. As shown in Figures 67 and 69, the lower strains in the top right and lower left hand corners have ESAL values that are much greater than those in the middle along the diagonal from the upper right to the bottom left hand corner. Therefore, to increase the fatigue life of the pavement, the surfaces should be either kept flexible and stiff or strong and thick.

The tire inflation pressure has a significant effect on the fatigue life, especially for surfaces that are less than or equal to 1.5 inches. Since the ESAL applications decrease dramatically in the lower left hand region, the tire inflation pressure has a significant effect on the fatigue life for these thin surface and weak modulus combinations.

Other studies conducted as a part of research study 2345 and reported by Roberts and Rosson (34) included the evaluation of a 14-inch granular base instead of the 8-inch base. These analyses showed that while the increased thickness did not significantly affect tensile strain at the bottom of the surface, it did significantly lower the subgrade vertical compressive strains.

Summary. Overall, these studies show the significant influence of increases in tire pressure on reduction in service lives of all the pavements included in the study. Of special importance is the effect of higher tire pressures on thinner pavements and the need to make these pavements either thin and flexible or thick and stiff.

PASSENGER CAR TIRE STUDIES WITH ILLIPAVE

In this study two tire models were used, the Tielking tire model and the uniform pressure model, to analyze the effect of radial passenger-car

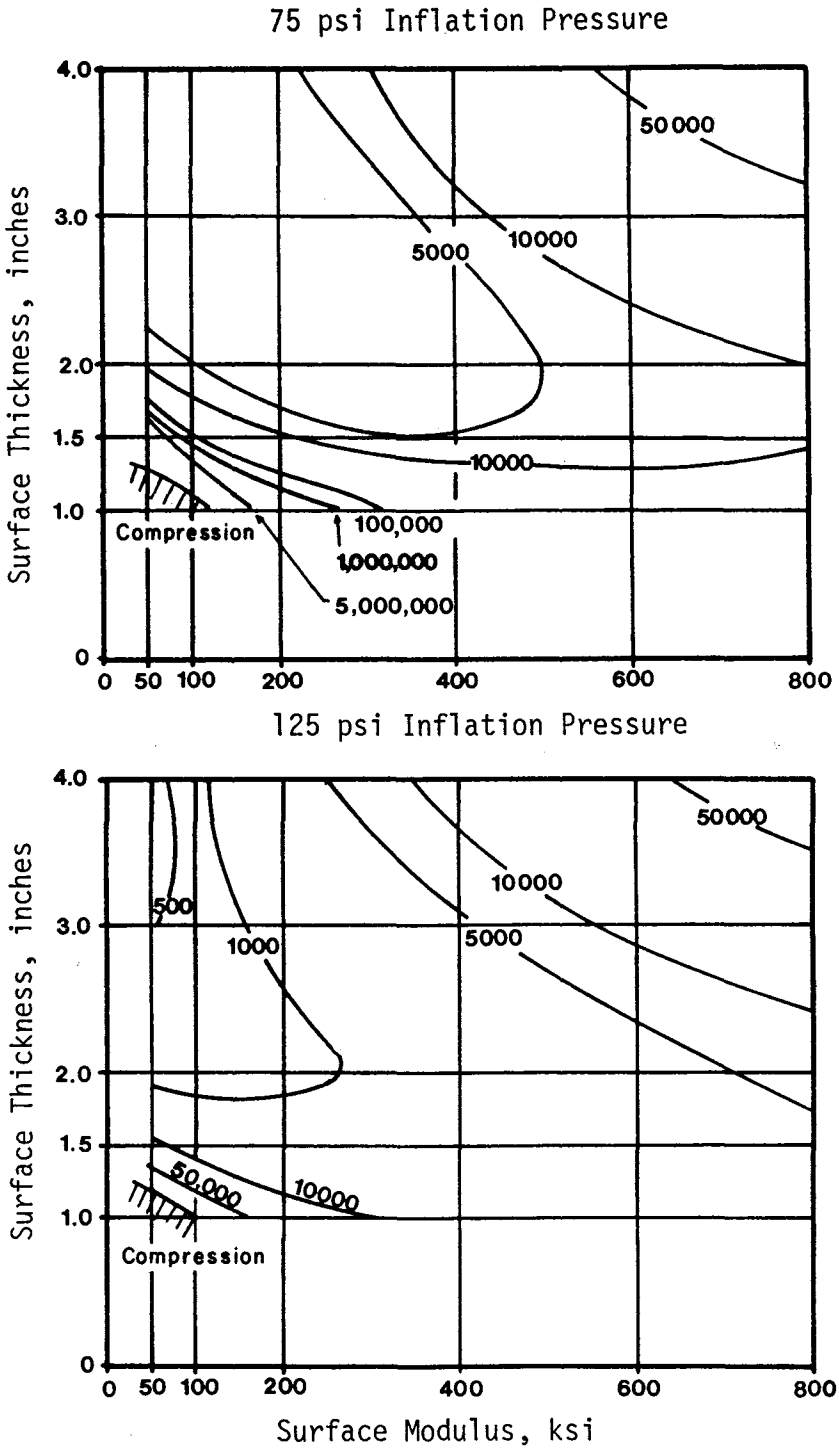

Figure 67. ESAL contours as a function of the tensile strain at the bottom of the surface for a $8787\theta^{0.365}$ base modulus and 8-inch base.

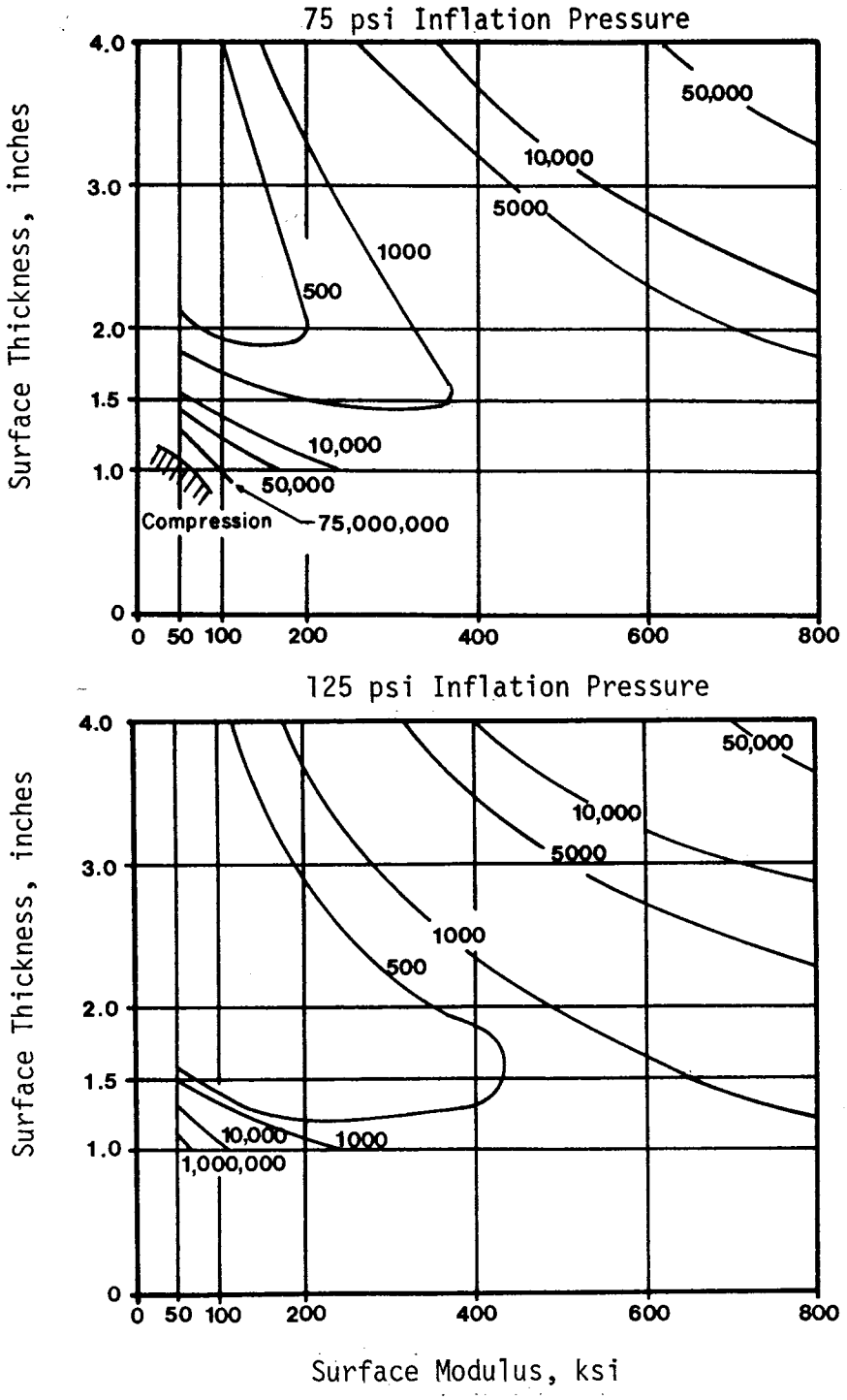

Figure 68. ESAL contours as a function of the tensile strain at the bottom of the surface for a $7000\,\theta^{0.325}$ base modulus and 8-inch base.

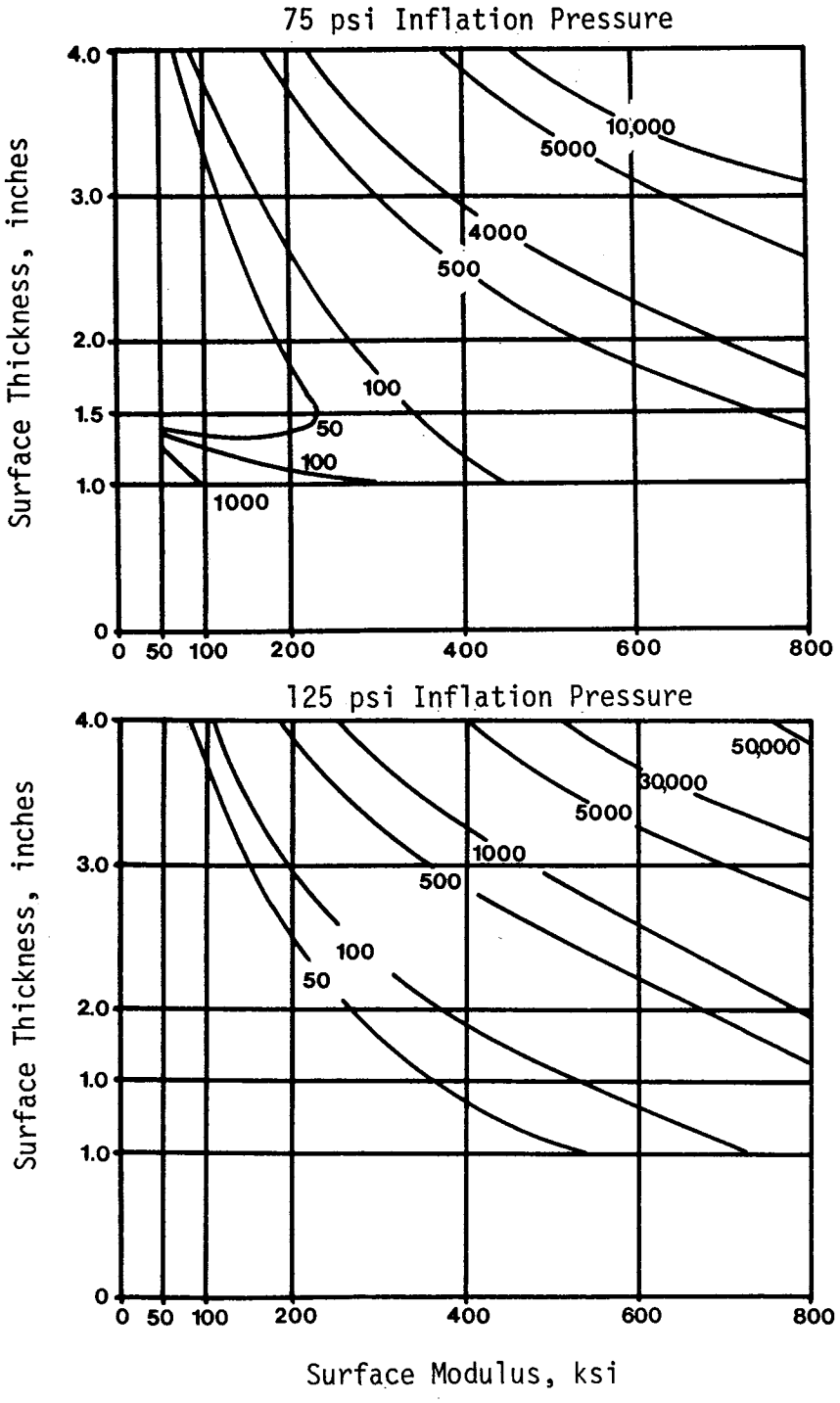

Figure 69. ESAL contours as a function of the tensile strain at the bottom of the surface for a $4886\theta^{0.239}$ base modulus and 8-inch base.

tires on thin asphalt pavements. The tire used in the study was a P205/75R14 with an inflation pressure of 26 psi. Results from the Tielking tire model in Figure 70 show that the contact pressure distribution is grossly larger than the inflation pressure. With the uniform pressure model the inflation pressure is assumed to be the same as the contact pressure. Two different tire loads were also used in the analysis: 800 and 1320 pounds. The 1320 pound load is the maximum rated load for the tire and 800 pounds is assumed to be a typical load.

To assess the difference in the tire pressure assumptions several types of comparisons have been made using results from ILLIPAVE computer runs. These comparisons include plots to show the effect of tire pressure on strains in the pavement.

The surface thicknesses included in the study were 1, 2, 3 and 4 inches. Taking into consideration the soil types, temperature ranges and moisture levels within the different regions of the state, the following range of material properties was selected for typical surface, base and subgrades.

Asphalt Concrete Surface:

Thickness: 1, 2, 3 and 4 inches
Elastic Moduli: 50, 200, 400 and 800 ksi
Poisson's Ratio: 0.3
Density: 145 pcf

Granular Base:

Thickness: 8 inches
Elastic Moduli: 30 and 60 ksi
Poisson's Ratio: 0.4
Density: 135 pcf

Subgrade:

Thickness: Infinite
Elastic Modulus: 5 ksi
Poisson's Ratio: 0.45
Density: 120 pcf

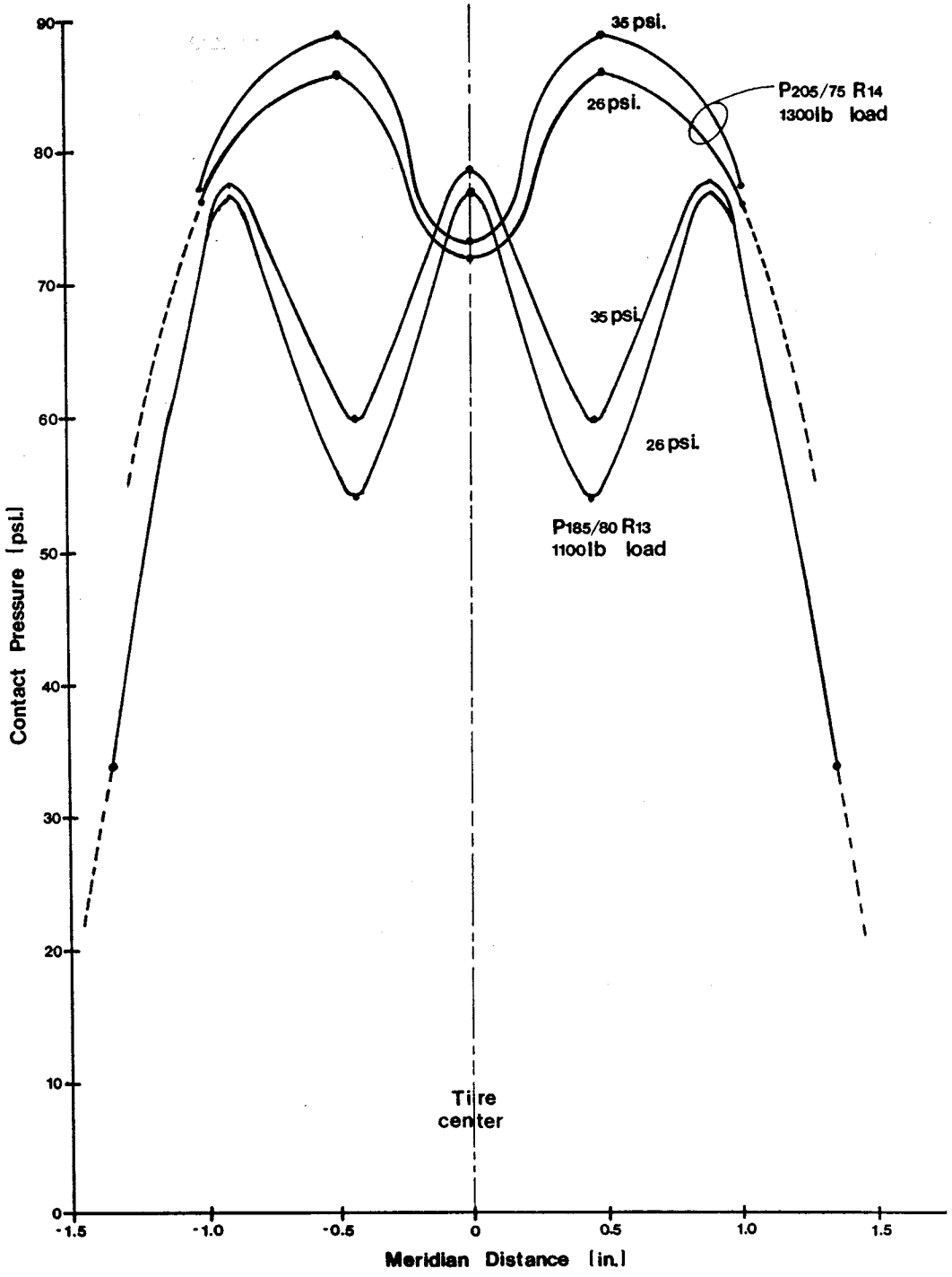

Figure 70. Effect of inflation pressure on footprint pressure distribution of radial passenger car tires.

Tire Pressure Effects

A series of computer runs were used to analyze the effects of tire pressure on thin pavements using both the Tielking Tire Model and the Uniform Tire Model.

To describe the effects of automobile tire pressure on tensile strains at the bottom of the surfaces, Figures 71 and 72 have been prepared. Figure 71 shows the change in tensile strain for a surface of varying thickness and with a modulus of 400 ksi on an 8-inch base with an increase in tire pressure. Figure 72 shows the same information for a surface with a modulus of 50 ksi. There is an increase in tensile strain when the tire contact pressure is increased for both the weak and strong bases. Notice that a 26 psi contact pressure on a 1 inch thick surface with a weak base causes a higher strain than the same pavement under a 65 psi contact pressure but with a stronger base. This demonstrates the importance of providing an adequate base especially for thin pavements. Strains are increased by approximately 100 percent when the tire pressure model is changed from 26 psi uniform to 65 psi for the 60 ksi base and almost as much for the 30 ksi base. Notice that, as the surface thickness decreases from 2 inches to 1-inch, the tensile strains decrease and move toward compression at the bottom of the surface.

The effect of the change in base modulus on tensile strain is comparable to that of the increase in contact pressure between the two models; indicating the importance of both modeling the tire contact pressure correctly and having a strong base.

The effect of reducing the surface modulus on tensile strains is shown in Figure 72. Observe that the tire contact pressure effects are greatest for the thinner surface and lower surface modulus combinations. The figure also indicates that for thin, low modulus surfaces, the pavement structure is in compression.

If both the surface and base modulus are low, these passenger car loads can lead to rapid fatigue failure because the tensile strains are quite high. For the very flexible surface, the change in contact pressure shown by the two models produces strains that are about twice as high for the Tielking Model as for the Uniform Model for both base moduli. Notice that for all cases, when the surface thickness is only 1-inch, the strain at the bottom of the surface is in compression.

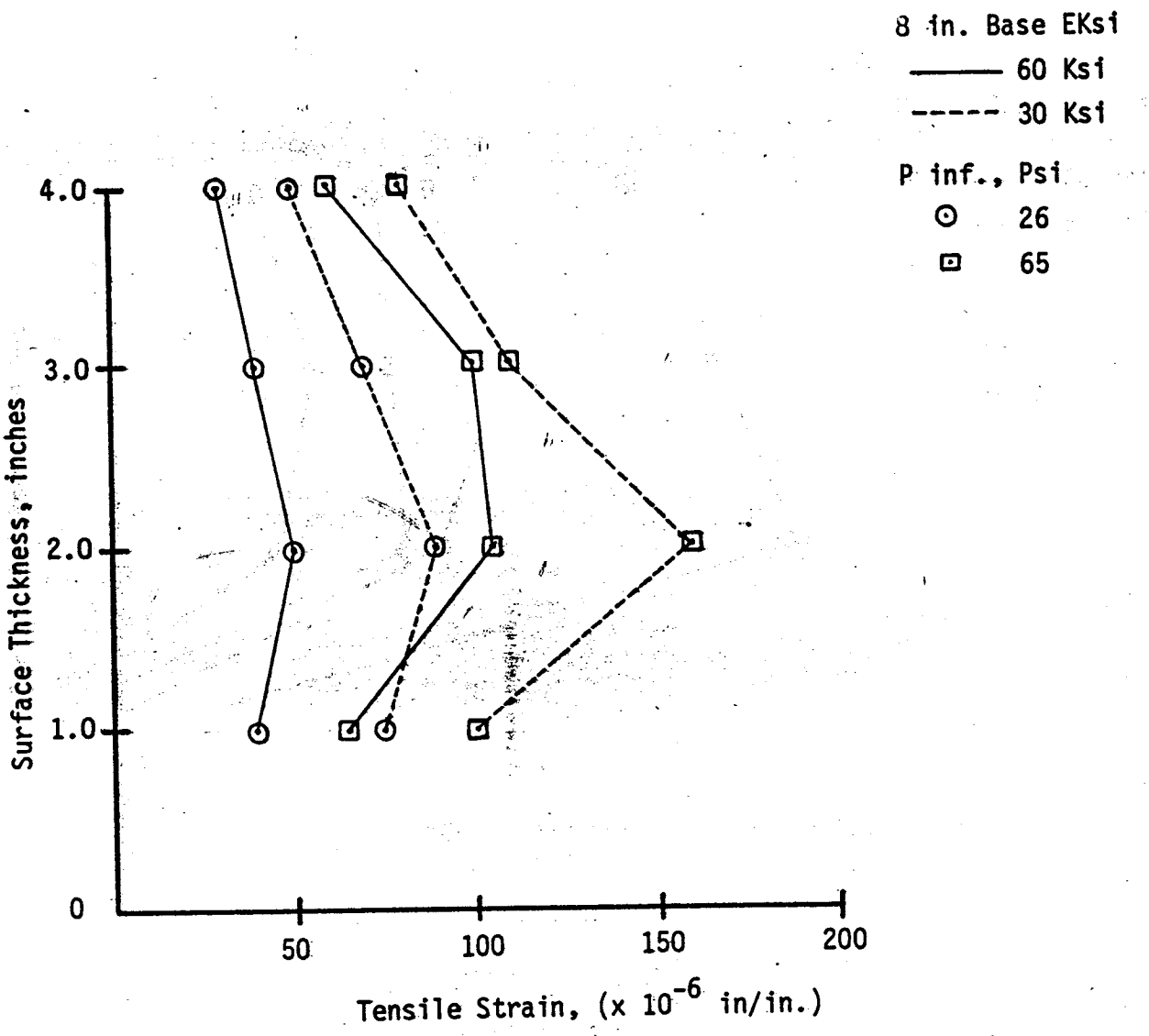

Figure 71. Effect of tire pressure on tensile strain at the bottom of a surface with a modulus of 400 ksi for a P205/75R passenger tire load of 1,320 lbs.

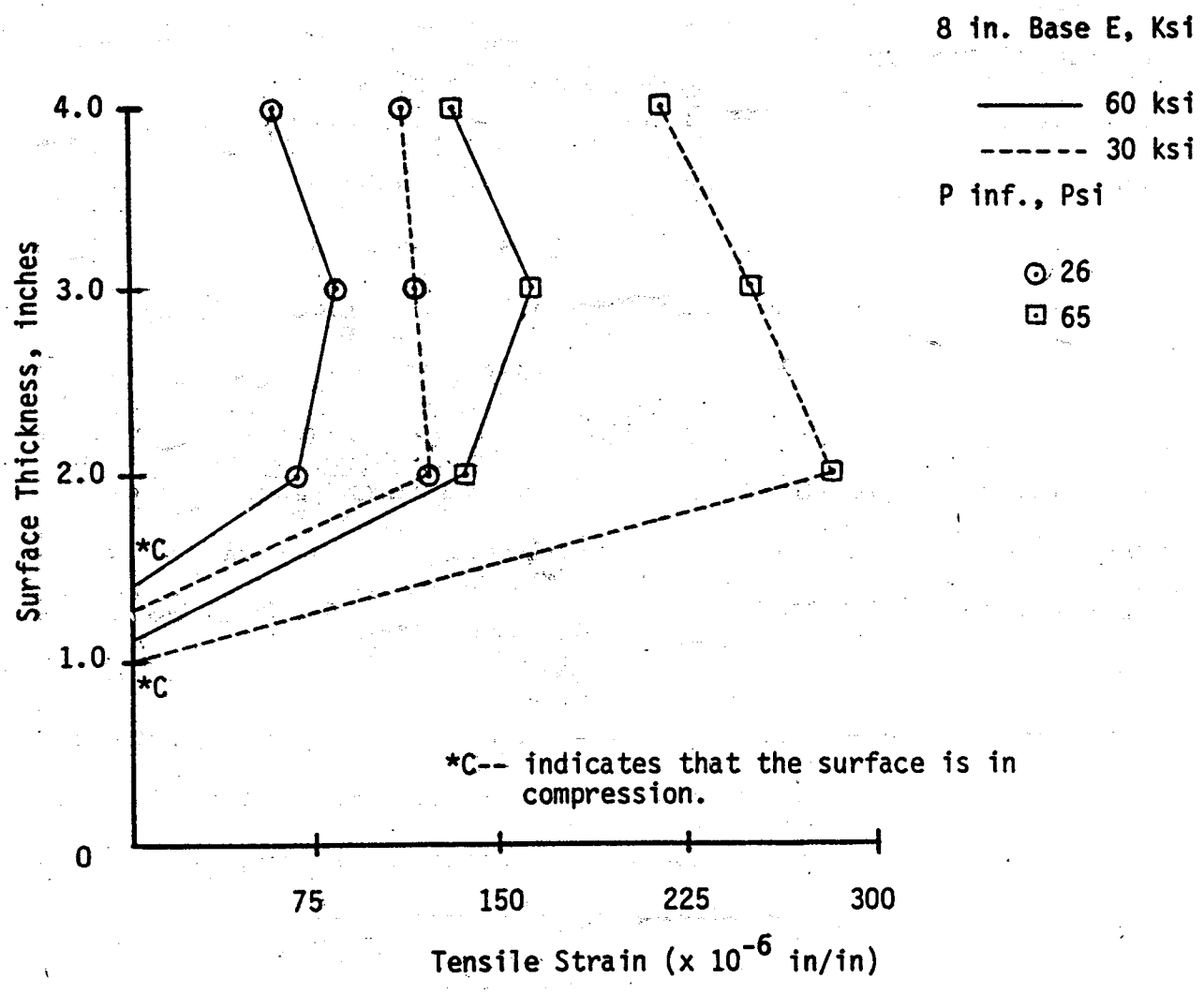

Figure 72. Effect of tire pressure on tensile strain at the bottom of the surface with a modulus of 50 ksi for a P205/75R passenger tire load of 1,320 lbs.

Tire Load Effects

With the trend of the automobile industry to build lighter and more efficient cars, two different tire loads were used in this study. The highest load was that for the maximum rated load and the second was a more typical value for vehicular loading.

To describe the effect of automobile tire load on tensile strains at the bottom of the surface, Figures 73 and 74 were prepared.

Figure 73 shows the effect of tire load and pressure on different surface thicknesses having a surface modulus of 400 ksi over an 8-inch base with a modulus of 30 ksi. The figure shows that at 26 psi contact pressure the tensile strain increases by about 20 to 25 micro-inches per inch when the tire load is increased from 800 lbs. to 1320 lbs. However, for 65 psi contact pressure, increasing the load substantially increases the strain, with increases ranging from 30 to 50 micro-inches per inch.

Figure 74 shows similar trends as those shown in Figure 73. The primary difference is that the difference in strains are lower because the base modulus is higher.

As seen in Figure 74, there is little difference in the tensile strains for the 4-inch surface carrying a tire load of either 800 or 1320 lbs. at 26 psi contact pressure. Notice too that the strains are about the same for a 1-inch surface subjected to the two tire loads at both 65 and 26 psi contact pressures. This means that the major effects on tensile strains due to tire load increments occur for the pavement surface thicknesses between 1 and 4 inches.

Tensile Strain at Bottom of Surface

As mentioned earlier in this report, the primary pavement response or significant indicator of fatigue cracking is the maximum tensile strain at the bottom of the asphalt concrete layer. To control the extent of fatigue damage, the tensile strains at the bottom of the surface must be kept fairly low.

Figures 75 through 78 show the different horizontal tensile strains as a function of surface thickness and modulus for various combinations of tire load and contact pressure. Figure 75 shows the effect on the horizontal tensile strains at the bottom of the surface layer of increasing the tire contact pressure for a tire load of 1320 pounds. As the contact pressure is increased, the tensile strains tend to increase. The lowest strains occur in the upper right and lower left corners with

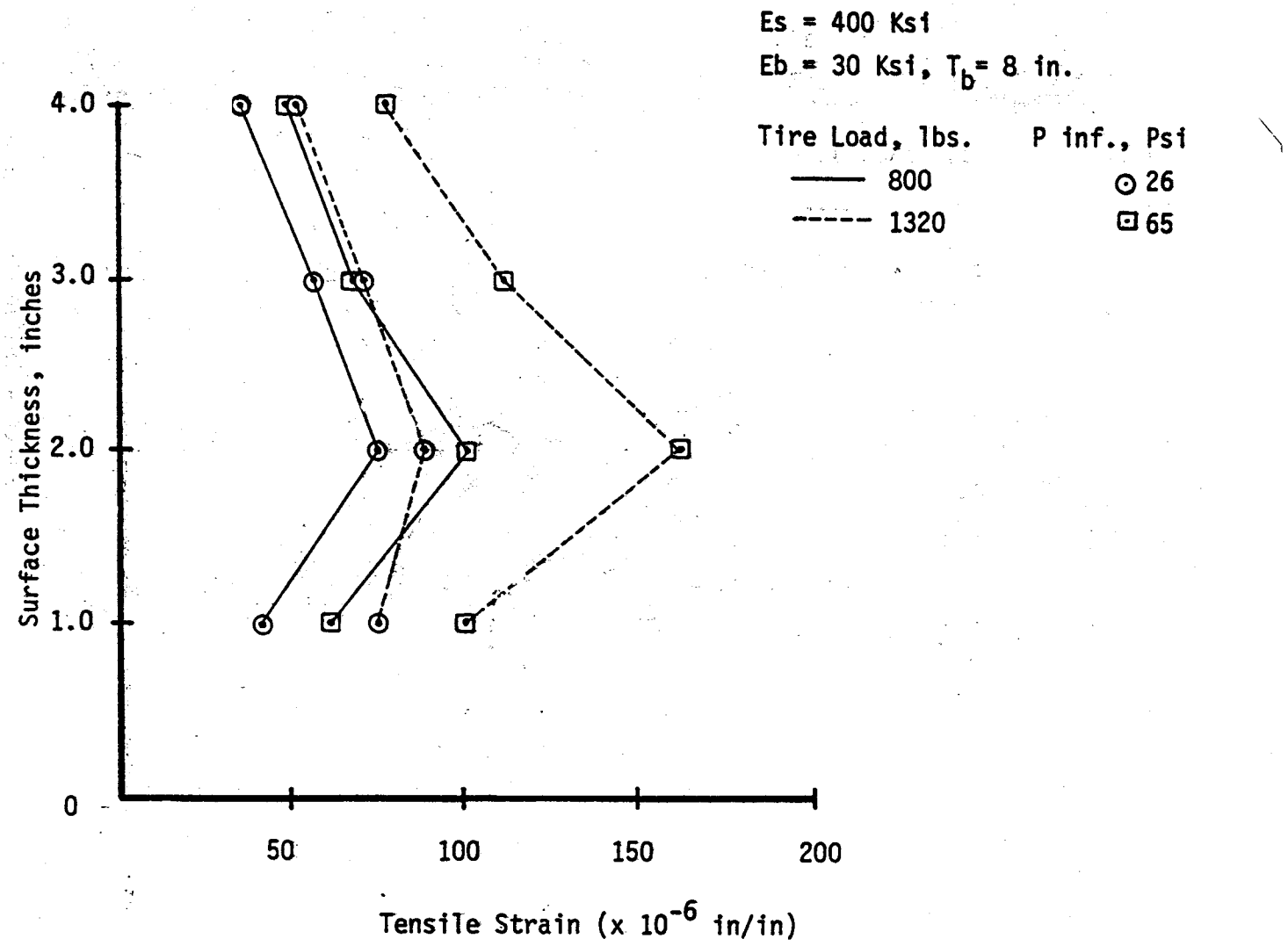

Figure 73. Effect of tire load on tensile strains at the bottom of the surface with a modulus of 400 ksi and a base modulus of 30 ksi.

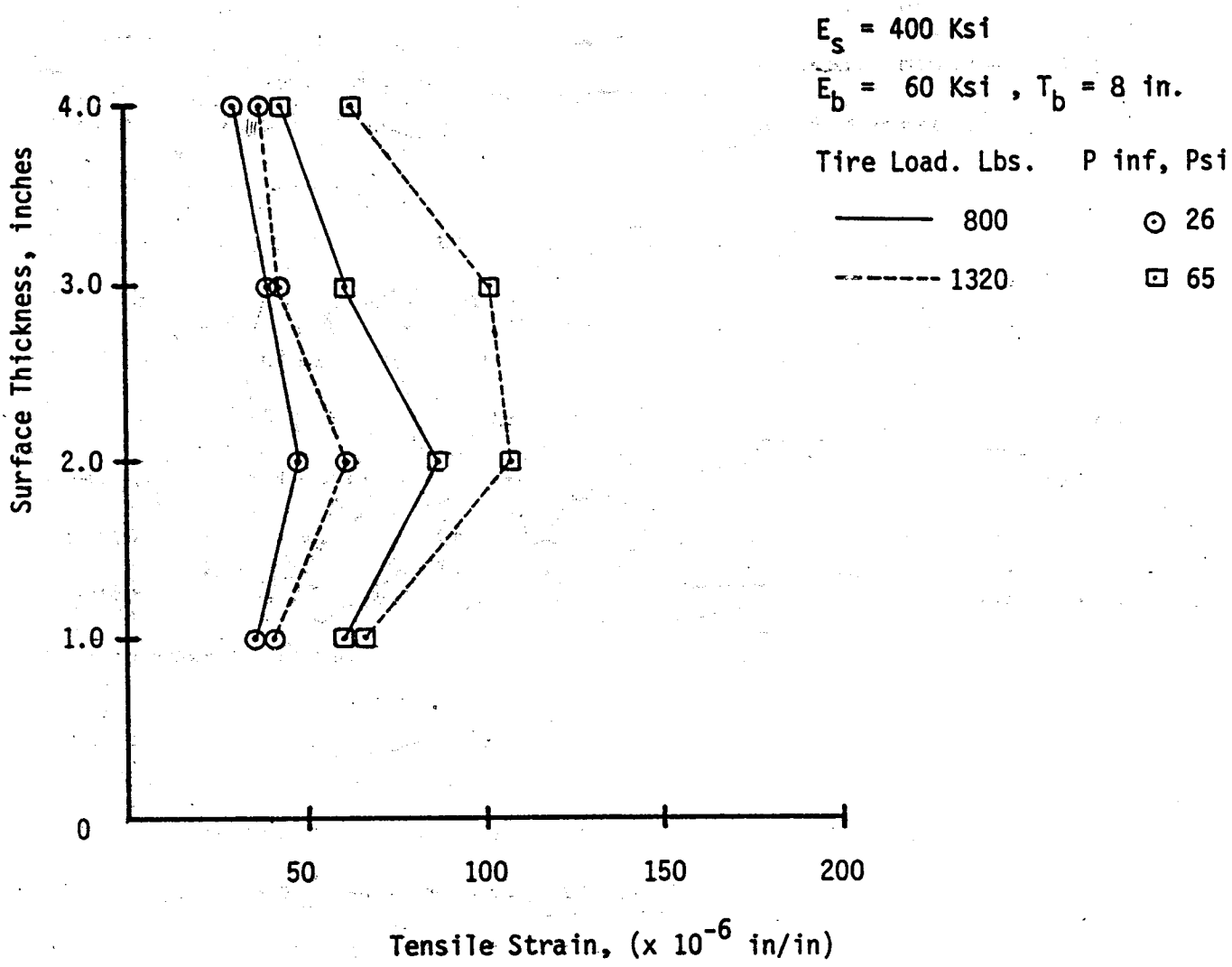

Figure 74. Effect of tire load on tensile strains at the bottom of the surface with a modulus of 400 ksi and a base modulus of 60 ksi.

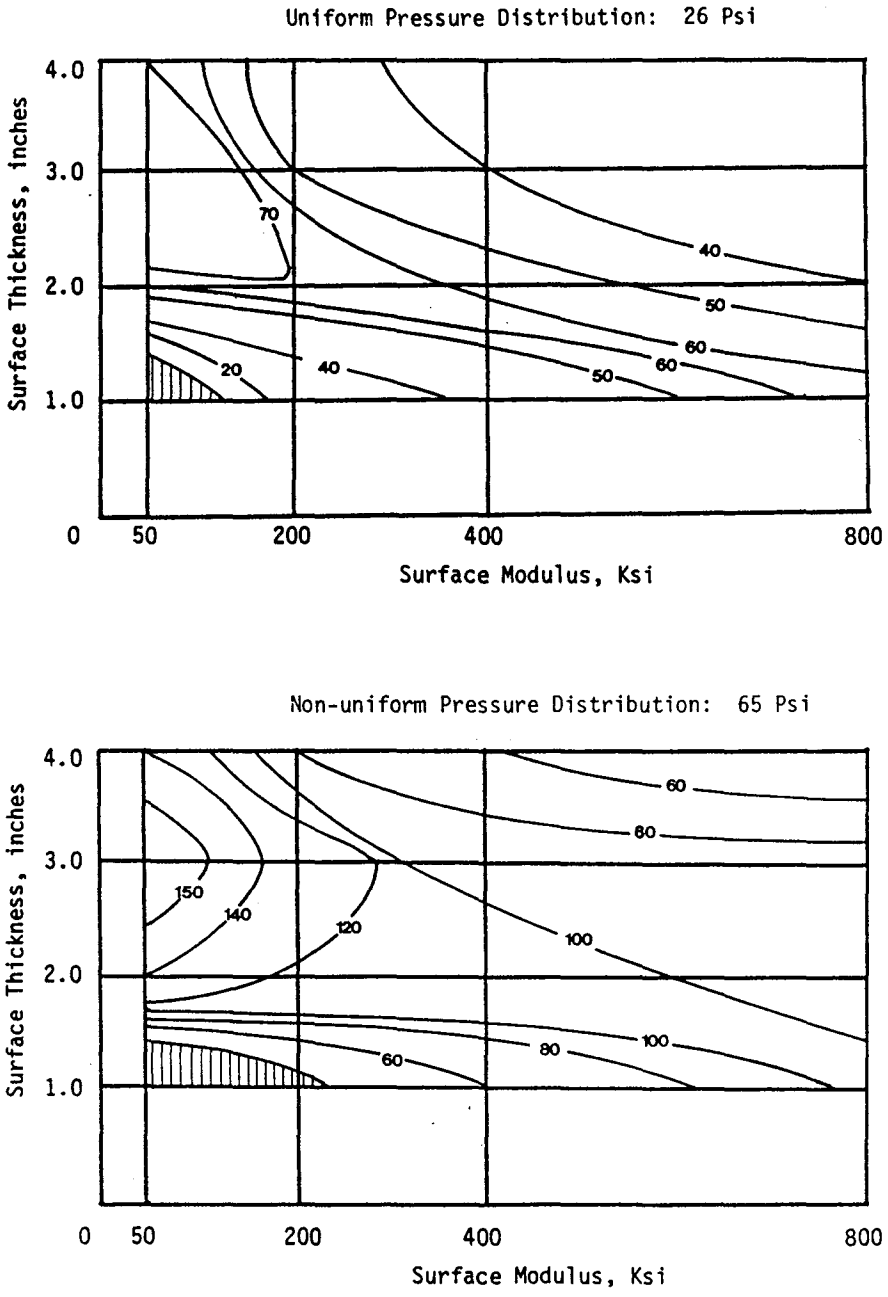

Figure 75. Tensile micro-strain contours at the bottom of the surface for a 60 ksi base modulus and a tire load of 1,320 lbs.

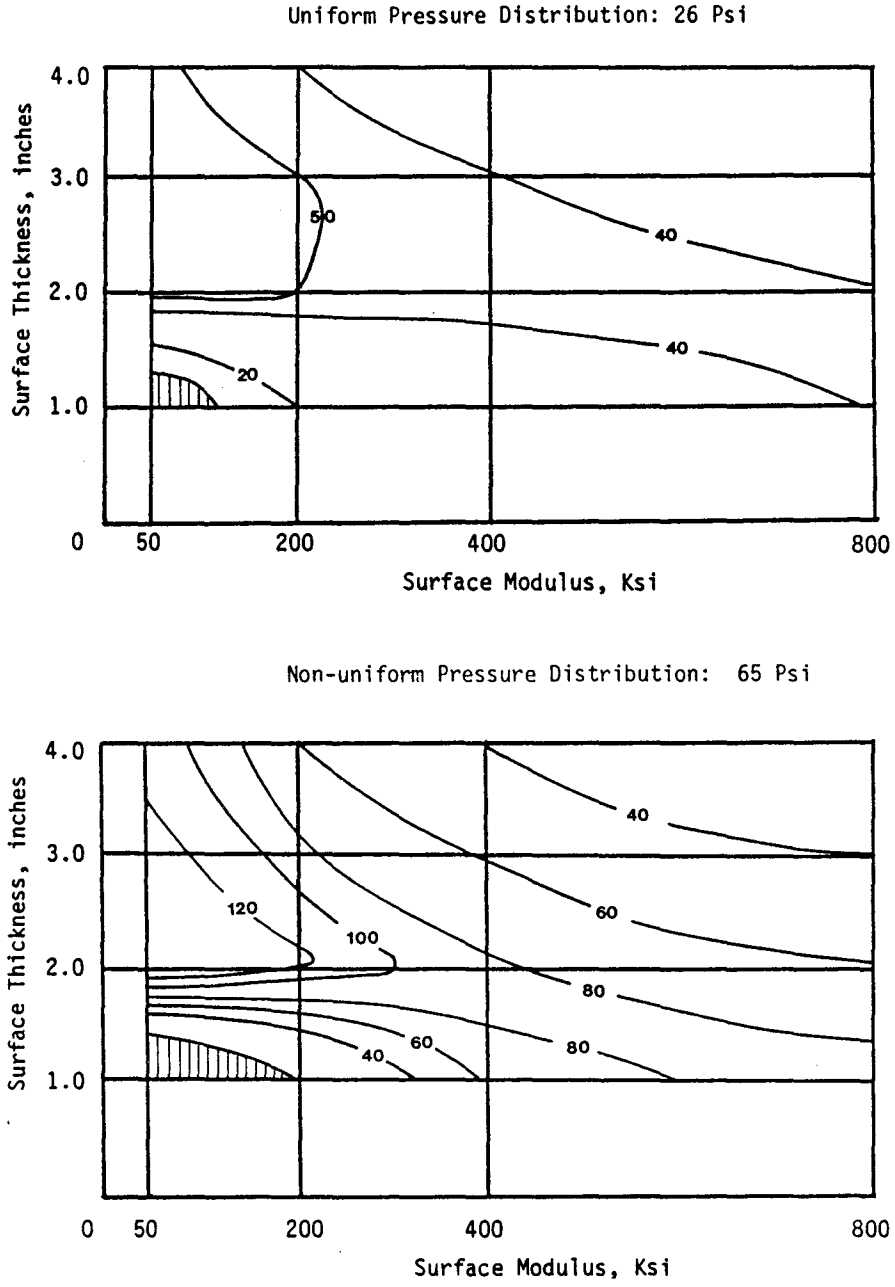

Figure 76. Tensile micro-strain contours at the bottom of the surface for a 60 ksi base modulus and a tire load of 800 lbs.

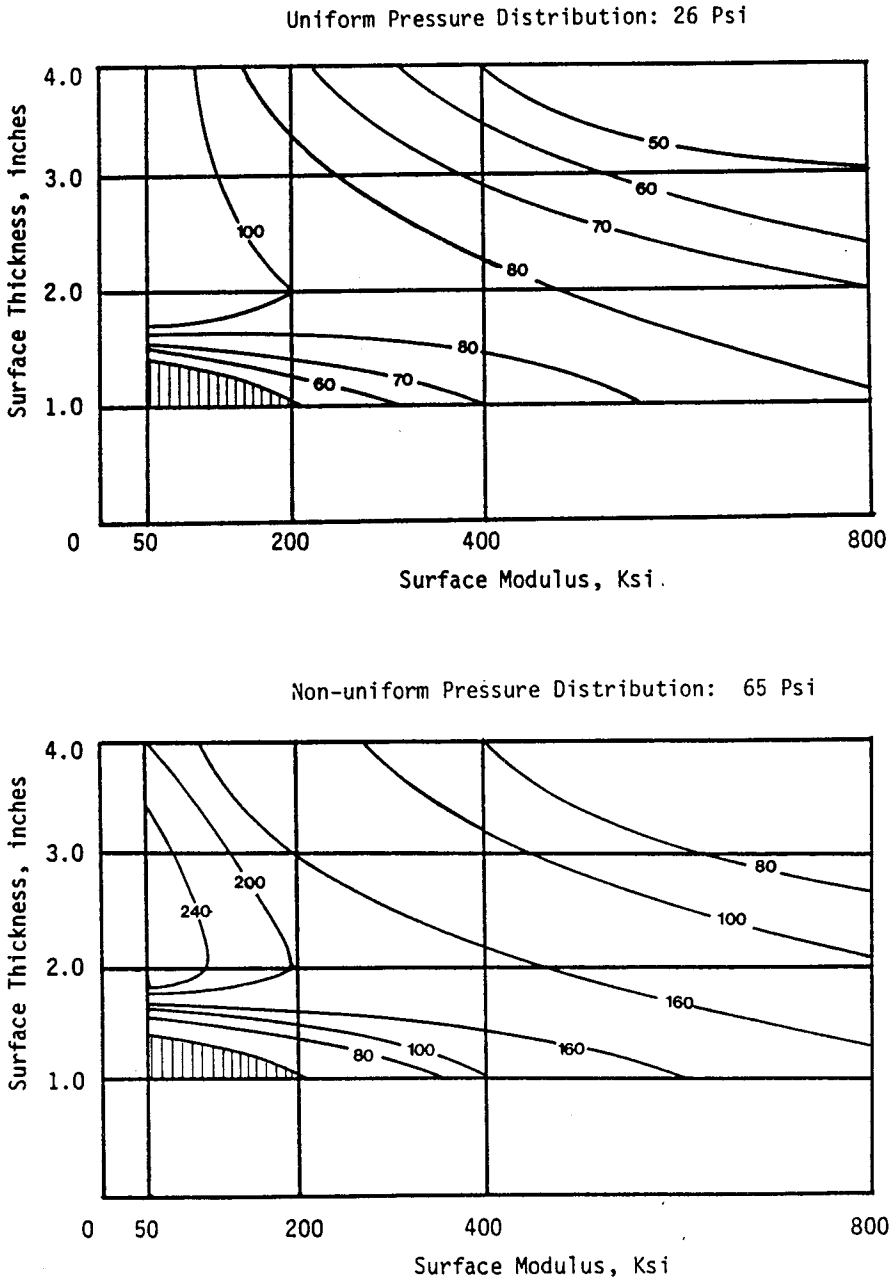

Figure 77. Tensile micro-strain contours at the bottom of the surface for a 30 ksi base modulus and a tire load of 1,320 lbs.

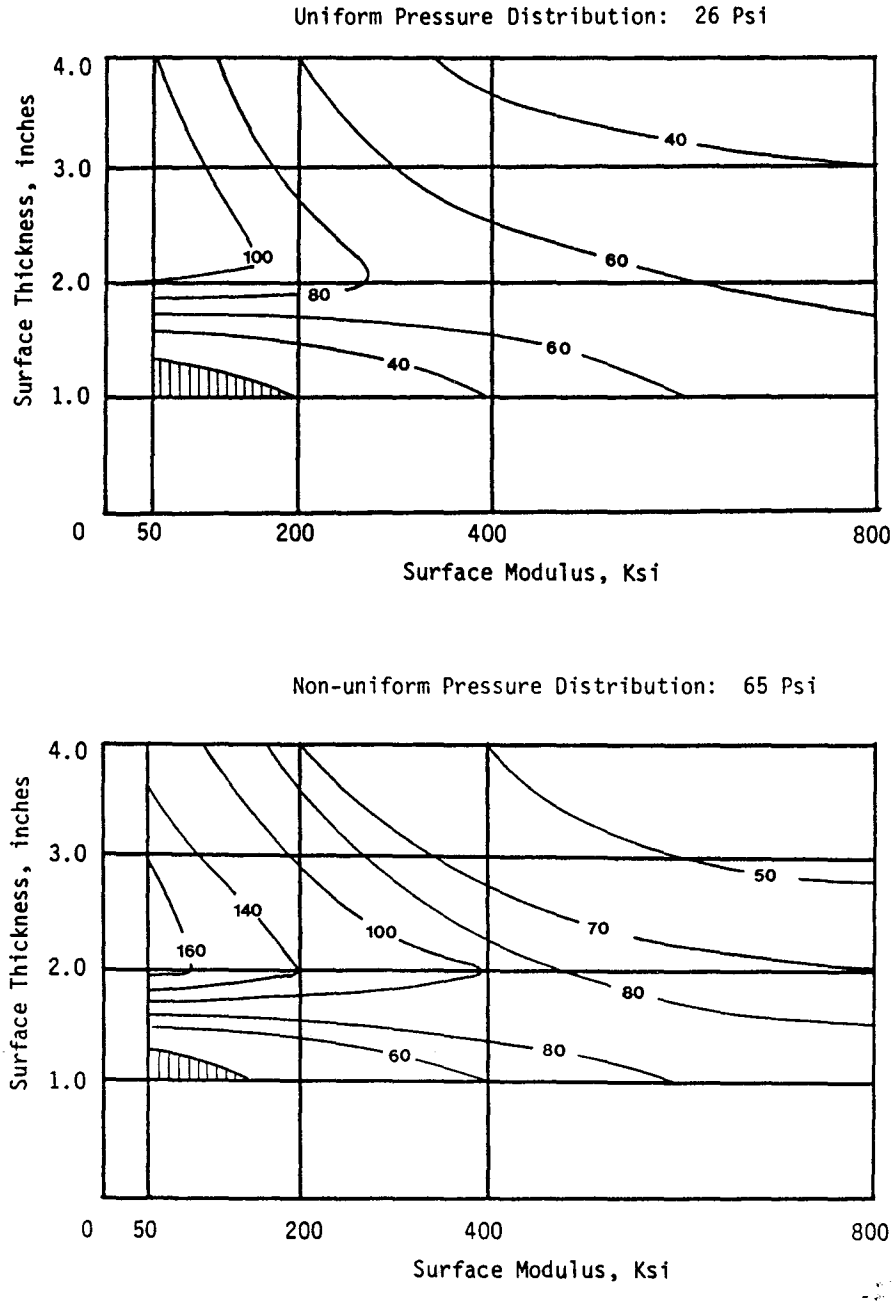

Figure 78. Tensile micro-strain contours at the bottom of the surface for a 30 ksi base modulus and a tire load of 800 lbs.

the highest strains occurring generally in the middle and upper left portions of the figures. Figure 76 shows the horizontal tensile strains of a pavement structure subjected to a tire load of 800 pounds. Comparing Figures 75 and 76, we can see that increasing the load increases the horizontal tensile strains for both tire contact pressures. The difference in tensile strains is not so significant due to the high moduli or strong base layer.

Figures 77 and 78 are of similiar form to the previous two figures with the primary difference that base modulus is lower. Observe in Figure 77 the effect on the tensile strains of increasing the tire contact pressure. When compared to Figure 75, a significant increase in tensile strains occurs as a result of the low modulus base. A comparison of the data plotted in Figure 77 and 78 shows a much greater effect for increasing the tire load for the low modulus base than for the high modulus base in Figures 75 and 76. Again, the lowest strains occur in the upper right and lower left corner of both figures and the highest strains occur in the middle and upper left at the low moduli, thicker surface combinations.

Fatigue Damage Effects

The calculated tensile strains at either the top or bottom of the asphalt concrete surface can be used to estimate the number of axle applications until class 2 cracking occurs. Class 2 cracking is defined as cracking that has progressed to the point where cracks have connected together to form a grid-type pattern. A pavement surface that has class 2 cracking is assumed to have failed in fatigue.

Figures 79 through 82 show the number of loads to failure, Nf, for different surface thickness and moduli. These figures show that the highest number of applications to failure occur in the upper right and lower left corners.

The surface modulus and thickness have a significant effect on the number of applications to failure. To increase the fatigue life of the pavement, the surface should be either flexible and thin or stiff and thick.

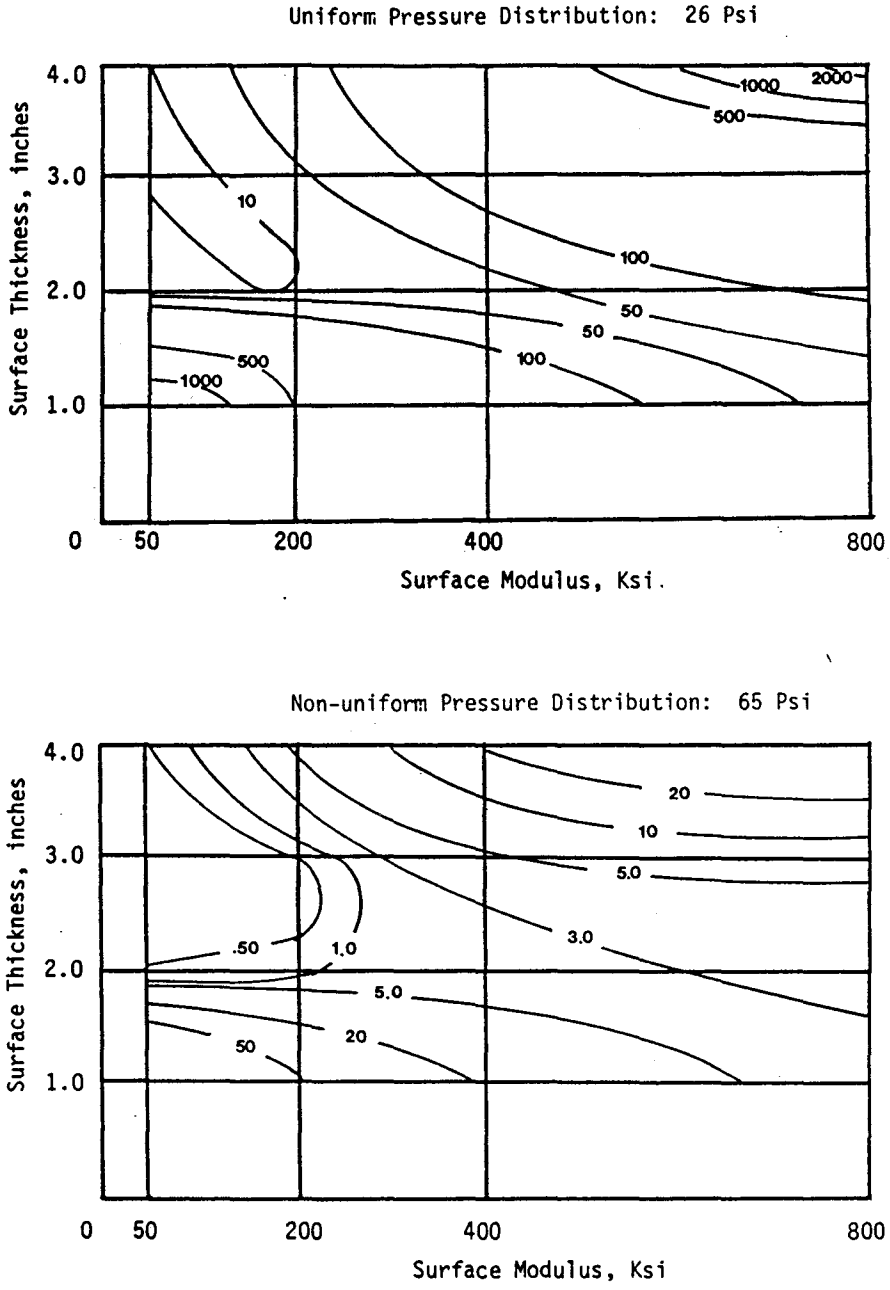

Figure 79. N_f contours in millions as a function of the tensile strain at the bottom of the surface for a 60 ksi base modulus and a tire load of 1,320 lbs.

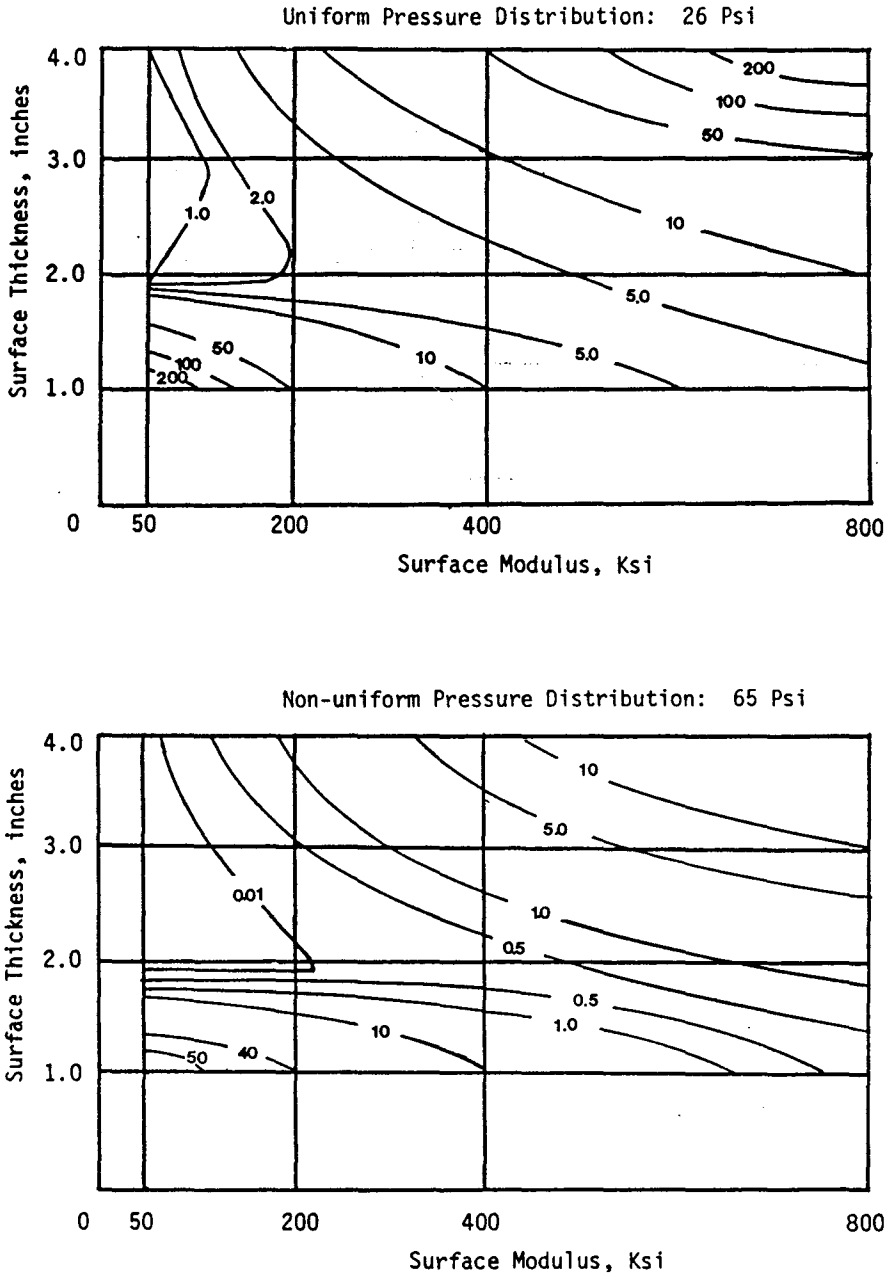

Figure 80. N_f contours in millions as a function of the tensile strain at the bottom of the surface for a 30 ksi base modulus and a tire load of 1,320 lbs.

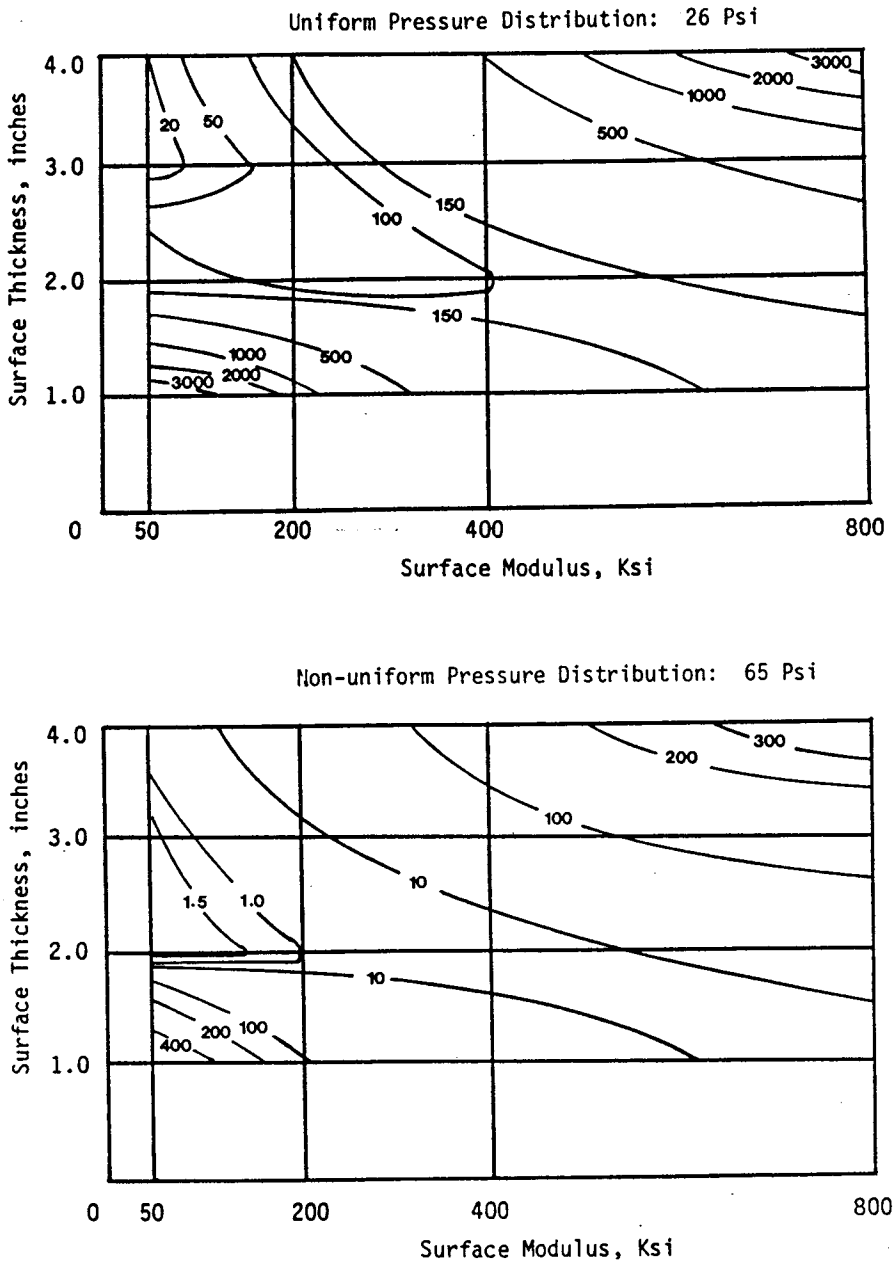

Figure 81. N_f contours in millions as a function of the tensile strain at the bottom of the surface for a 60 ksi base modulus and a tire load of 800 lbs.

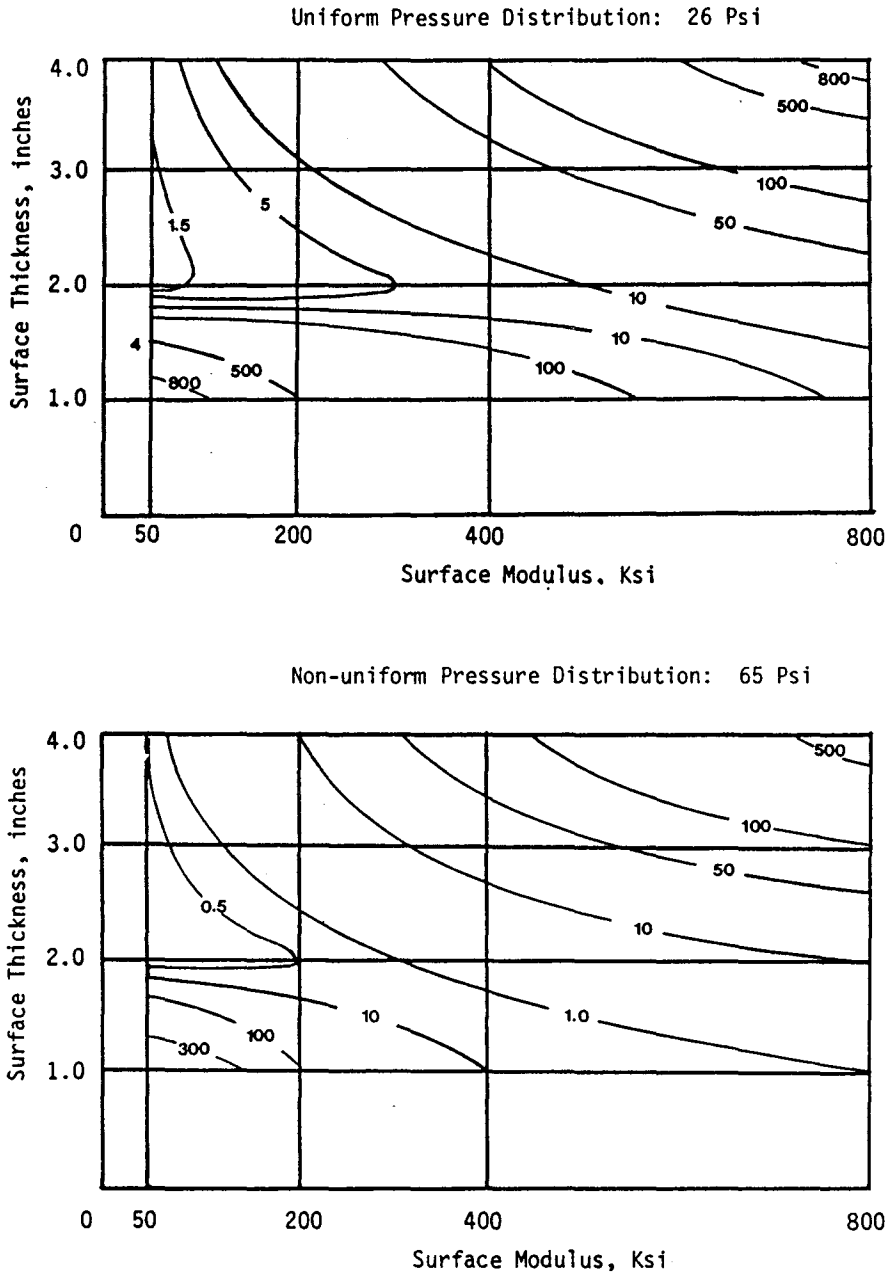

Figure 82. N_f contours in millions as a function of the tensile strain at the bottom of the surface for a 30 ksi base modulus and a tire load of 800 lbs.

A low volume road is considered to have approximately 500 ADT (average daily traffic). Figure 83 shows the cumulative number of vehicle load applications for a period of up to 20 years. Figure 79 indicates that thick, low moduli surfaces do not provide adequate service. Observe that these thick, low moduli surfaces provide less than 1,000,000 axle load applications. Data from Figure 83 indicates that a five year life pavement is subjected to approximately 1.9 million axle load applications.

The number of axle load applications is considerably reduced as the base modulus decreases as seen in Figure 80. Notice again that only thick, high moduli surfaces or thin, low moduli surfaces provide an adequate service.

Summary

These data show that for this pavement structure the effect of the contact pressures for automobile tires can have a significant effect in consuming the fatigue life of these pavements. The fact that the contact pressure distribution is much higher than the inflation pressure contributes very significantly to this observed effect.

TRUCK TIRE STUDY WITH MODIFIED ILLIPAVE

The purpose of this part of the study is to conduct an analytical study to evaluate the effects of different truck tire contact pressure distributions on Texas pavements using the modified ILLIPAVE computer program.

Input Data

Evaluations are made for different structural thickness combinations of surface, base and subgrade materials with the traffic levels shown in Table 21. The traffic is assumed to be uniform over the 20 year analysis

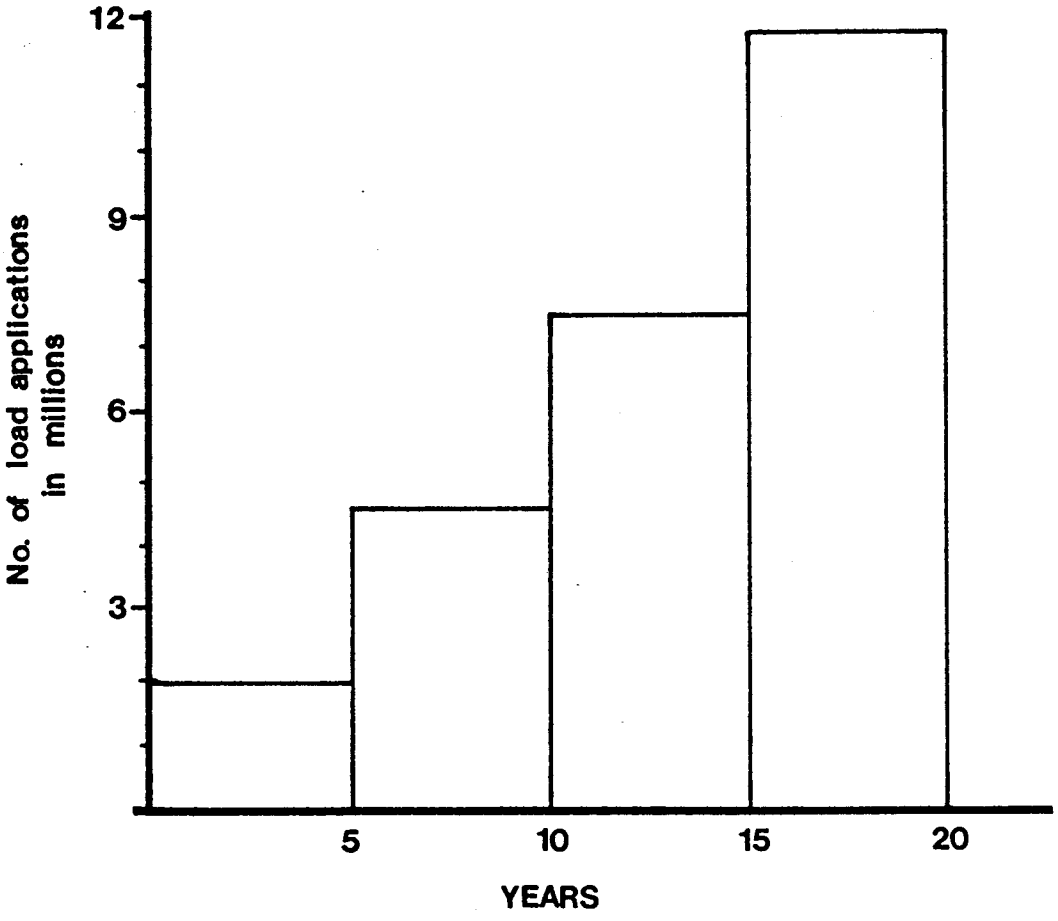

Figure 83. Cumulative number of automobile axle load applications.

Table 21. Input Data of Combinations of Thickness and Traffic Conditions

Layer Thickness, in.			Traffic
Surface	Base	Subgrade	18 kip EASL/day
1	8	521	15
2	8	521	30
4	8	521	150

period. The thicknesses of base and subgrade layers are 8-inches and 521-inches, repectively, for all combination cases.

Two different tire inflation pressures are used in the analysis. One is about 75 psi which is conventionally assumed to be a uniform vertical pressure applied over a circular area with a radius of 4.37 inches. The other is about 125 psi based on Tielking bias tire model over a circular area with a radius of 3.21 inches as mentioned in Chapter 3. The contact pressure distributions from the Tielking model include not only the nonuniformed vertical loads but also the horizontal shear pressure distribution. Figure 84 shows the vertical and horizontal load distributions for the bias truck tire for an inflation pressure of 125 psi.

Four representative Texas locations, Port Arthur, Brownsville, El Paso, and Amarillo, were selected for characterizing the effect of climate on the stress state of the selected pavements. Average monthly temperatures were gathered for these four locations from U.S. Weather Bureau records, and each year was divided into two seasons summer and winter. The length of summer is from April to October while the winter period was from November to March.

The surface layer consists of an asphalt concrete mixture (4.5 percent asphalt) with assumed resilient moduli of 2,200 , 500 , and 20 ksi at temperatures of 40, 72, and 120^{o}F, respectively. These data were obtained from laboratory tests included in Reference 21. The values of resilient moduli of the surface layer at each seasonal temperature (Table 22) were determined using the graphically method shown in Figure 59 of Chapter 4.

The characteristics of the base course were assumed to be stress sensitive and described as a function of the three principal stresses, Table 22. The subgrade soil is assumed to be a clay, classified by the Unified Soil Classification as CL. The resilient modulus of the subgrade soil is assumed to be constant over this layer, Table 22.

The permanent deformation properties of each pavement material were developed from the materials described in the example problem. The data are contained in Table 19. Other material properties such as density, Poissons ratio and coefficient of earth pressure at rest are shown in Table 23. The fatigue parameters K_1 and K_2 at different climate locations (24) as well as the stocastic coefficients such as roughness

Table 22. Input Data of Resilient Moduli of Each Pavement Materials, Representative Climate locations, and Temperature Variation.

Climate Location	Season	Length of Month	Average Temperature	Resilient Moduli, psi		
				Surface	Base	Subgrade
Port Arthur	Summer	7	77.1	380×10^3	$\varepsilon_r = k_1\theta^{k_2}$ k_1=37461 k_2=0.53	12,000
	Winter	5	56.3	$1,100 \times 10^3$		
Brownsville	Summer	7	80.4	310×10^3		
	Winter	5	64.5	760×10^3		
El Paso	Summer	7	73.9	440×10^3		
	Winter	5	48.5	$1,600 \times 10^3$		
Amarillo	Summer	7	68.9	600×10^3		
	Winter	5	41.2	$2,100 \times 10^3$		

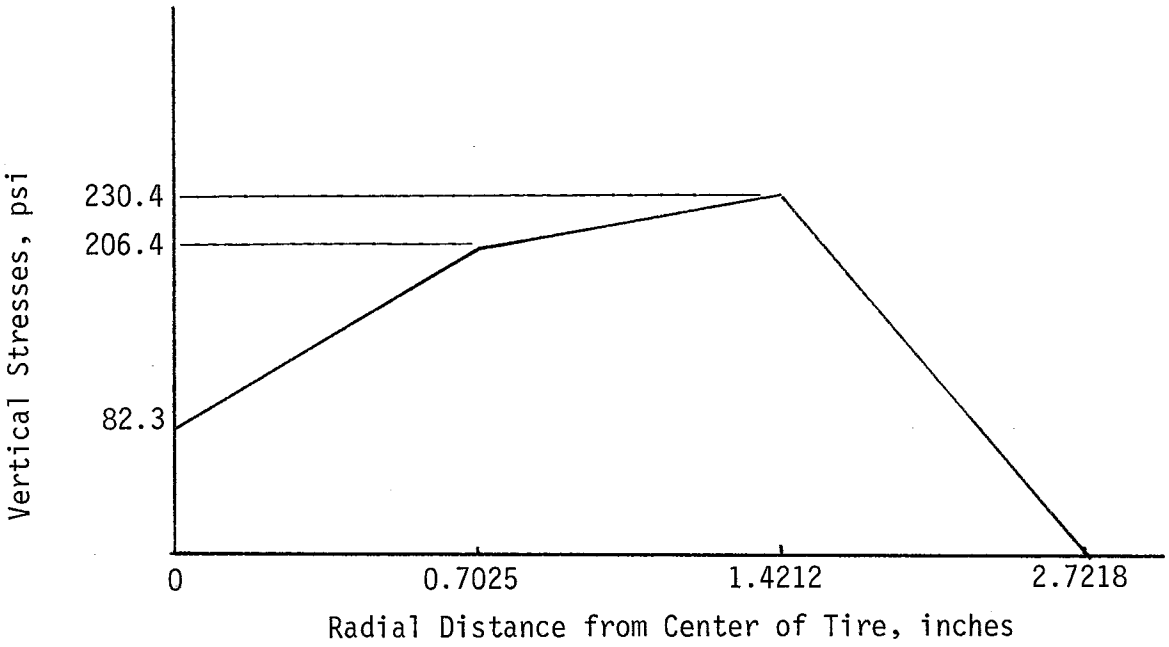

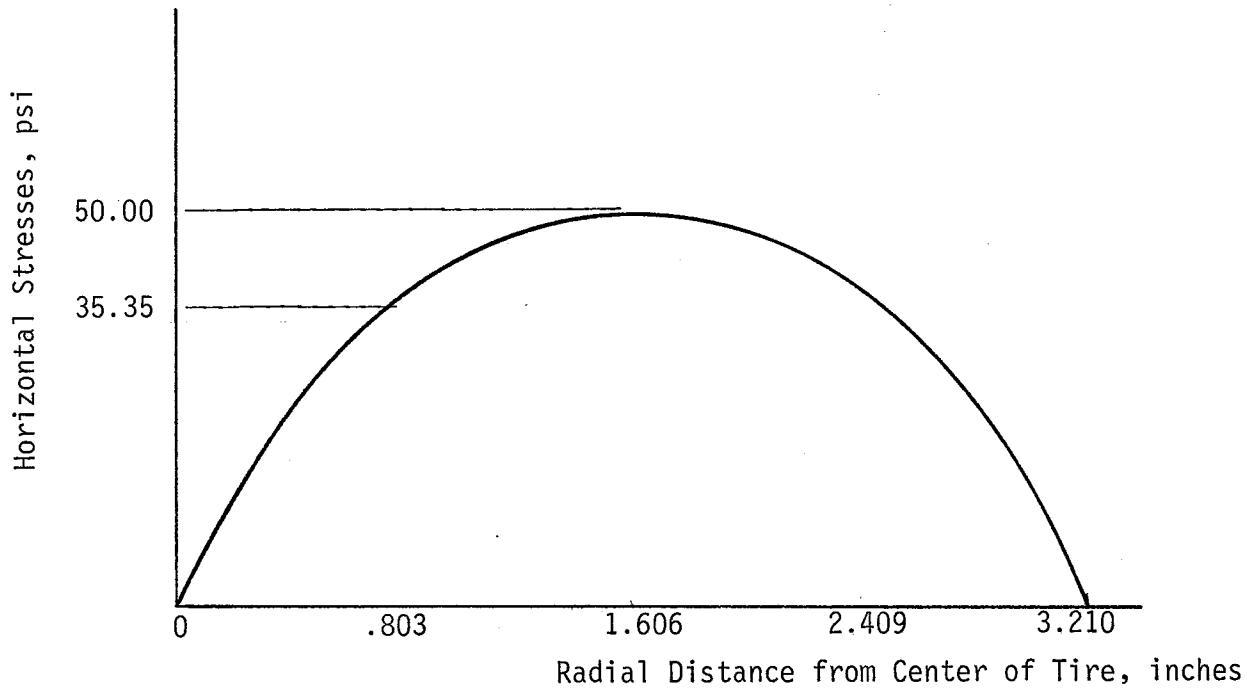

Figure 84. Vertical Stresses and Horizontal Stresses of Tire by Tielking Tire Model

Table 23. Input Data of Density, Poisson Ratio, and Coefficient of Earth at Rest of Each Pavement Materials

Structural Layer	Density, pcf	Poisson Ratio	Coefficient of Earth at Rest
Surface	145	0.35	0.67
Base	137	0.4	0.6
Subgrade	106	0.45	0.82

properties B and c, coefficients of variation of K_1 and K_2, and coefficient of co-variation of K_1K_2 used in this analysis are contained in Table 24.

Output Data

The 24 thickness and climatic zone combinations were run and the results will be described in the following sections. The discussions will be in terms of performance or distress measures of rut depth, cracking index, slope variance and serviceability.

Rutting. Rut depth is the permanent deformation in the wheel path created by repeated traffic loads. Graphs of the predicted rut depth with time for various combinations of pavement thickness, climates, and tire pressures are shown in Figures 85 to 88. From the results it is apparent that the predicted rut depth resulting from the 125 psi inflation pressures is larger than that from the 75 psi inflation pressure for all surface thicknesses. It should also be noted that the predicted rut depth is lower for the the locations with lower seasonal temperatures regardless of the tire pressure and that the thicker surfaces are more sensitive to increases in seasonal temperature than thinner ones. Although a rut depth of less than 0.5 inches in 20 years is considered excellent rutting performance, any additional increase in tire inflation pressures would accelerate the development of rutting and reduce the service life of the pavement.

Cracking. The criterion for cracking is based on fatigue produced by tensile strains at the bottom of the surface layer. The cracking index is defined using Miner's Hypothesis and failure of the pavement is assumed to occur when the cracking index is equal to 1.0. Figures 89 to 92 contain plots of cracking index as a function of time for the various combinations of pavement thickness, climate, and tire pressures. None of the pavements with a 1-inch surface thickness which were subjected to tire inflation pressures of 75 show very much cracking during the 20

Table 24. Input of Data of Fatigue Parameters and Stochastic Coefficients for Each Representative Climatic Location.

Climate Location	Season/ Temperature	k_1	k_2	c.v. $[k_1]$	c.v.$[k_2]$	c.v.$[k_1k_2]$	B	C
Port Arthur	Summer/77.1	3.177×10^{-6}	3.136					
	Winter/56.3	7.799×10^{-8}	3.541					
Brownsville	Summer/80.4	6.361×10^{-6}	3.060					
	Winter/64.5	2.927×10^{-7}	3.396	0.2	0.04	-0.9	1.0	0.058
El Paso	Summer/73.9	1.666×10^{-6}	3.206					
	Winter/48.5	2.617×10^{-8}	3.661					
Amarillo	Summer/68.9	6.417×10^{-7}	3.311					
	Winter/41.2	1.091×10^{-8}	3.756					

Climate Location	Season/Temp.	Resilient Moduli, psi Surface	Base	Subgrade
Port Arthur	Summer/77.1	380,000	k_1=3746.1 k_2=0.53	12,000
	Winter/56.3	1,100,000		

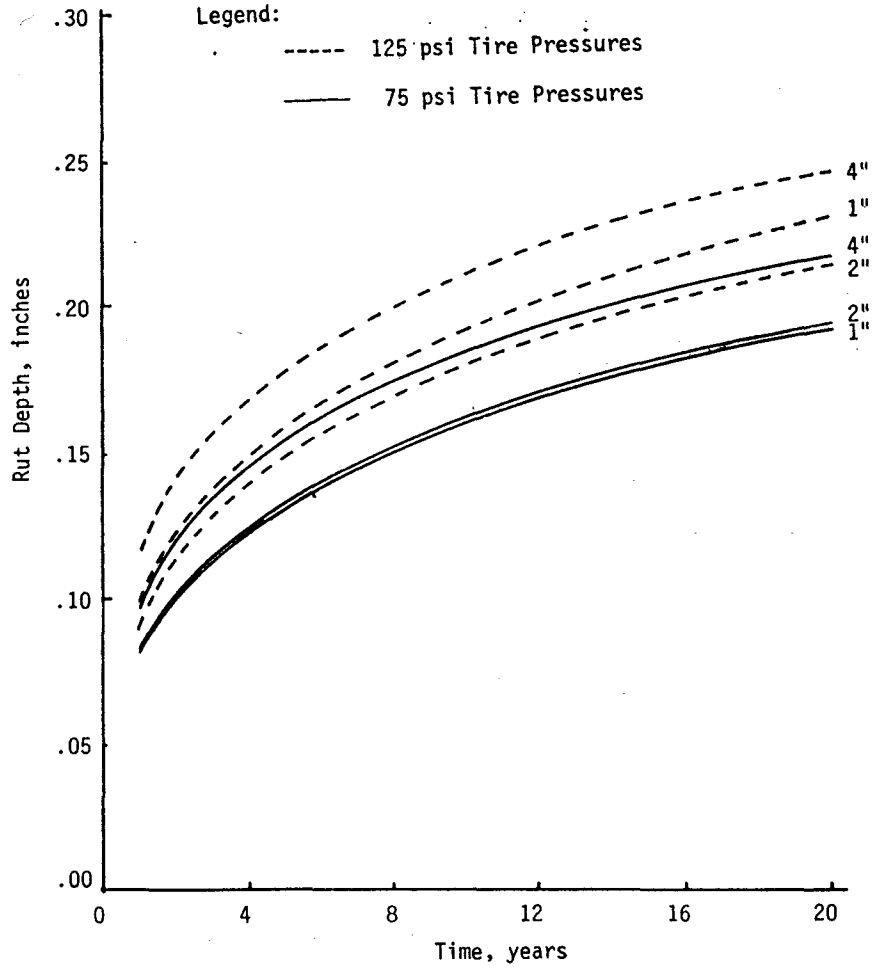

Figure 85. Predicted rutting for Port Arthur, Texas.

Climate Location	Season/Temp.	Resilient Moduli, psi Surface	Base	Subgrade
Brownsville	Summer/80.4	310,000	k_1=3746.1 k_2=0.53	12,000
	Winter/64.5	760.000		

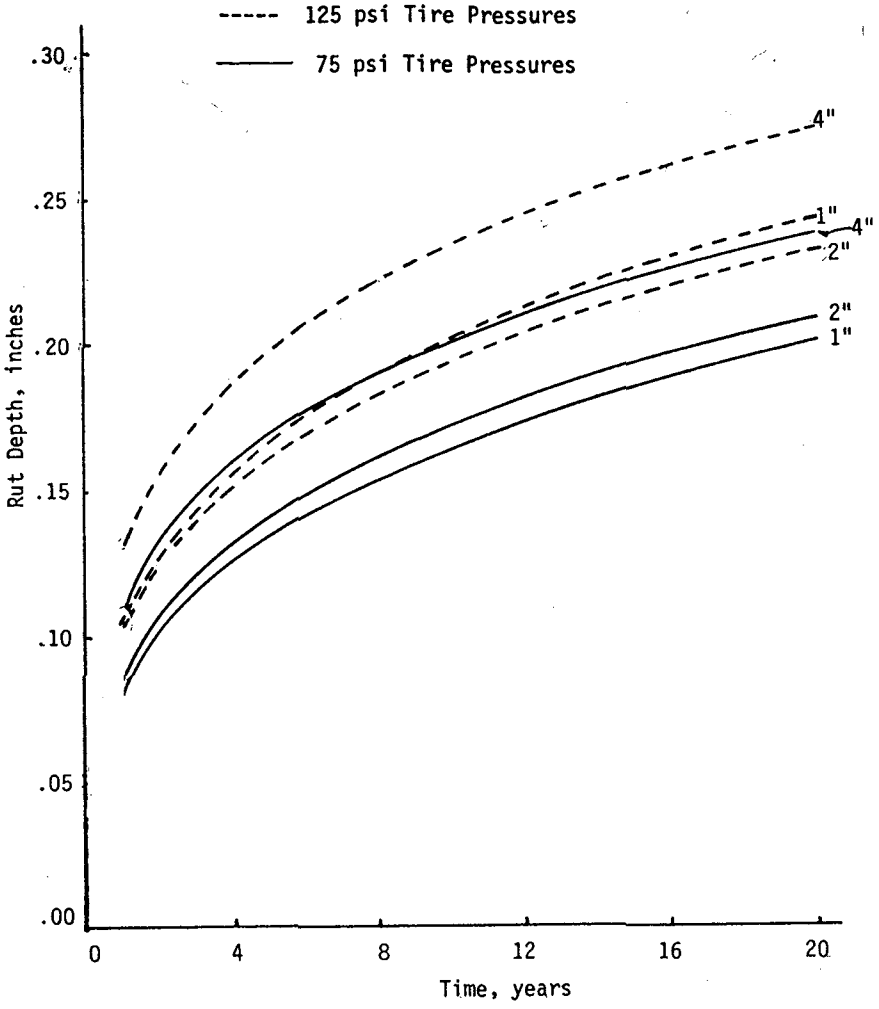

Figure 86. Predicted rutting for Brownsville, Texas.

Climate Location	Season/Temp.	Resilient Moduli, psi Surface	Base	Subgrade
El paso	Summer/73.9	440,000	k_1=3746.1 k_2=0.53	12,000
	Winter/48.5	1,600,000		

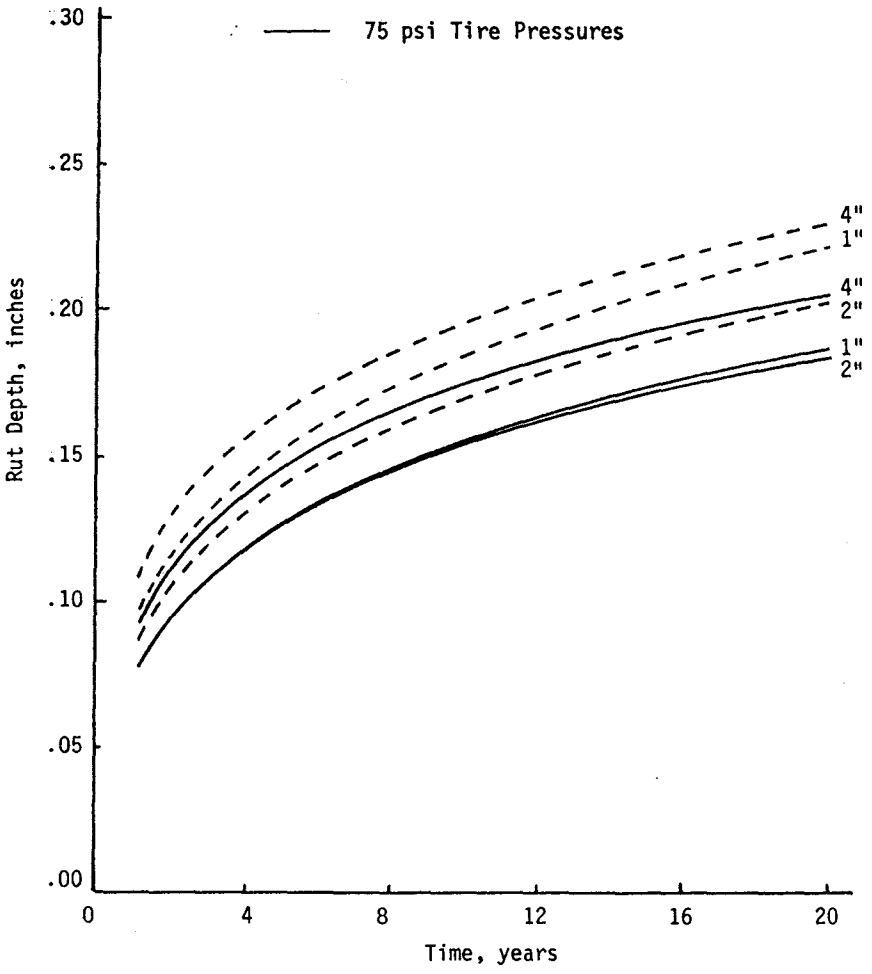

Figure 87. Predicted rutting for El Paso, Texas.

Climate Location	Season/Temp.	Resilient Moduli, psi Surface	Base	Subgrade
Amarillo	Summer/68.9	600,000	k_1=3746.1 k_2=0.53	12,000
	Winter/41.2	2,100,000		

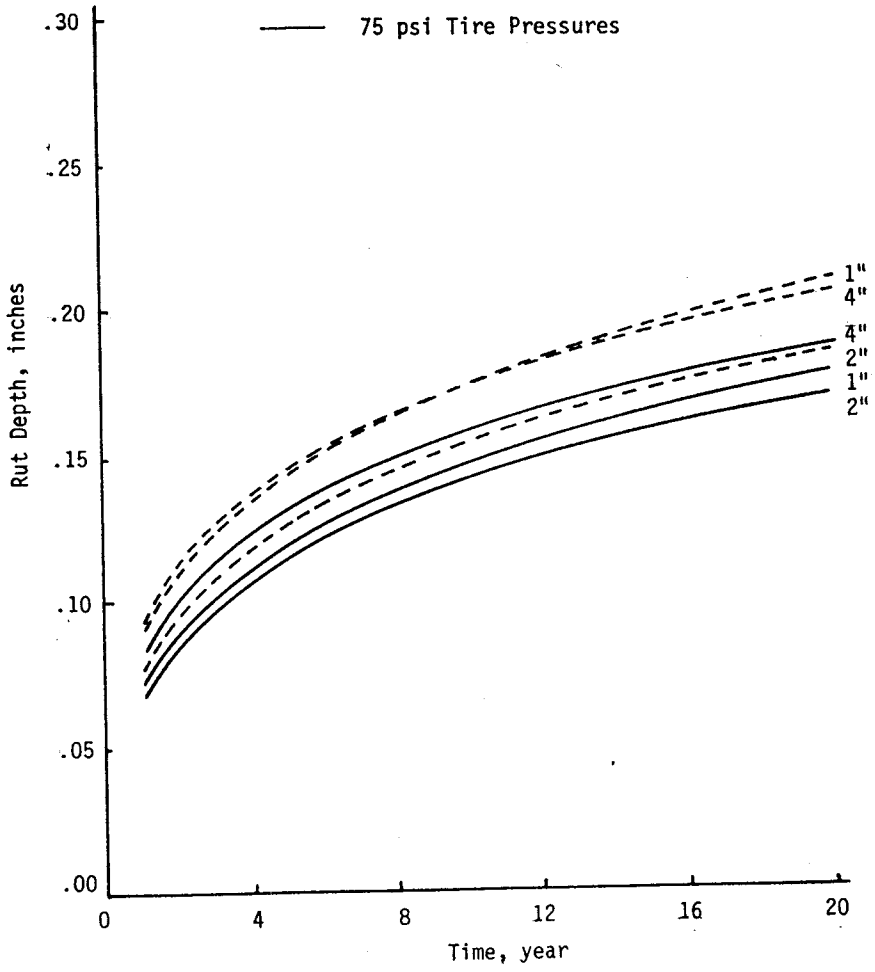

Figure 88. Predicted rutting for Amarillo, Texas.

Climate Location	Season/Temp.	Resilient Moduli, psi Surface	Base	Subgrade
Port Arthur	Summer/77.1	380,000	k_1=3746.1 k_2=0.53	12,000
	Winter/56.3	1,100,000		

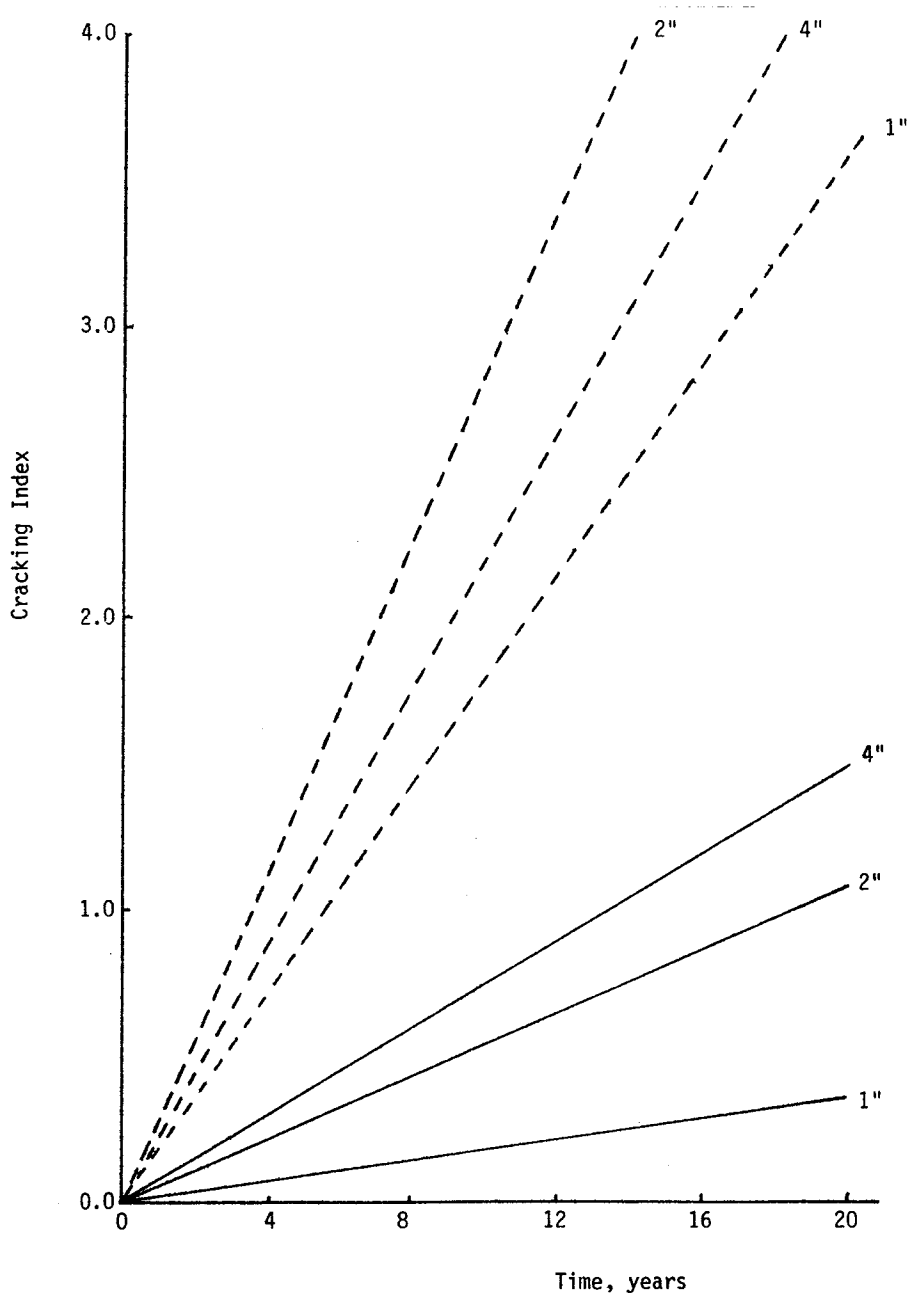

Figure 89. Prediced cracking index for Port Arthur, Texas.

Climate Location	Season/Temp.	Resilient Moduli, psi Surface	Base	Subgrade
Brownsville	Summer/80.4	310,000	k_1=3746.1 k_2=0.53	12,000
	Winter/64.5	760.000		

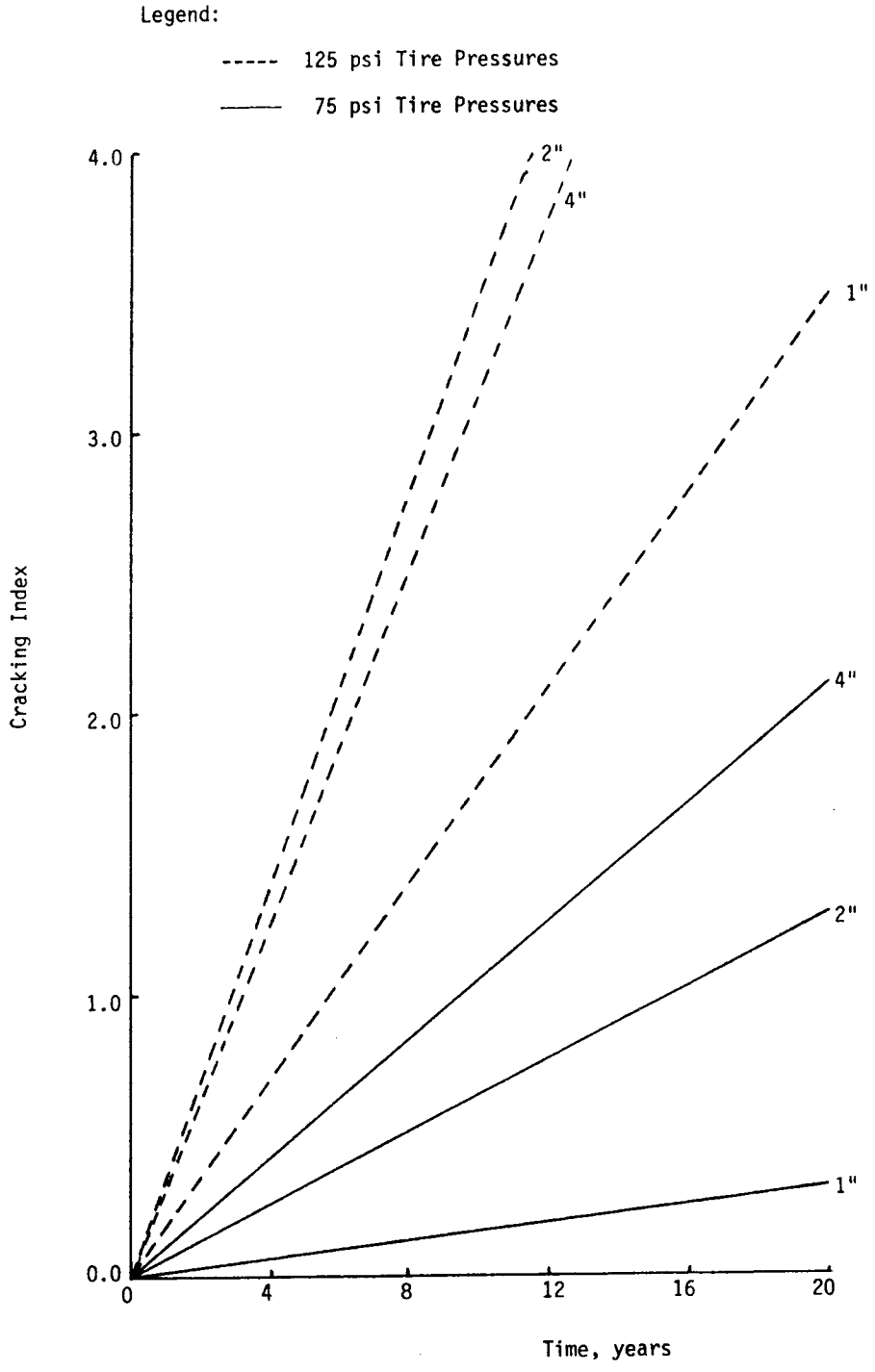

Figure 90. Predicted cracking index for Brownsville, Texas.

Climate Location	Season/Temp.	Resilient Moduli, psi Surface	Base	Subgrade
El paso	Summer/73.9	440,000	k_1=3746.1 k_2=0.53	12,000
	Winter/48.5	1,600,000		

Legend:

----- 125 psi Tire Pressures

——— 75 psi Tire Pressures

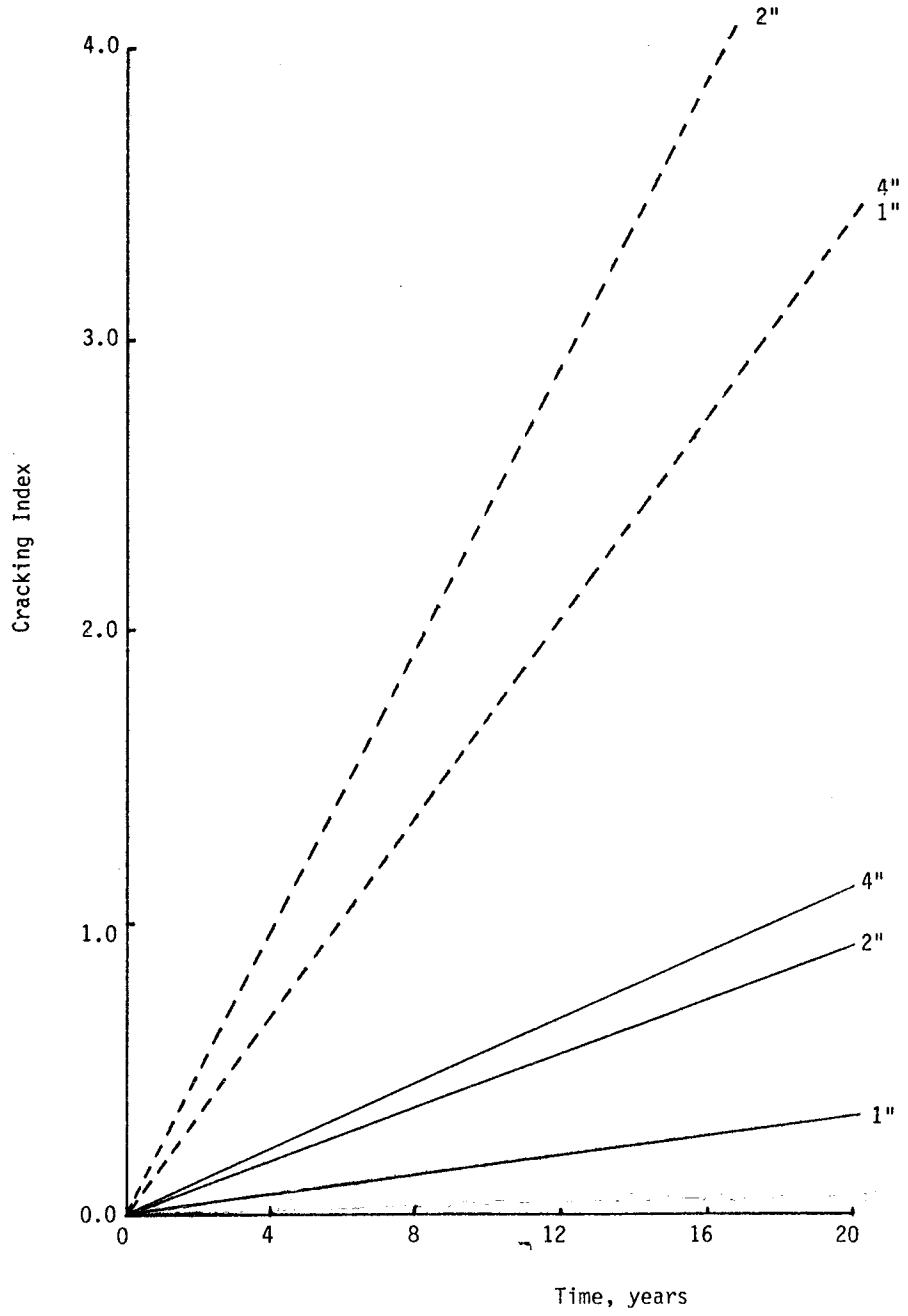

Figure 91. Predicted cracking index for El Paso, Texas.

Climate Location	Season/Temp.	Resilient Moduli, psi Surface	Base	Subgrade
Amarillo	Summer/68.9	600,000	k_1=3746.1 k_2=0.53	12,000
	Winter/41.2	2,100,000		

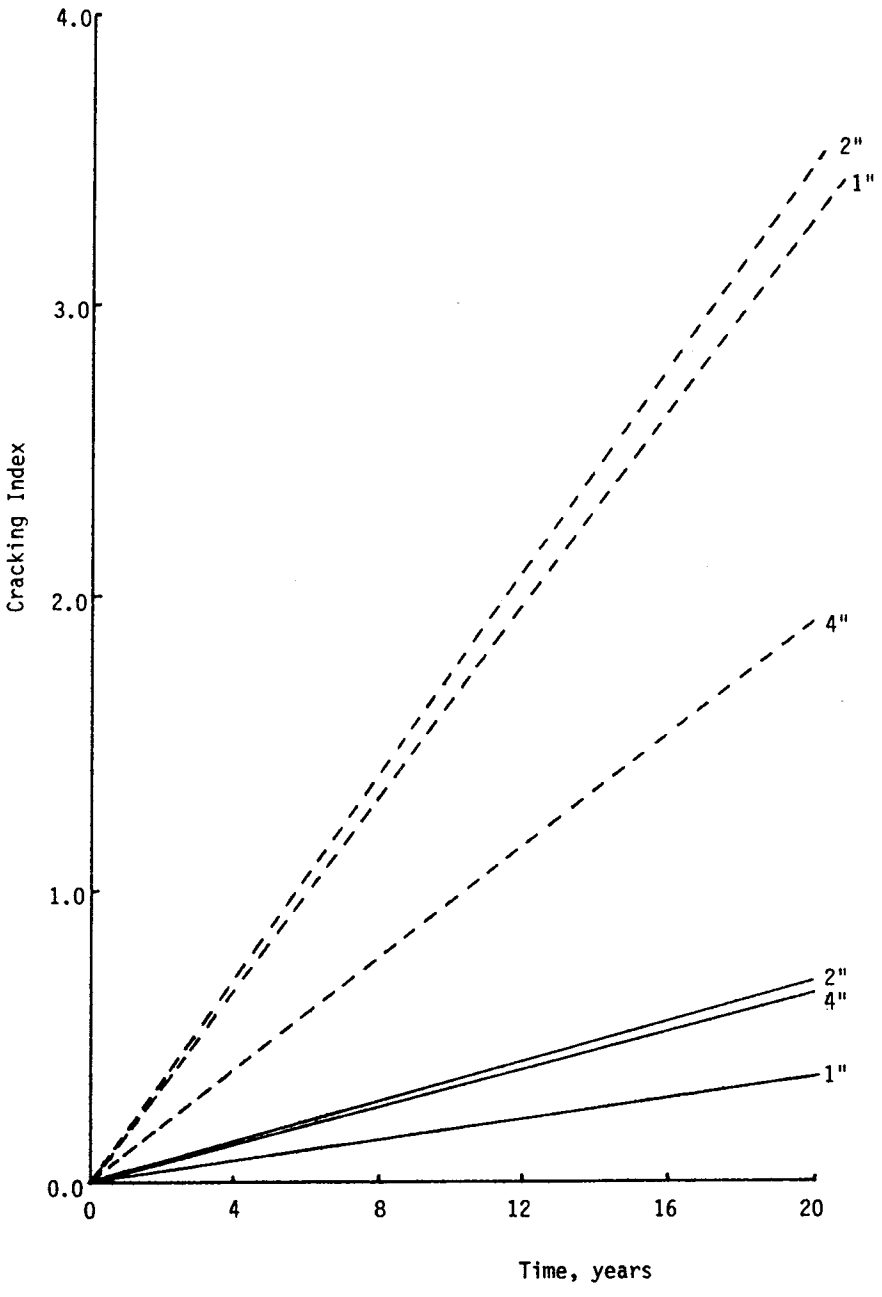

Figure 92. Predicted cracking index for Amarillo, Texas.

years. However, a cracking index of 1.0 occurs with both the 2-inch and 4-inch thick surface layers for all climatic zones except the Amarillo zone. For 125 psi inflation pressure, cracking occurs on the 1-inch, 2-inch, and 4-inch thick surface layers for all climatic zones within 10 years. Also shown in these figures is the fact that a 2-inch surface thickness cracks at a faster rate than the 1-inch and 4-inch layers. It is worth noting the relationship between the various surface thickness and inflation pressure interactions with different seasonal temperature changes. Analysis of the plots in Figure 89 and 92 shows that cracking dramatically decreases with decreasing temperature especially for 4-inch thick surfaces, regardless of whether the tires are inflated at 74 or 125 psi. Although cracking decreases with decreasing temperatures for the 2-inch and 4-inch surface, there appears to be no significant change with temperature for the 1-inch surface loaded at 75 and 125 psi inflation pressure.

Slope Variance. In the modified ILLIPAVE program, the variance of rut depth is computed in the rut depth model and then used to estimate the slope variance. The difference in rut depth occurs because of the stochastic material variability of each layer. Figures 93 to 96 present the predicted slope variance as a function of time for the four climatic locations and two tire pressure models for the different surface thicknesses. These results show that slope variance increases with increase in tire pressure and that the slope variance decreases with decrease in seasonal temperature regardless of the inflation pressures. The thinner surface experienced larger values of slope variance with increasing tire pressure.

Serviceability. The overall serviceability plots of the pavements in each climatic zone are shown in Figures 97 to 100. These plots show the predicted decline of present serviceability index with the time for each combination. These figures show that the PSI for pavements loaded at 125 psi inflation pressure is lower than for similiar pavements loaded at 75 psi inflation pressure. The plots also show that the pavements in warm

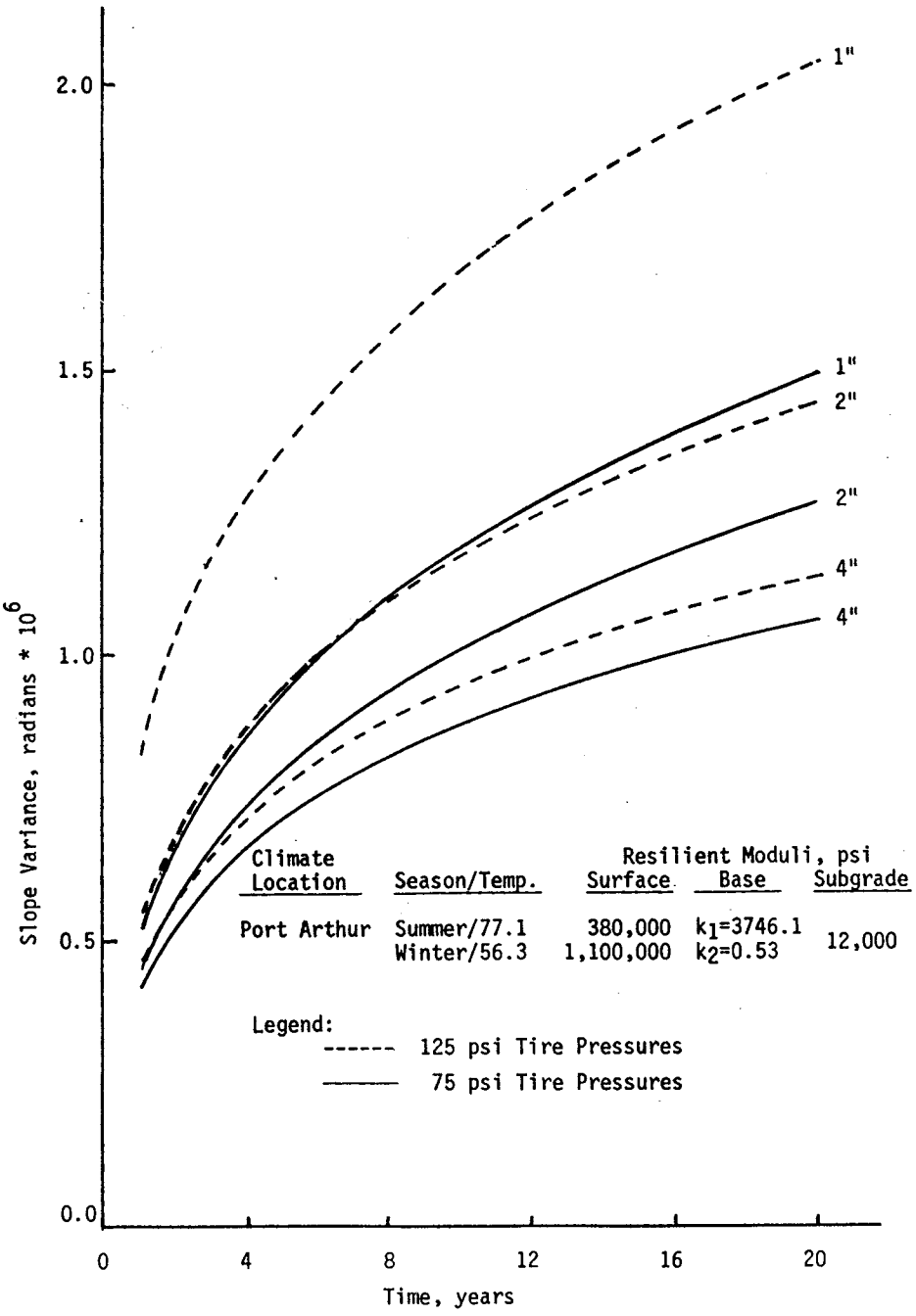

Figure 93. Predicted slope variance for Port Arthur, Texas.

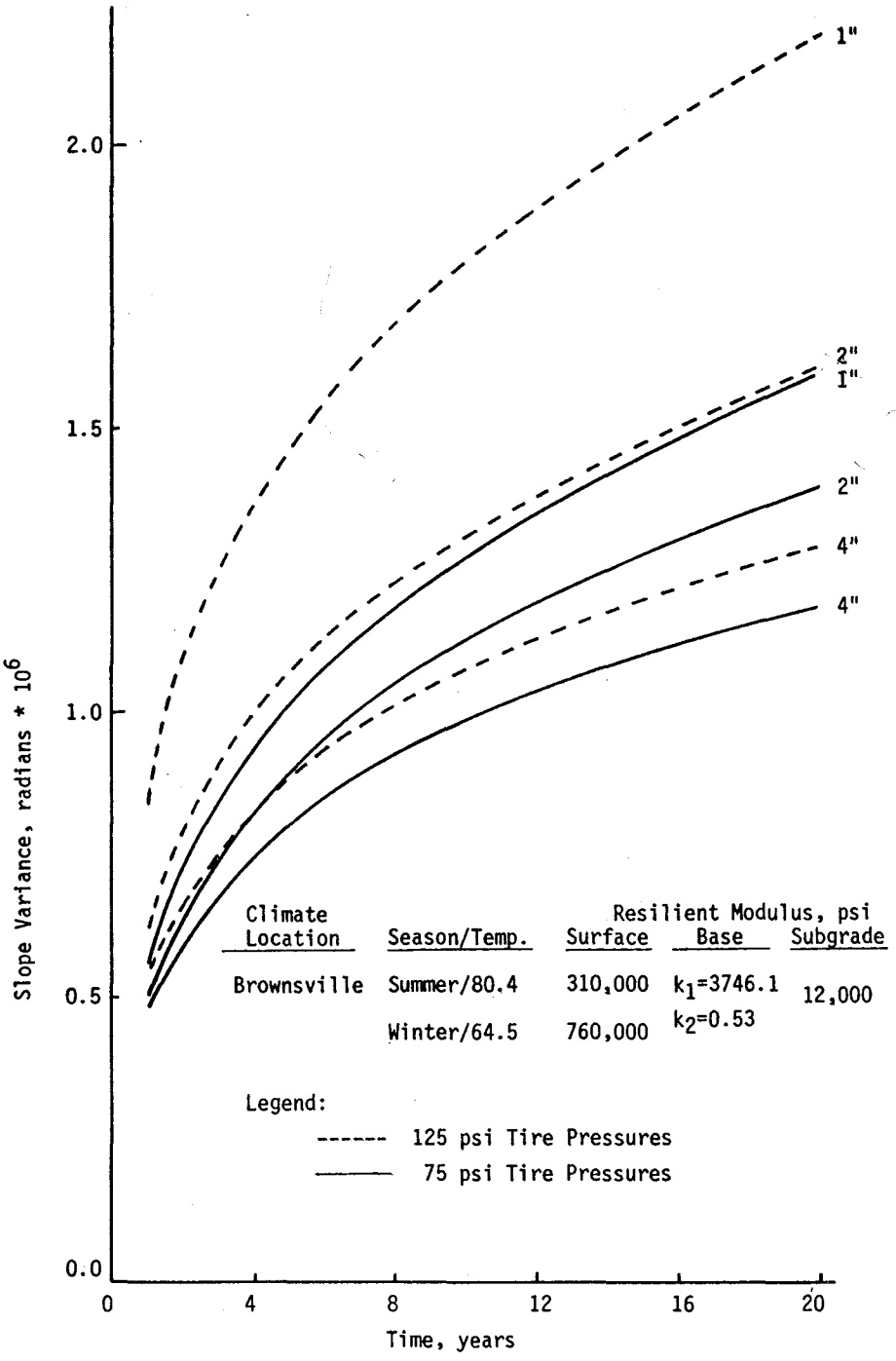

Figure 94. Predicted slope variance for Brownsville, Texas.

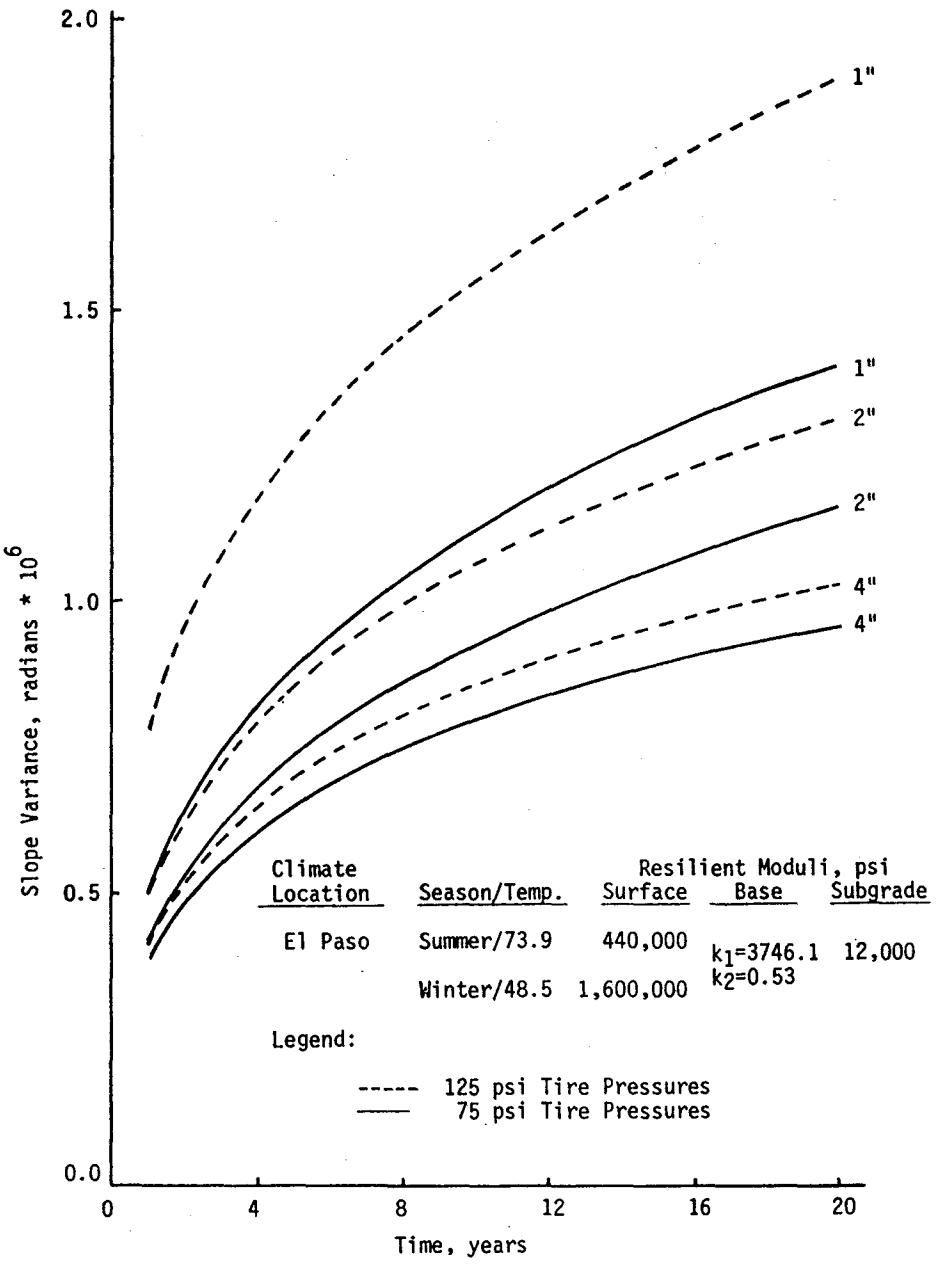

Figure 95. Predicted slope variance for El Paso, Texas.

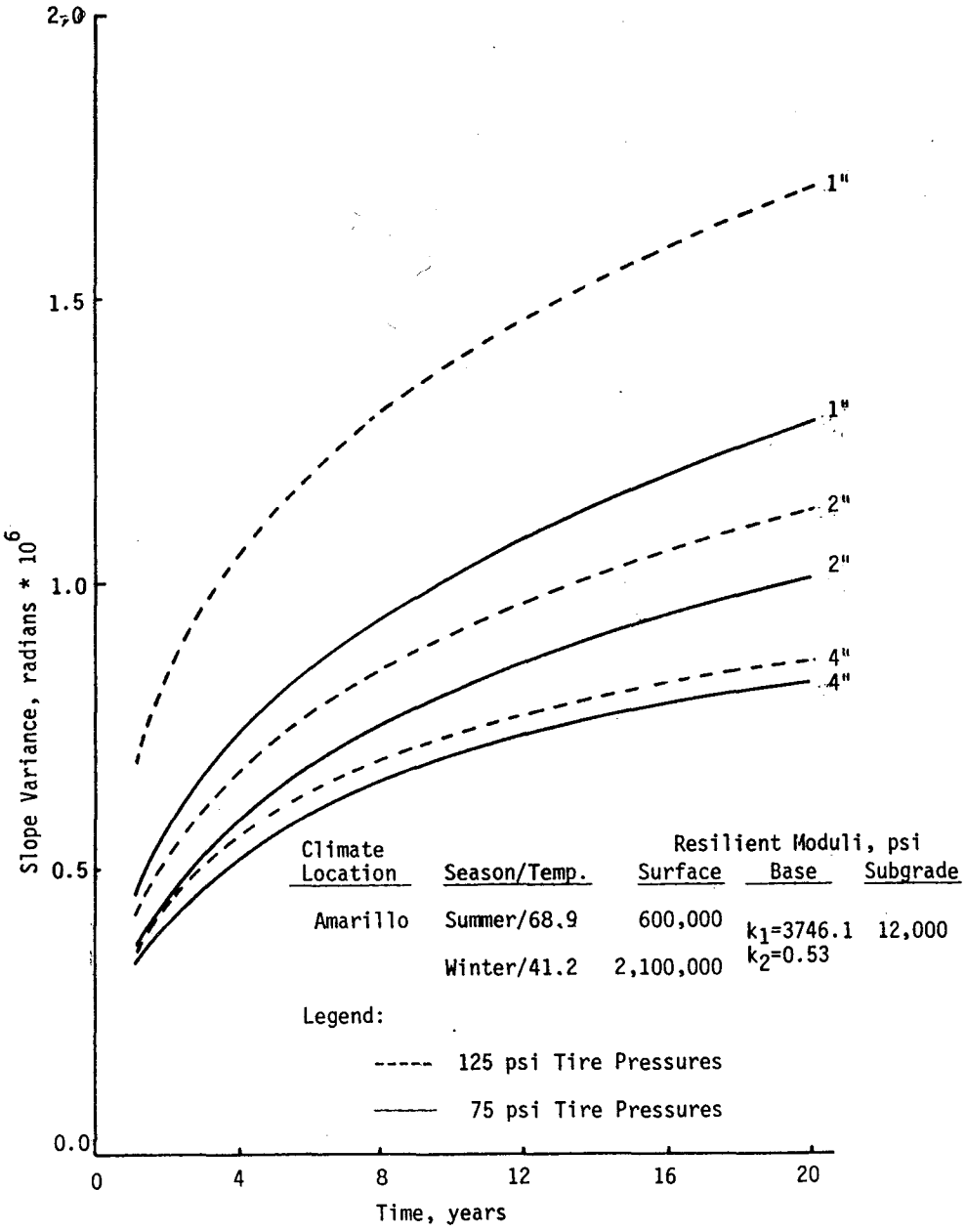

Figure 96. Predicted slope variance for Amarillo, Texas.

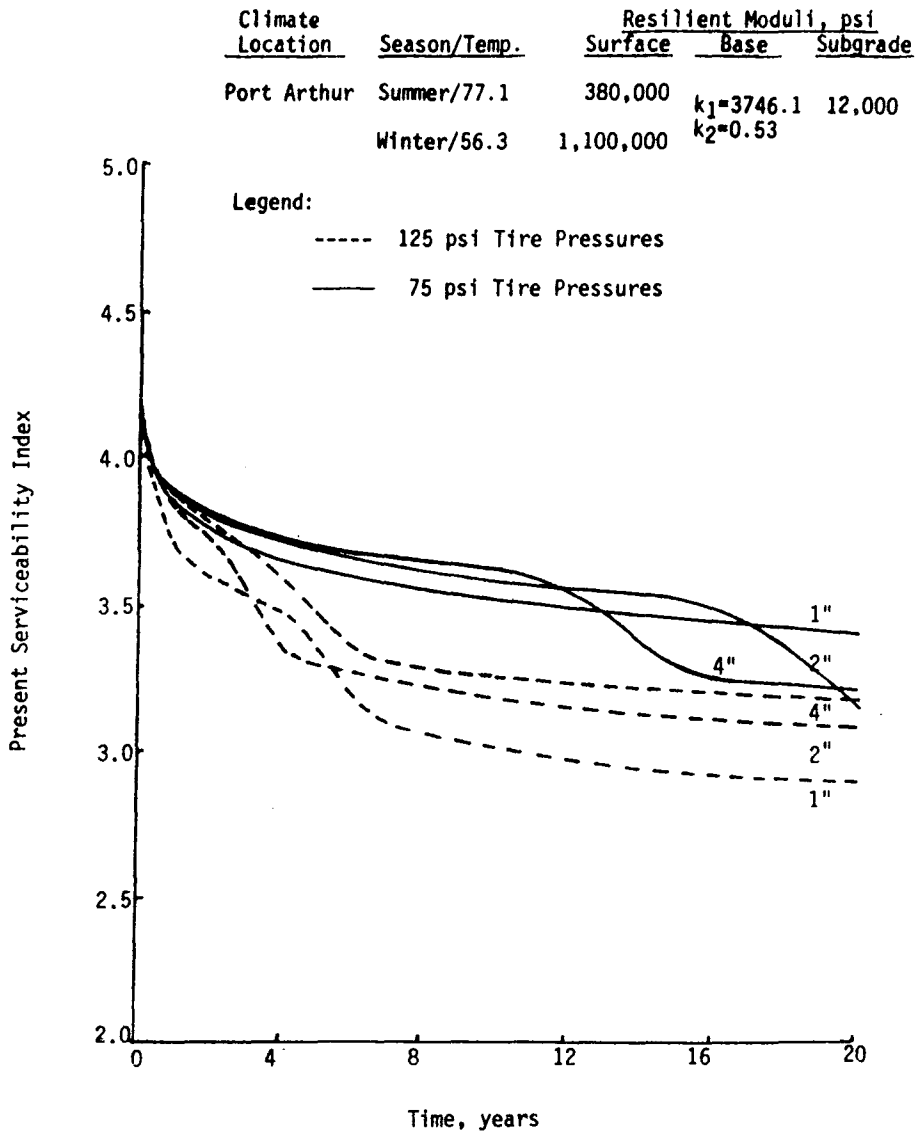

Figure 97. Predicted present serviceability index (PSI) for Port Arthur, Texas.

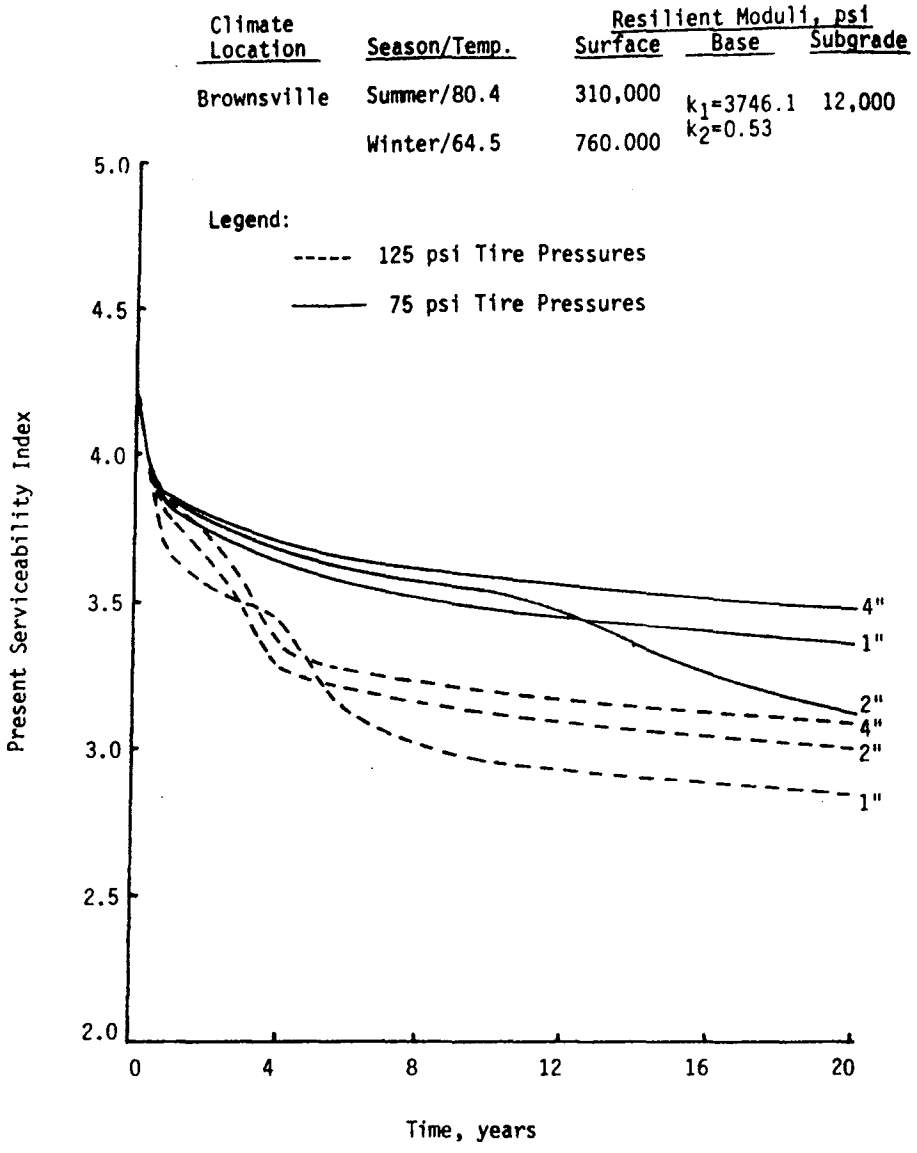

Figure 98. Predicted present serviceability index (PSI) for Brownsville, Texas.

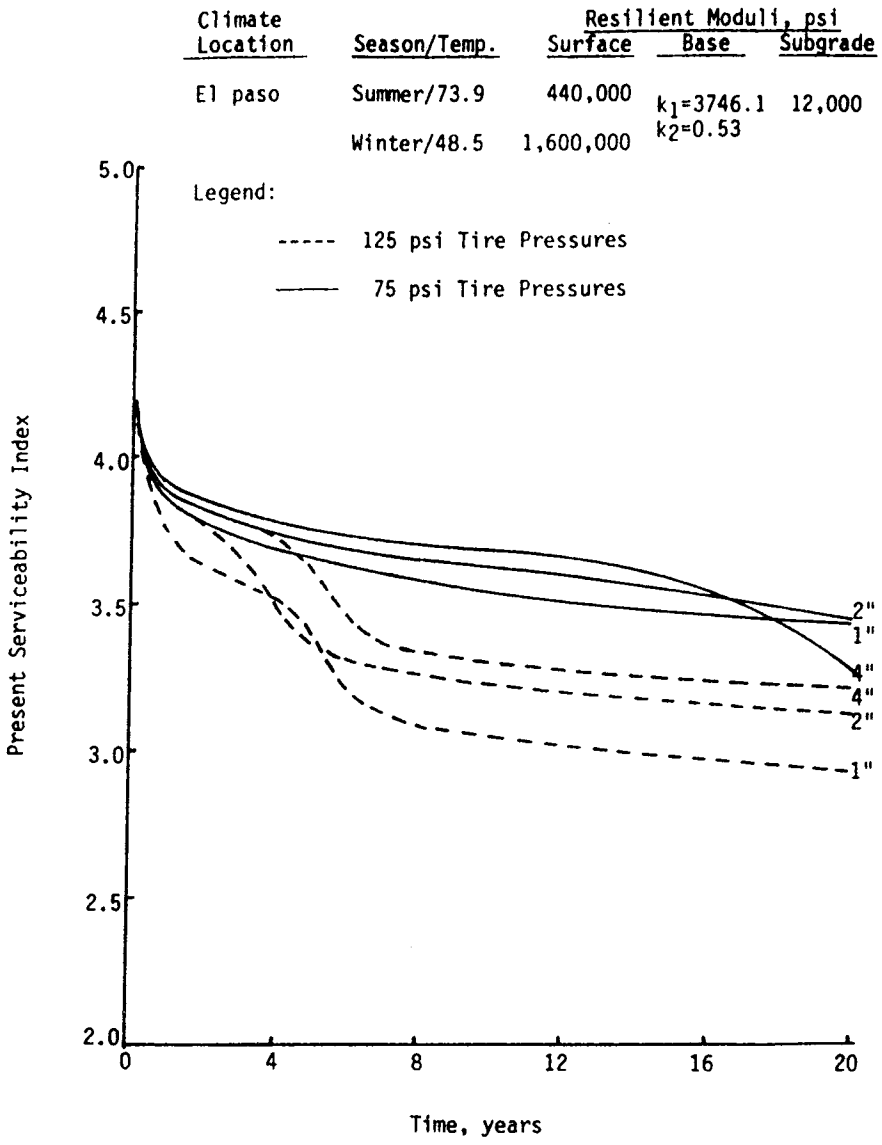

Figure 99. Predicted present serviceability index (PSI) for El Paso, Texas.

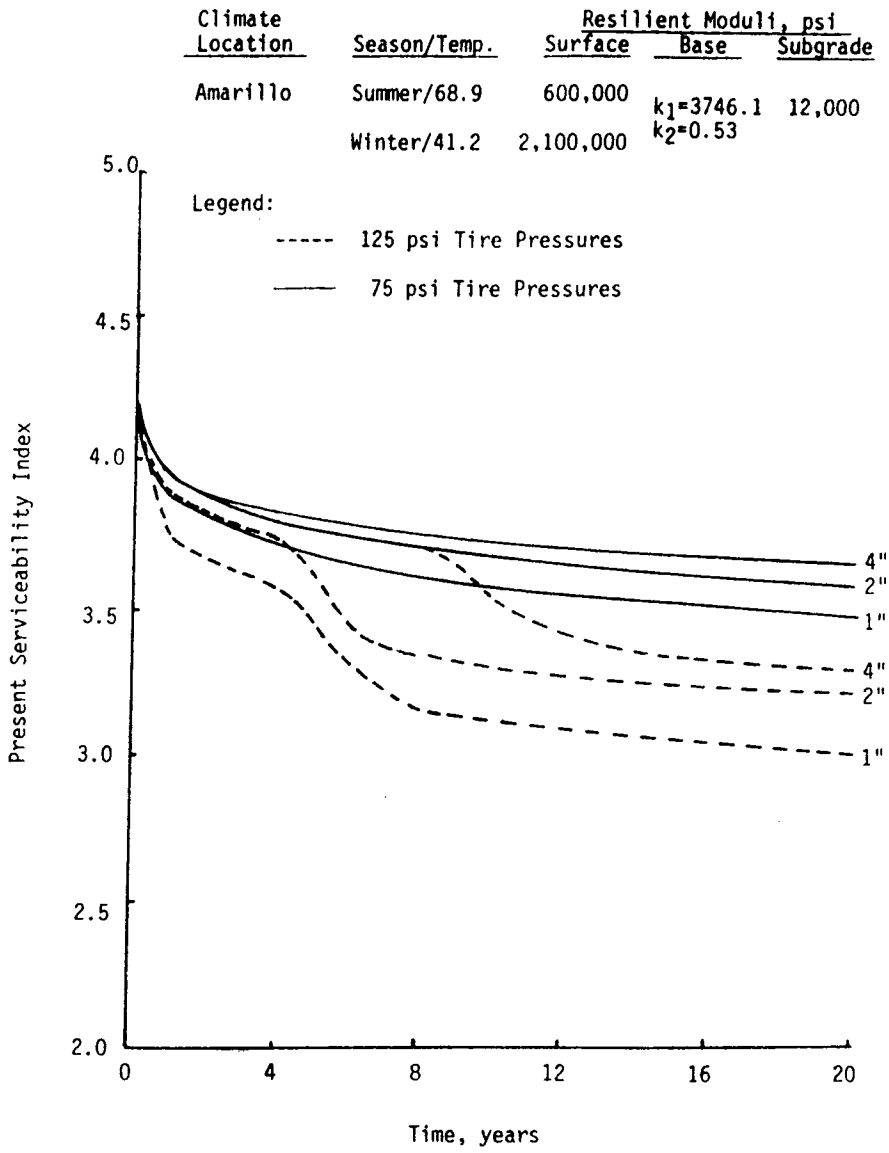

Figure 100. Predicted present serviceability index (PSI) for Amarillo, Texas.

climates have a lower value of PSI than similiar pavements in cold climates.

CHAPTER 6

CONCLUSIONS AND RECOMMENDATIONS

CONCLUSIONS

Field Studies indicate that for the 3-S2 vehicle, which is the predominant cargo vehicle on the highway system, the tire inflation pressures are considerably higher than those assumed for most pavement design procedures. Analytical studies of truck tires show that the inflation pressure is magnified about two times when the tire contacts the road surface. The magnification is a result of an interaction between the structure of the tire and the road. The end result is that for inflation pressures of 75 and 125 psi the peak contact pressures are about 150 and 220 psi, respectively. Contact pressures of this magnitude produce high strains in thin pavement surfaces which often lead to premature fatigue cracking failures. The analytical studies to evaluate the effect of tire contact pressures of flexible pavements, indicate that

(1) for truck tire loadings, premature fatigue cracking can occur when the surface thicknesses are between 1 and 3-inches and are placed over flexible bases,

(2) for passenger tire loadings, the strains at the bottom of the surface may be large enough to require the pavement designer to consider this class of vehicle in pavement design, especially for surfaces between 1 and 3-inches over weak granular bases,

(3) the high contact pressures from truck tires is expected to be a major factor causing the significant increase in rutting observed on Texas highways, and

(4) the Tielking tire model program produces very good estimates of tire contact pressure distributions that can be used in pavement studies.

RECOMMENDATIONS

Results from the field and analytical studies indicate that the pavement and rehabitation design procedures used by the Department should be expanded to explicitly consider the effects of tire contact pressure on stresses in flexible pavements. In addition, when thin asphalt surfaces are placed over granular bases, consideration should be given to the strains induced by the contact pressures from typical passenger vehicles.

Since the analytical studies of the effect of tire contact pressure distributions involved only a few tires, additional studies should be performed using other types of tires. Of particular interest is radial truck tires since the field study indicated that more than 50 percent of the truck tires measured were radials.

REFERENCES

1. Berger, M., "Kinematics of a Rolling Tire and Its Application to Tire Performance," Journal of Applied Polymer Science, Vol. II, No. 5, pp. 174-180, 1959.

2. Lippmann, S. A., and Oblizajek, K. L., "The Distributions of Stress Between the Tread and the Road for Freely Rolling Tires," SAE Paper 740072, Automotive Engineering Congress, 1974.

3. Moore, D. F., The Friction of Pneumatic Tyres, Elsevier, 1975.

4. Seitz, N., and Hussmann, A. W., "Forces and Displacement in Contact Area of Free Rolling Tires," SAE Transactions Vol. 80, Paper 710626, 1971.

5. Frank, F. and Hofferberth, W., "Mechanics of the Pneumatic Tire," Rubber Chemistry and Technology, Vol. 40, No. 1, pp. 271-322, 1967.

6. Clark, S. K., ed., Mechanics of Pneumatic Tires, U.S. Department of Transportation (NHTSA) 1981.

7. Ridha, R. A., et al., "Contact Loading of a Rubber Disk," Tire Science and Technology, Vol. 13, No. 1, pp. 3-15, 1985.

8. Ridha, R. A., et al., "Finite Element Modeling of a Homogeneous Pneumatic Tire Subjected to Footprint Loadings," Tire Science and Technology, Vol. 13, No. 2, pp. 91-110, 1985.

9. Tielking, J. T., "A Finite Element Tire Model," Tire Science and Technology, Vol. 11, Nos. 1-4, pp. 50-63, 1983.

10. Tillerson, J. R., and Haisler, W. E., "SAMMSOR II - A Finite Element Program to Determine Stiffness and Mass Matrices of Shells of Revolution," TEES-RPT-70-18, Texas A&M University, October, 1970.

11. Haisler, W. E., and Stricklin, J. A., "SNASOR II - A Finite Element Program for the Static Nonlinear Analysis of Shells of Revolution," TEES-RPT-70-20, Texas A&M University, October, 1970.

12. Tielking, J. T., and Schapery, R. A., "A Method for Shell Contact Analysis," Computer Methods in Applied Mechanics and Engineering, Vol. 26, No. 2, pp. 181-195, 1981.

13. Bonse, R.P.H., and Kuhn, S. H., "Dynamic Forces Exerted by Moving Vehicles On a Road Surface," Highway Research Board Bulletin, No. 233, pp. 9-32, 1959.

14. 1984 Year Book, The Tire and Rim Association, Inc., 3200 W. Market Street, Akron, Ohio 44313.

15. Burmister, D.M., "The Theory of Stresses and Displacements in layered system and Applications to the Design of Airport Runways." Proc., Highway Research Board, Vol. 23, 1943.

16. Duncan, J.M., C.L. Monismith, and E.L. Wilson, "Finite Element Analysis of Pavements." HRB, Highway Research Record 228, 1968. pp. 18-33.

17. Radd, L. and J.L. Figueroa, "Load Response of Transportation Systems." Transporation Engineering Journal, ASCE, Vol. 106, No.1, TEI, 1980. pp 111-128.

18. Taylor, M.L., "Characterization of Flexible Pavements by Non-Destruction Testing." Civil Engineering Department, University of Illinois at Urbana - Champaign, Ph.D. disertation, 1978.

19. ILLIPAVE User's Manual. Transportation Facilities Group, Department of Civil Engineering University of Illinois at Urbana - Champaign, May, 1982.

20. Pickett, D.E., D. Saylak, R.L. Lytton, W.E. Conger, D. Newcomb, and R.A. Schapery, "Extension and Replacement of Asphalt cement with Sulfur," Federal Highway Administration, Rept No. FHWA-RD-78-95, March, 1978.

21. Barksdale, R.D., "Laboratory Evaluation of Rutting in Base Course Materials," Proceedings, 3rd International Conference on Structural Design of Asphalt Pavements, University of Michigan, Ann Arbor, 1972.

22. Edris, E.V., and R.L. Lytton, "Dynamic Properties of Subgrade Soils, Including Environmental Effect," Research Report No. 164-3, Texas Transportation Institute, Texas A&M University, College Station, Tx., May 1976.

23. Soussou, J.E., F. Moavenzadek and H.K. Findakly, "Synthesis for Rational Design of Flexible Pavements, Part II," Federal Highway Administration, Contract No. FH-11-776, Washington D.C., January 1973.

24. Rauhut, J.B., J.C. O'Quin, and W.R. Hudson, "Sensitivity Analysis of FHWA Structural Model VESYS II," Vol. 1 and 2, Federal Highway Administration Report, No. FHWA-RD-76-23, Washington, D.C., March 1976.

25. Kenis, W.J., "A Design Method for Flexible Pavements Using the VESYS Structural Subsystem," Proceedings, 4th International Conference Structural Design of Asphalt Pavement, University of Michigan, Ann Arbor, Michigan, Vol. 1, 1977.

26. Witczak, M.W., "Development of Regression Model for Asphalt Concrete Modulus for Use in MS-1 Study," January, 1978.

27. Van der Poel, C., "A General System Describing the Visoelastic Properties of Bitumens and Its relation to Routine Test Data," Journal of Applied Chemistry, Vol 4, 1954.

28. Huekelom, W. and Klomp, A.J.G., "Road Design and Dynamic Loading," Proceedings, Association of Asphalt Paving Technologists, Dallas, Texas, Vol. 33, 1964.

29. Rada, G. & Witczak, M.W., "Comprehensive Evaluation of Laboratory Resilient Moduli Results from Granular Material." Transportation Research Record 810, Transportation Research Board, National Research Council, Washington D.C., 1981, pp23-33.

30. Claessen, A.I.M., Valkering, C.P., and Diturarch, R., "Pavement Evaluation with the Falling Weight Deflectometer." Proceedings, Association of Asphalt Paving Technologists, Vol 45, 1976.

31. "The AASHO Road Test: Report 5 - Pavement Research", Special Report 61E, Highway Research Board, National Academy of Sciences, National Research Council, 1962.

32. Witczak, M.W., "Design of Full-Depth Asphalt Airfield Pavements," Proceedings, Third International Conference on the Structural Design of Asphalt Pavements, London, England, 1972.

33. Roberts, F.L., Kennedy, T.W., and Elkins, G.E., "Material Properties to Minimize Distress in Zero-Maintenance Pavement," Report No. FHWA-RD-80, Federal Highway Administration, Office of Research and Development, Washington D.C., August 1979.

34. Roberts, F.L., and B.T. Rosson, "Establishing Material Properties for Thin Asphalt Concrete Surfaces on Granular Bases", Report No. FHWA-TX-85-345-1, Texas Transportation Institute, Texas A&M University, College Station, Texas, November 1985.

35. Roberts, F.L., and R. Urruela, "Effects of Automobile Tire Loads on Thin Flexible Pavements", Draft Report No. FHWA-TX-84-345-2, Texas Transportation Institute, Texas A&M University, College Station, Texas, January 1986.

36. Monismith, C.L., "Fatigue Characteristics of Asphalt Paving Mixtures and Their Use in Asphalt Pavements", University of New Mexico, Symposium on Fatigue in Asphalt Pavements, January 7, 1981.

37. "Asphalt Concrete Overlays of Flexible Pavements, Vol. 1, Development of New Design Criteria", Final Report, Federal Highway Administration, Washington, D.C. June, 1975.

38. Katona, M.G., "A Simple Contact - Friction Interface Element with Applications to Buried Culverts," International Journal for Numerical and Analytical Methods in Geomechanics, Vol. 7, 1983, pp 371-384.

39. Lytton, R.L. , Class notes for the course of Numerical Methods in Geotechnical Engineering, 1983.

40. DeJong, D.L., M.G.F. Poutz and A.R. Korswagon," Computer Program BISAR: Layered Systems under Normal and Tangential Surface Loads," External Report AMSR, 006.73. Koniklijke/Shell Laboratorium, Amsterdam, Netherlands, 1973.

2372 DATA COLLECTION

TEST NO. _____ STATE LIC._____ AASHTO CLASS. _____ COMMODITY _____ TEMP: PAVT. _____°F AIR _____°F DATE _____

LOCATION _____ WEATHER _____ COMMENTS _____

	TIRE MANUFACTURER	RAD/ BIAS	SIZE	PRESSURE (PSI) 1st	2nd*	TREAD DEPTH (1/32 IN)	PRINT BY CALIPER Width (IN)	Length(IN) CTR	OUT	WEIGHT (LB/TON)	LENGTH $x_1 x_2 x_3$	WIDTH	HEADLIGHT HEIGHT
(F)													
(1)													
(2)													
(3)													
(4)													

* Recorded Time after Vehicle Stops.

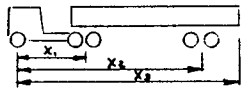

2372 DATA COLLECTION

TEST NO. _____ STATE LIC._____ AASHTO CLASS. _____ COMMODITY _____ TEMP: PAVT. _____°F AIR _____°F DATE _____

LOCATION _____ WEATHER _____ COMMENTS _____

	TIRE MANUFACTURER	RAD/ BIAS	SIZE	PRESSURE (PSI) 1st	2nd*	TREAD DEPTH (1/32 IN)	PRINT BY CALIPER Width (IN)	Length(IN) CTR	OUT	WEIGHT (LB/TON)	LENGTH $x_1 x_2 x_3$	WIDTH	HEADLIGHT HEIGHT
(F)													
(1)													
(2)													
(3)													
(4)													

* Recorded Time after Vehicle Stops.

APPENDIX B. SIGNIFICANCE TESTS FOR FACTORS AFFECTING TIRE PRESSURES

To test the effect of axle weights on tire pressures in the presence of tire construction, tread depth, and front/all-other axles, for 3-S2 trucks, the following model was used:

$$y = \beta_0 + \beta_1 X_1 + \beta_2 X_2 + \beta_3 X_1 X_2 + \beta_4 X_3 + \beta_5 X_1 X_3 + \beta_6 X_4 + \beta_7 X_1 X_4$$

where y = tire pressure

X_1 = axle weight

X_2 = 1 Bias
0 Radial

X_3 = 1 Tread Depth $\geq$8/32"
0 Tread Depth $<$8/32"

X_4 = 1 Other axle
0 Front axle

$\beta_0, \beta_1, \ldots, \beta_7$ are model parameters.

The result of the model estimation is shown below:

DEP VARIABLE: PRESSURE

SOURCE	DF	SUM OF SQUARES	MEAN SQUARE	F VALUE	PROB>F
MODEL	3	38938.508	12996.169	68.560	0.0001
ERROR	863	163589	189.559		
C TOTAL	866	202578			

ROOT MSE	13.768046	R-SQUARE	0.1925
DEP MEAN	95.764706	ADJ R-SQ	0.1897
C.V.	14.37695		

VARIABLE	DF	PARAMETER ESTIMATE	STANDARD ERROR	T FOR HO: PARAMETER=0	PROB > |T|
INTERCEP	1	83.029589	2.687891	30.890	0.0001
WEIGHT	1	0.0007662898	0.0001491228	5.139	0.0001
TYPE	1	-12.688041	1.085518	-11.688	0.0001
TREAD	1	5.682135	1.411034	4.027	0.0001

APPENDIX C. COMMODITY CODES FOR ANOVA

Recoded commodity types for ANOVA:

1. Produce
2. Grain, Feed, Milo
3. Cattle
4. Logs
5. Rock, Sand, Gravel, Limestone
6. Food and Beverage:
    - Beverage
    - Dairy
    - Food
    - Meat
    - Reefer
7. Solid Bulk:
    - Cement
    - Asphalt
    - Gypsum
    - Lime
    - Woodchips
    - Finished Lumber
    - Tar
8. Liquid and Gas Bulk:
    - Milk
    - Water
    - Liquid
    - Liquid Oxygen
    - Gas
    - Propane
    - Gasoline
9. Heavy Cargo:
    - Brick
    - Building Supply
    - Cable/Wire
    - Cotton
    - Metal
    - Paper
    - Concrete Pipe
    - Steel Pipe
    - Steel Re-Bar
    - Tile
    - Machinery
10. All Others

APPENDIX D

DEVELOPMENT AND VERIFICATION OF INTERFACE MODELS FOR MODIFIED ILLIPAVE

INTERFACE ELEMENT

(A) Implementation of Solution Methodology

Interface conditions can be considered as the interaction between two substructures as they come together or separate under loading. In pavements the sliding occurs between layers possibly due to poor tack coat or moisture at interface. Analyses which assume a perfectly bonded interface will over predict the shear transfer and will then underestimate strains in the layers.

The model to simulate interface conditions described herein in general is based on the one developed by Katona (38). The principle of this model is to incorporate an arbitrary set of constraint equations into a virtural work formulation. In finite element displacement formulation without constraining the internal virtual work is written as

$$\delta \underset{\sim}{u}^T = (K\underset{\sim}{u} - \underset{\sim}{P}) = 0 \qquad 1$$

in which

$\delta \underset{\sim}{u}^T$ = virtual displacement vectors

K = global stiffness matrix

$\underset{\sim}{u}$ = displacement vectors

$\underset{\sim}{P}$ = external force vectors

An arbitrary set of linear nodal point constraint equations with unknown internal constraint forces λ can be expressed as

$$\delta \underset{\sim}{\lambda}^T \quad (c\underset{\sim}{u} - \underset{\sim}{\Delta}) = 0 \qquad 2$$

in which

$\delta\underset{\sim}{\lambda}^T$ = arbituary variation of constraint force vectors.

c = constraint "stiffness" matrix

$\underset{\sim}{\Delta}$ = specified normal or tangential movement.

The constraint virtual work is then written by

$$\delta\,(c\underset{\sim}{u} - \underset{\sim}{\Delta})^T\ \underset{\sim}{\lambda} = \delta\,\underset{\sim}{u}^T c^T \underset{\sim}{\lambda} \qquad 3$$

Thus, the general virtual work including constraints is formulated by adding internal virtual work in Equation 1 to the constraint virtual work in Equation 3 in conjunction of Equation 2, as expressed in matrix form:

$$\delta \begin{Bmatrix} \underset{\sim}{u} \\ \underset{\sim}{\lambda} \end{Bmatrix}^T \left(\begin{bmatrix} K & C^T \\ C & O \end{bmatrix} \begin{Bmatrix} \underset{\sim}{u} \\ \underset{\sim}{\Delta} \end{Bmatrix} - \begin{Bmatrix} P \\ \underset{\sim}{\Delta} \end{Bmatrix} \right) = 0 \qquad 4$$

$\underset{\sim}{u}$ and $\underset{\sim}{\lambda}$ are unknowns to be solved in the global system.

To clarify the formulation of interface element, Equation 4 can be partitioned as

$$(K^* + C^*)\ U^* = F + f \qquad 5$$

in which

$$K^* = \begin{bmatrix} K & O \\ O & O \end{bmatrix}$$

$$C^* = \begin{bmatrix} O & C^* \\ C & O \end{bmatrix}$$

$$U^* = \begin{Bmatrix} \underset{\sim}{u} \\ \underset{\approx}{\lambda} \end{Bmatrix}$$

$$F = \begin{Bmatrix} \underset{\sim}{P} \\ o \end{Bmatrix}$$

$$f = \begin{Bmatrix} o \\ \underset{\approx}{\Delta} \end{Bmatrix}$$

C^* and f are the constraint element "stiffness" and load vector, respectively, which are formulated to describe the relations by the states between two interface nodes. As shown in Table D-1, there are three possible boundary states that can exist between the interface nodes. "Fixed - Fixed" refers to the interface nodes are constrained to move together in both the normal and tangential direction. "Fixed - Free" implies that relative normal movement is constrained and a tangential force is specified. And "Free - Free" is characterized by specifying the normal and tangential interface forces. Table D-2 shows the element constraint matrix and load vector for three boundary states. Detailed derivation appears in Reference 39. To implement the interface conditions to ILLIPAVE, the iterative procedures are made as following

1. Initially assumed that each constraint element "stiffness" is in a fixed-fixed state, and assign a zero vector to the load matrix.

2. Add each constraint element "stiffness" and load vectors into global system.

3. Solve the trial value of $\underset{\sim}{u}$ and $\underset{\sim}{\lambda}$

Table D-1. Boundary States for Interface Element

Normal Terminology	State	Normal Specified		Tangential Specified	
		Relative Displacement	Force	Relative Displacement	Force
Fixed-Fixed	A	x		x	
Fixed-Free	B	x			x
Free -Free	C		x		x

Table D-2. Element Constraint Matrix and Load Vector

State	u_i	v_i	u_i	v_i	λ_n	λ_s	"load"
State A Fixed-Fixed	0	0	0	0	-C	S	0
	0	0	0	0	-S	-C	0
	0	0	0	0	C	-S	0
	0	0	0	0	S	C	0
	-C	-S	C	S	0	0	Δ_n
	S	-C	-S	C	0	0	Δ_t
State B Fixed-Free	0	0	0	0	-C	0	-ST
	0	0	0	0	-S	0	CT
	0	0	0	0	C	0	ST
	0	0	0	0	S	0	-CT
	-C	-S	C	S	0	0	Δ_n
	0	0	0	0	0	1	T
State C Free-Free	0	0	0	0	0	0	CN-ST
	0	0	0	0	0	0	SN+CT
	0	0	0	0	0	0	-CN+ST
	0	0	0	0	0	0	-SN-CT
	0	0	0	0	1	0	N
	0	0	0	0	0	1	T

Δ_n, Δ_t, T, and N are specified values

c = cos ϕ

s = sin ϕ

ϕ = angle of the global co-ordinate to interface element co-ordinate

4. Examine the validity of the assumed state for each interface element by the decision criterion of Table D-3.
    a) If the state of every interface element corresponds to the criterion of Table D-3, then stop computing.
    b) Otherwise change the constraint to element "stiffness" and load vector to the proper state with aid of Table D-2, then return to step 2.

The steps described above to calculate the interface forces and displacements of nodes are also shown in the form of flowcharts as illustrated in Figure D-1.

(B) Comparisons between BISAR and Modified ILLIPAVE with SLIP Condition

The purpose of this section is to examine the validity of modified ILLIPAVE Computer program with interface element model as described previously. To do this, the results from linear elastic layered system computer program, BISAR (40), will be compared with that of the modified ILLIPAVE program. The pavement geometry used in comparisons is shown in Figure D-2. Since an infinite thickness of the subgrade layer used in BISAR can not be assigned in ILLIPAVE, a value of fifty times the loading radius is specified. The thickness of the base course is fixed with the value of 8-inches, while the thickness of asphalt layer is varied from 1, 1.5, 2, and 4-inches. Material properties are considered to be linear elastic because of the limitations of BISAR. The elastic moduli of the base and subgrade are 50,000 and 20,000 psi, respectively, while the elastic modulus of asphalt concrete is varied from 800,000 , 400,000 , and 50,000 psi. A circular uniform load with a pressure of 125 psi is applied on the surface for all cases, and the radius of loading area is 3.21-inches. A Full Slip condition (frictionless slip) is assigned between the surface and base course only. Table D-4 shows the comparisons of the radial strains at bottom of the surface course

Table D-3. Decision Matrix for Selecting New State

Previously Assumed State	New State for Next Iteration		
	State A Fixed-Fixed	State B Fixed-Free	State C Free-Free
State A Fixed-Fixed	$\lambda_n \leq \xi$ $\lambda_s < T_{max}$	$\lambda_n \leq \xi$ $\lambda_s > T_{max}$	$\lambda_n > \xi$
State B Fixed-Free	$\lambda_n \leq \xi$ $\Delta_s T_{max} < 0$	$\lambda_n \leq \xi$ $\Delta_s T_{max} > 0$	$\lambda_n > \xi$
State C Free-Free	$\Delta_n < 0$	Not applicable	$\Delta_n > 0$

ξ = tensile rupture resistance of interface

Tmax = Maximum friction force

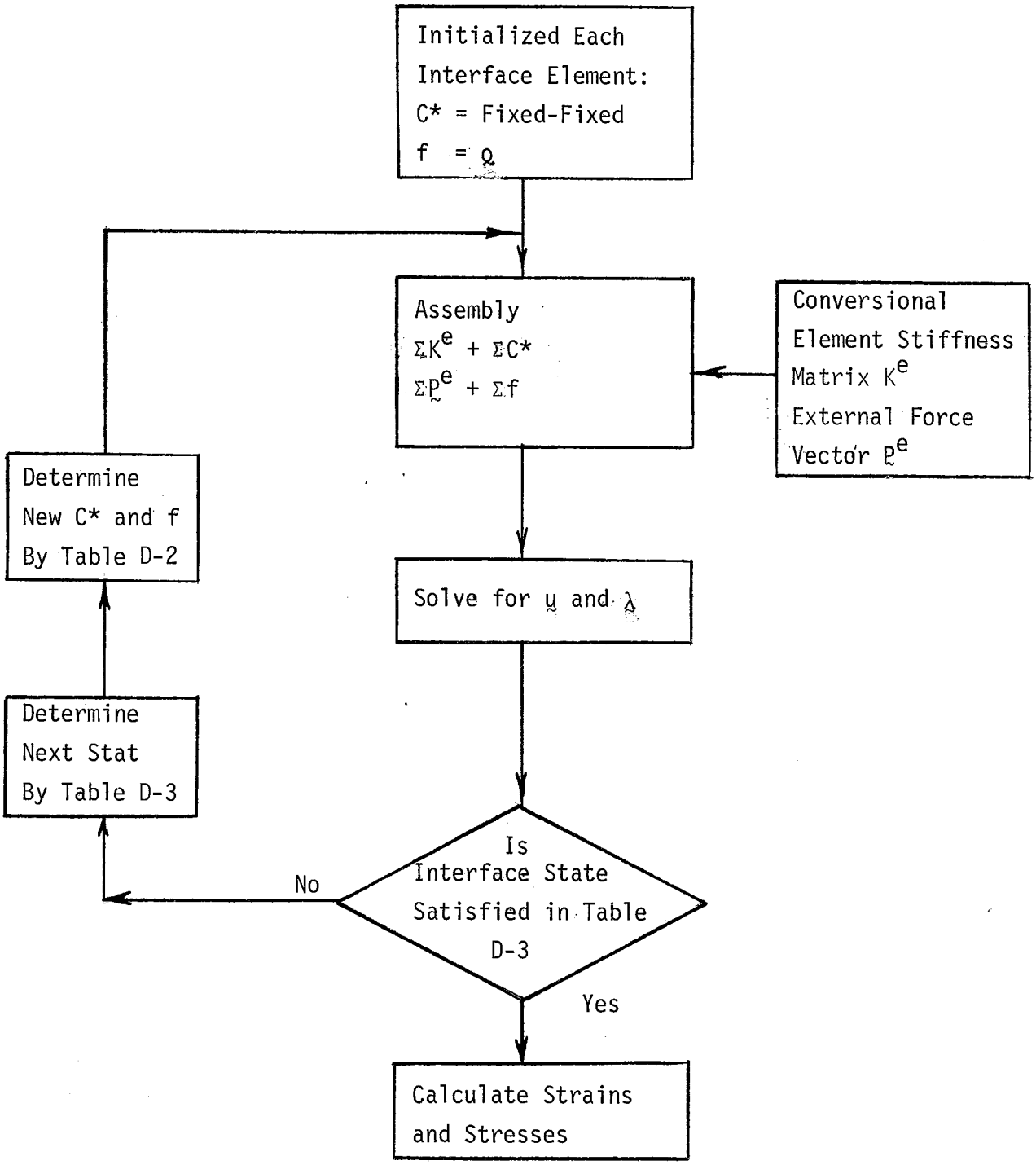

Figure D-1. Structural Analysis Including Interface Element

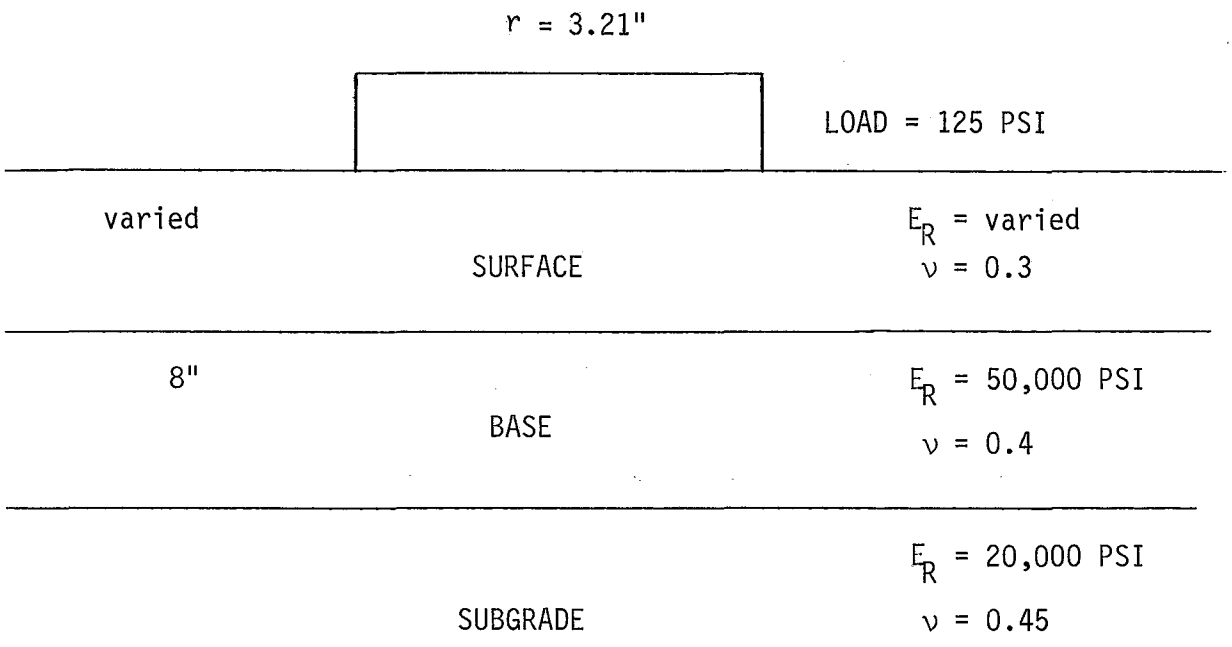

Figure D-2. Pavement Geometry for Comparison Analysis

Table D-4. Comparisons of Radial Strains at Bottom of Surface Course

Modulus of Surface (psi)	AC Thickness (inches)	Radial Strains, in/in x 10^{-4}	
		BISAR	Modified ILLIPAVE
800,000	1	4.009	4.005
	1.5	3.953	3.668
	2	3.400	3.151
	4	1.751	1.629
400,000	1	4.900	5.015
	1.5	5.410	5.160
	2	5.010	4.727
	4	2.897	2.716
50,000	1	8.864	9.226
	1.5	12.21	12.19
	2	14.00	13.53
	4	11.71	10.81

from BISAR and modified ILLIPAVE program. It is apparent that the layered elasticity solution and finite element solution are in good agreement. Thus, it is believed the modified ILLIPAVE program can accurately represent the response of pavement structure in practice.

APPENDIX E

FLOW CHARTS OF MODIFIED ILLIPAVE

The modified ILLIPAVE computer program to carry out all of the calculations, including structural analysis, distress analysis, and present serviceability index, are summarized in this appendix by way of a set of flow charts. Figure E-1 shows the methodology processes carried out in the computer program.

Three categories of input data are required in the computer program. The first category of input data includes geometric properties, including geometry of the layered system which in turn generates a finite element mesh automatically by the program, and loading conditions which can be either the uninform or non-uniform vertical and horizontal loads. The second category of input data is defined as material properties, including structure and distress properties, and stocastic coefficients which are detailed in chapter 4. The third category of input data includes daily traffic rate and seasonal temperatures.

Next come the calculations of structural response, including deflections, strains, and stresses, based on the finite element method. The interface conditions are optional that can be either a full bond or full slip between layers as defined in Appendix D.

Next the rut depth is calculated, which in turn calculates slope variance, and fatigue cracking of current analysis period using the equations that are described in the chapter 4. The detailed flow chart for each type of distress are shown in Figure E-2, E-3, and E-4. The present serviceability index is then calculated using initial serviceability index, rut depth, cracked area, and slope variance for the specified analysis period.

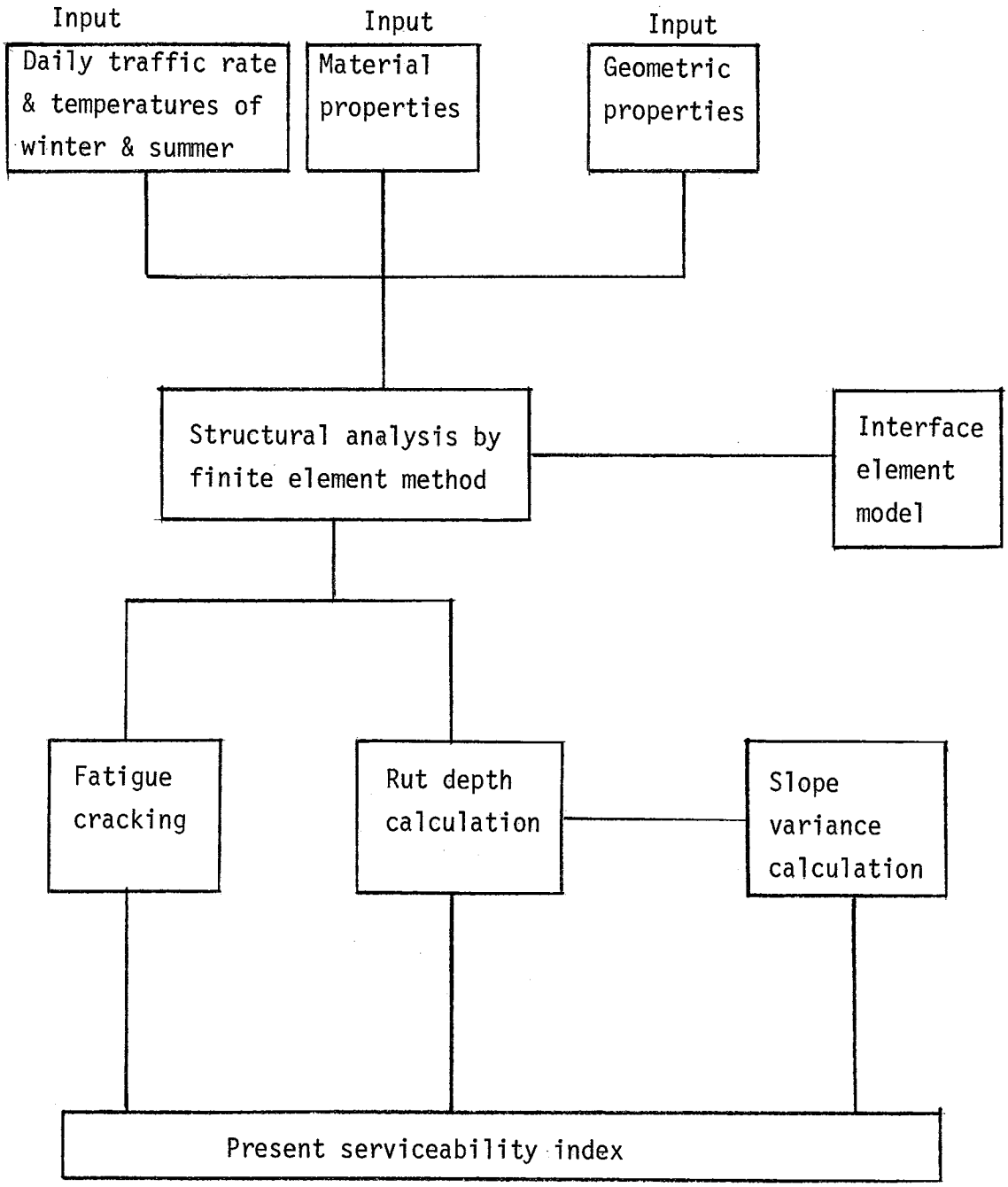

Figure E-1. Methodology process of modified ILLIPAVE.

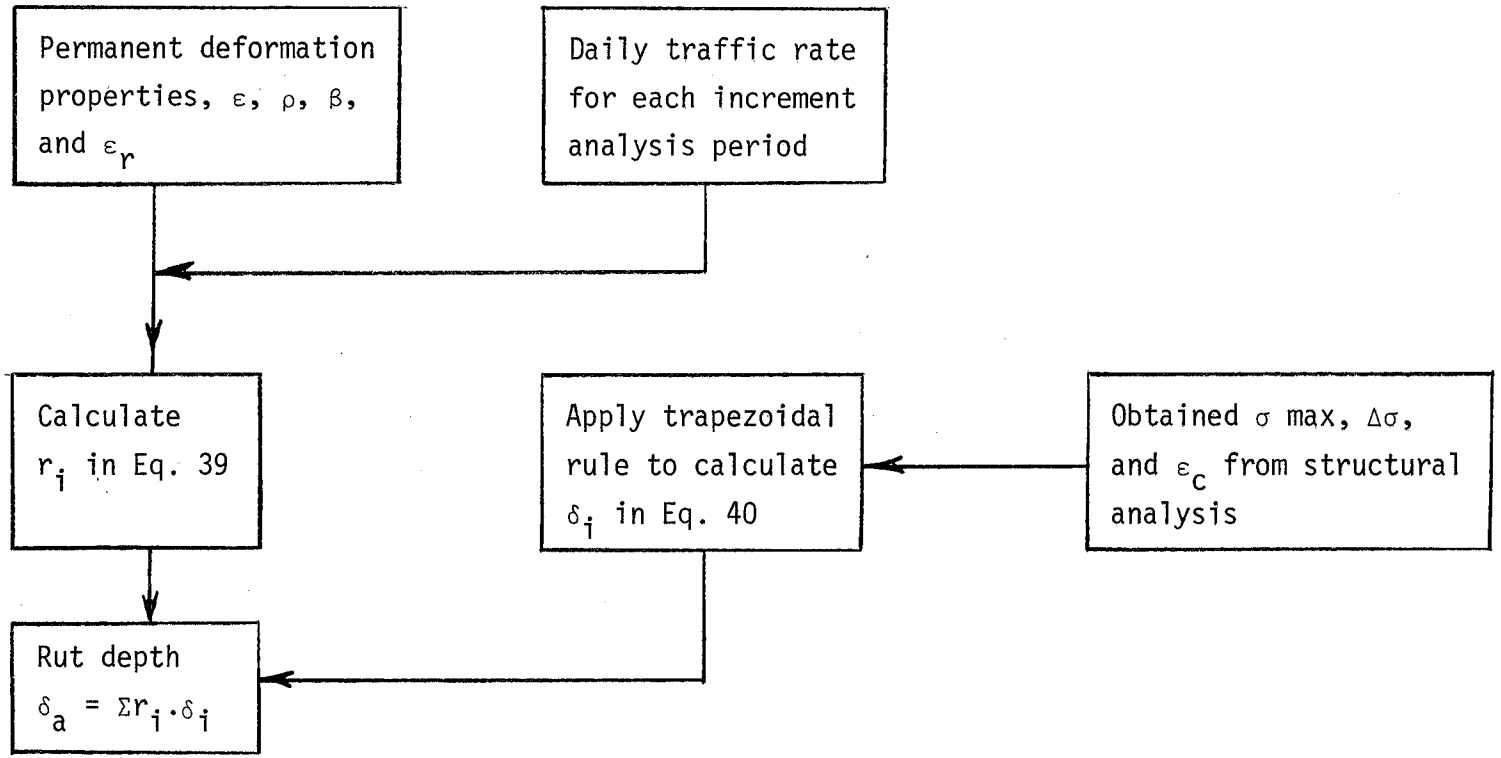

Figure E-2. Calculation of rut depth.

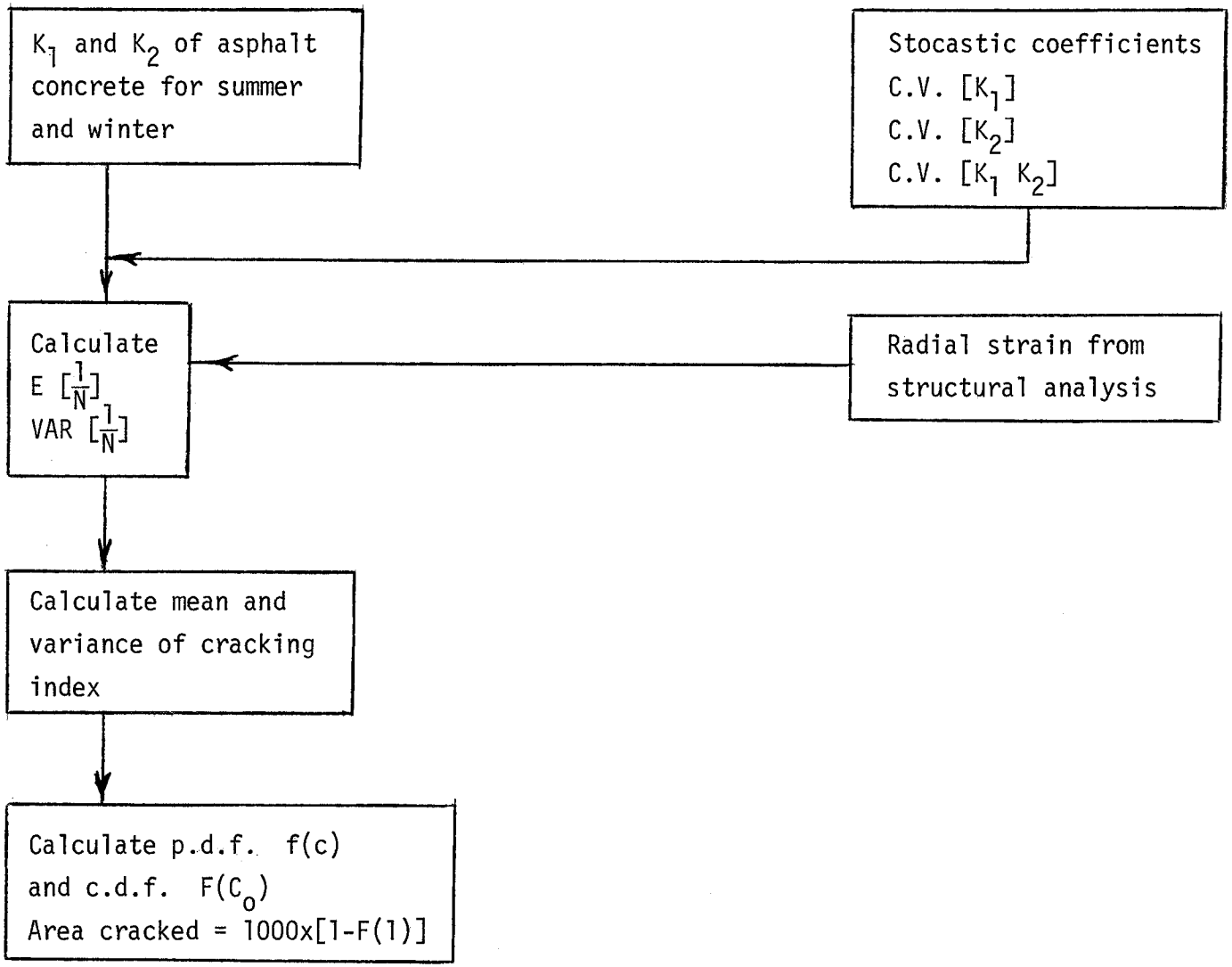

Figure E-3. Fatigue Cracking Calculation.

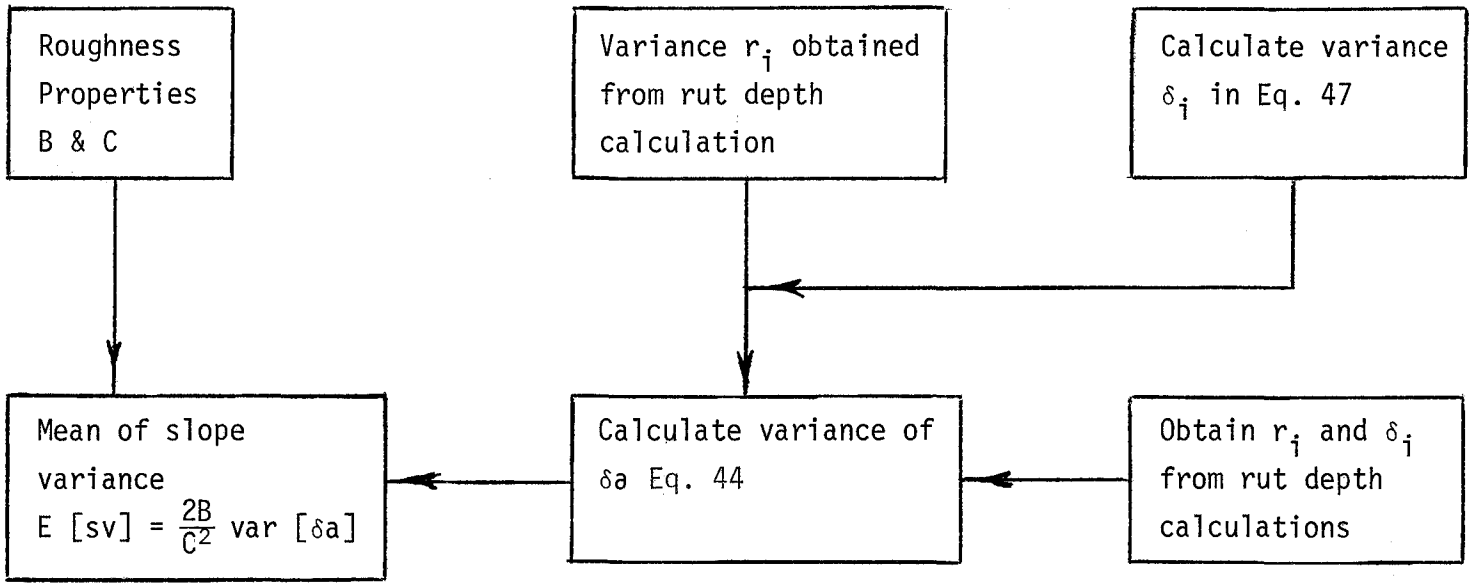

Figure E-4. Slope Variance Calculation.

APPENDIX F

PERMANENT DEFORMATION CHARACTERIZATION OF SAMPLE PAVEMENT MATERIALS

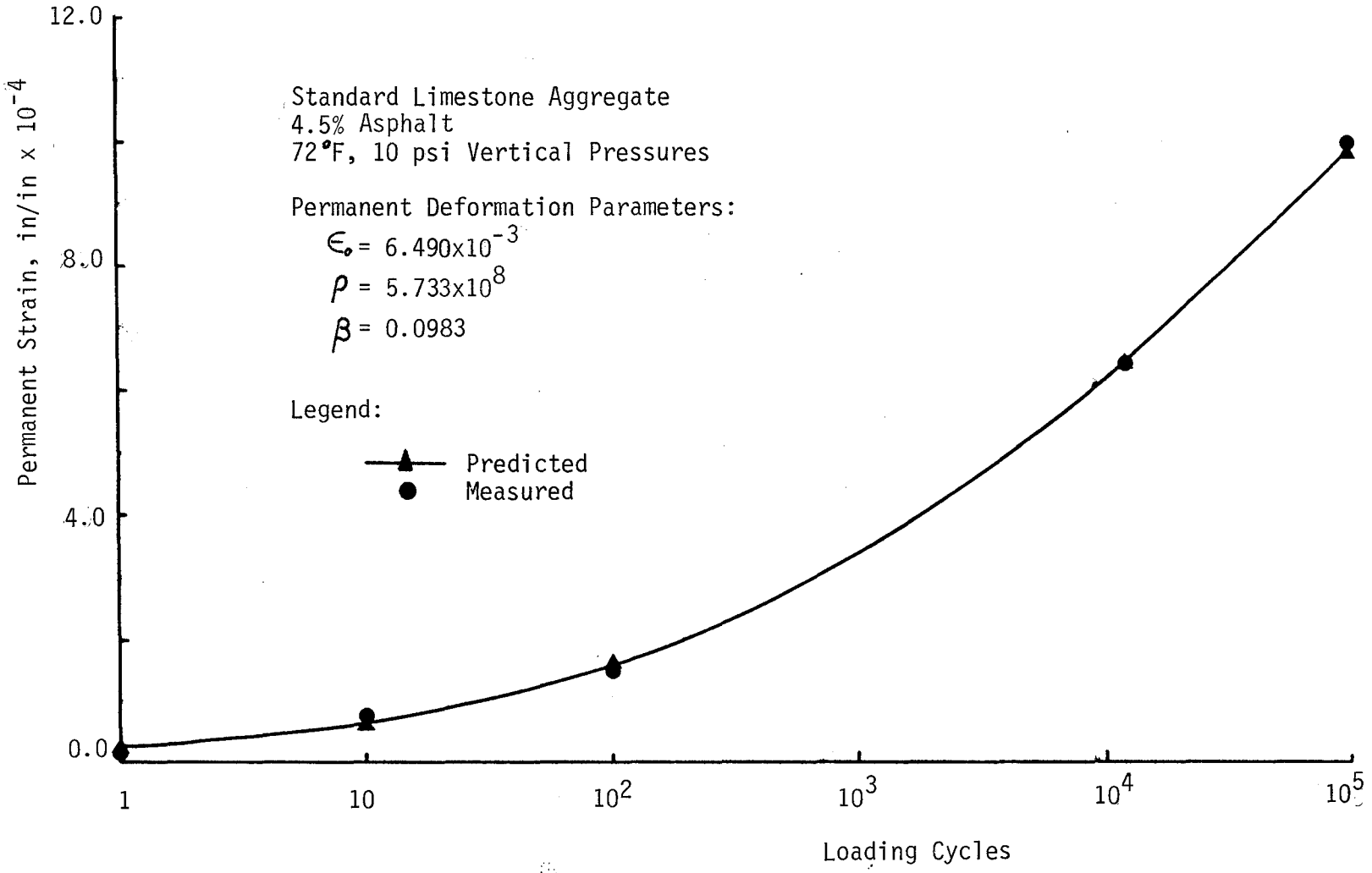

Figure F-1. Comparisons of Predicted And Measured Permanent Strains Versus Loading Cycles for Asphalt Concrete

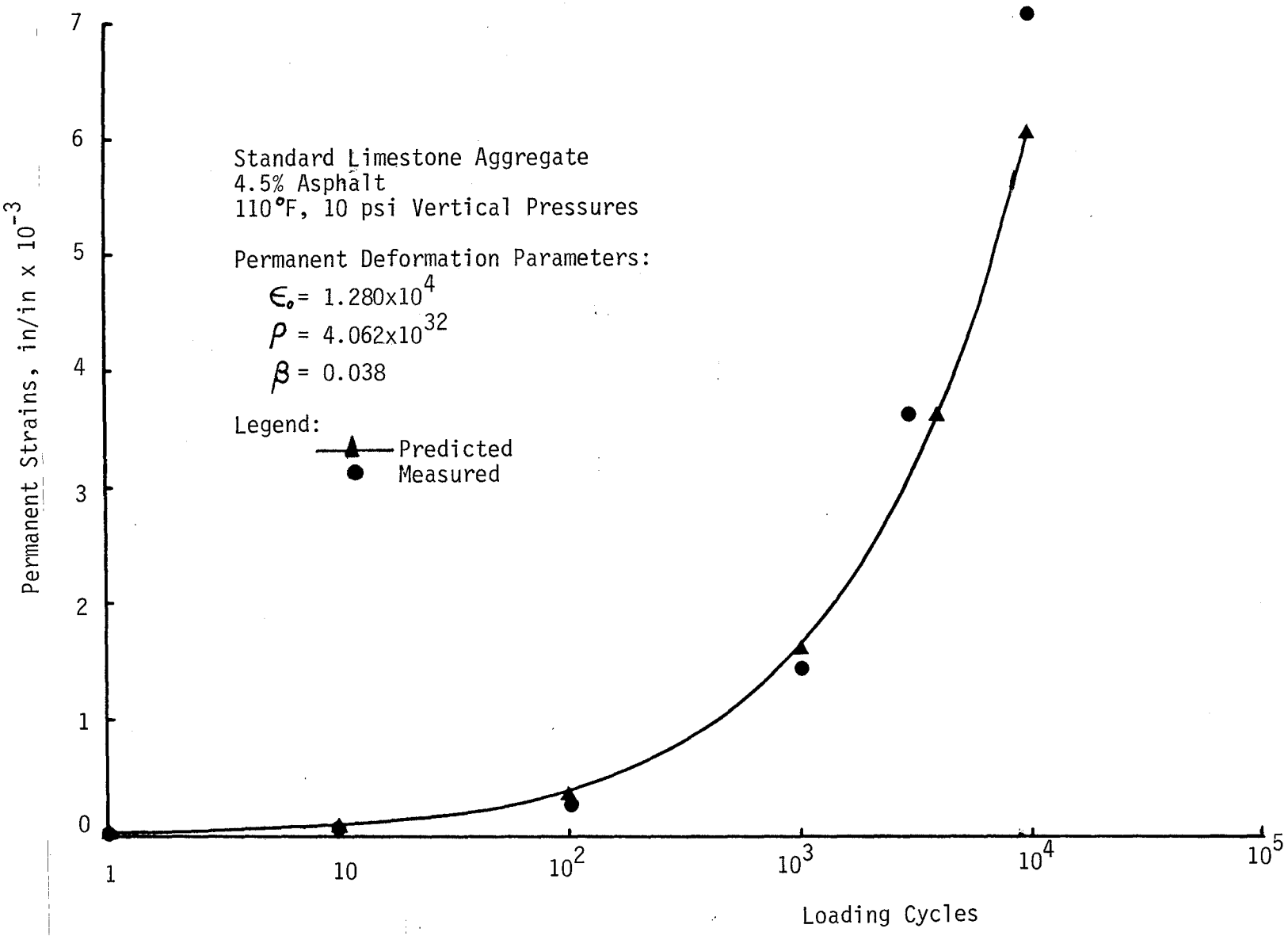

Figure F-2. Comparisons of Predicted and Measured Permanent Strains Versus Loading Cycles for Asphalt Concrete

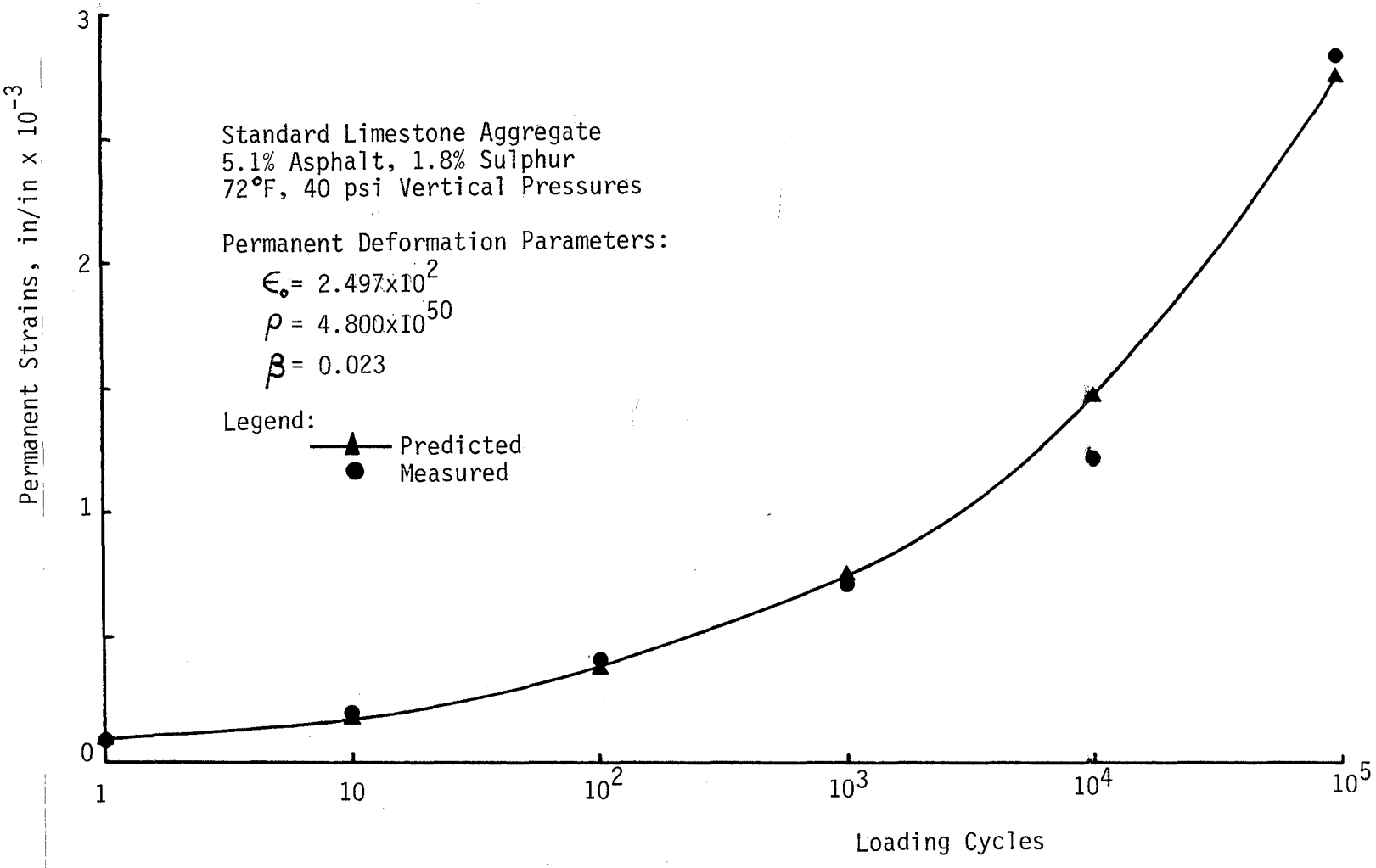

Figure F-3. Comparison of Predicted and Measured Permanent Strains Versus Loading Cycles for Asphalt Concrete

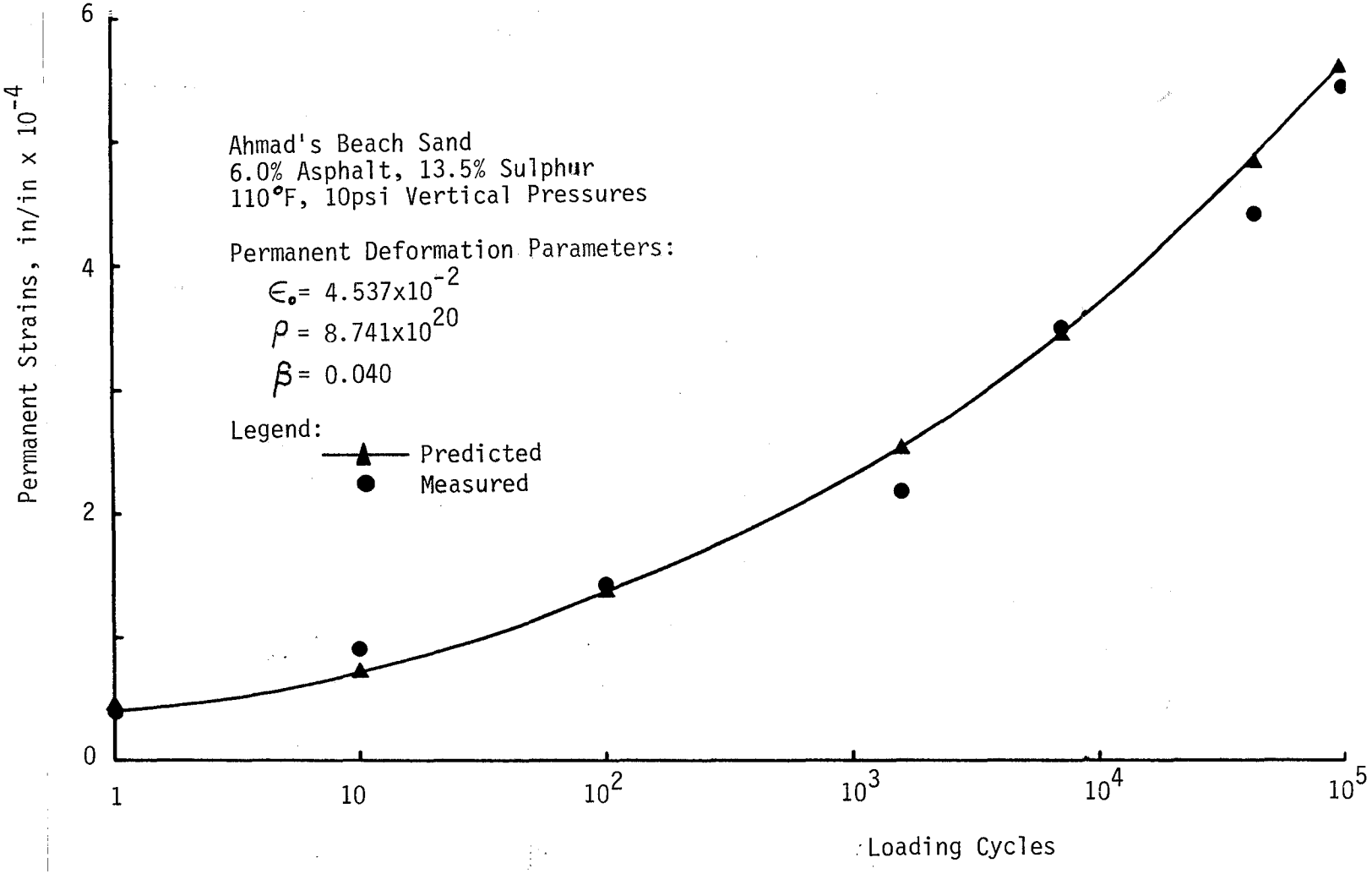

Figure F-4. Comparisons of Predicted and Measured Permanent Strains Versus Loading Cycles for Aspahalt Concrete with Sulphur

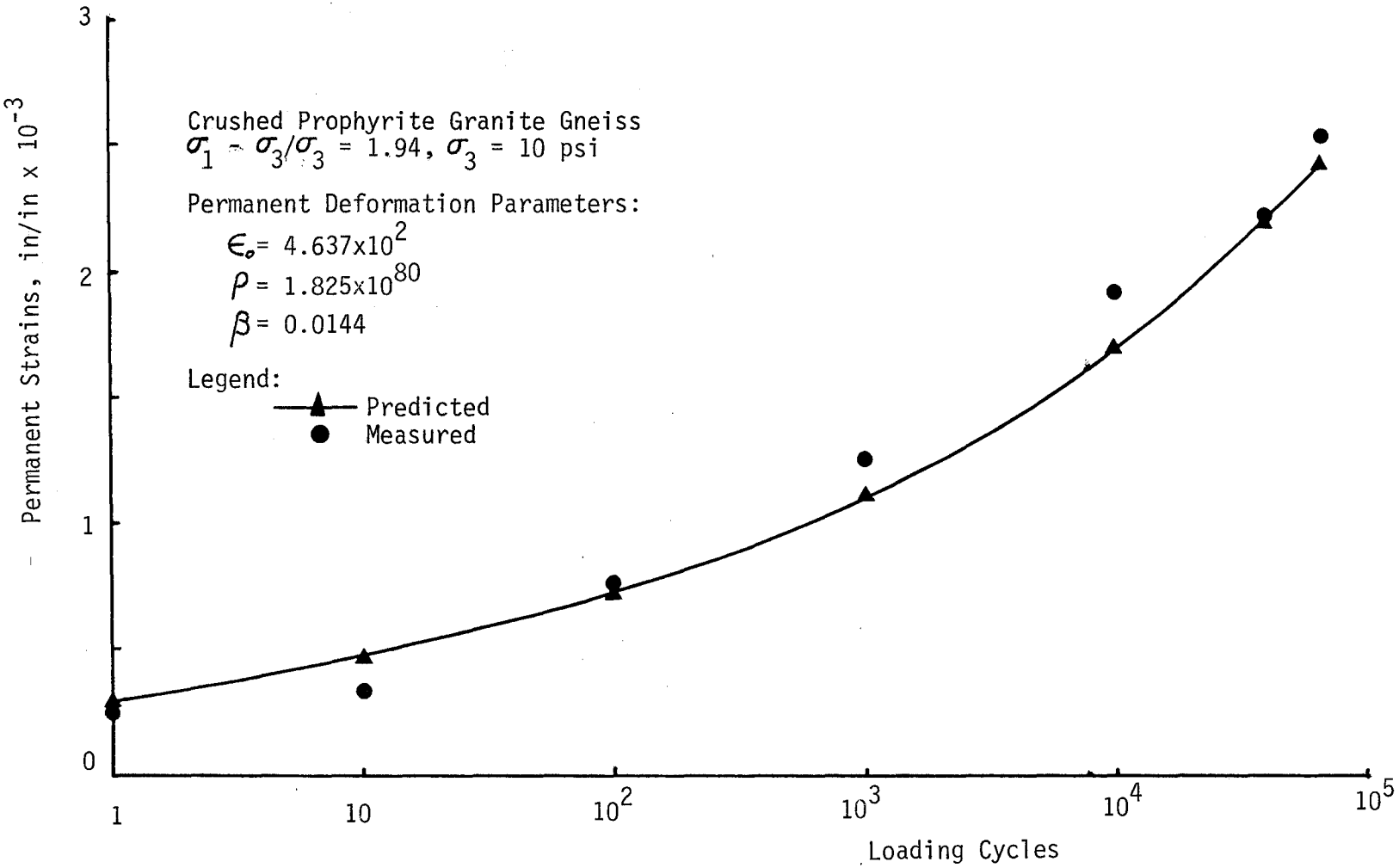

Figure F-5. Comparison of Predicted and Measured Permanent Strains Versus Loading Cycles for Base Course

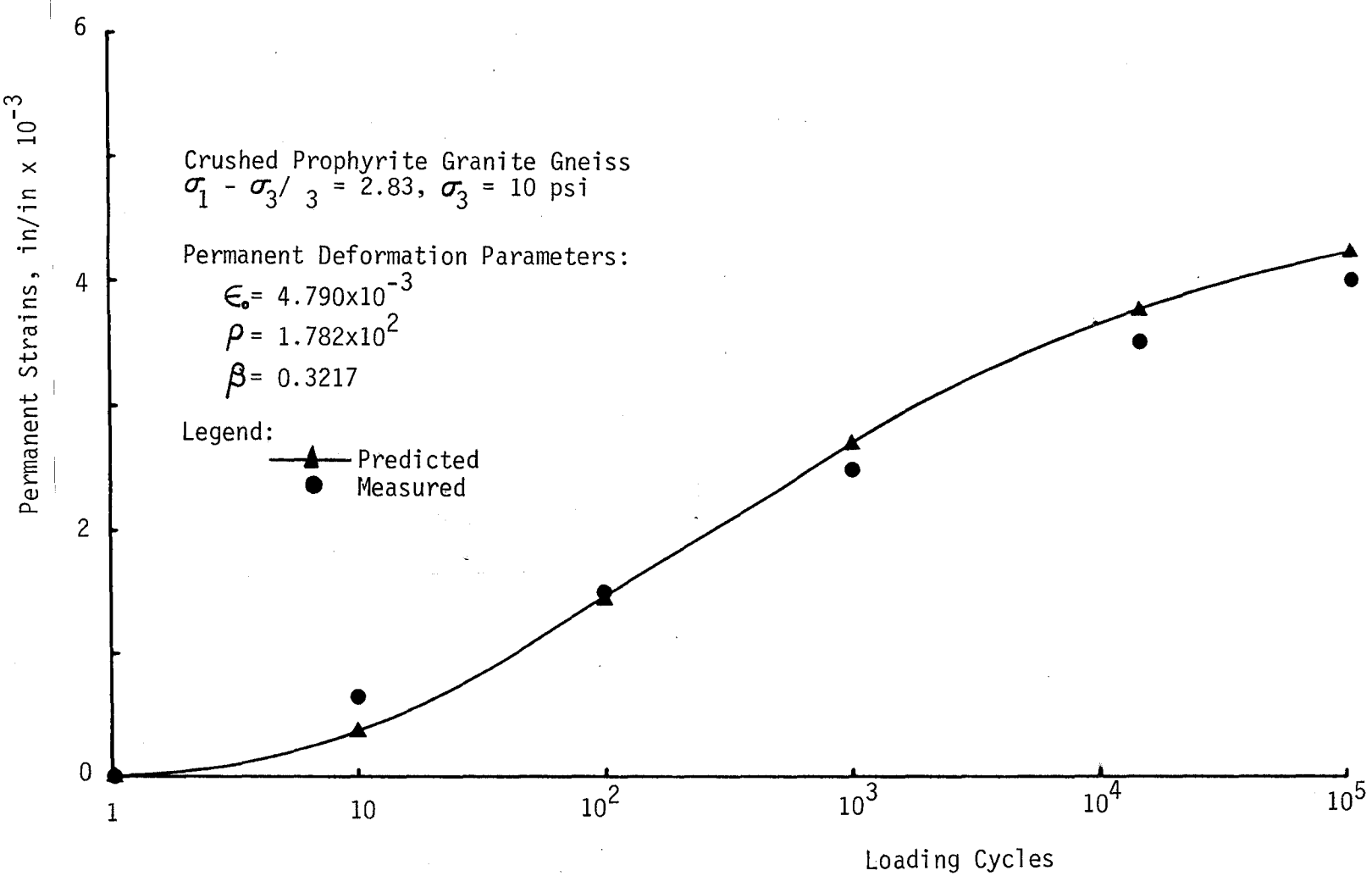

Figure F-6. Comparison of Predicted and Measured Permanent Strains Versus Loading Cycles for Base course

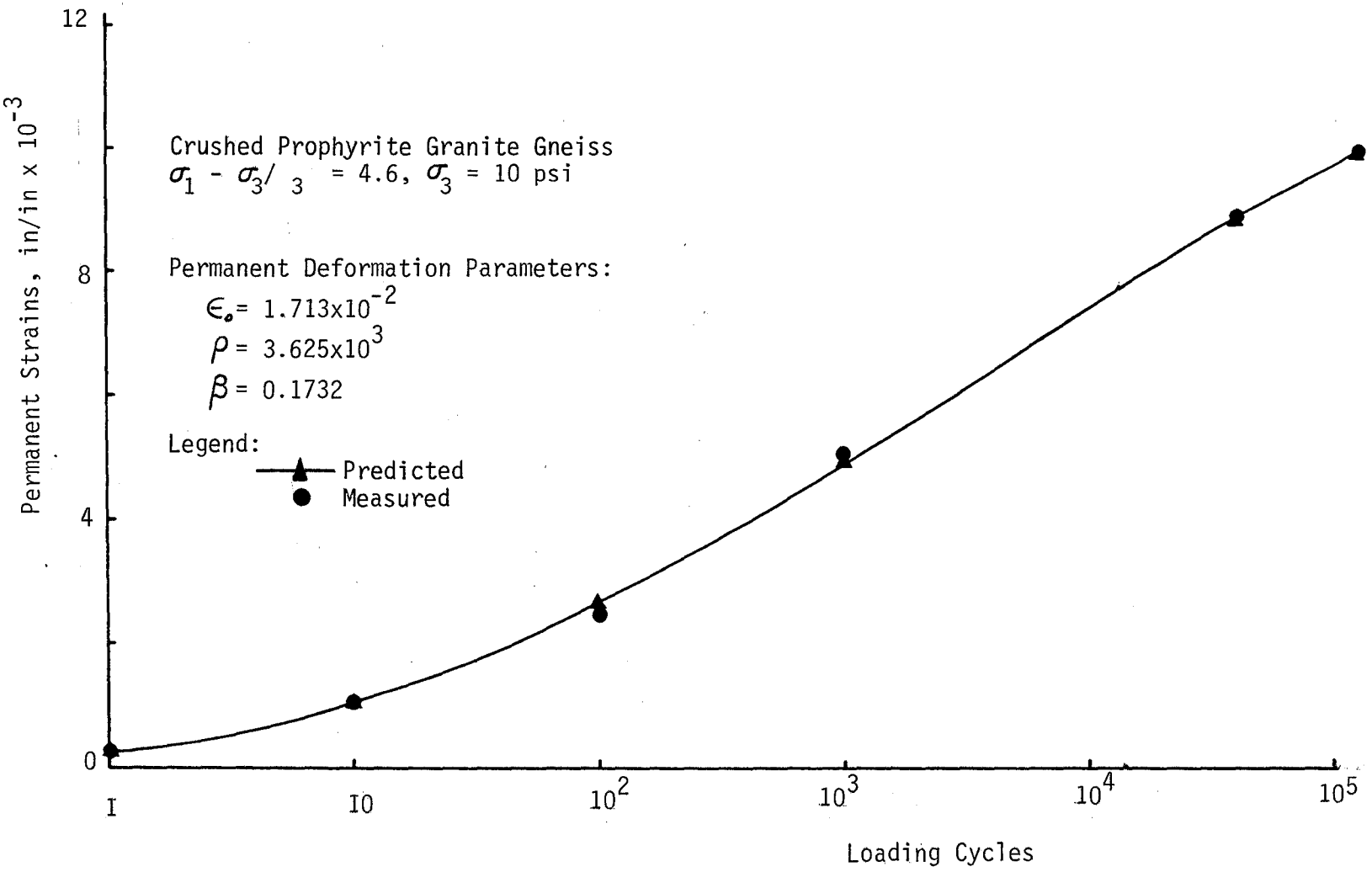

Figure F-7. Comparisons of Predicted and Measured Permanent Strains Versus Loading Cycles for Base Course

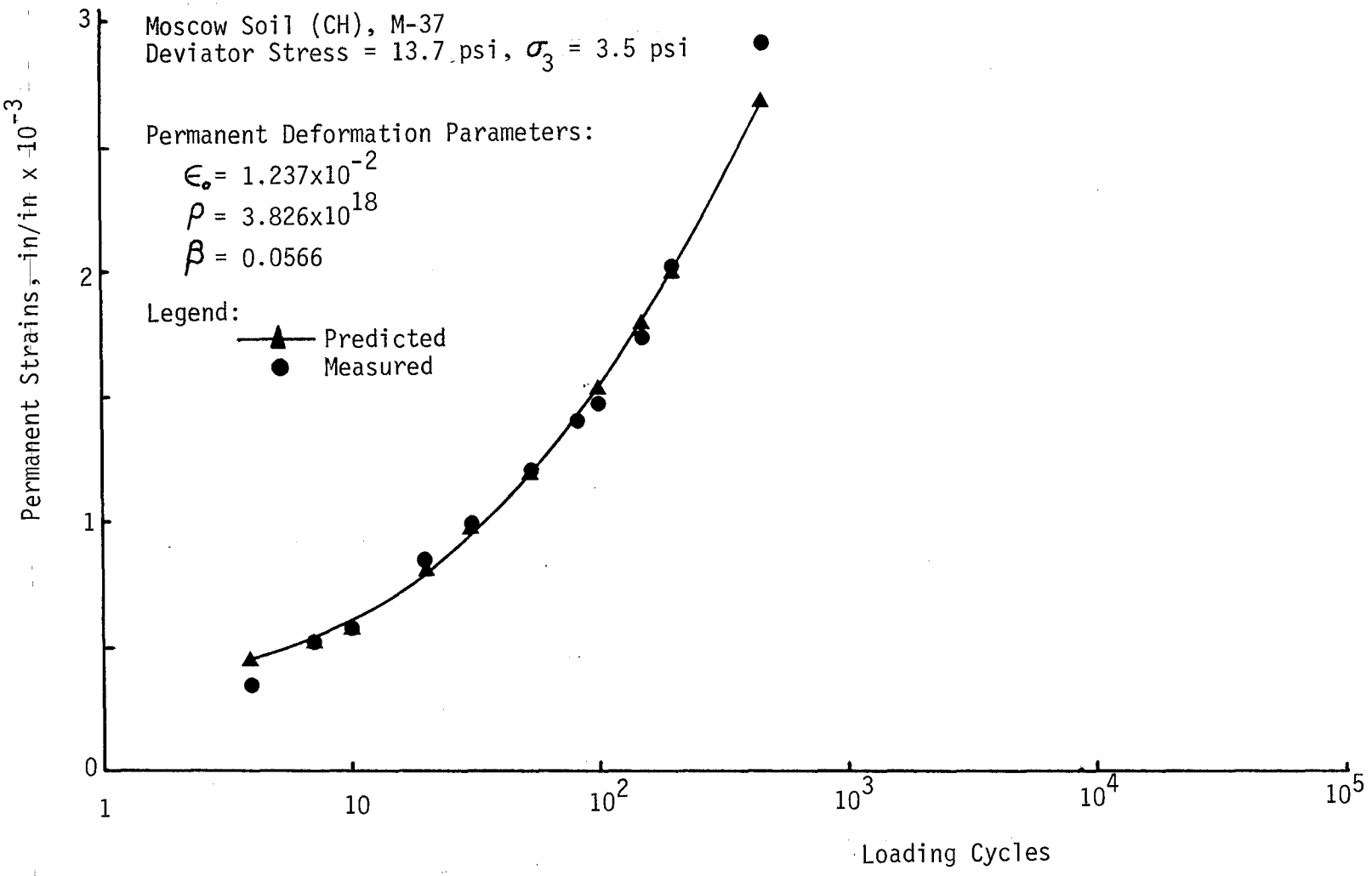

Figure F-8. Comparisons of Predicted and Measured Permanent Strains Versus Loading Cycles for Subgrade Soil

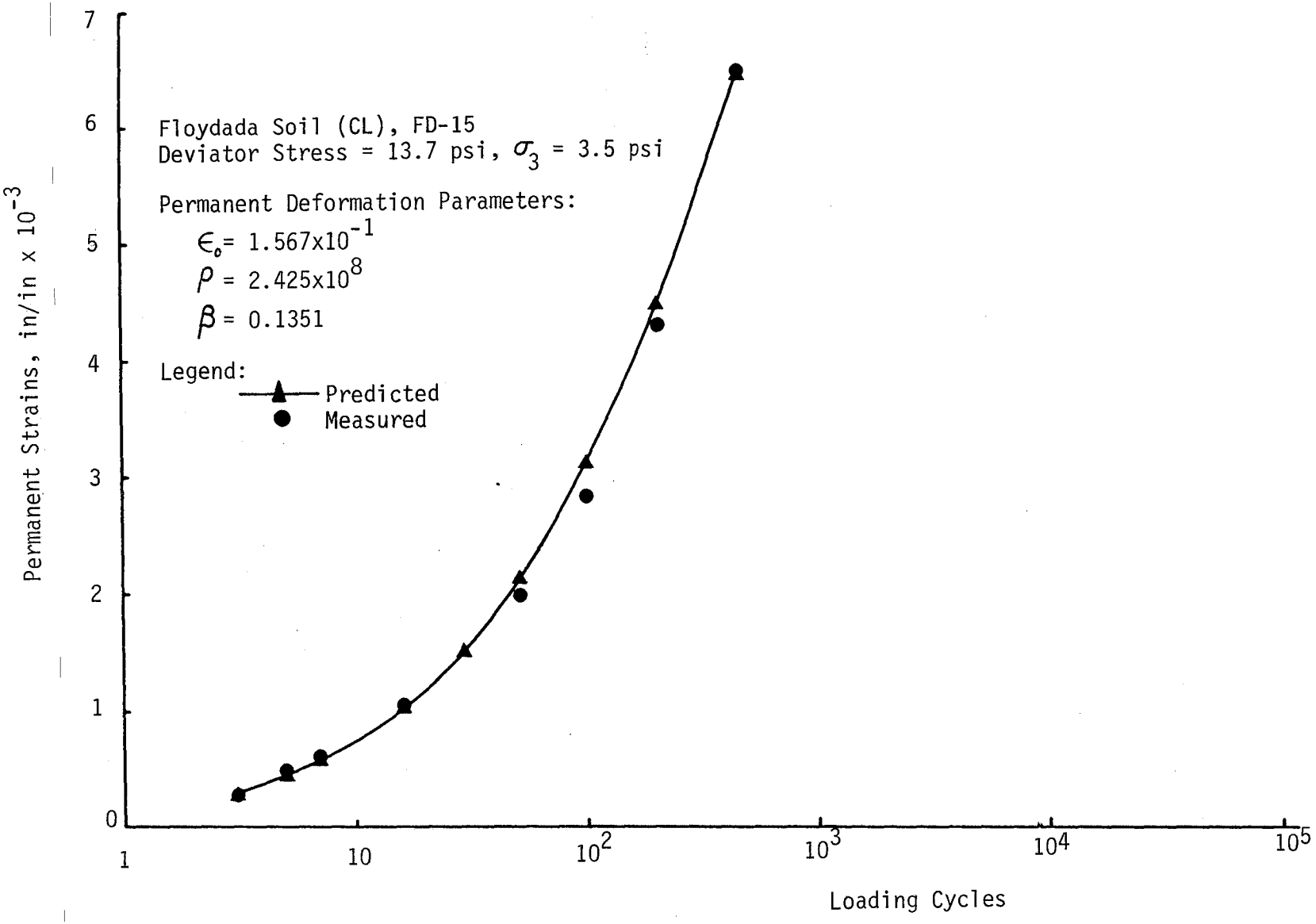

Figure F-9. Comparisons of Predicted and Measured Permanent Strains Versus Loading cycles for subgrade Soil

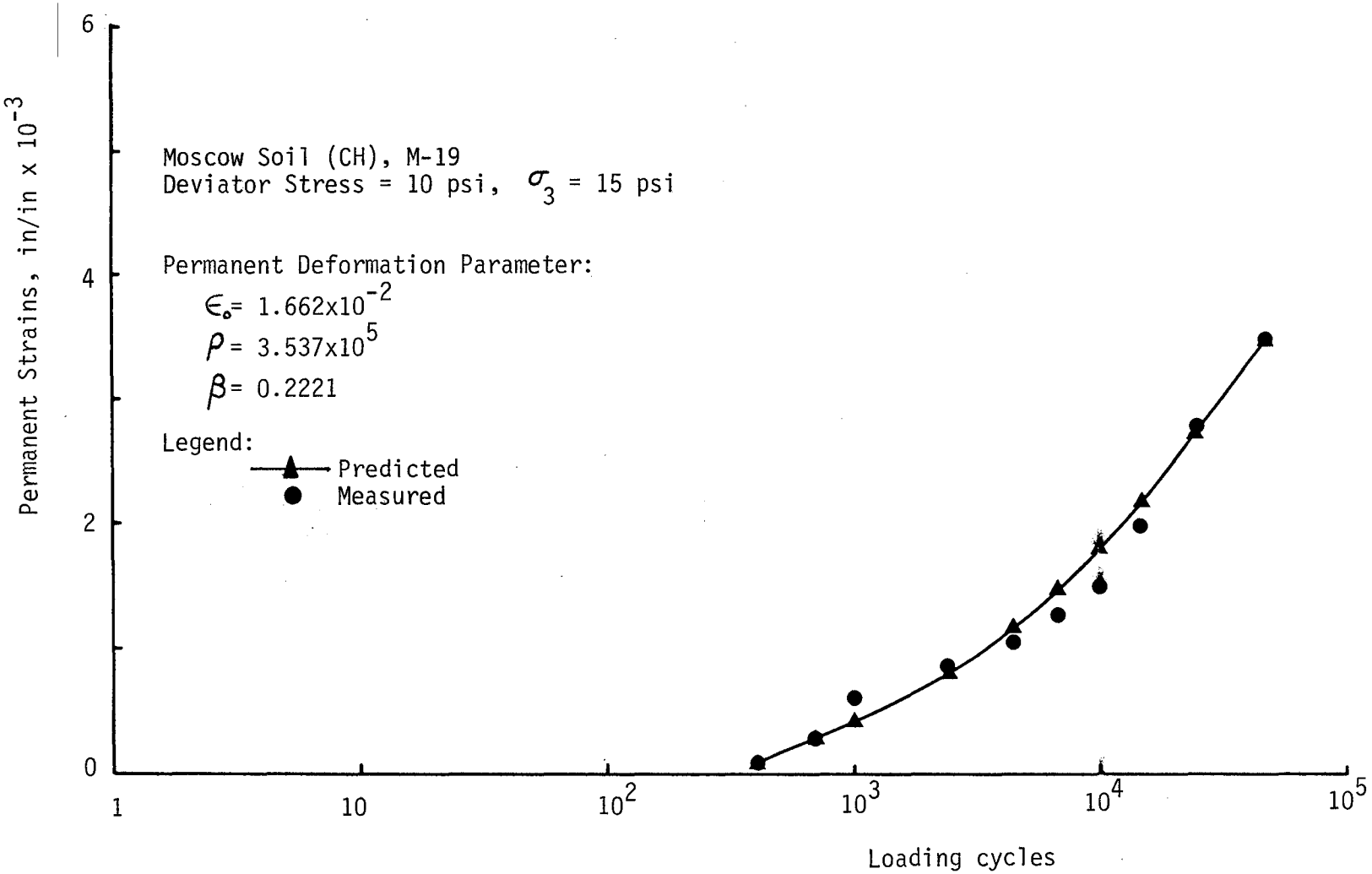

Figure F-10. Comparisons of Predicted and Measured Permanent Strains Versus Loading Cycles for Subgrade Soil

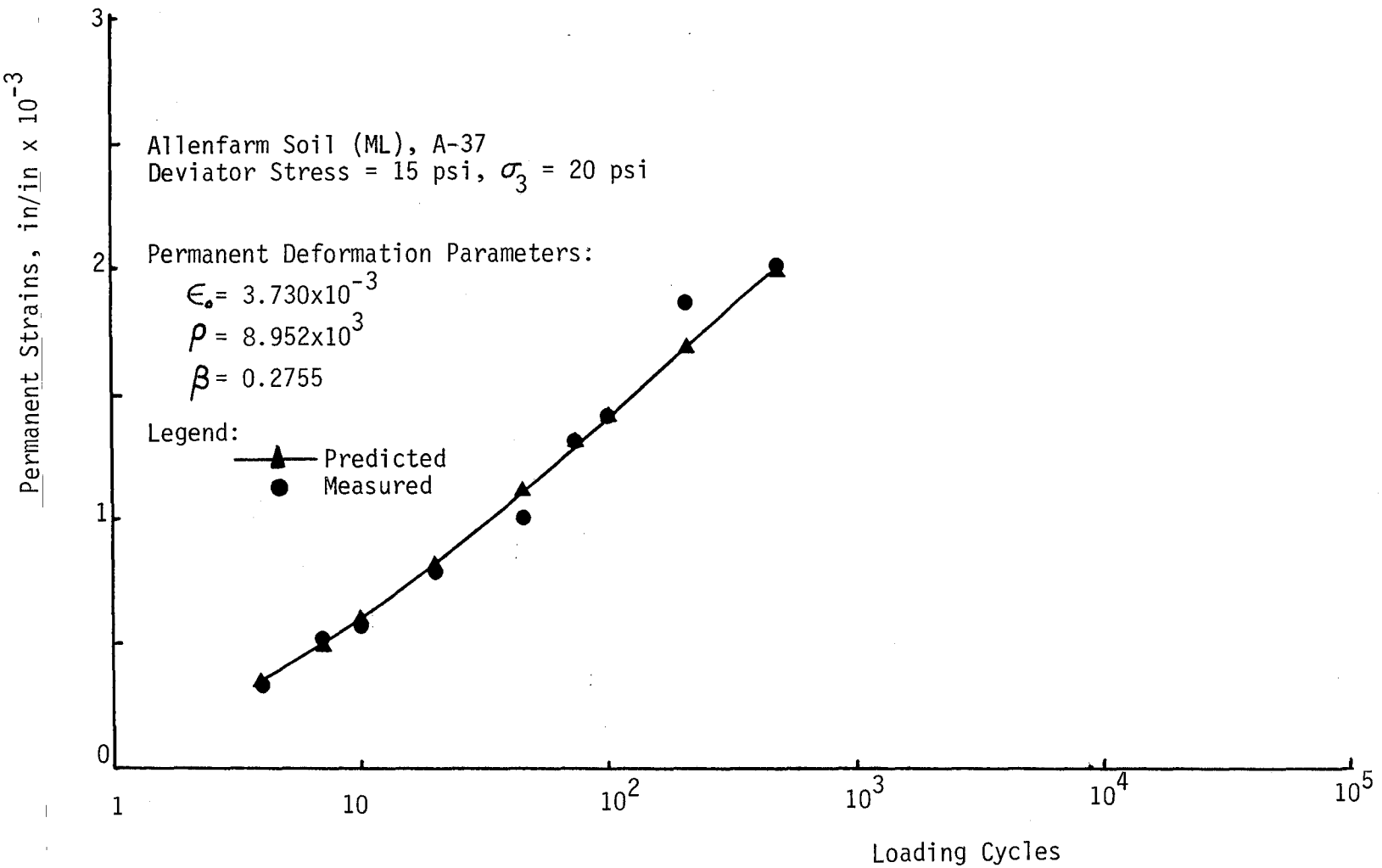

Figure F-11. Comparisons of Predicted and Measured Permanent Strains Versus Loading Cycles for Subgrade Soil

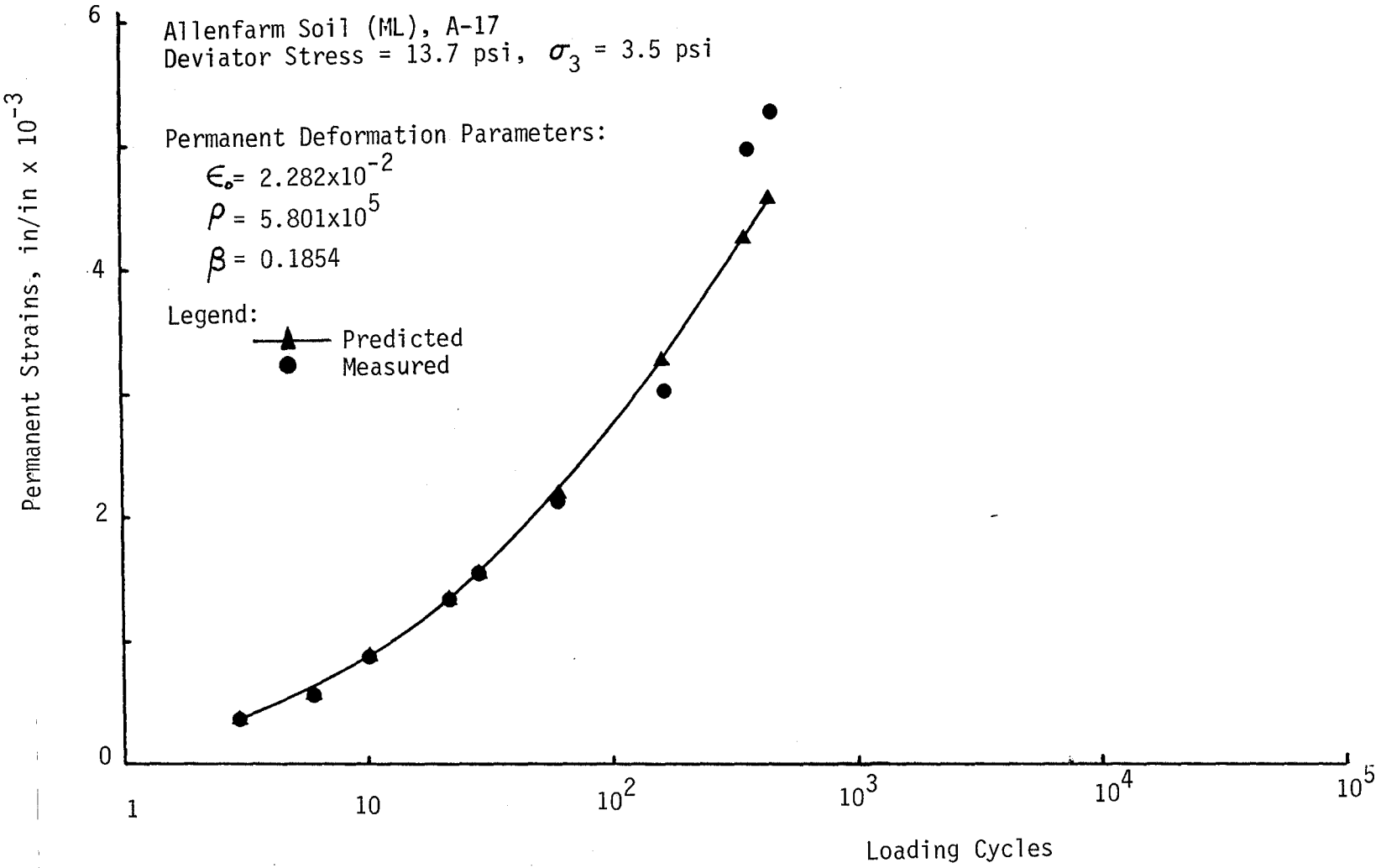

Figure F-12. Comparisons of Predicted and Measured Permanent Strains Versus Loading Cycles for Subgrade Soil

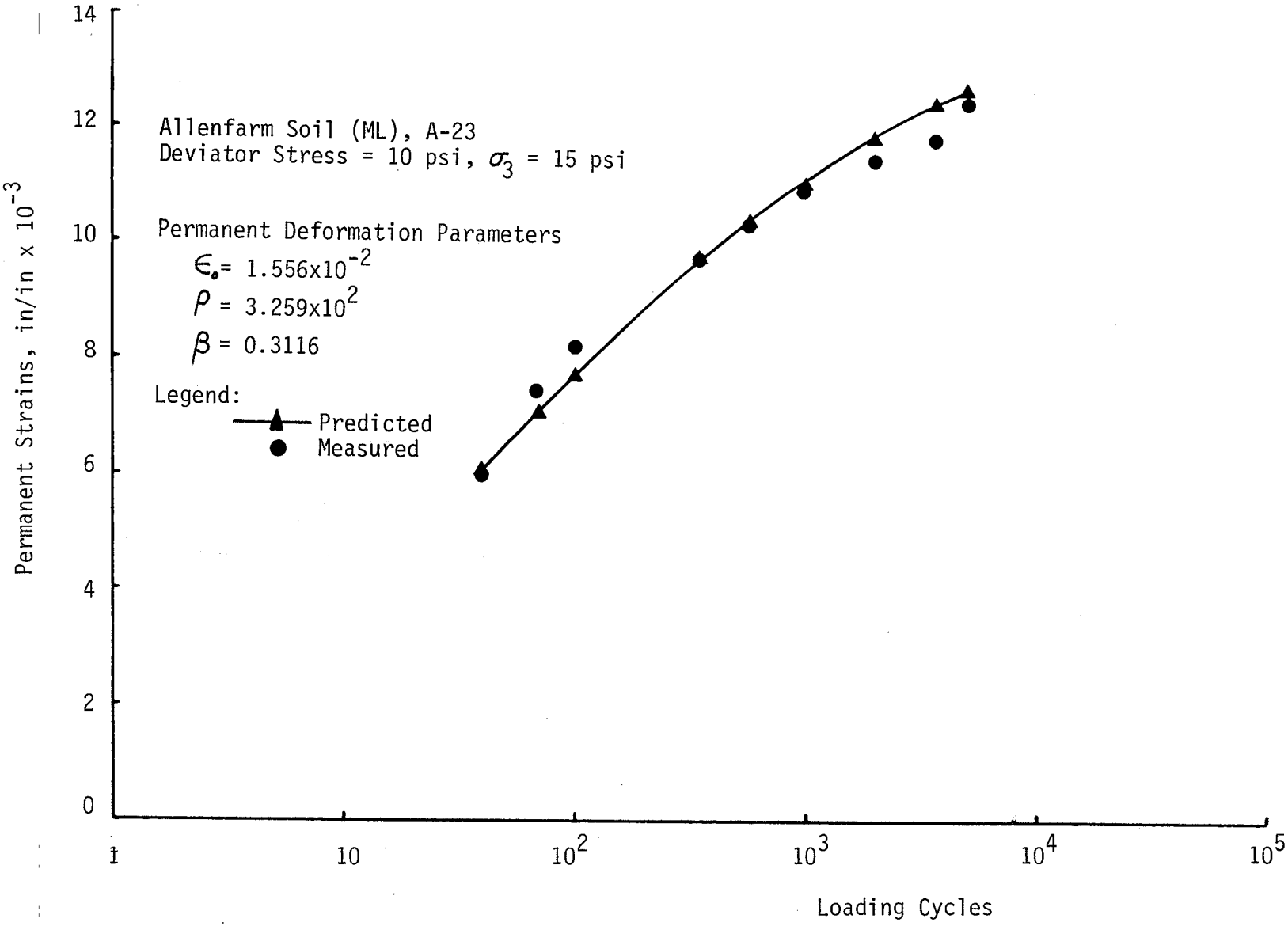

Figure F-13. Comparison of Predicted and Measured Permanent Strains Versus Loading Cycles for Subgrade Soil